

Electronic Thesis and Dissertation Repository

6-15-2017 12:00 AM

Comparative Investigation of Bored and Continuous Flight Auger Piles with Consideration of Green Concrete

Mahmoud Kassem
The University of Western Ontario

Supervisor
Hesham El Nagggar
The University of Western Ontario

Graduate Program in Civil and Environmental Engineering
A thesis submitted in partial fulfillment of the requirements for the degree in Doctor of Philosophy
© Mahmoud Kassem 2017

Follow this and additional works at: <https://ir.lib.uwo.ca/etd>



Part of the [Geotechnical Engineering Commons](#)

Recommended Citation

Kassem, Mahmoud, "Comparative Investigation of Bored and Continuous Flight Auger Piles with Consideration of Green Concrete" (2017). *Electronic Thesis and Dissertation Repository*. 4604.
<https://ir.lib.uwo.ca/etd/4604>

This Dissertation/Thesis is brought to you for free and open access by Scholarship@Western. It has been accepted for inclusion in Electronic Thesis and Dissertation Repository by an authorized administrator of Scholarship@Western. For more information, please contact wlsadmin@uwo.ca.

Abstract

Bored and continuous flight auger (CFA) piles are two widely used cast in place reinforced concrete pile types that are constructed employing different techniques, which affect their performance and capacity. However, both are classified as non-displacement piles and are designed accordingly using the same method. Therefore, the objective of this work is to comparatively investigate the axial and lateral performance of bored and CFA piles installed in sand. In addition, the potential of constructing sustainable piles utilizing green concrete mixture that incorporates treated oil sand waste (TOSW) was investigated. Fresh and hardened properties along with durability performance of CFA concrete mixtures incorporating 10%, 20%, 30% and 40% TOSW as partial replacement of sand were investigated. Six piles with the same nominal geometry were constructed using conventional and green concrete mixtures. The piles were subjected to axial monotonic compressive and uplift loading as well as monotonic and cyclic lateral loading. The test piles were exhumed after testing to investigate their dimensions and profile, surface roughness, and interface friction between soil and pile. The soil-pile interface conditions of bored and CFA piles were quantitatively characterized using fractal dimension to measure surface roughness. Finally, three-dimensional non-linear finite element models were developed utilizing Plaxis 3D software to simulate the behaviour of the bored and CFA piles under monotonic compression, uplift, and lateral loading. A parametric study was carried out to investigate the effect of the angle of internal friction and the pile diameter on its behaviour and capacity under different loading cases. The results showed that the addition of TOSW, up to 30% replacement of sand, did not adversely affect the performance of CFA concrete mixtures. CFA piles had higher compressive, pullout, and lateral

capacity compared to bored piles. This was attributed to the increase in diameter of the CFA piles compared to the bored piles owing to the high pressure used for placing the concrete in CFA construction, which led to higher lateral soil confinement. It was also found that piles constructed employing concrete mixture incorporating TOSW had the same geotechnical performance as those constructed utilizing conventional concrete mixture. Finally, the numerical analysis demonstrated that the effects of construction technique should be accounted for in order to properly simulate the CFA pile behaviour.

Keywords

Continuous flight auger piles, Bored piles, Axial, Lateral, Numerical analysis, Finite element, Oil sands waste, Construction sustainability, Waste reuse.

Co-Authorship Statement

The work summarized herein was carried out by the author under the supervision of Dr. M. H. El Naggar. That includes all the field and laboratory tests, numerical modelling, analysis of data, results interpretation, thesis writing and resulting publications. The following chapters will be submitted soon for possible publication in peer-reviewed journals.

Chapter 3: Implementation of treated drill cuttings solid waste in concrete mixtures

Chapter 4: Comparison of axial performance of bored and continuous flight augered large scale model piles in sand

Chapter 5: Lateral monotonic and cyclic behaviour of continuous flight auger and bored piles in sand

Chapter 6: Numerical investigation of performance of bored and continuous flight auger piles under monotonic loading

To my sons Malek, Mohamed, and Ibrahim

Acknowledgments

Firstly, I would like to express my sincere gratitude to my advisor Prof. M. Hesham El Naggar for the continuous support of my Ph.D study and related research, for his patience, motivation, and immense knowledge. His guidance helped me in all the time of research and writing of this thesis. I could not have imagined having a better advisor and mentor for my Ph.D. study.

All the love and gratitude to my adorable wife Nada. For the affection and care she provided, for believing in me when I had doubts and above all, for the fact that she was always there for me.

I also owe my deepest gratitude for my father Mohamed and my mother Nahla for their continuous support, encouragement, and unconditional love.

Special appreciation for all my friends especially Dr. Ahmed Soliman and Moustafa Aboutabikh who supported me and shared their valuable experience with me.

Table of Contents

Abstract.....	i
Co-Authorship Statement.....	iii
Acknowledgments.....	v
List of Tables	xi
List of Figures	xii
List of abbreviations and symbols	xix
Chapter 1.....	1
1 INTRODUCTION	1
1.1 Overview.....	1
1.2 Research objectives.....	2
1.3 Methodology.....	2
Chapter 2.....	4
2 LITERATURE REVIEW.....	4
2.1 Bored piles	4
2.2 Bored and Continuous flight auger piles	5
2.3 Axial loading.....	7
2.4 Lateral loading	9
2.5 Construction effect.....	10
2.6 Surface roughness	11
2.7 Sustainability in geotechnical applications.....	12
2.7.1 Road construction	12
2.7.2 Vehicle tires	13
2.7.3 Mine tailing waste.....	14
2.7.4 Oil sands waste	15

2.8	References.....	19
Chapter 3.....		26
3	IMPLEMENTATION OF TREATED OIL SANDS WASTE IN CONCRETE MIXTURES	26
3.1	Introduction.....	26
3.2	Experimental program	27
3.2.1	Materials	27
3.2.2	Testing procedures	28
3.3	Results and discussion	32
3.3.1	Fresh properties.....	32
3.3.2	Compressive strength.....	34
3.3.3	Splitting tensile strength	35
3.3.4	Flexural strength	38
3.3.5	Modulus of elasticity.....	40
3.3.6	Pullout strength.....	42
3.3.7	Freeze and thaw	44
3.3.8	Corrosion.....	46
3.3.9	Leaching.....	47
3.4	Conclusions.....	48
3.5	References.....	50
Chapter 4.....		53
4	COMPARISON OF AXIAL PERFORMANCE OF BORED AND CONTINUOUS FLIGHT AUGERED LARGE SCALE MODEL PILES IN SAND	53
4.1	Introduction.....	54
4.2	Experimental program	56
4.2.1	Materials	56

4.2.2	Piles description and installation	58
4.2.3	Piles instrumentation and testing setup.....	60
4.3	Results and discussion	64
4.3.1	Compression test.....	64
4.3.2	Pullout test	76
4.4	Pile surface.....	81
4.4.1	Piles profile	81
4.4.2	Compressive strength of in-situ concrete.....	83
4.4.3	Direct shear surface roughness	84
4.4.4	Roughness fractal dimension	87
4.5	Conclusions.....	91
4.6	References.....	93
Chapter 5	98
5	LATERAL MONOTONIC AND CYCLIC BEHAVIOUR OF CONTINUOUS FLIGHT AUGER AND BORED PILES IN SAND.....	98
5.1	Introduction.....	98
5.2	Experimental program	100
5.2.1	Soil preparation and investigation	100
5.2.2	Materials	101
5.2.3	Test piles and installation.....	101
5.3	Instrumentation and test setup	102
5.3.1	Lateral loading	102
5.3.2	Load test sequence and procedures.....	104
5.3.3	Pure bending test.....	107
5.4	Results and discussion	108
5.4.1	Monotonic loading	108

5.4.2	Cyclic loading	109
5.4.3	Moment curvature	124
5.4.4	Curvature and moment profiles curve fitting	124
5.4.5	Moment and deflection	126
5.4.6	Initial modulus of subgrade reaction.....	132
5.5	Conclusion	133
5.6	References.....	134
Chapter 6.....		137
6	NUMERICAL INVESTIGATION OF PERFORMANCE OF BORED AND CONTINUOUS FLIGHT AUGER PILES UNDER MONOTONIC LOADING	137
6.1	Introduction.....	137
6.2	Finite element model description.....	140
6.2.1	Soil model – Soil Hardening material model.....	143
6.2.2	Interface model	144
6.2.3	Test piles	145
6.2.4	Pile Model.....	146
6.2.5	Loading sequence.....	147
6.3	Model calibration	147
6.3.1	Compression loading	149
6.3.2	Pullout loading.....	152
6.3.3	Lateral loading	154
6.4	Verification	155
6.5	Parametric study.....	156
6.5.1	Effect of angle of internal friction	157
6.5.2	Effect of Pile diameter	167
6.5.3	Effect of pile length to diameter ratio	176

6.6 P-y curves..... 184

6.7 Conclusions..... 185

6.8 References..... 187

Chapter 7..... 189

7 SUMMARY, CONCLUSIONS, AND RECOMMENDATIONS..... 189

7.1 Summary and conclusions 189

7.2 Contribution 193

7.3 Recommendations..... 193

Curriculum Vitae 195

List of Tables

Table 3.1 Analysis of the TOSW	29
Table 3.2 Mixtures composition	30
Table 3.3 Measured metals in TOSW compared to different standards	47
Table 4.1 Piles configuration	59
Table 4.2 Piles ultimate load.....	65
Table 4.3 Soil-concrete interface properties	70
Table 4.4 Extracted cores compressive strength.....	84
Table 5.1 Piles configuration	102
Table 5.2 Variation of degradation parameter t for all cyclic tests.....	123
Table 6.1 Mesh sensitivity analysis	143
Table 6.2 pile properties of the different models	145
Table 6.3:Soil parameters before calibration	148
Table 6.4: Soil properties of the CFA pile model.....	151

List of Figures

Figure 3.1 TOSW and Cement Particle size distribution.....	30
Figure 3.2 Slump variation for all tested concrete over the investigated period	34
Figure 3.3 Compressive strength development for all tested mixtures over the investigated period	35
Figure 3.4 Splitting tensile strength development for all tested mixtures over the investigated period.	36
Figure 3.5 Correlation between the experimental data and predicted values for the splitting tensile strength	38
Figure 3.6 Flexural strength development for all tested mixtures over the investigated period	39
Figure 3.7 Correlation between the experimental data and predicted values for the flexural strength.....	40
Figure 3.8 Modulus of elasticity development for all tested mixtures over the investigated period	41
Figure 3.9 Correlation between the experimental data and predicted values for the modulus of elasticity	42
Figure 3.10 Pull-out strength development for all tested mixtures over the investigated period	43

Figure 3.11 Compressive strength and pull-out strength of the tested mixtures at age 28 days as percentage of the control mixture.....	44
Figure 3.12 Durability factor for different mixtures.....	45
Figure 3.13 Corrosion current through test time.....	46
Figure 4.1 Sand grain size distribution curve	57
Figure 4.2 Piles plan	59
Figure 4.3 Compression test setup.....	60
Figure 4.4 instrumentation distribution (a) along pile length (b) cross section	61
Figure 4.5 Direct shear (a) test configuration (b) sample slice.....	63
Figure 4.6 (a) pile coring process (b) Cylinder core specimen before and (c) after testing ...	63
Figure 4.7 Load-displacement curves for test piles	65
Figure 4.8 (a) Shaft resistance (b) End bearing	69
Figure 4.9 Shaft shear stresses variation with relative pile movement.....	70
Figure 4.10 Shaft load distribution along pile, (a) CFA C0, (b) CFA C1, (c) Bored C0, (d) Bored C1	72
Figure 4.11 Axial load distribution along pile, (a) CFA C0, (b) CFA C1, (c) Bored C0, (d) Bored C1	74
Figure 4.12 End bearing stress.....	77

Figure 4.13 Pullout load-displacement curves.....	78
Figure 4.14 Skin friction vs relative pile head movement	79
Figure 4.15 Load distribution along the piles, (a) CFA C0, (b) CFA C1, (c) Bored C0, (d) Bored C1	81
Figure 4.16 Pile profile, (a) pile extraction, (b) cross section.....	82
Figure 4.17 Pile sand cover intrusion (a) pile cross section, (b) bored pile, (c) CFA pile	83
Figure 4.18 Soil-concrete peak interface friction angle using direct shear test	85
Figure 4.19 Soil-concrete residual interface friction angle using direct shear test.....	85
Figure 4.20 Particles orientation on the piles surface, (a) CFA pile, (b) bored pile	86
Figure 4.21 Schematic of compass-walking method for determination of fractal dimension of a profile	88
Figure 4.22 Schematic of compass-walking method for determination of fractal dimension of a profile, (a) Bored pile, (b) CFA pile	89
Figure 4.23 Profile of pile surface used to calculate D_R for different profiles of a) bored pile (labeled by B1-B10), b) CFA pile (labeled by C1-C10).....	90
Figure 5.1 Piles configuration.....	103
Figure 5.2 Piles instrumentation distribution (a) along pile length (b) cross section	104

Figure 5.3 Lateral pile loading test patterns (a) Cyclic test (0-15 kN) (b) Cyclic test (10-25 kN) (c) Cyclic test (0-25 kN) (d) Monotonic test	106
Figure 5.4 Bending test setup on extracted pile	107
Figure 5.5 Lateral deflection curve of pile Bored C1 tested before cyclic loading	108
Figure 5.6 Lateral load deflection curves performed after the cyclic tests for piles CFA C1, Bored C0, and Bored C1	109
Figure 5.7 Lateral cyclic load displacement curve (0-15 kN range) (a) CFA C0 (b) CFA C1 (c) Bored C0 (d) Bored C1.....	112
Figure 5.8 Lateral cyclic load displacement curve (10-25 kN range) (a) CFA C0 (b) CFA C1 (c) Bored C0 (d) Bored C1.....	115
Figure 5.9 Lateral cyclic load displacement curve (0-25 kN range) (a) CFA C0 (b) CFA C1 (c) Bored C0 (d) Bored C1.....	118
Figure 5.10 Variation of lateral stiffness with loading cycles (a) 0 to 15 kN (b) 10 to 25 kN (c) 0 to 25 kN	120
Figure 5.11 Variation of degradation with loading cycles for amplitude (a) 0 to 15 kN (b) 10 to 25 kN (c) 0 to 25 kN	122
Figure 5.12 Piles moment-curvature.....	124
Figure 5.13 Monotonic test (a) deflection (b) moment.....	127
Figure 5.14 0-15 kN cyclic tests first and last cycle (a) deflection (b) moment.....	128

Figure 5.15 10-25 kN cyclic tests first and last cycle (a) deflection (b) moment..... 130

Figure 5.16 0-25 kN cyclic tests first and last cycle (a) deflection (b) moment..... 131

Figure 5.17 Experimental vs numerical load displacement 132

Figure 6.1 Boundaries sensitivity analysis for (a) bottom boundary (b) vertical boundary . 141

Figure 6.2 Pile model showing the different soil layers 142

Figure 6.3 Pile diagram..... 146

Figure 6.4: Comparison of measured and calculated compression load-settlement curves of bored pile 150

Figure 6.5:Plan view of the soil configuration around the CFA pile..... 150

Figure 6.6: CFA pile measured and calculated compression load deflection comparison ... 151

Figure 6.7: Comparison of measured and calculated pullout load-displacement curve for bored pile 152

Figure 6.8: CFA pile measured and calculated pullout load deflection comparison 153

Figure 6.9: Comparison of measured and calculated lateral load-deflection curve for bored pile..... 154

Figure 6.10: Comparison of CFA pile measured and calculated lateral load-deflection curves 155

Figure 6.11 Verification comparison between measured and calculated compression load deflection curves	156
Figure 6.12 Effect of friction angle on (a) shaft friction, (b) end bearing, and (c) total load of the bored pile, and (d) shaft friction, (e) end bearing, and (f) total load of the CFA pile.....	161
Figure 6.13 Effect of friction angle on pullout load displacement of (a) bored pile (b) CFA pile.....	163
Figure 6.14 Effect of friction angle on (a) load displacement, (b) pile deflection, and (c) moment distribution of bored pile, and (d) load displacement, (e) pile deflection, and (f) moment distribution of CFA pile	166
Figure 6.15 Effect of D on (a) shaft friction, (b) end bearing, and (c) total load of the bored pile, and (d) shaft friction, (e) end bearing, and (f) total load of the CFA.....	170
Figure 6.16 Effect of D on pullout load displacement of (a) bored pile (b) CFA pile	172
Figure 6.17 Effect of D on (a) load displacement, (b) pile deflection, and (c) moment distribution of bored pile, and (d) load displacement, (e) pile deflection, and (f) moment distribution of CFA pile	175
Figure 6.18 Effect of L/D on (a) shaft friction, (b) end bearing, and (c) total load of the bored pile, and (d) shaft friction, (e) end bearing, and (f) total load of the CFA pile.....	179
Figure 6.19 Effect of L/D on (a) load displacement, (b) pile deflection, and (c) moment distribution of bored pile, and (d) load displacement, (e) pile deflection, and (f) moment distribution of CFA pile	183

Figure 6.20 comparison between Bored, CFA and API p-y curves at several depths of the
piles..... 185

List of abbreviations and symbols

<i>ACIP</i>	Augured cast in-place
A_p	Actual average pile diameter
<i>C</i>	Cohesion
<i>CB</i>	Crushed bricks
<i>CFA</i>	Continuous flight auger pile
<i>D</i>	Pile diameter
D_{50}	Mean particle size
<i>DF</i>	Durability factor
D_R	Fractal dimension
<i>E</i>	Modulus of elasticity of concrete
E_{50}^{ref}	Secant stiffness from standard drained triaxial test
E_{oed}^{ref}	Tangent stiffness from primary odometer loading
E_p	Elastic modulus of the pile
E_{ur}^{ref}	Unloading/reloading stiffness
ε	Measured strain
f_c	Compressive strength
<i>FE</i>	Finite element
f_f	Flexural strength
f_{isp}	Splitting tensile strength
<i>HRWRA</i>	High range water reducer admixture
<i>HWP</i>	Hot water process
<i>IAE</i>	Integral absolute error
i_{corr}	Corrosion current density
k	Initial modulus of subgrade reaction
K_1	Lateral pile stiffness at the first cycle
K_L	Pile lateral stiffness
K_s	Coefficient of lateral earth pressure
<i>LVDT</i>	Linear variable displacement transducers
<i>N</i>	Number of freezing and thawing cycles
<i>OPC</i>	Ordinary portland cement

P	Relative dynamic modulus of elasticity
p	Contact pressure
P_{max}	Maximum lateral load
P_{min}	Minimum lateral load
P_s	Axial force at each strain gauge
RAP	Reclaimed asphalt pavement
RCA	Recycled concrete aggregates
RH	Relative humidity
R_p	Linear polarization resistance
t	Degradation parameter
$TMCC$	Thermo-mechanical cuttings cleaner
$TOSW$	Treated oil sand waste
y	Deflection
y_{max}	Maximum pile head deflection
γ	Unit weight
γ'	Effective unit weight
δ	Interface friction angle
ν	Poisson's ratio
τ_{avg}	Average mobilized shaft resistance
ϕ	Angle of internal friction
ϕ_p	Peak friction angle
ϕ_r	Residual friction angle
Ψ	Curvature
ψ	Dilation angle

Chapter 1

1 INTRODUCTION

1.1 Overview

Pile foundations are used to support structures by transferring their loads to deeper and stronger soil layers. They are considered as a favorable design option for sites with weak shallow soil layers or when supporting heavy structures. The complexity of the projects and the demands of their loading conditions have increased the need for more understanding of foundation systems and their behaviour.

Bored and CFA piles are constructed employing different construction techniques but both are classified as non-displacement piles. The behaviour of bored and CFA piles has been investigated by several authors (Albuquerque et al. 2005; Albuquerque et al. 2011; Farrell and Lawler 2008; Gavin et al. 2013; Gavin 2009; Ismael 2001). CFA piles used in the United Kingdom since 1966. Farrell and Lawler (2008) have reported that the ultimate capacity of the CFA piles was about double that of the bored piles, while Albuquerque et al. (2005) reported 40% increase in CFA pile capacity over that of bored piles. On the other hand, (2011) reported similar behaviour for CFA and bored piles. Therefore, a better understanding of the behaviour of CFA piles and their design parameters is required.

In recent years, green concrete has drawn serious attention of many researchers. Generally, green concrete mixtures incorporate waste materials as a partial or total replacement for cement (e.g. alkaline activated concrete (Das et al. 2014)) and/or aggregates. However, limited studies have investigated the direct role of replacing fine aggregate with similar

waste materials on concrete properties development. Implementing such waste materials as a partial replacement for the natural sand in concrete mixtures, without sacrificing their strength and durability performance, will lead to both economic and environmental benefits. Therefore, this study also aims at reducing the environmental and ecological impacts of concrete through incorporating treated oil sands waste as partial replacement of its fine aggregate.

1.2 Research objectives

In order to have better understanding of the behaviour of both bored and CFA piles and feasibility of reusing Treated Oil Sands Waste (TOSW), the following objectives were set for this study:

- Investigating the feasibility of reusing TOSW in the construction of CFA piles and its effect on different material or geotechnical behaviour.
- Investigate the behaviour of CFA and bored piles, and the factors that affect their distinctive behaviour
- To assess the behaviour of bored and CFA piles under axial compressive, uplift and lateral loading.

1.3 Methodology

To fulfill these objectives, comprehensive investigation was performed consisting of the following stages:

- ***Literature review:*** Literature review was conducted on piles subjected to different loading conditions and built with different construction methods to have better knowledge of the existing systems.
- ***Material testing:*** Material testing of concrete mixtures incorporating TOSW to investigate the effect of waste on the concrete mixtures properties. Hardened, fresh, and durability of concrete mixtures were investigated.
- ***Large model testing:*** six instrumented large-scale model piles were installed and tested. The tests conducted included monotonic compressive, and uplift, and monotonic and cyclic lateral loading. The test results were presented in load-displacement curves as well as load and moment distribution along the pile shaft. Piles were exhumed after testing to be inspected and to test the pile surface properties and the effect of the construction method.
- ***Numerical simulation:*** Three-dimensional finite element simulations were conducted on both bored and CFA piles using the commercial software package Plaxis. Calibration and verification against experimental data were performed. The effect of the angle of internal friction as well as the pile diameter on the response of the pile under different loading conditions were investigated.

Chapter 2

2 LITERATURE REVIEW

Piles can be categorized according to their methods of installation into driven or bored. However, this traditional way of categorizing may not be adequate for many forms of piles used now. Alternatively, the piles may be more suitably categorized into displacement and non-displacement piles. However, some piles are constructed with combination of both methods; therefore, their behaviour and performance need some clarification.

Displacement piles are installed by pushing or hammering the pile into the soil which leads to radial movement of the soil as it advances in the soil. Soil may also move vertically with the pile movement. In granular soils, particles may become compacted, but in clay, soil may heave with immediate volume change (Fleming 2009).

Non-displacement piles are constructed by first excavating a hole into the ground, which reduces the soil lateral stresses that may be partly reinstated by pumping concrete under pressure in the second stage of pile construction. Therefore, problems resulting from soil displacement as heave are eliminated, but the benefits of soil compaction in granular soil are then lost. In addition, there are concerns associated with soil spoils disposal, especially for contaminated soil (Fleming 1995).

2.1 Bored piles

Bored piles are cast-in-place concrete piles that are constructed in holes stabilized to facilitate reinforcement installation and concrete placement. Bored piles are distinguished

from other pile types by their large diameter that allow them to be used individually, e.g., as in bridge pier applications. The Diameter of bored piles typically range from 0.8 to 3.5 m, while the depth commonly used in transportation projects can reach up to 60 m. Bored piles can be constructed in a variety of soil and rocks, where its most efficient performance can be utilized when strong bearing layer exists. Large diameters can eliminate the usage of pile cap to distribute the load from the superstructure to the pile foundation, which is beneficial in tight spaces when foundation is constructed near an existing building. This is attributed to its high flexural capacity due to the large diameter.

2.2 Bored and Continuous flight auger piles

Continuous flight auger (CFA) is a type of pile that combines the properties of the displacement and no-displacement piles. It is bored the same way as the bored piles but without casing or slurry. During concreting, pressure is applied which results in radial displacement that improves the surrounding soil properties. So, the construction method of CFA pile makes it somewhere in between driven and bored piles. This type of pile was originally introduced in the 1950s (Van Impe 2004). However, it was not used widely until the 1980s (Fleming 1995). The technology advancement increased the potential of constructing CFA piles. CFA is constructed by drilling a hole using an auger to the final depth in one continuous step. While excavating into the ground, the auger flights filled with soil provide enough lateral support for the ground around the pile. Similarly, while withdrawing the auger from the ground, concrete/grout pumping starts through the hollow center of the auger. Synchronized auger withdrawal and concrete/grout pumping provide

support to the soil around the hole. After auger withdrawal and concrete pumping are done, reinforcement steel cage is placed inside the hole filled with fresh concrete/grout.

The diameter of the CFA piles is usually between 0.3 and 0.9 m and a length of up to 30 m. However, the trend in practice is towards using smaller pile diameters (0.3 to 0.6 m). In recent years, larger diameters with range of 0.6 to 0.9 m are being used in Europe. The steel reinforcement is usually installed in the top 10 to 15 m of the CFA pile. This is because it is difficult to push the steel reinforcement into the concrete, and bending stresses transferred below this level are usually low.

A CFA pile does not require a casing or slurry to support the hole walls during its construction. Moreover, the construction time of the CFA pile is less than that of the bored pile as the CFA is excavated in one continuous process, unlike the bored piles which requires lowering the drilling bit multiple times to finish excavation. On the other hand, the power and torque needed to excavate the CFA piles are higher than that required for the bored pile. As a result, CFA piles are limited to smaller diameters and lengths. Moreover, it is limited to soil and very weak rocks, while bored piles can be constructed with larger diameter and depth, and in harder materials.

Both bored and CFA piles require more refined quality assurance methods in order to ascertain the pile structural integrity. The soil spoils resulted from the pile excavation can be a major concern if the site was contaminated or has limited space to handle the excavated materials.

2.3 Axial loading

The axial behaviour of bored and CFA piles in compression has been investigated by several researchers (Albuquerque et al. 2005; Albuquerque et al. 2011; Farrell and Lawler 2008; Gavin et al. 2013; Gavin 2009; Gavin et al. 2009; Ismael 2001). The performance of CFA piles was found to be different from that of the bored piles. Mandolini (2002) conducted full scale tests on three CFA piles and concluded that the CFA piles have intermediate behaviour between bored and driven piles, and their performance is strongly influenced by the installation process. Farrell and Lawler (2008) investigated the CFA pile shaft resistance and found it to be similar to the driven pile. Moreover, they have reported that the ultimate capacity of the CFA piles was about double that of the bored piles, while Albuquerque et al.(2005) reported 40% increase in CFA pile capacity over that of bored piles. The difference between the results of both studies can be attributed to the difference in experience of the drilling rig operator. On the other hand, Albuquerque et al. (2011) reported similar behaviour for CFA and bored piles. Therefore, a better understanding of the behaviour of CFA piles and their design parameters is required.

Gavin et al. (2009) investigated the shaft capacity of CFA piles in sand. Two full scale CFA piles with different diameters and lengths were tested in compression. Their results showed that the load supported by the shaft friction ranged from 71% to 78% and it was suggested that the interface dilation was not significant.

The relationship between axial load, movement magnitude and rate of movement on CFA piles constructed in soft clay was investigated by King et al. (2000). Twelve full-scale instrumented CFA piles were constructed in soft silty clay and were tested in compression.

The loading scheme involved a) short duration with constant rate (< 6 hours), b) short duration with maintained load (45 to 55 hours), and c) long duration (> 300 hours). The results showed that the peak shaft resistance (highest resistance occurs due to soil peak shear strength) was found to be dependent on the rate of movement, while the ultimate shaft resistance (post peak resistance as a result of residual soil shear strength) was dependent only on the magnitude of movement.

Seward et al. (2013) investigated the remolded zone around the CFA piles constructed in Mercia mudstone. Four piles were installed with 5.5 m depth and 0.35 m diameter. The effect of water and piles over turning during installation were the two variables applied to study their effect on the remolded zone around the piles. It was found that the remolded soil had a distinct boundary with the surrounding soil. It was also noted that the thickness of this zone ranged from zero to 55 mm. The thickness of the remolded zone in the dry constructed piles and without over rotation (i.e., stopping the auger rotation immediately after reaching the required depth) was 12 mm.

The behaviour of bored piles under axial loading in cemented sands was investigated by Ismael (2001). Full scale load tests were conducted on four piles: two were tested in compression; and two were tested in pullout. The results showed that 70% of the total load was transferred through the skin friction and the axial load distribution was almost linear. Moreover, it was observed that shaft friction in compression and uplift is very similar.

Kenny et al. (1997) studied the effect of CFA pile auguring on the change in relative density of the surrounding soil. Small augers with different geometry were used in laboratory test with different auger penetration rate and rotation speed. It was concluded that the

disturbance in the surrounding soil is greatly affected by the rate of penetration and rotation speed. Moreover, it was found that the potential to densify the soil exists when penetrating at a rate greater than the optimum, using auger with steeper flight, and larger stem diameter.

2.4 Lateral loading

Bored and CFA piles are often subjected to static and cyclic lateral loads due to different hazards such as vessel impacts, traffic, waves, wind, and earthquakes that could lead to significant accumulated permanent pile displacements. In current design practice, similar procedure is being utilized to evaluate the lateral response of bored and CFA piles ignoring effect of installation method on the pile's behaviour under lateral load (Brown et al. 2007). This is mainly due to limited number of published experimental results especially for CFA piles under lateral cyclic loading.

Compared to the extensive experimental data on the lateral behaviour of bored piles subjected to static and cyclic loads (Ismael 2009; Little and Briaud 1988; Stewart et al. 2007), relatively few published results are available for the cyclic and even static response of laterally loaded CFA piles in sand. O'Neill et al. (2000) performed cyclic lateral load tests on a series of augered, cast-in-place piles in over-consolidated clay. They found that a p - y model, which relates the soil reaction to the pile deflection, modified from the Welch-Reese model developed in similar soils for drilled shafts, would give excellent predictions of pile performance. Frizzi and Meyer (2000) compared theoretical analysis output with experimental results obtained from six lateral load tests of auger cast piles in south Florida. Based on the limited published data on the lateral response of CFA piles, Brown et al. (2007) suggested that CFA piles behave essentially like drilled shafts if the differences

between the pile material properties are accounted for in the analysis. Recently, Hamid (2014) carried out three lateral load tests performed on auger cast piles and compared the measured lateral response with those predicted using the “ p - y ” method. It was found that reliable prediction of lateral displacement depends on the accurate estimation of pile’s modulus of elasticity. There is no doubt that the effect of pile properties is significant in the lateral load-deflection analysis of piles, however, the installation method has also a considerable influence on the mechanical characteristics of the surrounding soil (Fleming 2009). Therefore, it is not reasonable to utilize similar model, for example same load-transfer curves in the p - y approach, for the analysis of bored and CFA piles subjected to lateral loading.

2.5 Construction effect

Both the CFA and bored piles are classified as non-displacement piles, even though two different installation techniques are used for their construction. The construction of bored piles consists of boring a hole into the ground, installing rebar reinforcement and filling the hole with grout or concrete to construct the pile. In CFA pile construction, the pile is drilled to the final depth in one continuous process, simultaneous withdrawal and pumping of concrete/grout mix provides continuous support of the hole, and then steel reinforcement is immediately placed into the hole. The main difference in the construction method is related to pressurized concrete used for constructing CFA piles that can increase its volume by about 20% (Brown et al. 2007). Hence, the soil around the pile experiences densification. It was also found that the interface friction angle between the pile surface and the soil could be equal to soil’s internal friction angle, and the coefficient of lateral

earth pressure, K_s , could be equal to 0.9 for CFA piles compared with 0.7 for bored piles (Fleming 2009).

CFA pile has considerable advantages over the conventional bored pile, especially in water-bearing and unstable soils as temporary casing is not needed; however, its integrity and load-bearing capacity highly depends on strict control of workmanship compared to other in-situ types of pile (Tomlinson and Woodward 2014).

2.6 Surface roughness

The surface roughness of a pile is one of the key parameters affecting the shear resistance of the soil–pile interface (Zhu et al. 2012). It was demonstrated that the roughness of the pile surface has a dominant effect on the extent of the soil zone along the pile shaft controlling the mobilization of shaft resistance (Fioravante 2002). A thicker shear band forms when the sliding interface is rough due to the increase in interlocking between soil and pile surface (Uesugi et al. 1988). However, in-situ roughness of pile surfaces is always unpredictable due to drilling and underground casting conditions (Chen et al. 2015).

The roughness of pile surfaces is commonly estimated using factors based on soil type and pile material. However, these factors vary depending on different pile construction methods. The Fractal dimension technique offers an opportunity to quantify the roughness of the pile shaft by performing surface image processing. In this approach, the fractal dimension (D_R) is the amount of variation in a curve from a line; it can vary from 1 for smooth surface up to 2 for very rough surface profile (Mandelbrot 1985). In the present study, the soil-pile interface of bored and CFA piles is quantitatively characterized using

fractal dimension as a measure of surface roughness. The roughness quantification will aid in understanding the shear behaviour of soil-pile interface and evaluating shear strength for bored and CFA piles.

2.7 Sustainability in geotechnical applications

Recycling/reusing of the massive amounts of waste produced in many industrial applications is a major concern all over the world. The high cost associated with waste disposal and environmental and health concerns associated with such processes presents a pressing need to find a feasible solution. In the next sections, the reuse of construction/demolition waste, vehicle tires, and mine tailings wastes in geotechnical applications will be discussed.

2.7.1 Road construction

Road construction is one of the main applications that can benefit from construction/demolition waste. It can be used as a recycled aggregate to increase the pavement capacity. Irali et al. (2013) investigated the capability of using recycled concrete aggregates (RCA) on the performance of the subgrade. Four pavement sections were constructed and they were monitored for five years to study the effect of different weather conditions on the performance of the pavement. It was found that the pavement sections constructed with RCA showed comparable performance with that constructed with natural aggregates.

The effect of using crushed bricks (CB) on the pavement sub-base performance was investigated by Arulrajah et al. (2011). It was reported that its performance was good at

low moisture content. But, it was recommended to mix the CB with high quality recycled aggregates to enhance the overall performance. By mixing CB and RCA with 25% of crushed excavated rocks, Arulrajah et al. (2012) found that this combination satisfies the sub-base material requirements.

The applicability of using reclaimed asphalt pavement (RAP) stabilized with cement to enhance the performance of sub-grade was investigated by Taha et al. (2002). It was found that the pavement sub-grade strength and stiffness satisfied the material requirements by using the stabilized RAP.

2.7.2 Vehicle tires

Tire rubber is a major source of waste worldwide. Every year 13.5 million tons of scrap tires are disposed globally (Jan et al. 2015). Therefore, the need to reuse this kind of waste can have beneficial effects environmentally and economically. The reuse of shredded tire wires was investigated by Bosscher et al. (1992) to be used as a reinforcement material for embankments. Embankments with and without scrap tires were constructed and the performance and behaviour was evaluated. It was found that the embankment constructed with the shredded tire wire exhibited higher settlement, but its performance was equivalent to that constructed with sand. These results were in agreement with the findings of Edil and Bosscher (1994). They found that the soil-tire shred mixture exhibited high plastic compression at low pressure.

The effect of using shredded waste tires on the shear strength of sand was investigated by Foose et al. (1996). Effect of normal stress, shred content, unit weight, shred length, and shred orientation were studied. It was found that the mixture unit weight, normal stress,

and shred content controlled the shear strength. The angle of internal friction of the sand-tire mixture was 67° compared to the pure sand which was 34° , at the same unit weight. A similar study was done on clay to investigate the effect scrap tire wire on clay behaviour (Akbulut et al. 2007). Different length and content of scrap tires were used to check their effect on the unconfined compressive strength, cohesion, and the angle of internal friction. The results showed that both fibers length and content affected the soil strength parameters. Moreover, it was found that the unconfined compressive strength increased by increasing the tire content up to 2% then it decreased.

2.7.3 Mine tailing waste

Tuncan et al. (2000) investigated the effect of using petroleum contaminated drilling waste as a sub-base material. The petroleum waste was stabilized by adding pozzolanic fly ash, lime, and cement. Their results showed that the new mixture has better properties than that normally used as sub-base material. Similarly, Hassan et al. (2005) investigated the use of petroleum contaminated soil in highway construction. They studied the effect of using new soil with cement and crushed stones mixture as a replacement for the fine aggregates in the asphalt concrete mixtures. Leaching was investigated using the toxicity characteristic leaching procedure and results were found to be non-hazardous. Results showed that the unconfined compressive strength remained constant for cement-contaminated sand mixture with percentage up to 5%. Hassan et al. (2008) partially replaced the fine aggregates of the asphalt concrete mixture with oil-contaminated sand. They studied the effect of the replacement on the asphalt permeability and leaching. It was found that the asphalt concrete mixture permeability decreased by increasing the replacement percent up to 30%.

Aboutabikh et al. (2016) investigated the effect of incorporating treated oil sand waste (TOSW) in micropiles grout mixture as a partial replacement of cement. TOSW replaced cement with percentage up to 50% and its effects on fresh and hardened properties of the grout were investigated. The results showed that by increasing the TOSW percent, the flowability increased but the compressive strength decreased. However, all the grout mixtures satisfied the required compressive strength specified by the Federal Highway Administration for micropiles applications.

2.7.4 Oil sands waste

Alberta's crude oil reserve is considered the second largest in the world after Saudi Arabia (ERCB 2010). According to Alberta's Energy Resources Conservation Board, there are around 400 billion m³ of bitumen-in-place; 27 billion m³ of them can be economically recovered.

Generally, oil sands deposits exist within a depth of 30 to 90 m from the ground surface. Oil sands typically contain 8 to 14 % (by weight) bitumen and 3 to 5 % (by weight) water, and the rest are mineral solids (i.e. sand, silt, and clay) (Gosselin et al. 2010). Two common methods are applied to extract bitumen from oil sands: in-situ mining and open pit mining. In-situ mining is suitable for bitumen deposits deeper than 70 m. Bitumen has a very high viscosity which decreases at high temperatures. Therefore, bitumen is thermally treated to reduce its viscosity to a value similar to water using steam with temperature above 250 °C pumped to the ground. This makes the pumping bitumen from the ground easier.

Open pit mining is applicable for formations with depth up to 70 m. Oil sands are excavated and then the bitumen rich sands transported to crushers where oil sands ore is broken to

smaller lumps. After crushing, the ore is transported through conveyor into hot water to make slurry with temperature between 45 °C to 60 °C. By pumping air pebbles into the slurry, the bitumen droplets attaches to the air pebbles and float on the surface, while the solids settle to the bottom and then separated and discharged into large ponds (Gosselin et al. 2010). This process is called hot water process. Hot water process (HWP), developed in early 1960s by Dr. Karl Clark, is the most widely used bitumen extraction process. HWP involves using hot water, steam, caustic soda (NaOH), and other chemical compounds to separate the bitumen from the oil sand. The resulting products from this process are bitumen and tailings (i.e. a warm aqueous suspension of sand, silt, clay, and residual bitumen) (Fine Tailings Fundamentals Consortium 1995). Tailings are pumped into large tailing ponds. Once the tailings pumped, the coarse sand settles to form the dykes of the ponds while the fines and the residual bitumen are carried as slurry. The fines in the slurry then begin to settle with time. The water containing bitumen remaining at the surface is recycled, and the bitumen is recovered (Fine Tailings Fundamentals Consortium 1995).

Current inventories of the volume of tailings indicate a total volume of 720 million-m³ covering a total area of 130 km² (ERCB 2009). This volume continues to increase with the expansion of oil sands extraction process. However, site investigations conducted by (Mackinnon et al. 2005) demonstrated that the contaminated tailing water reached the ground water at a point a few kilometers away from the pond. Hence, there is an urgent need to find alternative ways for disposing or reusing the oil sands tailings.

Recently, a Thermomechanical Cuttings Cleaner (TMCC) technology was utilized to recover and reduce the hydrocarbons content in the oil sands tailings. TMCC is based on the idea of thermal desorption. Tailings are heated to a temperature high enough to

evaporate hydrocarbons and water. This high temperature is generated by friction created between particles in the TMCC. The driving unit utilizes a set of mounted hammers in motion inside a barrel shaped process unit (also referred to as the mill).

The tailings particles are forced towards the inner walls of the process unit by the rotating arms, converting the kinetic energy produced from the hammer arms to thermal energy. Evaporated oil and water are taken out from the heating chamber then condensed to their liquid state. The clean solids discharged from a valve in the bottom of the unit, and then new tailings are pumped in. The solids hydrocarbons content is usually less than 1% by weight (1,000 mg/kg) and the solids leaves the chamber at 350°C. After cooling, these treated solids discharged from the TMCC are referred to as Treated Oil Sands Waste (TOSW). The by-product of TMCC (i.e. the remaining solids) is very fine quartz powder. Hence, it has a potential to be used as a filler material for many construction applications.

Addition of filler to cementitious materials can modify the hydration kinetics of cement (Lawrence et al. 2003). Generally, filler materials composition can chemically interact with the hydration reactions of cement (i.e. accelerate or retard) by altering ionic species equilibrium in its pore solution. The degree of fineness for filler materials can affect cement hydration through modifying the particle size distribution and/or providing nucleation sites for hydrates.

In recent years, green concrete mixtures that incorporate waste materials as partial or total replacements for cement (e.g. alkaline activated concrete (Das et al. 2014)) and/or aggregates have become popular. However, limited studies investigated the direct role of replacing fine aggregate with waste materials on concrete properties development.

Implementing such waste materials as partial replacement of sand in concrete mixtures, without sacrificing their strength and durability performance, will lead to both economic and environmental benefits.

Concrete mixtures for bored and CFA piles consist of cement, water, sand, gravel and additives such as superplasticizers to enhance pumpability and workability (Brown et al. 2007; Brown et al. 2010). Concrete forms the body of the pile and has the responsibility to i) carry the structural load, ii) transfer the load to the reinforcement, the adjacent soil and the bearing soil, and iii) protect the steel reinforcement from corrosion. One of the main components of concrete is sand, which is a non-renewable natural resource. The rapid increase in construction activity has increased the demand on sand and consequently its cost, and in some cases lead to acute shortage in its supply such as in India and Malaysia (Balamurugan and Perumal 2013; Raman et al. 2007). In addition, the construction industry is intensifying efforts to develop sustainable construction practices while remaining economically efficient. Therefore, research efforts are focused recently on identifying opportunities to use mining waste in construction as replacement for natural sand.

2.8 References

- Aboutabikh, M., Soliman, A.M., and El Naggar, M.H. 2016. Properties of cementitious material incorporating treated oil sands drill cuttings waste. *Construction and Building Materials* **111**: 751-757. doi: <http://dx.doi.org/10.1016/j.conbuildmat.2016.02.163>.
- Akbulut, S., Arasan, S., and Kalkan, E. 2007. Modification of clayey soils using scrap tire rubber and synthetic fibers. *Applied Clay Science* **38**(1–2): 23-32. doi: <http://doi.org/10.1016/j.clay.2007.02.001>.
- Albuquerque, P., Carvalho, D., and Massad, F. 2005. Bored, continuous flight auger and omega instrumented piles: Behaviour under compression. *In Proceedings of The International Conference on Soil Mechanics and Geotechnical Engineering*. Osaka, Japan. p. 2075-2078.
- Albuquerque, P., da Fonseca, A.V., Santos, J., Esteves, E.C., Massad, F., and Carvalho, D. 2011. Effects of the construction method on pile performance: evaluation by instrumentation-part 2: experimental site at the Faculty of Engineering of the University of Porto.
- Arulrajah, A., Piratheepan, J., Aatheesan, T., and Bo, M.W. 2011. Geotechnical Properties of Recycled Crushed Brick in Pavement Applications. *Journal of Materials in Civil Engineering* **23**(10): 1444-1452. doi: [doi:10.1061/\(ASCE\)MT.1943-5533.0000319](https://doi.org/10.1061/(ASCE)MT.1943-5533.0000319).
- Arulrajah, A., Piratheepan, J., Bo, M.W., and Sivakugan, N. 2012. Geotechnical characteristics of recycled crushed brick blends for pavement sub-base applications. *Canadian Geotechnical Journal* **49**(7): 796-811. doi: [10.1139/T2012-041](https://doi.org/10.1139/T2012-041).
- Balamurugan, G., and Perumal, P. 2013. Use of quarry dust to replace sand in concrete—An experimental study. *International Journal of Scientific and Research Publications* **3**(12).

- Bosscher, P.J., Edil, T.B., and Eldin, N.N. 1992. Construction and performance of a shredded waste tire test embankment. *Transportation research record.*(1345).
- Bowles, J.E. 1996. *Foundation analysis and design*. McGraw-Hill, New York.
- Brown, D.A., Dapp, S.D., Thompson, W.R., and Lazarte, C.A. 2007. *Design and Construction of Continuous Flight Auger (CFA) Piles*. Federal Highway Administration. Technical Report.
- Brown, D.A., Turner, J.P., and Castelli, R.J. 2010. *Drilled shafts: Construction procedures and LRFD design methods*. US Department of Transportation, Federal Highway Administration.
- Chen, X.B., Zhang, J.S., Xiao, Y.J., and Li, J. 2015. Effect of roughness on shear behaviour of red clay - concrete interface in large-scale direct shear tests. *Canadian Geotechnical Journal* **52**(8): 1122-1135. doi: 10.1139/cgj-2014-0399.
- Das, S.K., Mohapatra, A.K., and Rath, A. 2014. Geo-polymer Concrete—Green Concrete for the Future—A Review. *International Journal of Civil Engineering Research*. **5**(1): 21-28.
- Edil, T., and Bosscher, P. 1994. *Engineering Properties of Tire Chips and Soil Mixtures*.
- ERCB. 2009. *Tailings Performance Criteria and Requirements for Oil Sands Mining Schemes*. Energy Resources Conservation Board.
- ERCB. 2010. *Alberta's Energy Reserves 2009 and Supply/Demand Outlook 2010-2019*. Energy Resources Conservation Board.
- Farrell, E.R., and Lawler, M.L. 2008. CFA pile behaviour in very stiff lodgement till. *Proceedings of the Institution of Civil Engineers-Geotechnical Engineering* **161**(1): 49-57.
- Fine Tailings Fundamentals Consortium, A. 1995. *Advances in oil Sands Tailings Research*. Department of Energy, Oil Sands and Research Division.

- Fioravante, V. 2002. On The Shaft Friction Modelling of Non-Displacement Piles in Sand Soils and Foundations **42**(2): 23-33. doi: 10.3208/sandf.42.2_23.
- Fleming, W.G.K. 1995. The Understanding of Continuous Flight Auger Piling, Its Monitoring and Control. (Includes appendix). Proceedings of the Institution of Civil Engineers - Geotechnical Engineering **113**(3): 157-165. doi: doi:10.1680/igeng.1995.27811.
- Fleming, W.G.K. 2009. Piling engineering. Taylor & Francis, New York;London;.
- Foose, G.J., Benson, C.H., and Bosscher, P.J. 1996. Sand Reinforced with Shredded Waste Tires. Journal of Geotechnical Engineering **122**(9): 760-767. doi: doi:10.1061/(ASCE)0733-9410(1996)122:9(760).
- Frizzi, R.P., and Meyer, M.E. 2000. Augercast Piles: South Florida Experience. *In* New Technological and Design Developments in Deep Foundations. pp. 382-396.
- Gavin, K., Cadogan, D., Tolooiyan, A., and Casey, P. 2013. The base resistance of non-displacement piles in sand. Part I: field tests. Proceedings of the Institution of Civil Engineers-Geotechnical Engineering **166**(6): 540-548.
- Gavin, K.G. 2009. Shaft capacity of continuous flight auger piles in sand. Journal of geotechnical and geoenvironmental engineering **135**(6): 790-798.
- Gavin, K.G., Cadogan, D., and Casey, P. 2009. Shaft Capacity of Continuous Flight Auger Piles in Sand. Journal of Geotechnical and Geoenvironmental Engineering **135**(6): 790-798. doi: doi:10.1061/(ASCE)GT.1943-5606.0000073.
- Gosselin, P., Hruday, S.E., Naeth, M.A., Plourde, A., Therrien, R., Kraak, G.V.D., and Xu, Z. 2010. Environmental and Health Impacts of Canada's Oil Sands Industry. The Royal Society of Canada.

- Hamid, T.B. 2014. Analysis of Lateral Load Tests on Auger Cast Piles. *In Tunneling and Underground Construction*.
- Hassan, H.F., Al Rawas, A., Hago, A.W., Jamrah, A., Al-Futaisi, A., and Al-Sabqi, T. 2008. Investigation of permeability and leaching of hot mix asphalt concrete containing oil-contaminated soils. *Construction and Building Materials* **22**(6): 1239-1246. doi: <http://doi.org/10.1016/j.conbuildmat.2007.01.017>.
- Hassan, H.F., Taha, R., Al Rawas, A., Al Shandoudi, B., Al Gheithi, K., and Al Barami, A.M. 2005. Potential uses of petroleum-contaminated soil in highway construction. *Construction and Building Materials* **19**(8): 646-652. doi: <http://doi.org/10.1016/j.conbuildmat.2005.01.001>.
- Irali, F., KIVI, A., SMITH, J., TIGHE, S., and Sangiorgi, C. 2013. Recycled Concrete Aggregate in Concrete Pavements: A Five Year Study on Its Effect on Pavement Performance. *In 2013 Conference and Exhibition of The Transportation Association of Canada-Transportation: Better-Fater-Safer*.
- Ismael, N.F. 2001. Axial Load Tests on Bored Piles and Pile Groups in Cemented Sands. *Journal of Geotechnical and Geoenvironmental Engineering* **127**(9): 766-773. doi: [doi:10.1061/\(ASCE\)1090-0241\(2001\)127:9\(766\)](https://doi.org/10.1061/(ASCE)1090-0241(2001)127:9(766)).
- Ismael, N.F. 2009. Behaviour of step tapered bored piles in sand under static lateral loading. *Journal of geotechnical and geoenvironmental engineering* **136**(5): 669-676.
- Jan, U., Sonthwal, V.K., Duggal, A.K., Rattan, E.J.S., and Irfan, M. 2015. Soil stabilization using shredded rubber tyre. *International Journal of Engineering and Innovative Technology (IJEIT)* **2**(4).

- Kenny, M., Canakci, H., and Andrawes, K. 1997. Densification of granular soils during CFA pile augering. *Ground improvement geosystems: densification and reinforcement*, Davies & Schlosser (eds.), Thomas Telford, London: 134-140.
- King, G.J.W., Dickin, E.A., Lyndon, A., and Wei, M.J. 2000. The Influence of Rate of Loading on the Behaviour of Continuous-Flight-Auger Bored Piles in Soft Clay. *Geotechnical & Geological Engineering* **18**(2): 139-153. doi: 10.1023/a:1008996419840.
- Lawrence, P., Cyr, M., and Ringot, E. 2003. Mineral admixtures in mortars: Effect of inert materials on short-term hydration. *Cement and Concrete Research* **33**(12): 1939-1947. doi: 10.1016/S0008-8846(03)00183-2.
- Little, R., and Briaud, J. 1988. Cyclic Horizontal Load Tests on 6 Piles in Sands at Houston Ship Channel. Research Report 5640 to USAE Waterways Experiment Station, Civil Engineering, Texas A&M University.
- Mackinnon, M., Kampala, G., Marsh, B., Fedorak, P., and Guigard, S. 2005. Indicators for assessing transport of oil sands process-affected waters. *In*. IAHS Press. pp. 71-80.
- Mandelbrot, B.B. 1985. Self-Affine Fractals and Fractal Dimension. *Physica Scripta* **32**(4): 257-260. doi: 10.1088/0031-8949/32/4/001.
- Mandolini, A. 2002. Full scale loading tests on instrumented CFA piles. *Geotechnical Special Publication*(116): 1088-1097.
- O'Neill, M.W., Vipulanandan, C., and Hassan, K. 2000. Modeling of Laterally Loaded ACIP Piles in Overconsolidated Clay. *In* *New Technological and Design Developments in Deep Foundations*. pp. 471-485.

- Raman, S., Safiuddin, M., and Zain, M. 2007. Non-destructive evaluation of flowing concretes incorporating quarry waste. *Asian journal of civil engineering (Building and Housing)* **8**(6): 597-614.
- Seward, L.J., Stallebrass, S.E., and Skipper, J. 2013. Remoulding of the Mercia Mudstone Group around CFA pile shafts. *Quarterly Journal of Engineering Geology and Hydrogeology* **46**(1): 41-51. doi: 10.1144/qjegh2011-053.
- Stewart, J.P., Taciroglu, E., Wallace, J.W., Ahlberg, E.R., Lemnitzer, A., Rha, C., Tehrani, P., Keowen, S., Nigbor, R.L., and Salamanca, A. 2007. Full scale cyclic testing of foundation support systems for highway bridges. Part II: Abutment backwalls. UCLA Structural and Geotechnical Engineering Laboratory(UCLA-SGEL 2007/02).
- Taha, R., Al-Harthy, A., Al-Shamsi, K., and Al-Zubeidi, M. 2002. Cement Stabilization of Reclaimed Asphalt Pavement Aggregate for Road Bases and Subbases. *Journal of Materials in Civil Engineering* **14**(3): 239-245. doi: doi:10.1061/(ASCE)0899-1561(2002)14:3(239).
- Tomlinson, M., and Woodward, J. 2014. *Pile design and construction practice*. CRC Press.
- Tuncan, A., Tuncan, M., and Koyuncu, H. 2000. Use of petroleum-contaminated drilling wastes as sub-base material for road construction. *Waste Management & Research* **18**(5): 489-505. doi: doi:10.1177/0734242X0001800511.
- Uesugi, M., Kishida, H., and Tsubakihara, Y. 1988. Behaviour of Sand Particles in Sand-Steel Friction. *Soils and Foundations* **28**(1): 107-118. doi: 10.3208/sandf1972.28.107.
- Van Impe, W. 2004. Two decades of full scale research on screw piles: An overview. Published by The Laboratory of Soil Mechanics, Ghent University, Belgium.

Zhu, H.H., Ho, A.N.L., Yin, J.H., Sun, H.W., Pei, H.F., and Hong, C.Y. 2012. An optical fibre monitoring system for evaluating the performance of a soil nailed slope. *Smart Structures and Systems* **9**(5): 393-410.

Chapter 3

3 IMPLEMENTATION OF TREATED OIL SANDS WASTE IN CONCRETE MIXTURES

This chapter presents an attempt to increase concrete sustainability through reusing treated oil sands waste (TOSW) as a replacement for natural sand. The environmental and ecological impacts associated with concrete industry represent a major sustainability challenge. Therefore, this study fresh and hardened properties along with durability performance of CFA concrete mixtures incorporating 10%, 20%, 30% and 40% TOSW as partial replacement of sand were investigated. The results show that the addition of TOSW, up to 30% replacement of sand, did not adversely affect the performance of CFA concrete mixtures. Moreover, the leaching of heavy metals from tested concrete was very low leading to a less harmful environment impact. Reusing of TOSW as partial replacement for sand in concrete mixtures for CFA piles is potentially feasible with environmental ecological and economic benefits.

3.1 Introduction

The oil sands industry is a major driver for economic activity in Canada (Carson 2011). Concurrently, solid waste generated by the oil sands mining sector has serious environmental and ecological impacts (Söderbergh et al. 2007). Therefore, several techniques have been used as a pre-treatment process to convert this solid waste to a reusable product instead of sending it to landfills. One of these innovative techniques is

Thermo-Mechanical Cuttings Cleaner (TMCC). In this pre-treatment technique, drill cuttings solid waste is thermally treated to recover hydrocarbons (Ormeloh 2014). The by-product of TMCC (i.e. the remaining solids) is very fine quartz powder. Hence, it has a potential to be used as a filler material for many construction applications.

Filler added to cementitious materials can alter the behaviour and hydration kinetics of the cement (Lawrence et al. 2003). Physically, if the filler was finer than the cement particles, it can affect its distribution in the concrete matrix, in which it can work as a nucleation site for hydrates and increase the its strength.

Sustainability in construction applications is one of the most important research topics in recent years. Incorporating waste materials in the concrete mixtures have been found to be a practical solution to waste disposal and saving natural resources. Therefore, this study aims at reducing the environmental and ecological impacts of concrete through incorporating TOSW as partial replacement of its fine aggregate. Continuous flight auger (CFA) piles concrete mixtures, which are widely used in North America, were chosen as a practical example. It is anticipated that results of this study will contribute to a wider acceptance of TOSW in different construction applications converting it into a valuable resource.

3.2 Experimental program

3.2.1 Materials

An ordinary Portland cement (OPC) Type 10 was used in all mixtures as the main binder. It consisted of 61% Tricalcium silicate (3CaOSiO_2), 11% Dicalcium silicate (2CaOSiO_2),

9% Tri-calcium aluminate ($3\text{CaO} \cdot \text{Al}_2\text{O}_3$), 7% tetracalcium aluminoferrite ($4\text{CaO} \cdot \text{Al}_2\text{O}_3 \cdot \text{Fe}_2\text{O}_3$), 3% sulfur trioxide (SO_3) and 0.82% equivalent alkalis was used as a binder material. Oil sands waste was treated using TMCC before it was brought to be investigated from Saskatchewan, Canada. TOSW was added as partial replacement of sand by volume. Table 3.1 shows the trace elements of TOSW. Particle size distribution curves for OPC and TOSW are shown in Figure 3.1. Coarse aggregate was a washed round gravel with sizes 5 to 10 mm, absorption of 0.8% and fines content lower than 1%. Natural siliceous sand with an absorption of 1.5% was used as fine aggregates. A water to cement ratio of 0.42 was used in all tested mixtures. A polycarboxylate ether based superplasticizer (HRWRA) was used to adjust mixture flowability. Air entraining admixture complying with ASTM C260 was used. In order to satisfy strength, workability and durability requirements for CFA piles, all mixtures were designed to achieve a slump of $220 \text{ mm} \pm 50 \text{ mm}$ and minimum 28-day compressive strength of 35 MPa (Brown et al. 2007). Table 3.2 shows the composition for all tested mixtures.

3.2.2 Testing procedures

3.2.2.1 Fresh properties

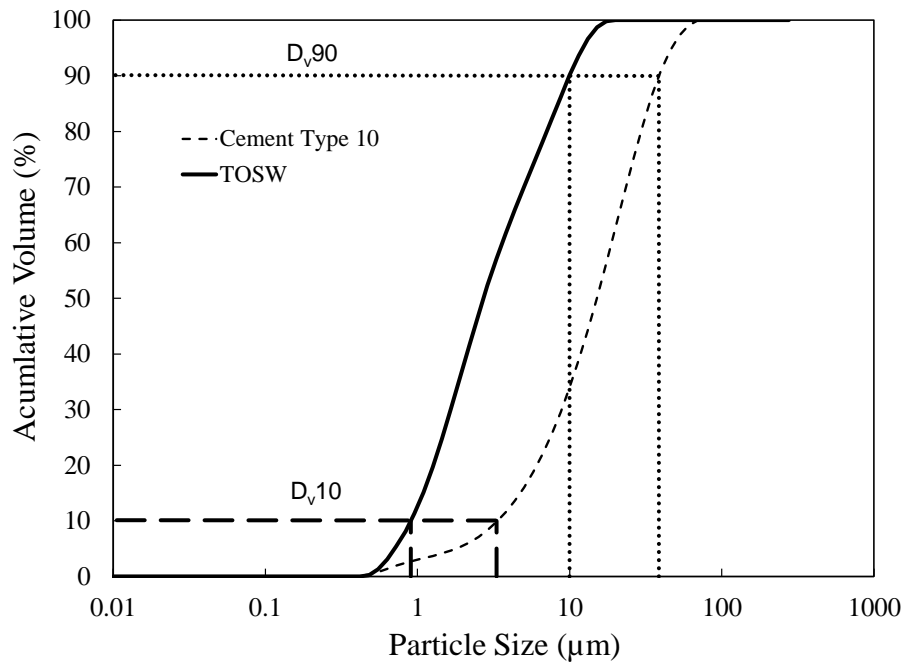
Slump and bleeding tests were conducted according to ASTM C143 (Standard Test Method for Slump of Hydraulic-Cement Concrete) and ASTM C232 (Standard Test Method for Bleeding of Concrete) to evaluate fresh properties for concrete mixtures, respectively. Moreover, the slump retention for concrete mixtures was conducted by measuring the slump loss at specific time intervals over the investigated period.

Table 3.1 Analysis of the TOSW

Element	Symbol	ICP-AES Analysis
		($\mu\text{g/g}$)
Silver	Ag	< 0.05
Aluminum	Al	7399
Arsenic	As	20
Barium	Ba	4795
Cadmium	Cd	< 0.05
Cobalt	Co	5
Copper	Cu	13
Iron	Fe	14024
Manganese	Mn	201
Molybdenum	Mo	< 0.05
Nickel	Ni	25
Vanadium	V	30
Zinc	Zn	101
Lithium	Li	4
Lead	Pb	33

Table 3.2 Mixtures composition

Property	Control	10%	20%	30%	40%
		TOSW	TOSW	TOSW	TOSW
Cement	1	1	1	1	1
Sand	1.79	1.6	1.42	1.24	1.07
Gravel	2.45	2.45	2.45	2.45	2.45
TOSW (%)	0	10	20	30	40
Superplasticizer (%)	0.80%	0.85%	1.0%	1.15%	1.6%
Air entrainment (%)	0.05	0.05	0.05	0.05	0.05
Slump (mm)	225	225	220	220	215
Concrete temperature (C°)	17	18	18	23	23
Air temperature (C°)	22	24	24	23	23

**Figure 3.1 TOSW and Cement Particle size distribution**

3.2.2.2 Hardened properties

Mechanical properties including compressive and tensile strengths, and modulus of elasticity were evaluated according to ASTM C39, ASTM C496, respectively. Flexural strength was evaluated using $100 \times 100 \times 400$ mm specimens according to ASTM C78. In addition, the bond strength between the concrete and the rebar was evaluated by pulling a steel rebar out of the 150×300 mm concrete cylinder. All specimens were produced in triplicate and were cured in a moist curing room (i.e. temperature (T) = $23 \text{ }^\circ\text{C} \pm 2 \text{ }^\circ\text{C}$ and relative humidity (RH) = $95\% \pm 5\%$) until testing ages 7, 28 and 120 days.

3.2.2.3 Durability performance

Freezing and thawing tests were conducted on prismatic concrete specimens following ASTM C666. Initially, specimens were inserted in metal boxes and then water was added up to 3 mm above the upper face of the concrete specimens (Method A of ASTM C666). Specimens were subjected to the freeze and thaw cycles adjusted according to ASTM C666 inside a freeze and thaw chamber. Meanwhile, non-destructive ultrasonic pulse velocity test was performed.

For corrosion test, the electrochemical linear polarization resistance method (Alghamdi and Ahmad 2014; Bentur et al. 1997; Broomfield 2007) was utilized to determine the corrosion current density (i_{corr}). In this method, a three-electrode system is used to measure i_{corr} . More details about the test setup can be found elsewhere (Broomfield 2007).

After a suitable initial delay, typically 60 s, the steel was polarized. The product of surface area of rebar under polarization and the slope of applied potential versus measured current

plot was taken as the linear polarization resistance R_p ($k\Omega \text{ cm}^2$) and i_{corr} (A/cm^2) can be calculated using:

$$i_{corr} = \frac{B}{R_p} \quad \text{Eq. 3.1}$$

Where, B is a constant, the value of B depends on the steel state. In case of active steel it has a value of 26 mV, while in case of passive steel its value is 52 mV. The value of B used in this test was 26 mV. All specimens were exposed to an accelerated scenario adopted from previous study by Palumbo (1991) at which specimens were connected to a direct electric current while being immersed in a 3.5% sodium chloride (NaCl) solution.

3.2.2.4 Leaching test

Leaching test was conducted according to EPA 1315 method (1315 2013). Test was conducted on an unsolidified sample of TOSW soaked as a row material in a certain volume of water. Simultaneously, concrete specimen with and without TOSW were submerged separately in the same water volume. Water samples were analyzed every 3 days using inductively coupled plasma mass spectrometry (ICP-MS).

3.3 Results and discussion

3.3.1 Fresh properties

Fresh properties of concrete have a significant effect on its placement quality (Kosmatka et al. 2002). Concrete with adequate workability and stability against segregation will have high strength and durability performance (Wu et al. 2009). Concrete slump test measures the concrete flowability before it sets. The testing method uses a cone with upper diameter

of 10 cm and base diameter of 20 cm and height of 30 cm. The cone is filled with concrete and then removed. The height of the concrete is then measured and the shape is assessed to determine the concrete workability. The proper workability is then determined according to the required application. In order to examine the effect of TOSW addition on the workability, all concrete mixtures slump was adjusted to 220 ± 5 mm while monitoring the change in HRWRA demand. Several trial concrete batches were conducted in order to identify the optimum HRWRA dosage that meets the targeted slump. As shown in Table 3.2 addition of TOSW reduced slump, hence, an increase in HRWRA dosage was required to maintain the slump within the desired range. For instance, mixture incorporating 20% TOSW required an increase in the HRWRA with about 0.2% to achieve the same slump of that of the control mixture. This can be ascribed to the fact that TOSW is a very fine material which reflects a very high viscosity to the fresh mixture, leading to a greater cohesivity and lower slump (Frontera et al. 2014). Eventually, all tested mixtures had not shown any sign of segregation or bleeding. On the other hand, from practicality point of view, failing to maintain the concrete workable for at least 30 min can jeopardize the entire installation process of CFA piles (Zayed 2005). This time frame is required to finish concrete pumping and reinforcement steel cage installation. Figure 3.2 illustrates the change in slump with time for all tested mixtures. All concrete mixtures incorporating TOSW had satisfied the 30 minutes slump retention time and maintained up to 90 min after mixing within the required slump range for CFA piles (180 to 220 mm) according to Brown et al. (2007). Therefore, mixtures incorporating TOSW can be used successfully for CFA application from workability point of view.

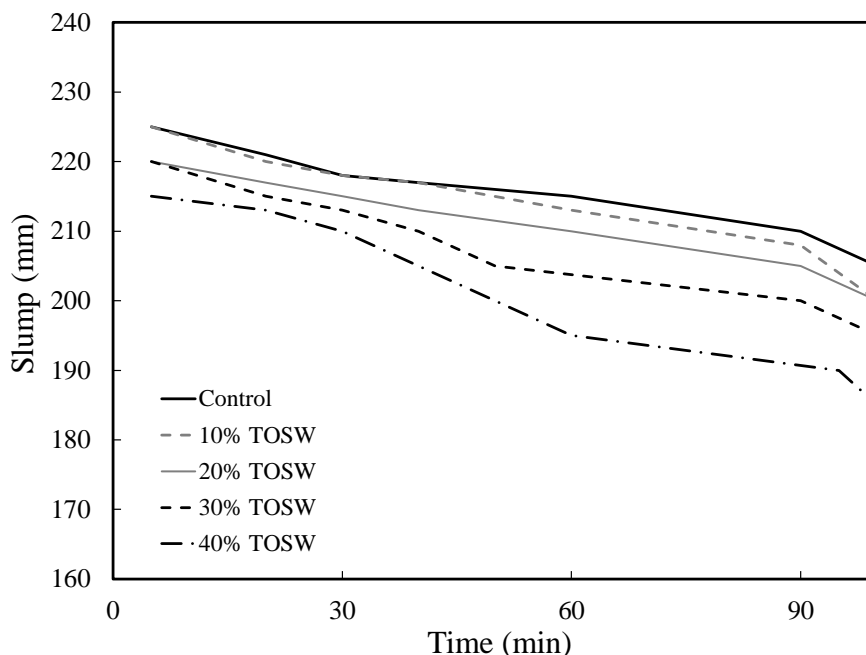


Figure 3.2 Slump variation for all tested concrete over the investigated period

3.3.2 Compressive strength

Compressive strength results for control and TOSW mixtures are given in Figure 3.3. Compressive strength has decreased by the addition of TOSW as partial replacement of sand. The higher the replacement rate, the greater was the reduction in the compressive strength. For instance, adding 10% and 30% of TOSW had induced a reduction in the compressive strength at age 28 days with about 4% and 16% than that of the control mixture, respectively. This reduction in strength can be ascribed to the increase in the amount of fine materials in mixtures (i.e. TOSW addition) (Muhammed et al. 2014). Simultaneously, inadequate dispersion of TOSW particles due to coagulation could induce weak points in the concrete microstructure resulting in a lower achieved strength (Felekoglu 2008). However, all tested mixtures meet the targeted compressive strength for CFA pile concrete mixtures at age 28 days (i.e. 35 MPa) (Brown et al. 2007), except

mixture incorporating 40% TOSW. For instance, compressive strength at age 28 days for mixtures incorporating 20% and 30% were 52.31 MPa and 46.75 MPa, respectively. It is interesting to note that the development rate of concrete strength did not alter by the addition of TOSW. The increase in compressive strength for the mixture with and without TOSW from age 7 to 28 days and from 28 to 120 days was about $10\% \pm 1\%$ and $12\% \pm 2\%$, respectively.

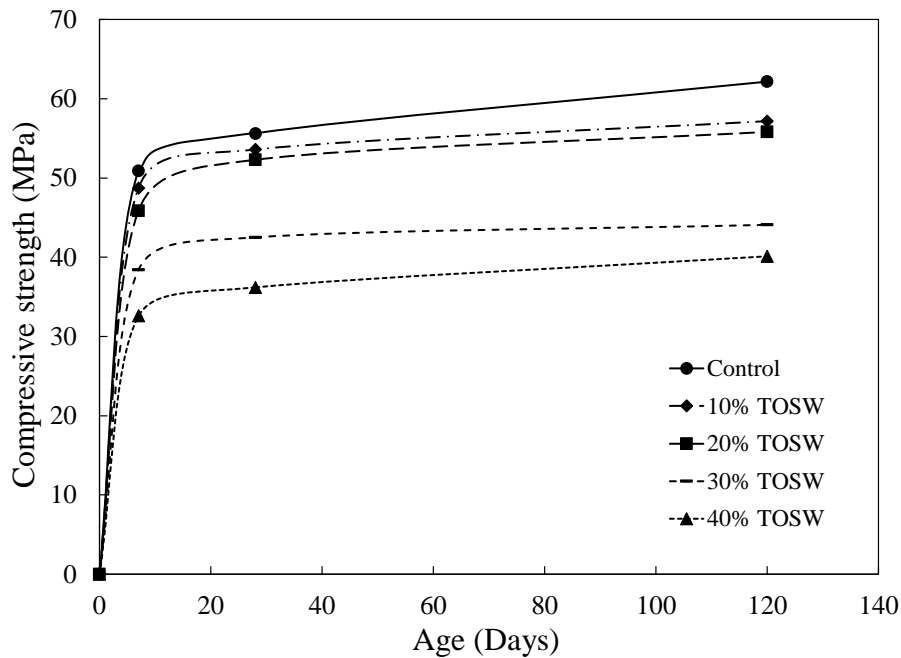


Figure 3.3 Compressive strength development for all tested mixtures over the investigated period

3.3.3 Splitting tensile strength

Splitting tensile strength test is a method of measuring the concrete cylinder tensile strength. Figure 3.4 illustrates the variation of splitting tensile strength with time for all tested mixtures. Tensile strength results followed the same trend as that of compressive

strength results. The higher the replacement rate, the greater was the reduction in the tensile strength. For instance, adding 10% and 40% of TOSW had induced a reduction in the tensile strength at age 28 days with about 6% and 23% than that of the control mixture, respectively. Similar to compressive strength, addition of TOSW had insignificant effect on the development rate of the tensile strength. All mixtures with and without TOSW had tensile strength developing rate of about 14% from age 7 to 28 days and less than 10% from age 28 to 120 days.

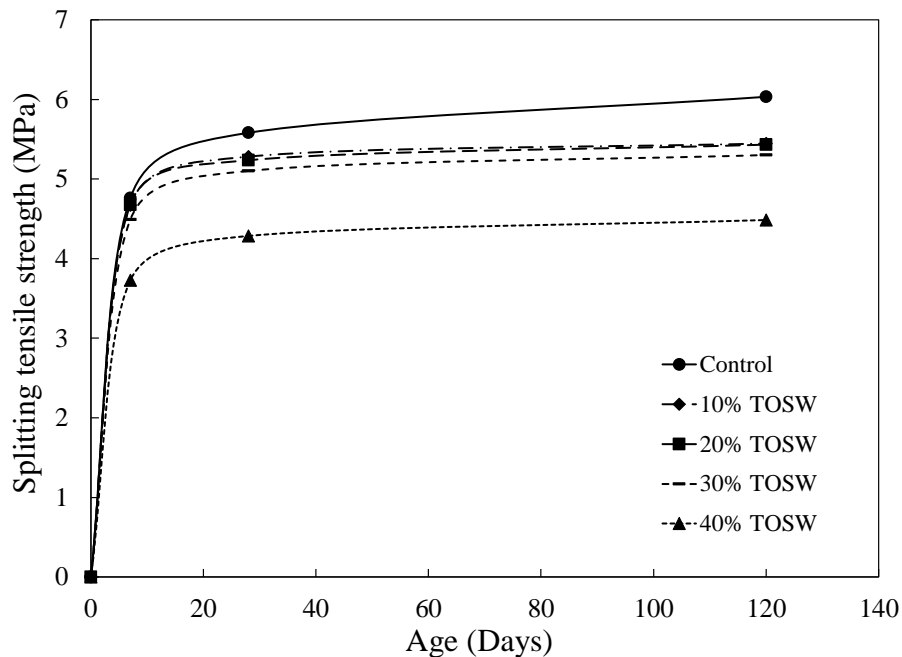


Figure 3.4 Splitting tensile strength development for all tested mixtures over the investigated period.

Generally, the ratio between tensile and compressive strengths for mixtures with and without TOSW at different concrete ages was about 10% which is a common value in the literature (Nihal et al. 2006). Moreover, several national building codes had proposed various formulas for the relationship between splitting tensile and compressive strengths

for concrete. In this study, ACI 318 (318 2008), ACI 363R (ACI 2010) and CEB-FIP (Taerwe and Matthys 2013) formulas were used to predict the TOSW mixture splitting tensile. The general formula is as follows (Eq. 3.2):

$$f_{tsp} = a f_c^b \quad \text{Eq. 3.2}$$

Where, f_{tsp} = splitting tensile strength, and f_c = compressive strength, in MPa, a and b are constants (i.e. ACI 318: $a=0.56$, $b=0.50$; ACI 363R: $a=0.59$, $b=0.50$; and CEB-FIP: $a=0.3$, $b=0.67$). The deviation between experimental data and predicted values is assessed statistically based on the integral absolute error (IAE , %), and it is computed from the following equation (Eq. 3.3):

$$IAE = \sum \frac{Q - P}{\sum Q} \times 100\% \quad \text{Eq. 3.3}$$

Where, Q = observed value and P = predicted value. The IAE value reflects the difference between predicted and observed values. If IAE is zero, this indicates that the predicted and observed values are identical, which rarely occurs. Hence, if there are different regression equations, the one having the smallest value of the IAE is the most reliable. Generally, an acceptable regression equation will have IAE in the range from 0 to 10% (Arioglu et al. 2006).

Figure 3.5 illustrates the correlation between the experimental data and predicted values for the splitting tensile strength. It seems that all the proposed formulas underestimate the splitting tensile strength of concrete mixtures incorporating TOSW. However, IAE values for CEB-FIP and ACI 363R were less than 10%, hence, both equations can be used to

estimate the splitting tensile strength of TOSW concrete mixtures based on the achieved compressive strength.

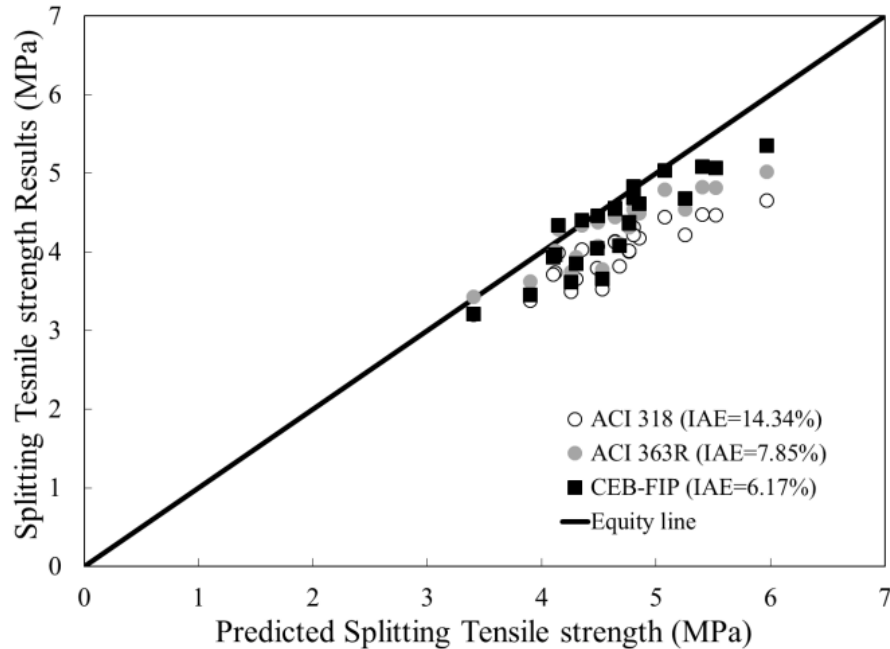


Figure 3.5 Correlation between the experimental data and predicted values for the splitting tensile strength

3.3.4 Flexural strength

Figure 3.6 shows the development of the flexural strength with time. It is clear that flexural strength results were consistent with compressive and tensile strength results. The flexural strength for control mixture was around $13\% \pm 1\%$ of its compressive strength at all testing ages. Similar trend was exhibited by mixtures incorporating different contents of TOSW. For instance, ratios between the flexural and compressive strength for mixtures incorporating 20% and 40% of TOSW were 11.6% and 13.2% at age 28 days, respectively.

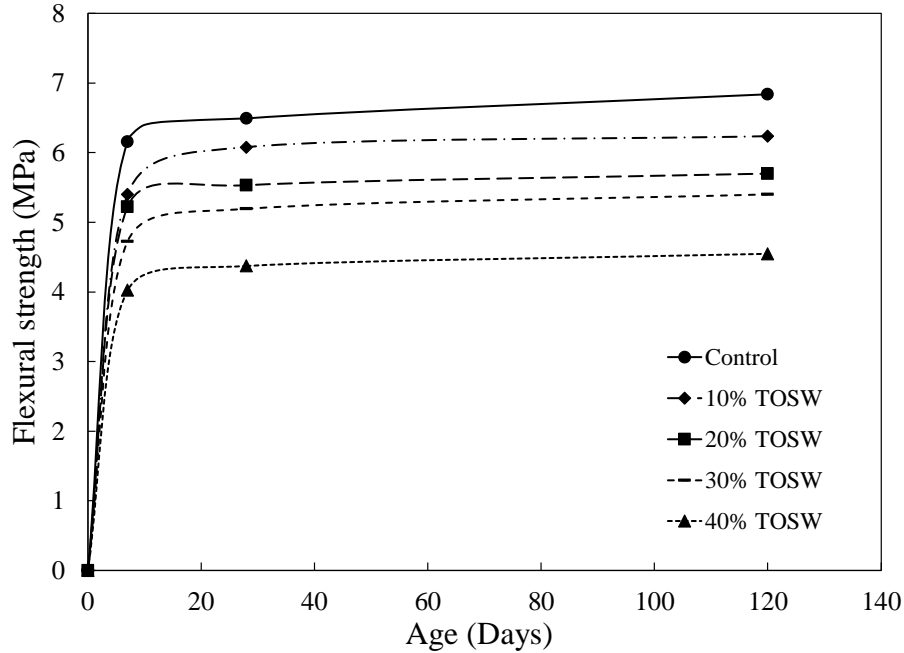


Figure 3.6 Flexural strength development for all tested mixtures over the investigated period

Similar to splitting tensile strength, various formulas for the relationship between flexural and compressive strengths were adopted. The ACI 318, ACI 363R and formula proposed by Shah and Ahmad (Shah and Ahmad 1985) were used to predict the TOSW mixture flexural strength. The general formula is similar to the equation as follows:

$$f_f = a f_c^b \quad \text{Eq. 3.4}$$

Where, f_f = flexural strength, and f_c = compressive strength, in MPa, a and b are constants (i.e. ACI 318: $a=0.62$, $b=0.50$; ACI 363R: $a=0.94$, $b=0.50$; and Ahmad and Shah (1985): $a=0.44$, $b=0.67$). The deviation between experimental data and predicted values was also assessed on the basis of IAE (%). Figure 3.7 shows the correlation between the experimental data and predicted values for the flexural strength. It can be seen that the formula proposed by Shah and Ahmed (Shah and Ahmad 1985) is capable to predict the

flexural strength for mixtures incorporating TOSW with an acceptable accuracy (i.e. *IAE* less than 10%).

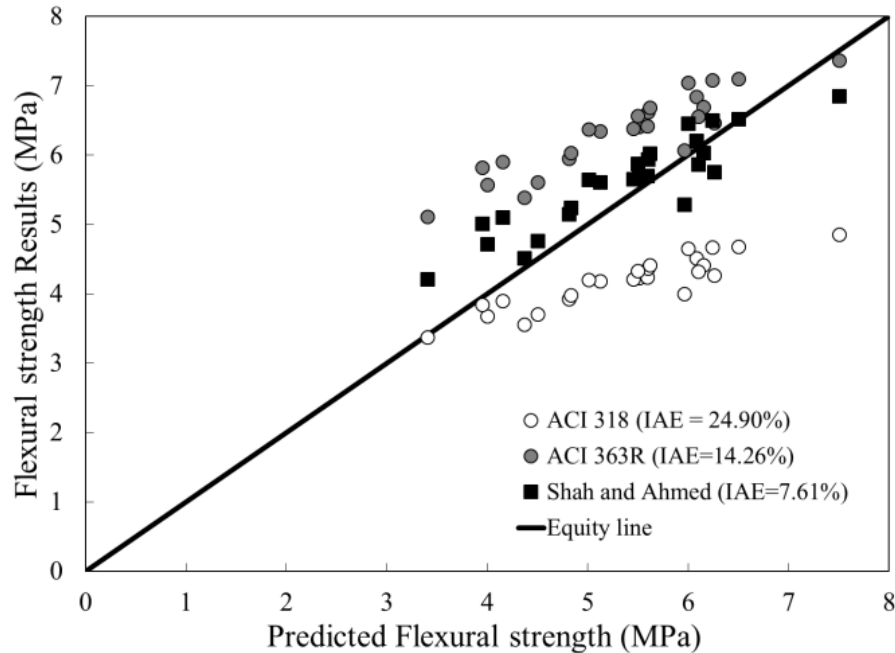


Figure 3.7 Correlation between the experimental data and predicted values for the flexural strength

3.3.5 Modulus of elasticity

The modulus of elasticity of concrete (E) represents the relationship between the stress and strain and provides an understanding of their effect on each other. As shown in Figure 3.8, increasing the TOSW content leads to a reduction in the measured modulus of elasticity. For instance, at age 28 days, increasing the TOSW content from 10% to 30% resulted in a higher reduction in the modulus of elasticity with about 12%. Moreover, the reduction in the modulus of elasticity induced by TOSW addition was in the same reduction order of that of the compressive strength.

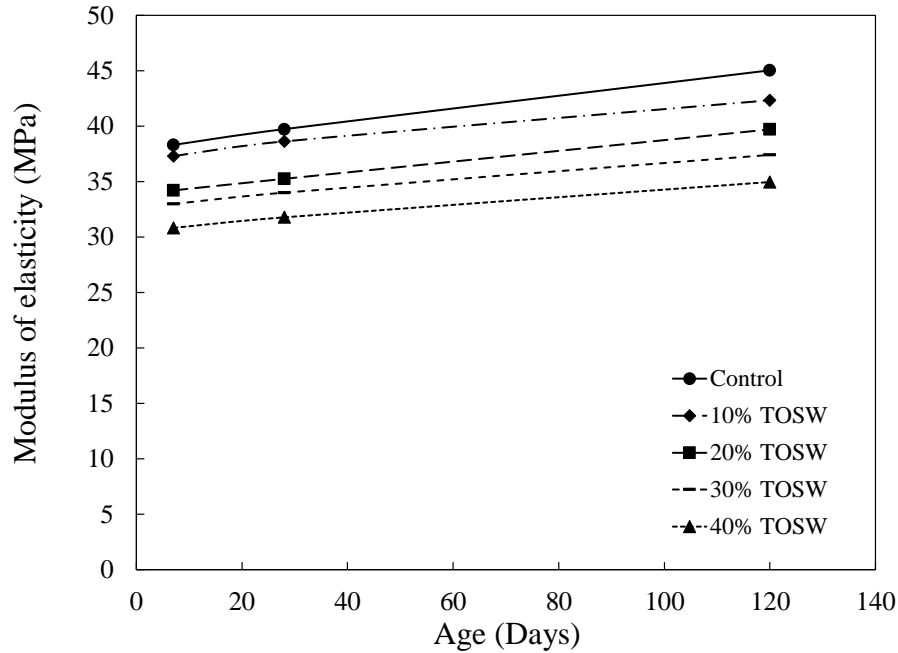


Figure 3.8 Modulus of elasticity development for all tested mixtures over the investigated period

This is in agreement with the literature as concrete modulus of elasticity is strongly related to its compressive strength. Generally, in the quality control program, modulus of elasticity is expressed as function of compressive strength which is determined routinely, while modulus of elasticity test is ignored as it is laborious and time-consuming. Therefore, various researchers have proposed a number of expressions that can be categorized into two groups. The first group of expressions may be written in the general formula as shown in (Eq. 3.5):

$$E = af_c^b + c \quad \text{Eq. 3.5}$$

Where a , b , and c are coefficients. This formula is recommended by ACI 363R ($a=3320$, $b=0.5$, $c=6900$). In the second category, the expression is similar to Eq. 3.2. The ACI 318 and CEB-FIP use values of 4730 and 8981 for a coefficient and 0.5 and 0.33 for b

coefficient, respectively. Figure 3.9 shows the correlation between the experimental data and predicted values for the modulus of elasticity. All proposed formulas are capable to predict the modulus of elasticity for mixtures incorporating TOSW with an acceptable accuracy (i.e. *IAE* less than 10%).

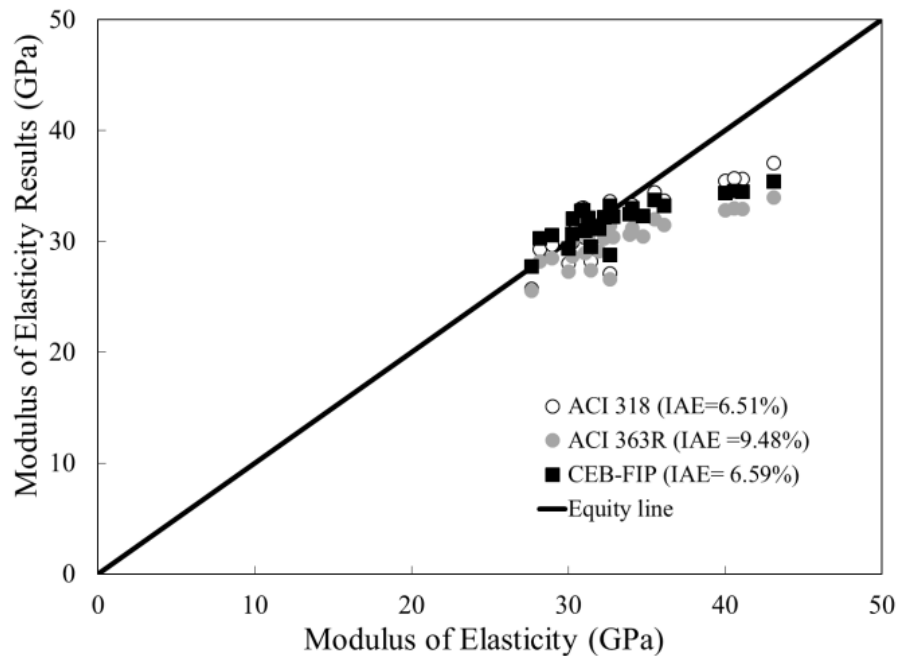


Figure 3.9 Correlation between the experimental data and predicted values for the modulus of elasticity

3.3.6 Pullout strength

One of the main assumptions in design of reinforced concrete structures is the strain compatibility between concrete and reinforcement steel. Hence, bond between them (i.e. concrete and steel) is an essential parameter which is significantly affected by the quality and properties of the holding concrete (Valcuende and Parra 2009). Figure 3.10 shows pullout strength development for all tested mixtures over the investigated period. All tested mixtures achieved more than 75% of the final pull-out strength at age 7 days. For instance,

control mixture and mixture incorporating 30% TOSW exhibited 77% and 87% of their final pull-out strength at age 7 days, respectively. Moreover, the addition of TOSW has resulted in a lower pull-out strength with respect to that of the control mixture without TOSW. The higher the TOSW content, the higher was the reduction in the pull-out strength. For example, increasing the TOSW content from 10% to 40% had led to a higher reduction in pull-out strength with about 30% with respect to that of the control mixture at age 28 days.

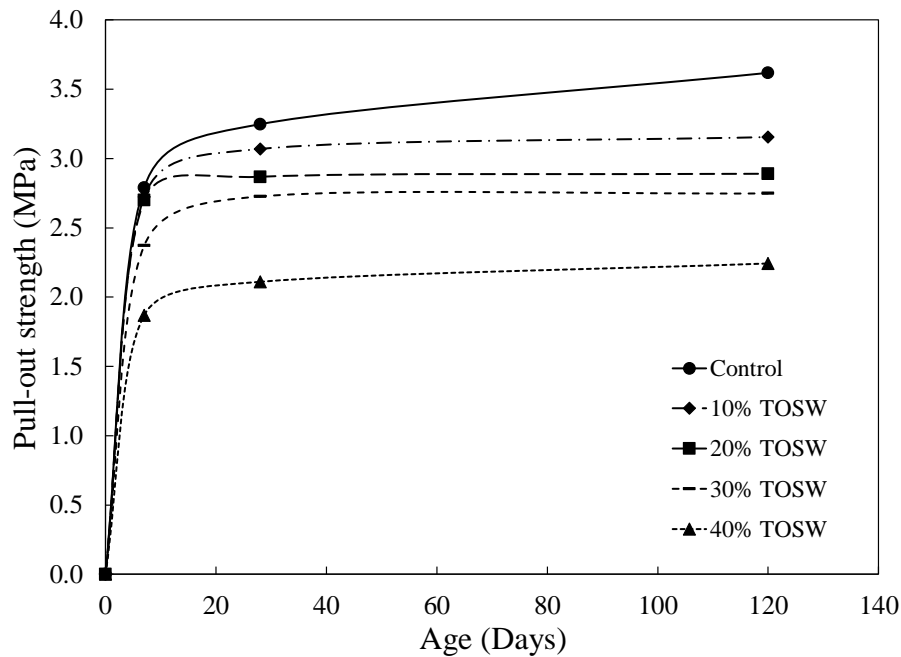


Figure 3.10 Pull-out strength development for all tested mixtures over the investigated period

Figure 4.11 shows the compressive strength and pull-out strength of the tested mixtures at age 28 days as a percentage of the control mixture. The reduction in both compressive and pull-out strengths due to TOSW addition were almost the same. This is expected since the

bond behaviour between the rebar and concrete is mainly controlled by concrete mechanical properties (i.e. compressive and tensile strengths) (Ahmad et al. 2014).

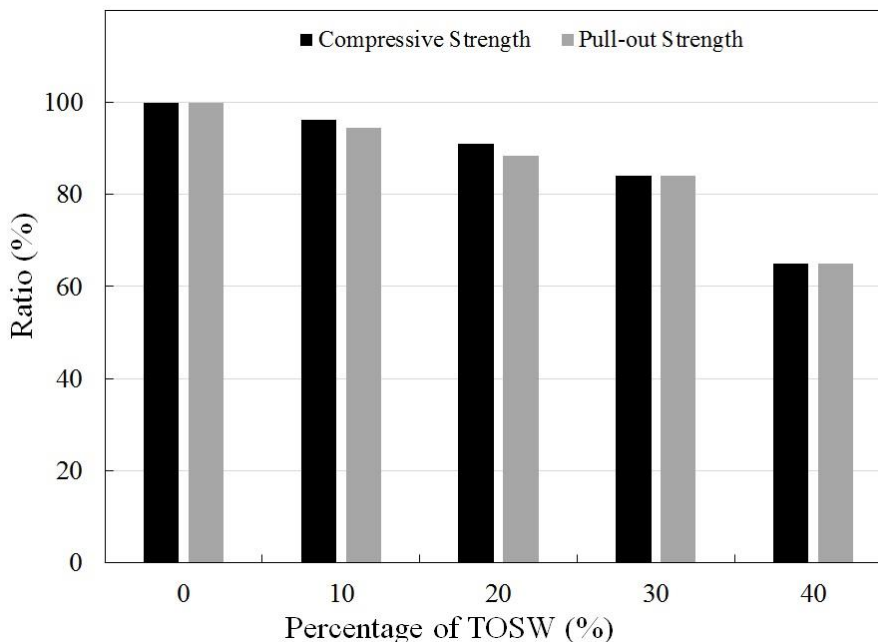


Figure 3.11 Compressive strength and pull-out strength of the tested mixtures at age 28 days as percentage of the control mixture

3.3.7 Freeze and thaw

Frost action is among the prominent durability problems of concrete structures exposed to cold climates. Hence, the freeze-thaw resistance for each tested mixtures was assessed according to ASTM C666 in which a durability factor (DF) is calculated after exposing each specimen to a number of freezing and thawing cycles (N) equals to M , which is a specified number of cycles at which the exposure is to be terminated (i.e. 300 cycles according to ASTM C666) or until its relative dynamic modulus of elasticity (P) reaches 60 % of its initial value using Eq. 3.6:

$$DF = \frac{P \times N}{M} \quad \text{Eq. 3.6}$$

Durability factors for all tested concrete mixtures after 300 freezing and thawing cycles are shown in Figure 3.12. All mixtures incorporating TOSW met the 60% threshold recommended by ASTM C666 guidelines for durable concrete subjected to freezing-thawing cycles, except mixture incorporating 40% TOSW. Mixture incorporating 40% TOSW was markedly deteriorated at about 210 freezing-thawing cycles with a durability factor less than 50%.

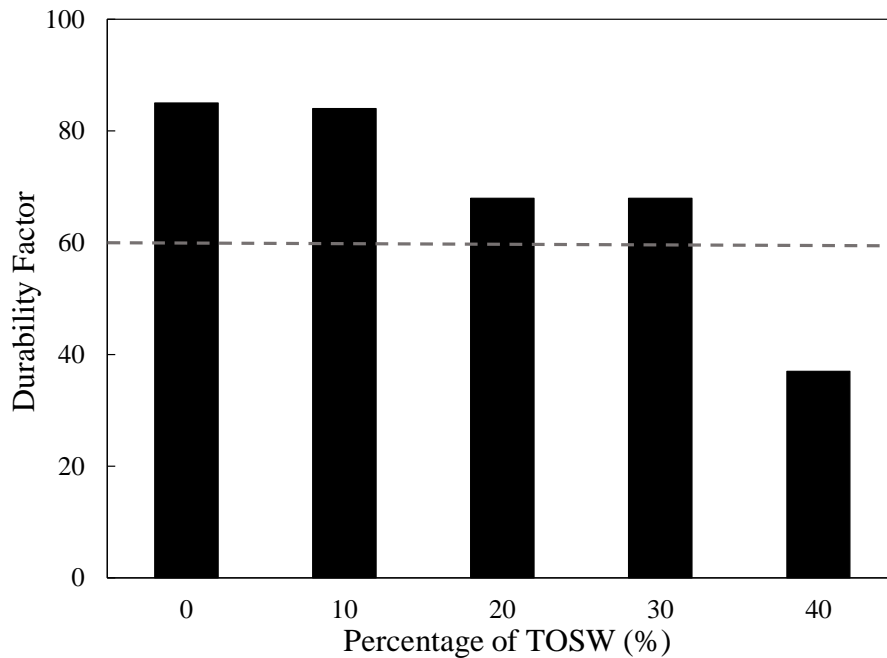


Figure 3.12 Durability factor for different mixtures

Generally, the relative dynamic modulus of elasticity was found to decrease as the TOSW content increased. Addition of TOSW compromised the concrete properties, especially tensile strength. Simultaneously, deterioration of concrete exposed to freezing and thawing cycles has been ascribed to the migration of super-cooled water between small and large

surface pores in order to freeze and form ice. The gradual build-up of ice in capillary pores exerts tensile stresses (Powers 1945, 1975). As these tensile stress exceeds the cement matrix tensile strength, micro cracks are formed and start to grow and propagate with the repeating of the freeze and thaw cycle (Litvan 1976). Hence, the addition of TOSW to concrete exposed to frost action makes it more vulnerable to crack due to the reduction in its tensile strength.

3.3.8 Corrosion

Figure 3.13 illustrates the variation of corrosion current density (i_{corr}) with exposure time to NaCl solution for different specimens. It was observed that TOSW addition increases the corrosion current. However, the calculated corrosion current for all mixtures was below the threshold value of $0.10 \mu\text{A}/\text{cm}^2$ indicating passive condition according to the criteria developed by Broomfield and Clear (Broomfield 1996; Clear 1989).

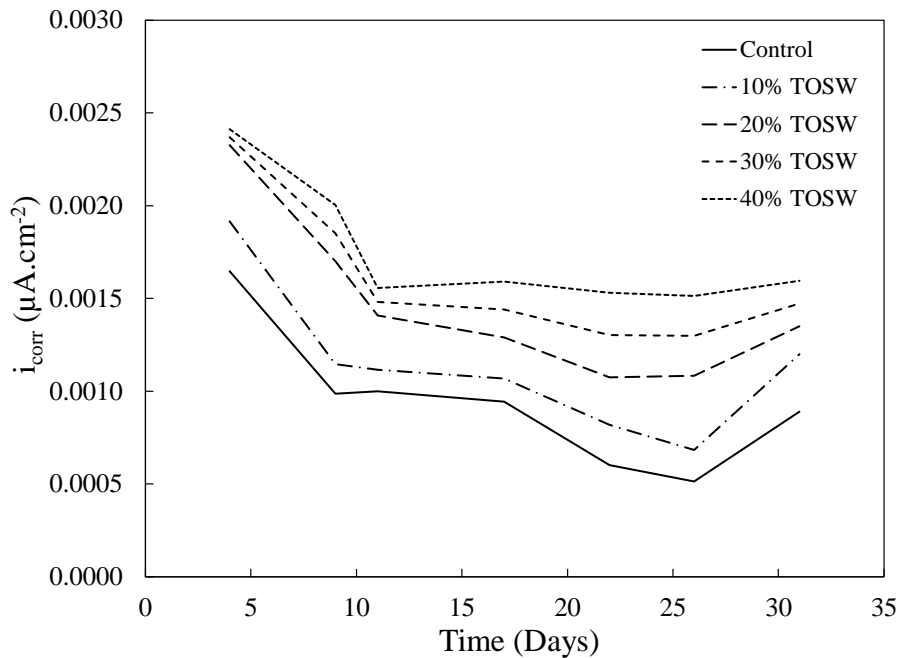


Figure 3.13 Corrosion current through test time

3.3.9 Leaching

Concrete mixtures incorporating 40% TOSW did not meet the performance requirements for CFA. Hence, the focus in the leaching evaluation was directed to concrete mixtures incorporating up to 30% of TOSW as partial replacement of sand. Leaching of heavy metals from the TOSW was initially identified through testing a sample of raw TOSW (Table 3.3).

Table 3.3 Measured metals in TOSW compared to different standards

Element	Symbol	CCME* guideline (mg/l)	Raw TOSW leaching (mg/l)	Concrete leaching (mg/l)		
				10% TOSW	20% TOSW	30% TOSW
Silver	Ag	N.A.	0.005	0.005	0.004	0.003
Aluminum	Al	5.000 ^b	1.656	0.349	0.615	0.975
Arsenic	As	0.005 ^a	0.012	0.004	0.002	BDL*
Barium	Ba	N.A.	1.113	0.700	0.105	0.119
Cadmium	Cd	N.A.	0.066	0.010	0.004	BDL
Cobalt	Co	0.050 ^b	0.001	BDL	BDL	BDL
Copper	Cu	0.004 ^a	0.012	BDL	BDL	BDL
Iron	Fe	0.300 ^a	0.451	0.028	0.013	0.004
Manganese	Mn	0.200 ^b	0.011	BDL	BDL	BDL
Molybdenum	Mo	0.073 ^a	0.056	0.005	0.005	0.004
Nickel	Ni	0.150 ^a	0.017	0.030	0.027	0.023
Vanadium	V	0.100 ^b	0.038	0.026	0.018	0.011
Zinc	Zn	0.030 ^a	0.001	BDL	BDL	BDL
Lithium	Li	2.500 ^b	0.013	0.023	0.025	0.024
Lead	Pb	0.006 ^a	0.004	0.001	0.002	0.002

^a CCME (Canadian Council of Ministers of Environment) guide lines for protection of fresh water

^b CCME guide lines for protection of agriculture (irrigation)

*BDL: Below Detecting Limits

According to the Canadian Council of Ministers of Environment (CCME) guideline limits, incorporation of TOSW in concrete mixtures had significantly reduced the leaching for different metals with respect to raw TOSW as shown in Table 3.3. For example, incorporation of TOSW in concrete had led to leaching values for Vanadium, Arsenic, and Aluminum, below CCME standards by about 20% to 93%. This can be ascribed to the solidification of the TOSW in the cementitious matrix of concrete. In addition, the densification and reduction in porosity of concrete microstructure induced by the addition of the very fine TOSW assisted in entrapping higher amount of metals (Sabatini et al.). However, some metals leaching increased but it was still below the CCME guidelines. This increase can be the contribution of the concrete from its components.

3.4 Conclusions

This study provides a new application for TOSW. It proved experimentally the high potential of recycling/reusing TOSW in concrete mixtures for different construction applications. Besides converting TOSW to a valuable product, this study provides an alternative solution for waste management of TOSW instead of sending to landfill. The following conclusions can be drawn from the experimental results:

- Increasing the HRWRA dosage can overcome the reduction in concrete slump induced by TOSW addition and maintain its workability within the required range for CFA application.
- Mixtures incorporating up 30% TOSW as a partial replacement of sand met the targeted compressive strength for CFA pile concrete mixtures at age 28 days (i.e. 35 MPa) along with adequate durability performance.

- Addition of TOSW did not alter the correlation between compressive strength and other mechanical properties.
- Solidification of TOSW in the cementitious matrix of concrete along with reduction in concrete porosity due to TOSW addition produced a mixture with leaching below the CCME guidelines.

3.5 References

- Carson, B. (2011). "Sustainable solutions in the oil sands." *Policy Options Magazine*, 12-22.
- Söderbergh, B., Robelius, F., and Aleklett, K. (2007). "A crash program scenario for the Canadian oil sands industry." *Energy Policy*, 1931-1947.
- Ormeloh, J. (2014). "Thermomechanical cuttings cleaner—qualification for offshore treatment of oil contaminated cuttings on the norwegian continental shelf and martin linge case study."
- Lawrence, P., Cyr, M., and Ringot, E. (2003). "Mineral admixtures in mortars: Effect of inert materials on short-term hydration." *Cement and Concrete Research*, 33(12), 1939-1947.
- Das, S. K., Mohapatra, A. K., and Rath, A. (2014). "Geo-polymer Concrete—Green Concrete for the Future—A Review." *International Journal of Civil Engineering Research*, 5(1), 21-28.
- Brown, D. A., Dapp, S. D., Thompson, W. R., and Lazarte, C. A. (2007). "Design and Construction of Continuous Flight Auger (CFA) Piles." Federal Highway Administration.
- Alghamdi, S. A., and Ahmad, S. (2014). "Service life prediction of RC structures based on correlation between electrochemical and gravimetric reinforcement corrosion rates." *Cement and Concrete Composites*, 47, 64-68.
- Bentur, A., Diamond, S., and Berke, N. S. (1997). *Steel corrosion in concrete*, E. & F.N. Spon, London.
- Broomfield, J. P. (2007). *Corrosion of steel in concrete: understanding, investigation and repair*, Taylor & Francis, New York.
- Palumbo, N. (1991). "Accelerated corrosion testing of steel reinforcement in concrete." Dissertation/Thesis, ProQuest Dissertations Publishing.
- EPA 1315, E. (2013). "Mass Transfer Rates of Constituents in Monolithic or Compacted Granular Materials Using a Semi-Dynamic Tank Leaching Procedure." Environmental Protection Agency. Washington, D.C.

- Kosmatka, S. H., Kerkhoff, B., and Panarese, W. C. (2002). *Design and Control of Concrete Mixtures*, 13th ed. Vol. EB001.13T;EB001.13T.; Stokie, Ill: Portland Cement Association, 1988.
- Wu, Z., Zhang, Y., Zheng, J., and Ding, Y. (2009). "An experimental study on the workability of self-compacting lightweight concrete." *Construction and Building Materials*, 23(5), 2087-2092.
- Frontera, P., Candamano, S., Iacobini, I., and Crea, F. "Eco-efficient self-compacting concrete with silica sand waste." *Proc., 2013 3rd International Conference on Advanced Materials and Information Technology Processing, AMITP 2013, October 1, 2013 - October 2, 2013*, WITPress, 205-212.
- Zayed, T. M. (2005). "Productivity and cost assessment for continuous flight auger piles." *Journal of Construction Engineering and Management*, 131(6), 677-688.
- Muhammed, H. S., Kadum, K. T., Ahmed, M. A., Getfan, N., and Zehra, A. A. (2014). "Effect of Fine Materials on the Compressive Strength and Workability of Concrete." *مجلة الكوفة الهندسية / Kufa journal of Engineering*, 4(1).
- Felekoglu, B. (2008). "A comparative study on the performance of sands rich and poor in fines in self-compacting concrete." *Construction & building materials*, 22(4), 646-654.
- Nihal, A., Girgin, Z. C., and Ergin, A. (2006). "Evaluation of Ratio between Splitting Tensile Strength and Compressive Strength for Concretes up to 120 MPa and its Application in Strength Criterion." *ACI Materials Journal*, 103(1), 18-24.
- American Concrete Institute, ACI Committee 318, and International Organization for Standardization. *Building Code Requirements for Structural Concrete (ACI 318M-08) and Commentary*. Farmington Hills, Mich: American Concrete Institute, 2008.
- ACI. (2010). "Report on high-strength concrete." ACI 363R-10, Farmington Hills, MI
- Taerwe, L., and Matthys, S. (2013). *fib model code for concrete structures 2010*, Ernst & Sohn, Wiley.
- Arioglu, N., Canan Girgin, Z., and Arioglu, E. (2006). "Evaluation of ratio between splitting tensile strength and compressive strength for concretes up to 120 MPa and its application in strength criterion." *ACI Materials Journal*, 103(1), 18-24.

- Shah, S. P., and Ahmad, S. H. (1985). "Structural properties of high strength concrete and its implications for precast prestressed concrete." *Journal - Prestressed Concrete Institute*, 30(6), 92-119.
- Valcuende, M., and Parra, C. (2009). "Bond behaviour of reinforcement in self-compacting concretes." *Construction and Building Materials*, 23(1), 162-170.
- Ahmad, S., Adekunle, S. K., Maslehuddin, M., and Azad, A. K. (2014). "Properties of self-consolidating concrete made utilizing alternative mineral fillers." *Construction and Building Materials*, 68, 268-276.
- Powers, T. C. (1945). "Working hypothesis for further studies of frost resistance of concrete." *American Concrete Institute*, 16(4), 245-272.
- Powers, T. C. (1975). "FREEZING EFFECTS IN CONCRETE." *American Society of Mechanical Engineers (Paper)*, 1-11.
- Litvan, G. G. (1976). "Frost action in cement in the presence of De-Icers." *Cement and Concrete Research*, 6(3), 351-356.
- Broomfield, J. P. (1996). "Field measurement of the corrosion rate of steel in concrete using a microprocessor controlled unit with a monitored guard ring for signal confinement." *ASTM Special Technical Publication*, 1276, 91-106.
- Clear, K. C. (1989). "Measuring rate of corrosion of steel in field concrete structures." *Transportation research record*(1211), 28-37.
- Sabatini, D. A., Knox, R. C., and American Chemical Society. Division of Colloid and Surface, C. "Transport and remediation of subsurface contaminants: colloidal, interfacial, and surfactant phenomena." American Chemical Society.

Chapter 4

4 COMPARISON OF AXIAL PERFORMANCE OF BORED AND CONTINUOUS FLIGHT AUGERED LARGE SCALE MODEL PILES IN SAND

Bored and continuous flight auger (CFA) piles are two widely used cast in place reinforced concrete pile types that are constructed employing different techniques, which affects their axial performance and capacity. In this regard, the work presented herein has two main objectives: to compare the axial performance of CFA and bored concrete piles in sand; and to investigate utilizing a green concrete mixture (i.e. incorporating treated oil sand waste (TOSW)) in their construction. Instrumented piles with the same nominal geometry were constructed using conventional as well the green concrete mixtures. The piles were subjected to axial compressive and uplift loading. The test piles were exhumed after testing to investigate their dimensions and profile, surface roughness, and interface friction between soil and pile. The soil-pile interface conditions of CFA and bored piles were quantitatively characterized using fractal dimension to measure surface roughness. The results showed that CFA piles compressive and pullout capacity was higher than that of the bored piles. This was attributed to the increase in diameter of the CFA piles compared to the bored piles owing to the high pressure used for placing the concrete in CFA construction, which resulted in a higher lateral confinement. It was also found that piles constructed employing concrete mixture incorporating TOSW, both CFA and bored piles, had the same geotechnical performance.

4.1 Introduction

Different types of pile foundations are used to meet different geotechnical challenges in construction sites. Bored and continuous flight auger (CFA) piles are two popular cast-in-place reinforced concrete piles that are used worldwide in many applications owing to their demonstrated reliable and safe performance as well as large load carrying capacity. The bored piles offer generally low cost large capacity deep foundation option with excellent performance suitable for different geotechnical conditions. On the other hand, CFA piles, also known as augered cast in-place (ACIP), can be installed rapidly with no noise or vibration during installation, and offer relatively high skin friction compared to bored piles (Bowles 1996).

Bored and CFA piles constructed with conventional concrete mixture that consists of cement, water, sand, gravel, and additives (Brown et al. 2007; Brown et al. 2010). The pile body carry the structure load, transfer the load to the reinforcement, the surrounding soil and reduce the steel corrosion. Sand is a main component of the concrete mixture and it is a non-renewable resource. The high demand on sand due to the increasing construction activity lead to increase in its cost and shortage in its supply as in India and Malaysia (Balamurugan and Perumal 2013; Raman et al. 2007). Moreover, efforts by the construction industry has increased to develop sustainable construction practice.

Oil sands industry is a major driver of economic activity in Canada (Carson 2011). Concurrently, solid waste generated by oil sands mining sector has severe environmental and ecological impacts (Söderbergh et al. 2007). Therefore, several techniques have been used as a pre-treatment process to convert this solid waste to a reusable product. One of

these innovative oil sand waste management techniques is Thermomechanical Cuttings Cleaner (TMCC) (Ormeloh 2014). The by-product of TMCC is very fine quartzes powder named as Treated Oil Sand Waste (TOSW). TOSW has been used successfully as a cement replacement in grout mixtures for micropiles (Aboutabikh et al. 2016). In the current research, its use as a sand replacement in the concrete mixtures for construction of bored and CFA piles is investigated.

The Axial behaviour of bored and CFA piles is affected by the construction method of each type. Several authors investigated the behaviour of both types under compression loading (Albuquerque et al. 2005; Albuquerque et al. 2011; Farrell and Lawler 2008; Gavin et al. 2013; Gavin 2009; Ismael 2001). However, the difference between the performance of both types was not clear. As an example, Albuquerque et al. (2005) reported 40% increase in the CFA pile capacity over the bored pile. On the other hand, Farrell and Lawler (2008) reported that the CFA pile ultimate capacity is double that of the bored pile. Therefore, a better understanding of the CFA pile behaviour, design parameters and its reasons is required.

The pressurized concrete used for constructing CFA piles can increase its volume by about 20% (Brown et al. 2007). Therefore, the soil around the pile experiences densification, which in turn enhances the skin friction of CFA piles. It was also found that the interface friction angle between the pile surface and the soil could be equal to soil's internal friction angle, and the coefficient of lateral earth pressure, K_s , could be equal to 0.9 for CFA piles compared with 0.7 for bored piles (Fleming 2009).

This chapter investigates the behaviour of CFA and bored piles, and the factors that affect their distinctive behaviour. In addition, the effect of incorporating TOSW on the behaviour of CFA and bored piles is investigated.

4.2 Experimental program

4.2.1 Materials

Six piles were installed in a test soil pit 4.5x4.5m in plan and 6.0 m deep. Four piles were CFA piles, while two piles were bored piles. The test pit was backfilled with natural washed concrete sand with fines less than 2%, and grain size distribution as shown in Figure 4.1. The sand was placed in layers, 25 cm each, and was compacted by vibrating plate compactor on three passes. Sand cone test was performed on each layer to measure the soil density and calculate the relative density to ensure uniform consistency. During backfilling the soil pit, sand samples were collected and were tested to determine the sand physical and mechanical properties.

The average water content and specific gravity of the sand were 3.3% and 2.71, and its maximum and minimum dry density were 20 and 16.2 kN/m³. The sand particles were angular with mean particle size (D_{50}) = 0.95 mm. The peak friction angle (ϕ_p) and residual friction angle (ϕ_r) were measured from direct shear tests and were 43 and 36°, respectively.

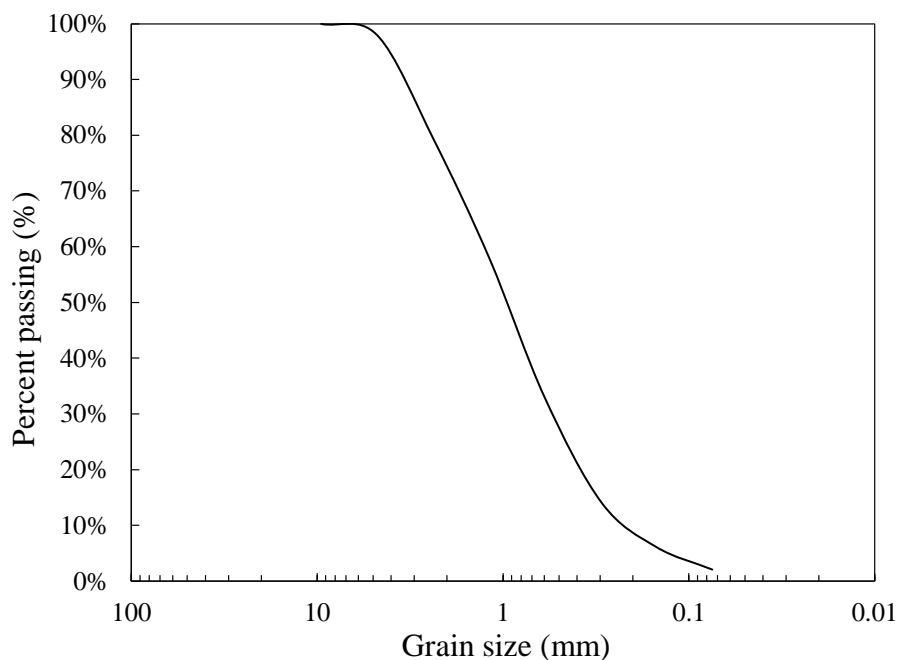


Figure 4.1 Sand grain size distribution curve

Ordinary Portland cement type 10 was used as a binder. The same natural washed concrete sand used for backfilling was utilized as fine aggregates, while the coarse aggregates constituted 9 mm rounded gravel. The TOSW was added as a sand replacement. The specific gravity and surface area of the TOSW were 2.81 and 4.85 m²/g, respectively.

In order to evaluate the effect of incorporating TOSW on the behaviour of bored and CFA piles, two concrete mixtures were used to construct the piles. The first mixture does not contain TOSW (C0). In the second mixture (C1), 30% of the sand was replaced by TOSW (C1). The 30% TOSW mixture was the only mixture with the highest percentage of TOSW that was satisfying the piles material requirements according to the FHWA (Brown et al. 2007). The concrete mixtures were tested according to ASTM C143 and ASTM C39 (2016) (2015) to confirm their workability to be 200±20 mm and 28 days compressive strength to be 35 MPa.

4.2.2 Piles description and installation

A Big Beaver auger drill rig was used to excavate the piles using a hollow stem auger. The outer diameter (D) of the auger was 0.27 m for all piles except pile No. 6, which was 21.6 cm. The spacing between piles was $> 5D$ to ensure that the piles capacity will not be affected by the interaction between them (Phillips and Valsangkar 1987). To decrease sand caving during excavation, the highest downward pressure was applied by the drilling rig with the slowest rotation possible. Moreover, as a quality assurance during the excavation of each pile, sand coming out of the hole was collected and weighed to calculate the occupied volume based on the measured density. The measured volume was compared with the theoretical volume of the hole to make sure that no caving occurred. After reaching the required depth, the drilling rig was removed and the hollow stem auger left in the hole preventing it from failure, Afterwards, pouring concrete started. For concreting the bored piles, the hollow stem auger was filled with concrete under its own weight (i.e. without pressure) and the auger was then pulled out of the ground using overhead crane without rotation. For CFA piles, a concrete pump was utilized to supply the concrete under pressure until the auger withdrawal was completed. The maximum delivery pressure at the pump outlet was 120 psi. The piles layout in the test pit is shown in Figure 4.2. Piles 1, 2, 3, and 4 were reinforced along their length with four 10M bars and 6M round stirrups every 15 cm. It was not possible to install the reinforcement cages into Piles 5 and 6 as the slump needed to be increased to facilitate the reinforcement cage insertion, thus they were not reinforced.

Piles 1 and 2 were bored piles, while piles 3, 4, 5 and 6 were CFA piles. Conventional concrete mixture (C0) was used in piles 1, 3, 5 and 6, while concrete mixture C1 was used in piles 2 and 4 (Figure 4.2). Table 4.1 illustrates the piles method of construction, material, and acronyms.

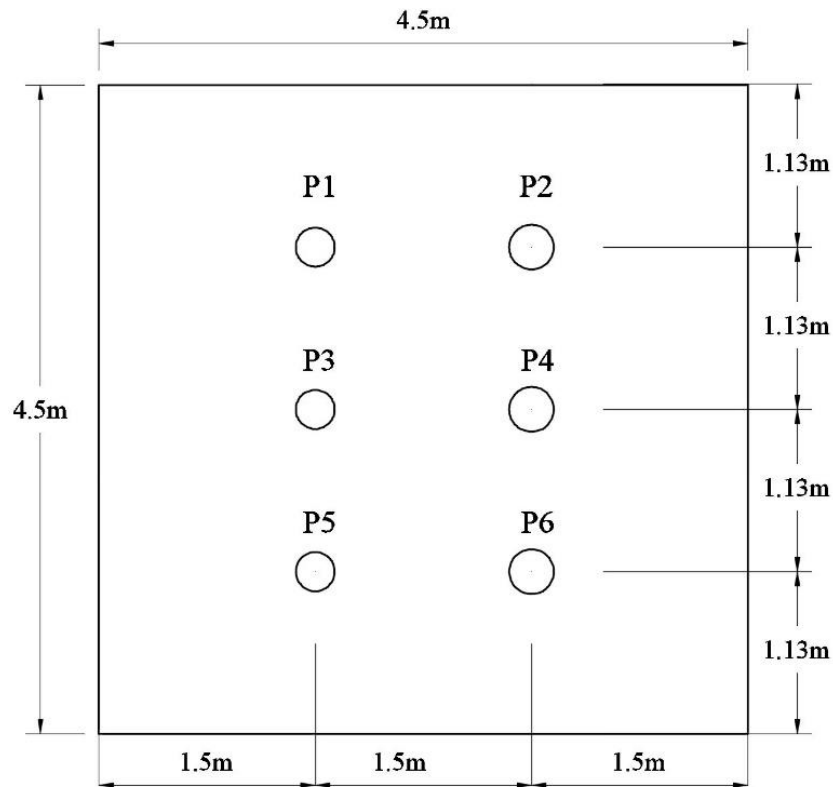


Figure 4.2 Piles plan

Table 4.1 Piles configuration

Pile	Type	Concrete mixture	Acronym
P1	Bored	C0	Bored C0
P2	Bored	C1	Bored C1
P3	CFA	C0	CFA C0
P4	CFA	C1	CFA C1
P5	CFA	C0	CFA C01
P6	CFA	C0	CFA C02

4.2.3 Piles instrumentation and testing setup

Figure 4.3 shows the compression test setup. The load was applied using a hydraulic jack with capacity of 996 kN and maximum stroke of 50 mm, reacting against a steel reaction beam affixed to the reinforced concrete wall of the test pit. The applied load at the pile head was measured using a load cell of 444 kN capacity, which was connected to a data acquisition system to record the load. The pile head was smoothed and leveled using a sulfur compound to ensure the load is distributed evenly. The vertical displacement was measured employing four linear variable displacement transducers (LVDTs) positioned across each other to measure any rotation in the pile head during loading. The average of the four LVDTs provided the displacement of the pile head at each load increment.

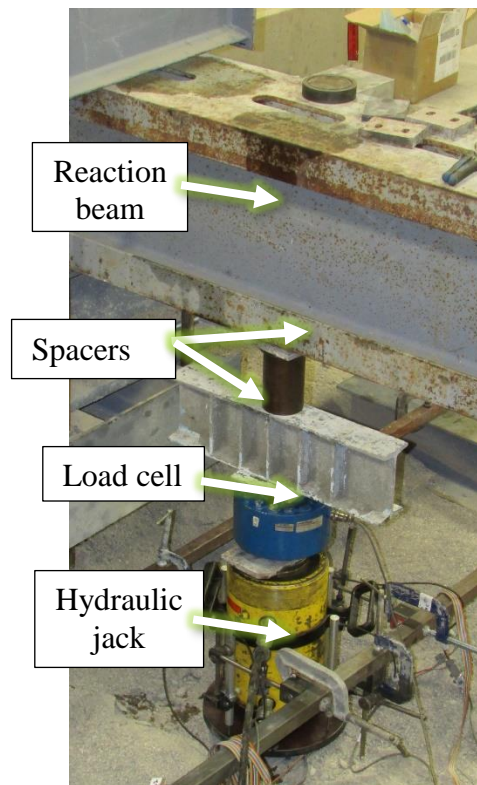


Figure 4.3 Compression test setup

Each pile was instrumented with strain gauges attached to the reinforcement cage at four levels spread along the pile shaft at distances from pile head of 0.88, 1.75, 2.63, and 3.50 m as shown in Figure 4.4a. Each strain gauge level comprised 4 strain gauges (Figure 4.4b) type CEA-06-250UW-120 provided by Micro-Measurements. The strain gauges were connected to the data acquisition system through lead wires that were protected by 3 layers of M coat A, 2 layers of M coat B Nitrile Rubber and 2 layers of silicon inside the concrete body. The load distribution along the pile shaft and the load transfer to the soil were calculated from the strain gauges' readings.

As mentioned previously, six piles were constructed but it was not possible to install the reinforcement in 2 piles as the concrete slump was low and reinforcement insertion was hard; hence, the piles without reinforcement were only tested in compression while the other piles were tested in compression, followed by uplift loading.

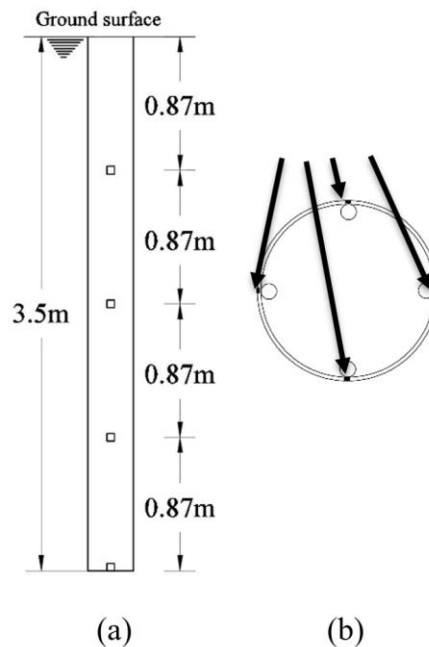


Figure 4.4 instrumentation distribution (a) along pile length (b) cross section

The compression and pullout pile load tests were performed according to ASTM D1143 (2013a) and ASTM D3689 (2013b) standards, respectively. Each compression and pullout load test consisted of a single cycle of loading from zero to maximum load, followed by unloading. The piles were pulled out through 8 threaded anchors embedded in the pile head.

The piles were exhumed after completing the load tests to investigate their effective diameters, interface properties (i.e. surface roughness, and soil-concrete friction angle), and compressive strength of concrete mixtures. The pile diameter was measured along its length to determine the actual diameter of the bored and CFA piles constructed with C0 and C1 mixtures. Direct shear test with constant normal stress was conducted to measure the skin friction mobilized at the soil-pile interface (Fioravante 2002). This was accomplished employing the direct shear test in accordance with ASTM D3080 (2011) for the sand and pile material interface. The shear box inside dimensions were 60 mm \times 60 mm and 25.5 mm height (Figure 4.5a). The applied normal stress ranged from 6 to 110 kPa, which simulated the range of in-situ confining stress for the test piles along the pile shaft. Slice specimens with dimensions 60 mm \times 60 mm were cut from the concrete surface of the pile (Figure 4.5b). Concrete cylinder cores were extracted from the center of the piles as shown in Figure 4.6. The cores were taken at the top, middle, and bottom of each pile to measure the in-situ compressive strength and the effect of pile installation method.

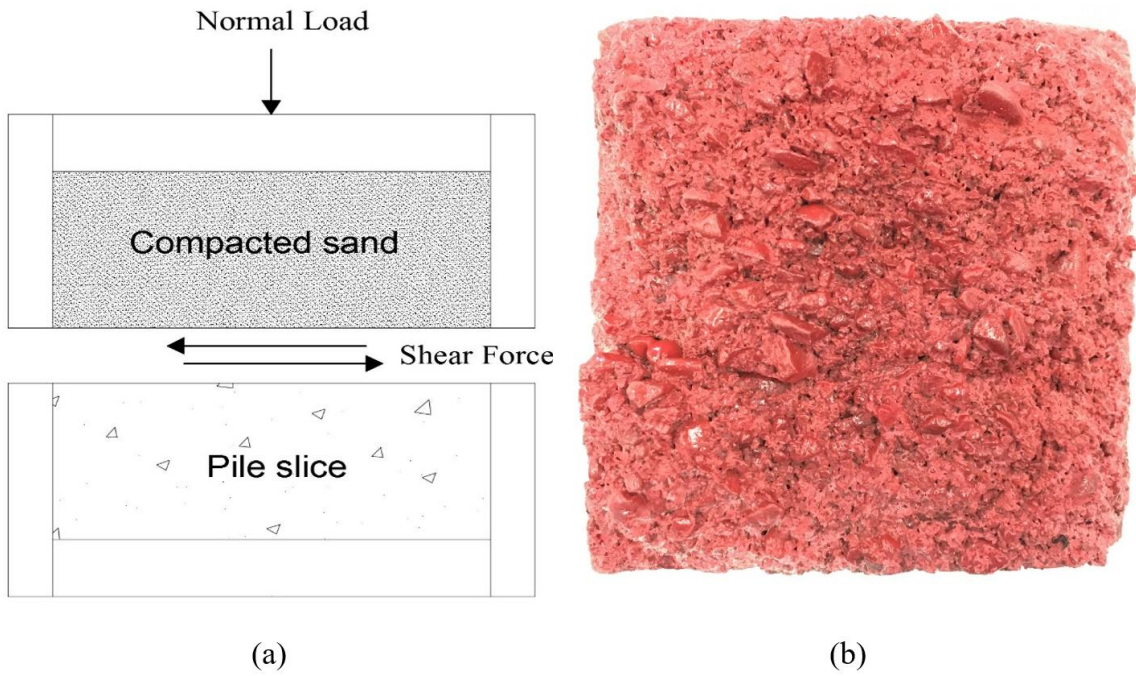


Figure 4.5 Direct shear (a) test configuration (b) sample slice

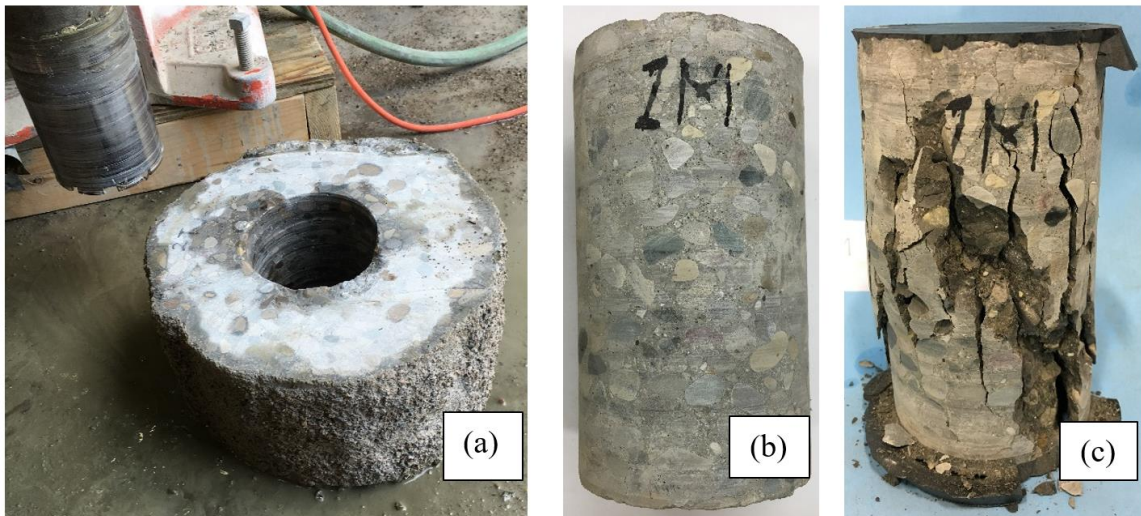


Figure 4.6 (a) pile coring process (b) Cylinder core specimen before and (c) after testing

4.3 Results and discussion

4.3.1 Compression test

4.3.1.1 Total load

The load-displacement responses of the test piles are shown in Figure 4.7. It is noted from Figure 4.7 that all piles displayed the same general load-displacement performance trend, but with varying initial stiffness (i.e. slope of tangent to load-displacement curve at initial load increments) and maximum load. The average initial stiffness of the CFA and bored piles were 90 and 50 kN/mm, respectively, which demonstrates the different behaviour of the two pile types.

The interpreted failure load (i.e. ultimate load) was defined as load applied at pile head corresponding to settlement equal to 10% of the pile diameter (Brown et al. 2007; Fleming 2009; Galbraith et al. 2014; Gavin 2009). Table 4.2 presents the ultimate load values of the tested piles. It can be seen from Figure 4.7 that the CFA piles exhibited much higher ultimate load capacity compared to the bored piles. This can be attributed to the additional confining pressure induced by the concrete pressure during installation, increase in pile diameter and improved piles' surface properties (at the macro scale). The average CFA piles ultimate load was about double that of the bored piles which can be attributed to the construction method which increased the surrounding soil stiffness, pile diameter, and pile surface roughness. This value agrees with the increase reported by (Busch et al. 2010) (i.e. 67% increase).

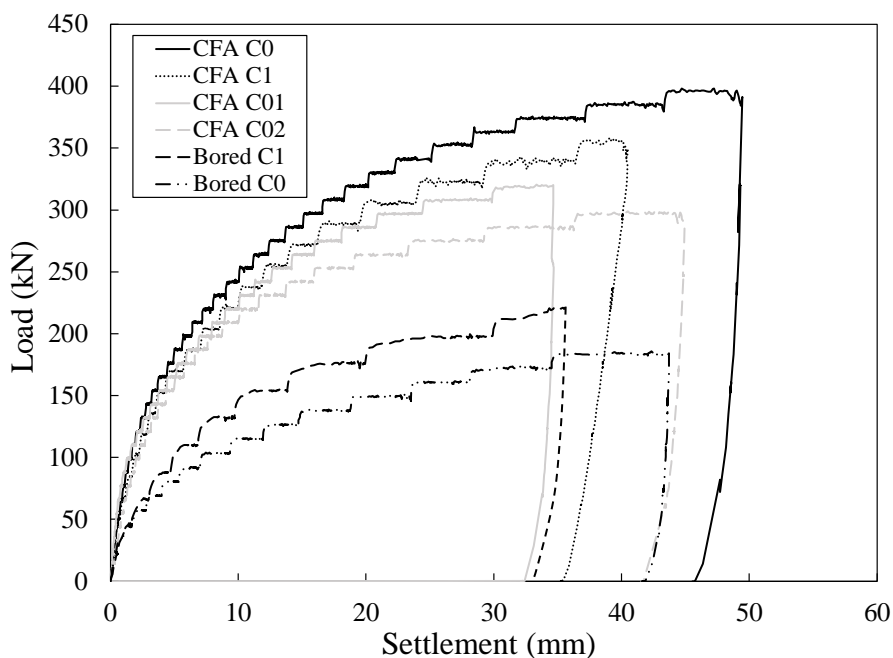


Figure 4.7 Load-displacement curves for test piles

Table 4.2 Piles ultimate load

Pile	Ultimate load (kN)
CFA C0	375
CFA C1	340
CFA C01	306
CFA C02	275
Bored C0	160
Bored C1	195

The behaviour of the piles incorporating TOSW was similar to that of the control pile (i.e. conventional concrete mixture). The average ultimate load of piles CFA C0 and CFA C01 was 340 kN, which is equal to that of CFA C1 pile. Pile CFA C02 had lower ultimate load which can be attributed to their smaller pile diameter as will be discussed later. The ultimate capacity of the bored pile C1 was larger than that of bored pile C0 by about 20%. On the

other hand, pile CFA C1 compressive capacity was lower than that of pile CFA C0 by 10%. Hence, this indicates that the incorporation of TOSW has indiscernible effect on the geotechnical capacity of the pile.

4.3.1.2 Shaft resistance

The strain gauge readings were used to calculate the load distribution along the pile. The axial force at each strain gauge (P_s) was calculated based on the strain gauge reading as follows:

$$P_s = \varepsilon A_p E_p \quad \text{Eq. 4.1}$$

where, ε is the measured strain, A_p is the actual average pile diameter, and E_p is the elastic modulus of the pile. The modulus of elasticity of the piles was calculated based on the elastic modulus of concrete and the cross-section of the pile and the reinforcement steel as follows:

$$E_p A_p = E_c A_c + E_s A_s \quad \text{Eq. 4.2}$$

where, A_p is the corresponding cross section area, $E_c = 36$ or 31 GPa is the elastic modulus measured for concrete mixture C0 or C1, respectively, and $E_s = 210$ GPa is the elastic modulus of the steel reinforcement.

The loading tests continued until the final settlement reached more than 10% of the nominal pile diameter, which exceeds the interpreted failure load. The load transferred to soil was calculated as the difference between the loads at different strain gauge levels. The shaft load was considered as the applied load minus the end bearing load. While, the bearing

load is obtained from the bottom strain gauge reading. The shaft load-settlement curves obtained for four piles are shown in Figure 4.8a, while their base load-settlement curves are presented in Figure 4.8b,

The shaft resistance of CFA piles was significantly higher than that of the bored piles over the entire range of loading (i.e. both stiffness and capacity of CFA piles are higher than that of bored piles). In addition, the load transfer of different piles was evaluated at the same pile head displacement of 25 mm for the sake of comparison. At this displacement level, the shaft resistance contributed 77% of the total load supported by the CFA piles, while the shaft resistance contributed only 66% of the total capacity for the bored piles. The shaft friction for piles CFA C01 and CFA C02 was estimated based on the ratio of the load transferred by the shaft to the total load for piles CFA C0 and CFA C1. This improvement in CFA pile shaft resistance is attributed to its installation method. It was also observed that the shaft resistance at 25 mm pile head displacement for the CFA C1 pile was 12% less than that of CFA C0 pile. Thus, it could be concluded that incorporating TOSW in the pile's concrete mixture had no effect on its geotechnical performance.

Figure 4.8b shows that the end bearing resistance of the CFA piles was significantly higher than that of the bored piles due to increased diameter of CFA piles.

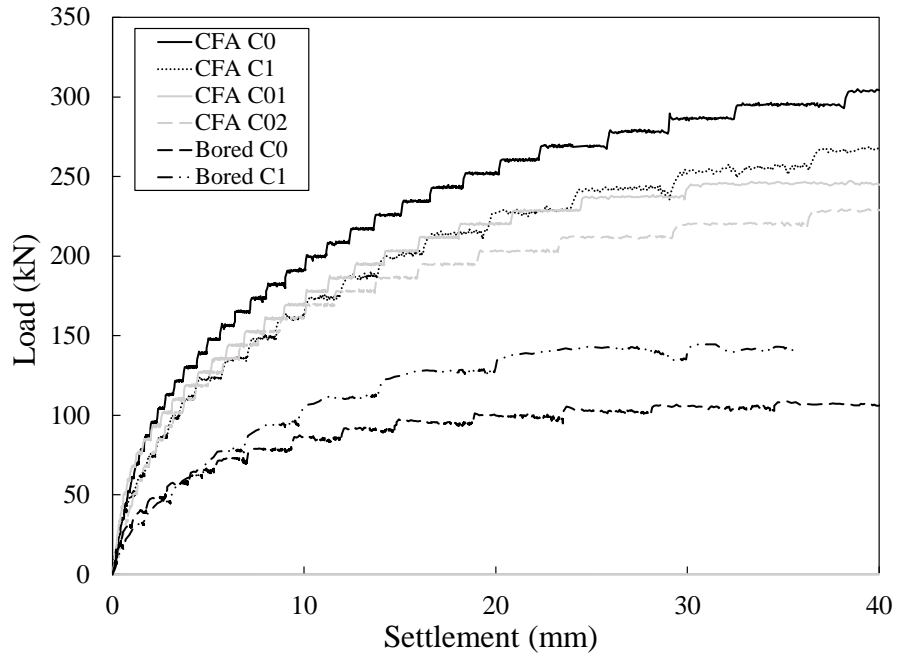
Figure 4.9 shows the average mobilized shaft resistance (τ_{avg}) for all piles during the compression test versus the normalized pile head settlement (w/D (%)) considering the actual pile geometry. The ultimate τ_{avg} value for the CFA piles was significantly higher than that of the bored piles, suggesting that the radial soil displacement during concrete pumping increased the soil coefficient of lateral earth pressure, which in turn increased the

shaft friction. The maximum average shaft resistance for the bored piles was 18 kPa and has been fully mobilized at normalized pile head displacement of 4 to 5 % of pile diameter. On the other side, The CFA piles shaft friction kept increasing until it reached the maximum stress at 10 % of pile diameter.

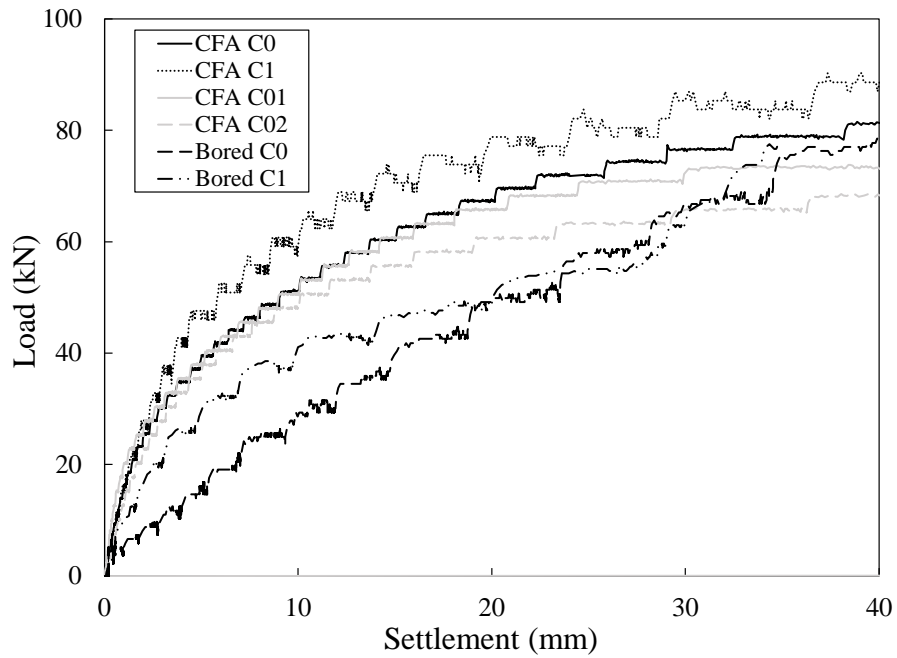
The shaft friction can be calculated using the conventional formula:

$$f_{su} = K_s * \sigma_o * \tan \delta \quad \text{Eq. 4.3}$$

where, K_s is the coefficient of lateral earth pressure, σ_o is the vertical earth pressure, and δ is the interface friction angle between the pile surface and the soil (Table 4.3). The interface friction angle was found to be higher than the angle of internal friction (ϕ) as discussed later. Therefore, the angle of interface friction angle used in the calculations was equal to angle of internal friction angle (i.e., 43°) as the failure occurred within the soil surrounding the pile surface. The coefficient of lateral earth pressure was back-calculated from the measured shaft friction and it was found to be 1.6 and 0.8 for the CFA and bored piles, respectively. The higher value of K_s for CFA piles should be attributed to higher concrete pressure experienced at the end point because of its shorter supply line length and hence lower resistance.



(a)



(b)

Figure 4.8 (a) Shaft resistance (b) End bearing

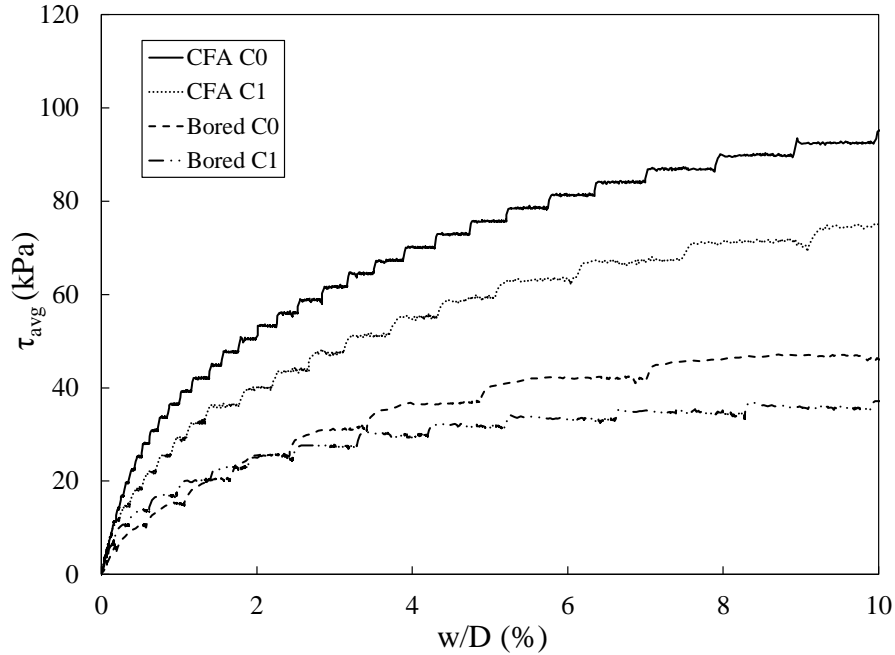


Figure 4.9 Shaft shear stresses variation with relative pile movement

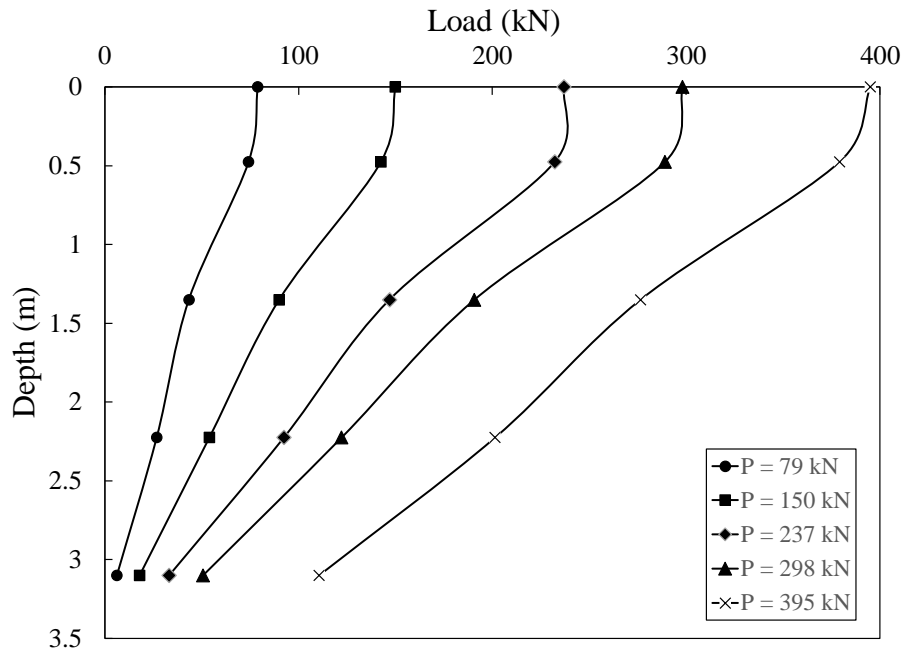
Table 4.3 Soil-concrete interface properties

Interface	ϕ°	δ_p°	δ_r°	δ/ϕ	$\tan\delta/\tan\phi$
CFA C0	43	51	45	1.18	1.28
CFA C1	43	51	43	1.18	1.32
Bored C0	43	49	45	1.14	1.37
Bored C1	43	48	43	1.12	1.23

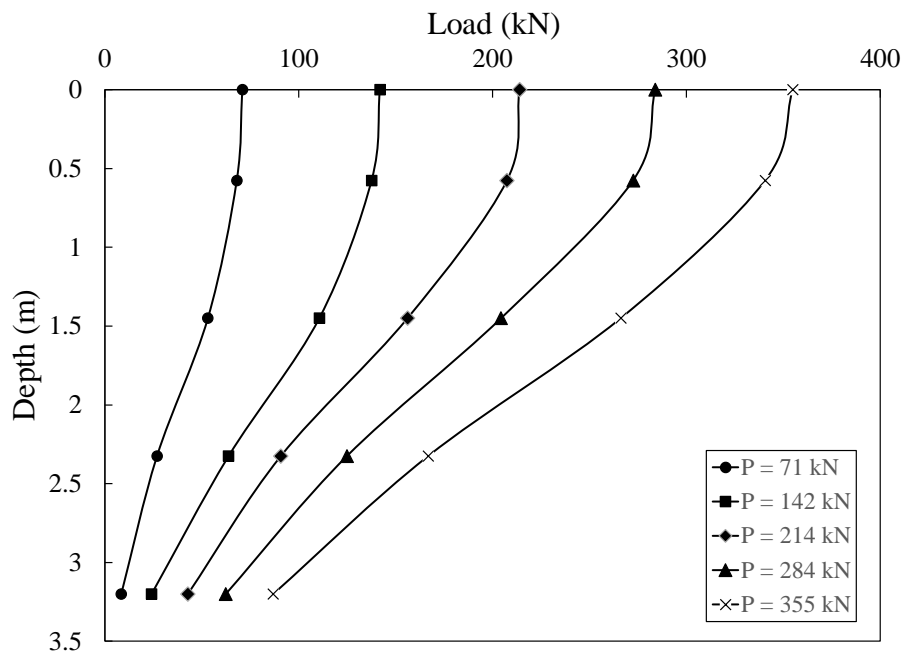
The load distribution and unit shaft friction distribution along the pile shaft are illustrated in Figure 4.10 and Figure 4.11, respectively. It is noted from Figure 4.10 that the load distribution pattern along the bored piles was following the same trend as that of the CFA piles. Similarly, Figure 4.11 shows that the unit shaft friction distribution along pile was the same for all piles except for pile CFA C0, which exhibited lower unit shaft friction at depth equal to 2 m. The reduction in resistance at this elevation is attributed to a drop in concrete pumping pressure during installation, which resulted in reduced pile diameter.

The maximum unit shaft friction value was observed at about two third of the piles length.

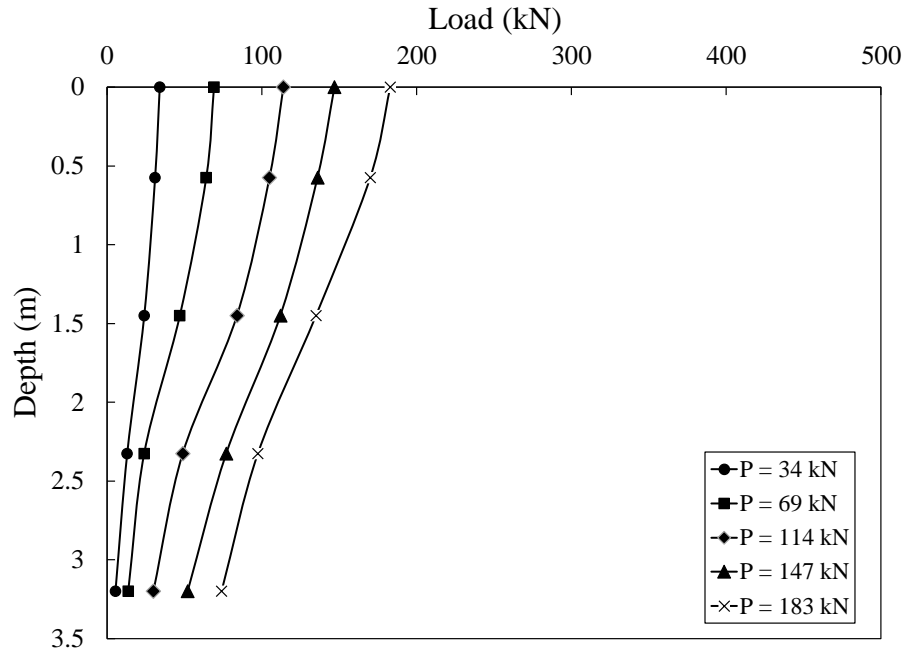
The maximum unit shaft resistance for both CFA piles was about 120 kPa, while it varied from 50 to 80 kPa for the bored piles.



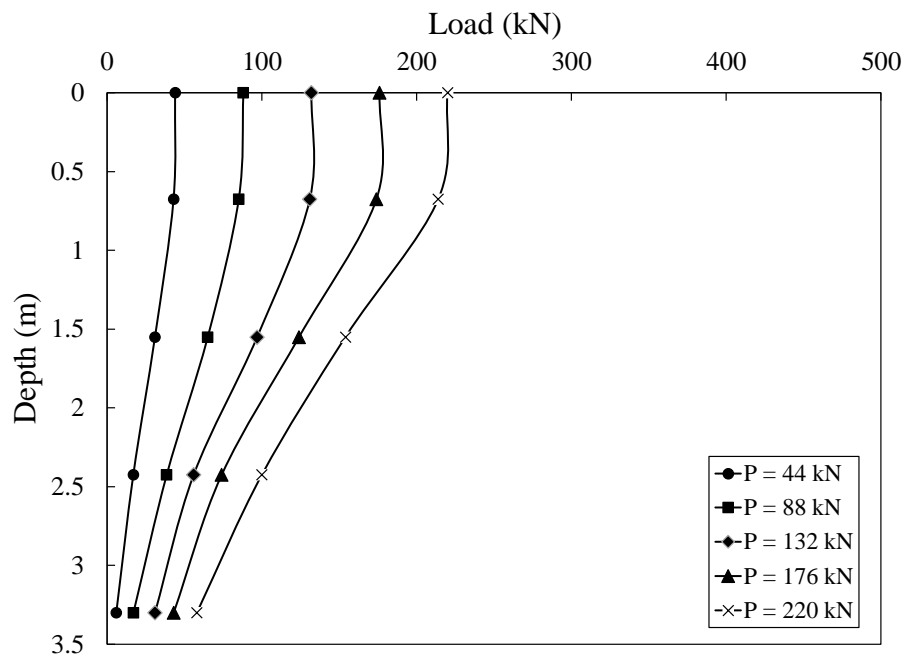
(a)



(b)

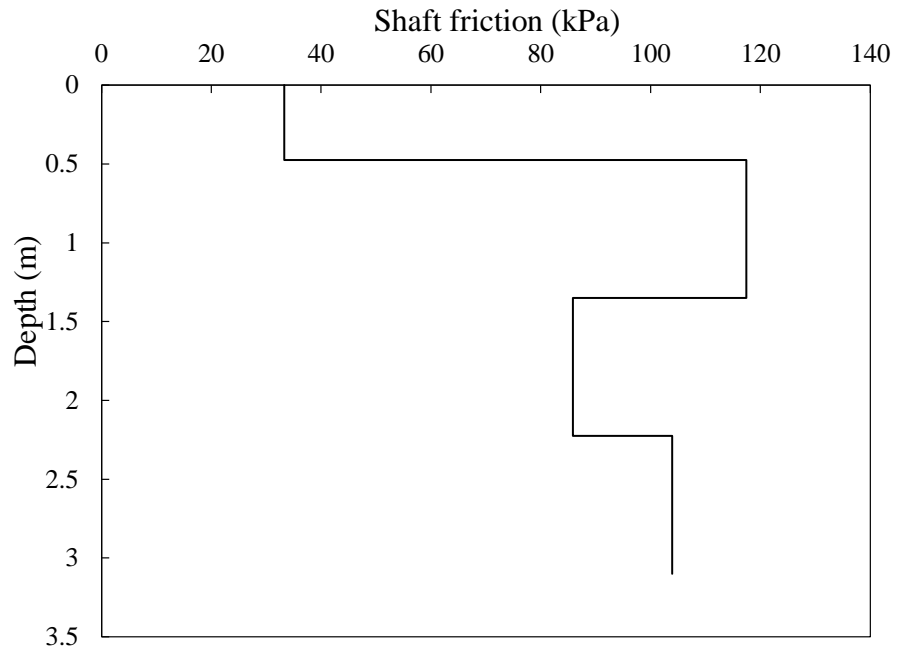


(c)

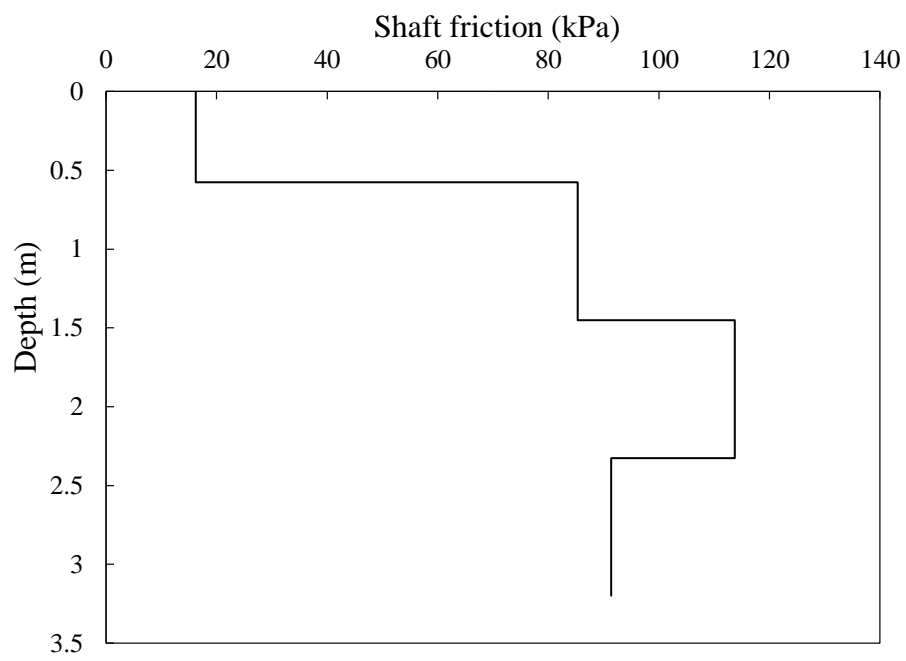


(d)

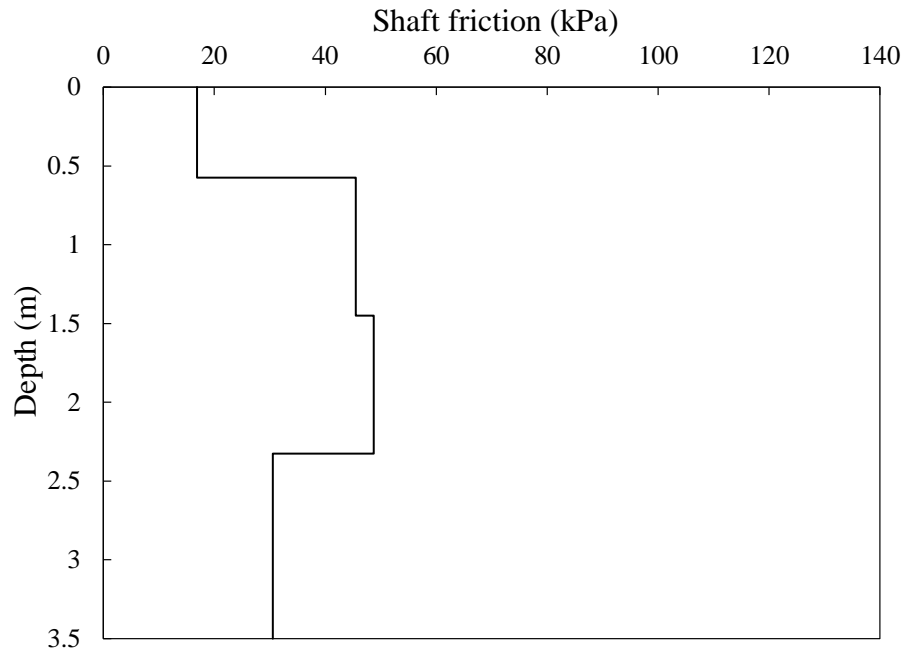
Figure 4.10 Shaft load distribution along pile, (a) CFA C0, (b) CFA C1, (c) Bored C0, (d) Bored C1



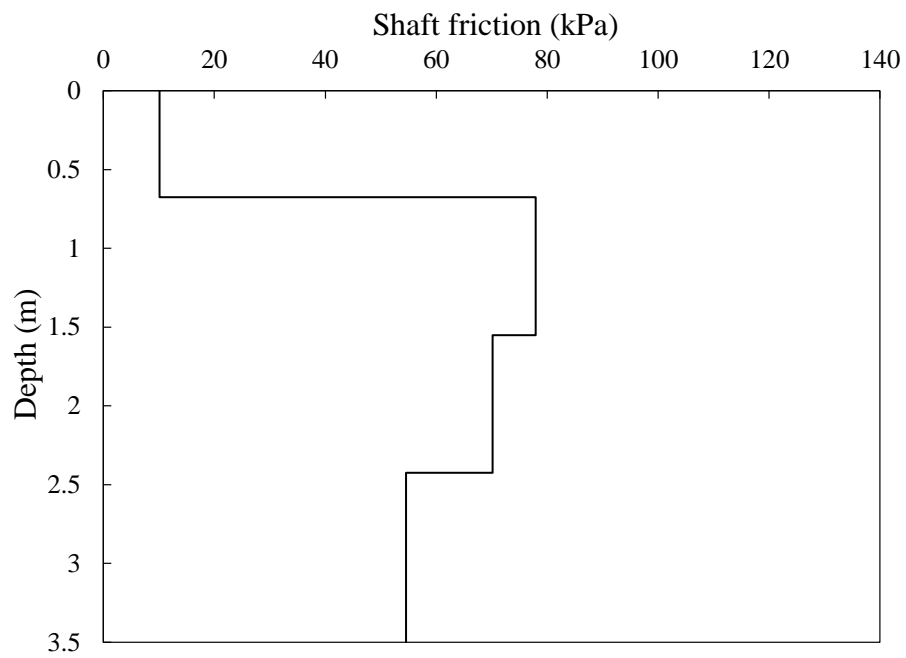
(a)



(b)



(c)



(d)

Figure 4.11 Axial load distribution along pile, (a) CFA C0, (b) CFA C1, (c) Bored C0, (d) Bored C1

4.3.1.3 End bearing

The variation of end bearing load with pile head displacement for the six piles are shown in Figure 4.8b. The end bearing for piles CFA C01 and CFA C02 was estimated based on the ratio of the load transferred by the end bearing to the total load for piles CFA C0 and CFA C1. As can be noted from Figure 4.8b, the end bearing resistance values for CFA piles were close to each other, and were much higher than the end bearing resistance of the bored piles. In addition, the toe stiffness of the CFA piles, defined as the initial slope of end bearing load-displacement curve, was almost identical and much higher than the stiffness of the bored piles. As the applied load increased, the CFA piles stiffness remained high and both piles CFA C0 and CFA C1, continued to display similar response. The end bearing resistance at 25 mm pile head movement represented 21% and 25% of the total applied load supported for piles CFA C0 and CFA C1, respectively. However, the end bearing load of pile CFA C1 was higher than pile CFA C0 by 13% at 25 mm displacement.

The end bearing resistance of bored piles was initially different from each other, as Pile C0 displayed much softer response than Pile C1. This may be attributed to the disturbance of the soil at the toe of Pile C0 during installation was greater than that of Pile C1. However, at 20 mm settlement both piles displayed almost the same end bearing resistance. The proportion of the total load supported by the pile toe at 25 mm settlement for bored pile C0 and bored C1 was 35% and 28%, respectively. The end bearing of the bored piles, at 25 mm settlement, was lower than that of the CFA piles by about 35%.

The installation method of the piles has also an effect on the pile cross-sectional area and hence its load carrying capacity. To understand the behaviour at the pile toe, end bearing

stress (toe load over cross-sectional area) was plotted against relative pile head movement (w/D %) (Figure 4.12). Except for pile Bored C0, the bearing stresses of all pile was close to each other with the CFA slightly higher than the bored piles. As mentioned previously, it appears that the soil at the toe of bored pile C0 was disturbed more than the other piles.

4.3.2 Pullout test

The results of the pullout test on the four piles are presented in terms of load-displacement curves as shown in Figure 4.13. Pile CFA C0 pullout test was stopped, at 25 mm displacement, after the anchors were pulled out from the pile head as can be noted from Figure 4.13, the uplift resistance of both CFA piles was almost 100% higher than that of the bored piles at 25 mm movement. This could be attributed to the densification experienced by the soil around the CFA piles during installation. Initially, the slope of the load-displacement curve was high due to the pile self-weight. As the applied uplift load exceeded the pile weight, the slope of the load-displacement curve (i.e. the uplift stiffness of the pile) decreased. It is noted that this stiffness was lower than the observed stiffness during the compressive loading. The difference in stiffness may be attributed to the absence of the end bearing resistance. However, CFA piles displayed stiffer response than bored piles, especially as the displacement exceeded 20 mm. In addition, the uplift load for pile CFA C0 at 25 mm was 20% higher than that of Pile CFA C1. On the other hand, the uplift load of bored pile C1 was higher than pile Bored C0 by about 58%.

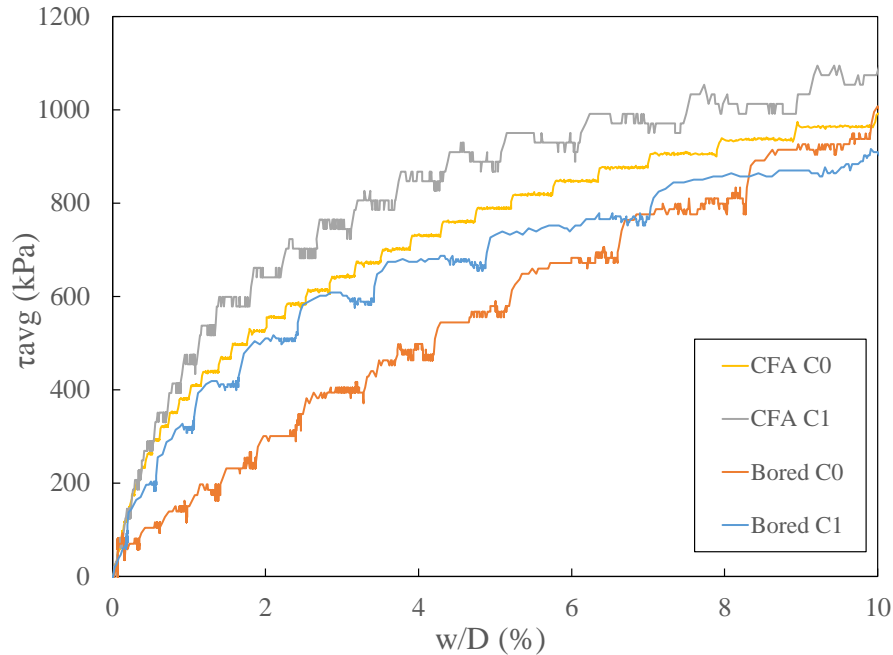


Figure 4.12 End bearing stress

The variation of the unit shaft resistance during pullout test with pile head relative movement is shown in Figure 4.14 . The unit shaft resistance increased almost linearly throughout the pullout tests. The initial linear behaviour may be attributed to the residual shear stress associated with the large displacement that occurred during the prior compression loading. At 5% relative movement, the unit shaft friction of pile CFA C0 was higher than that of pile CFA C1 by about 6%. At the same relative displacement, bored pile C0 unit shaft friction was 56% of that of bored pile C1. The values of the unit shaft friction measured in pullout test was found to be lower than the average values obtained during the compression test. This difference may be attributed to the loading history of the piles, which can reduce the shaft friction up to 53% (Joshi et al. 1992).

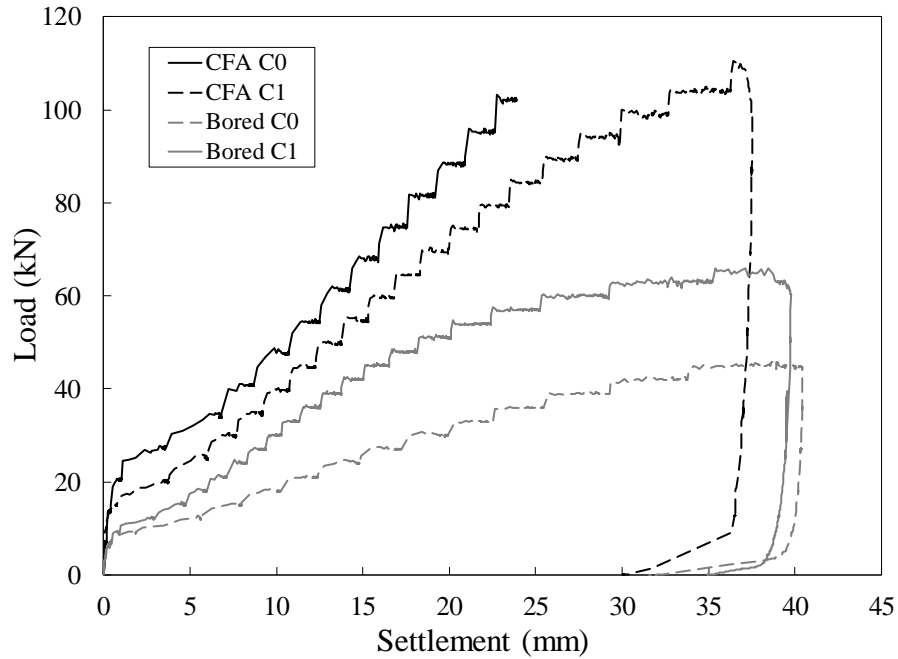


Figure 4.13 Pullout load-displacement curves

Figure 4.15 shows the load distribution during pullout along each pile. It can be noticed the difference in resistance between CFA and bored piles in the first one meter. For example, the load transferred through the pile to depth 0.75 m decreased by about 12% in the CFA pile and by about 30% for the bored pile.

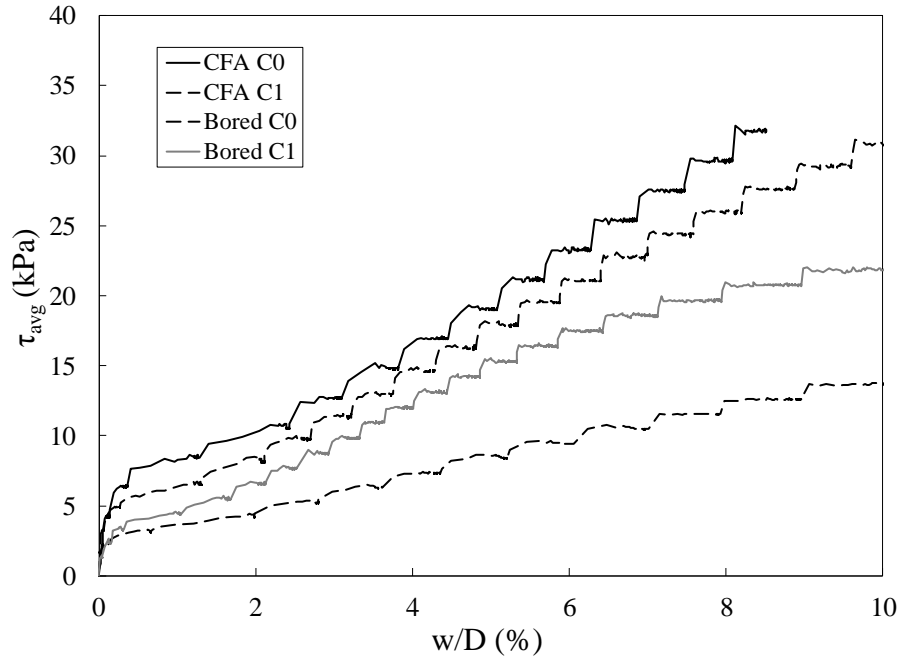
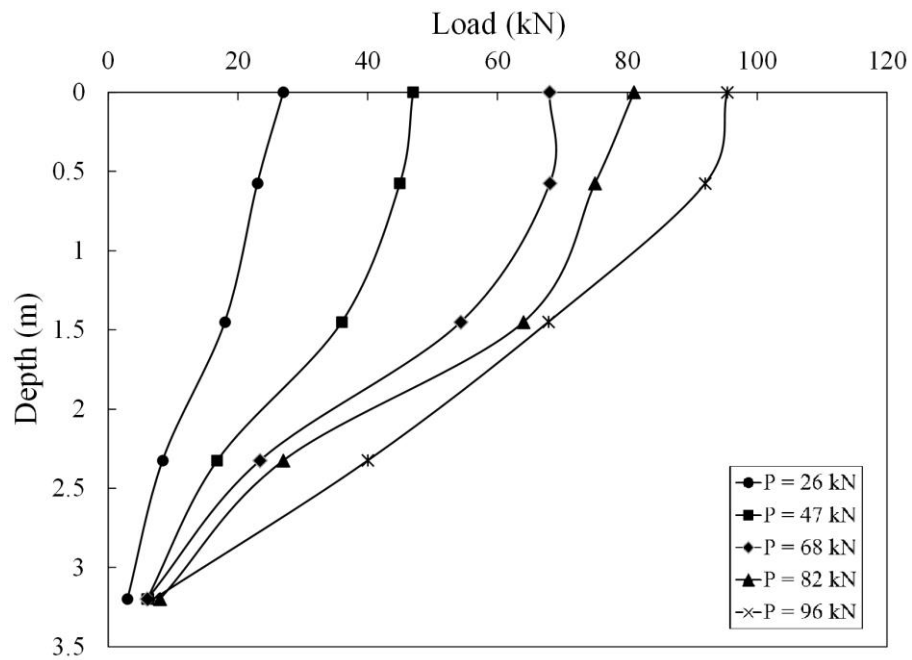
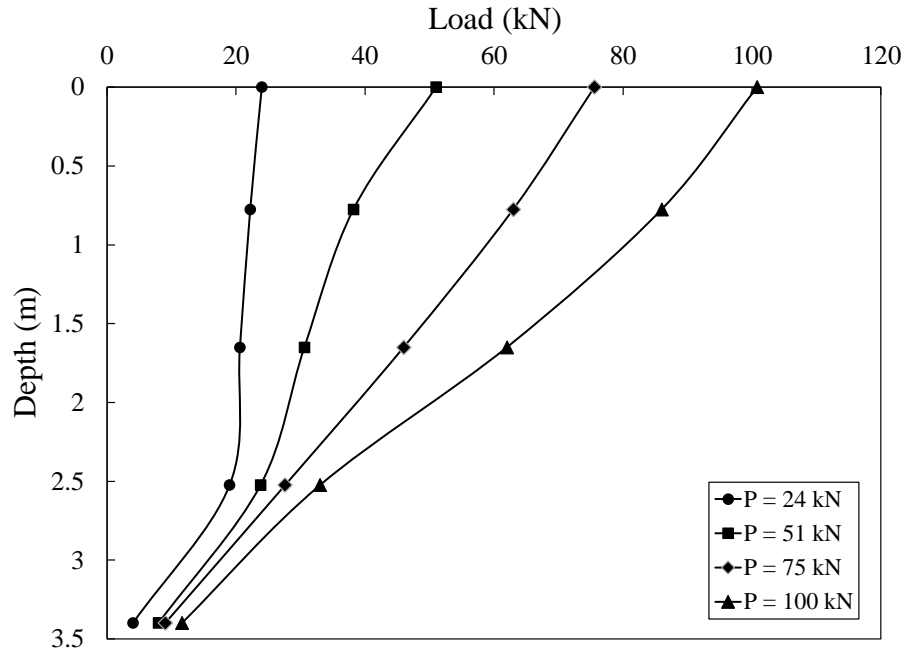


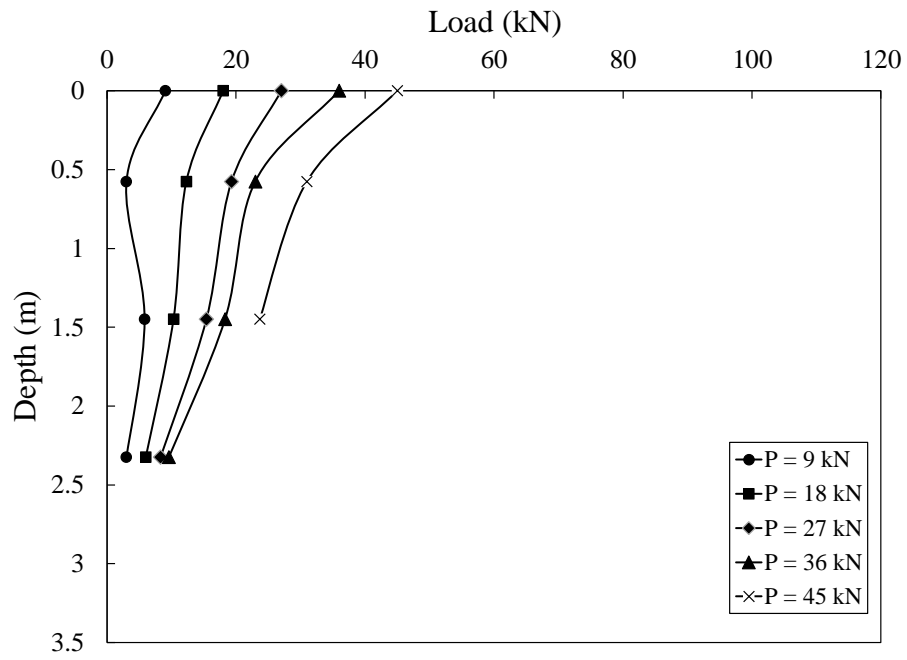
Figure 4.14 Skin friction vs relative pile head movement



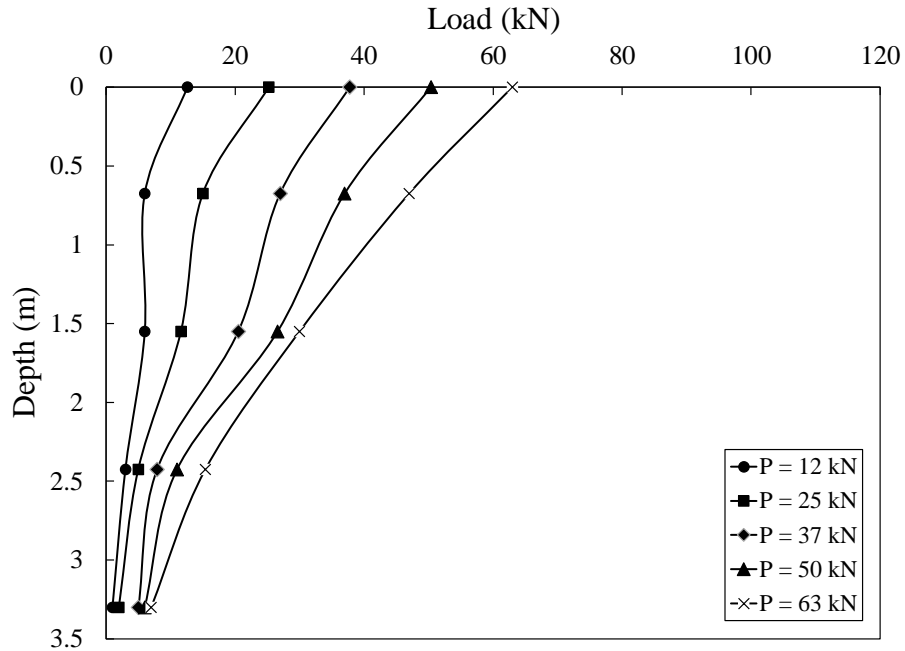
(a)



(b)



(c)



(d)

Figure 4.15 Load distribution along the piles, (a) CFA C0, (b) CFA C1, (c) Bored C0, (d) Bored C1

4.4 Pile surface

4.4.1 Piles profile

CFA and bored piles were exhumed after completing the load tests as shown in Figure 4.16a. Figure 4.16b shows the variation of measured diameter along each pile length. The average diameter for the test piles was found to be 318, 314, 315, 241, 284, and 282 mm for piles CFA C0, CFA C1, CFA C01, CFA C02, Bored C0, and Bored C1, respectively. It was found that the CFA piles diameter and total volume were about 13% and 28%, respectively, larger than the bored piles.

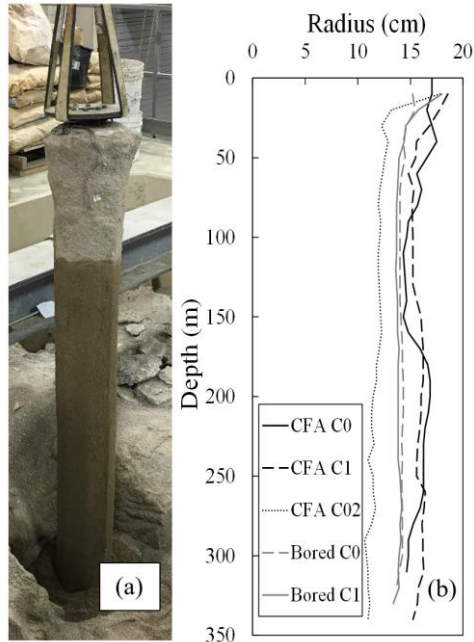


Figure 4.16 Pile profile, (a) pile extraction, (b) cross section

Furthermore, Figure 4.17a shows a cut through the cross-section of a bored pile. The pile cross-section consisted of reinforcement bars, concrete and a layer of cemented sand. The thickness of the cemented sand layer in the CFA ranged from 2 to 9 mm (Figure 4.17b), while it varied between 1 and 4 mm for the bored pile (Figure 4.17c). The increased thickness of the cemented sand layer in the CFA pile may be attributed to the permeation of concrete into the surrounded sand due to the concrete pumping pressure during construction. Thus, the surface roughness of the CFA piles was higher than that of the bored piles.

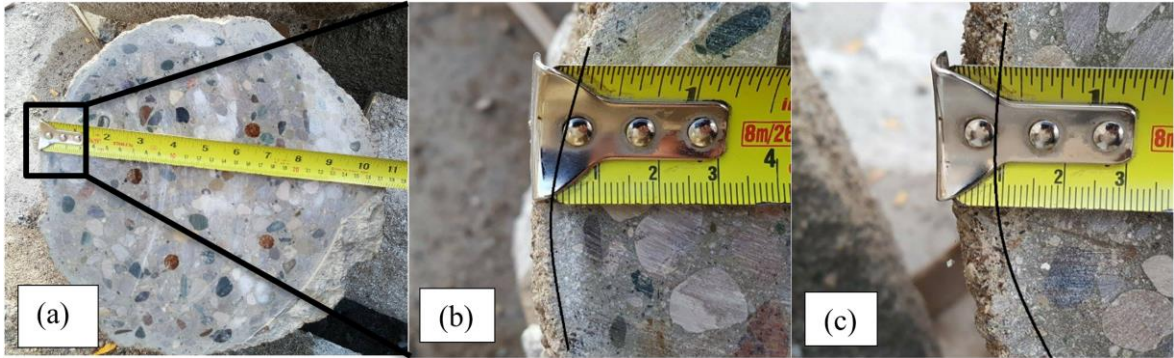


Figure 4.17 Pile sand cover intrusion (a) pile cross section, (b) bored pile, (c) CFA pile

4.4.2 Compressive strength of in-situ concrete

Three cross sections were cut from each pile as shown in Figure 4.6a. The cross sections were cut from the top, middle, and bottom of the pile to access the concrete compressive strength. Cores were extracted from the cross sections as shown in Figure 4.6b using Husqvarna diamond coring machine. The diameter of the samples was 9.2 mm and the height to diameter ratio ranged from 1.9 to 2. The compressive strength test was performed according to ASTM C39 (2016), and the results were presented as the average of three tests in Table 4.4. The lowest compressive strength measured was that of the bored C1 pile. However, it was higher than the minimum compressive strength specified by FHWA(Brown et al. 2007) by about 45%. The average compressive strength of the CFA piles was found to be higher than the bored pile by about 19%. The higher compressive strength of the CFA pile is attributed to the compaction of the concrete due to pumping pressure during pile installation (Gambhir 2013; Gonen 2016; Jamwal 2014).

4.4.3 Direct shear surface roughness

Figure 4.18 shows the results of direct shear tests between sand and slices from the piles surface. The interface friction angle (δ) results were close for all piles. The values ranged between 49° and 52° with an average value of 50° . The residual friction angle was in the range 43° to 45° (Figure 4.19). The difference between the peak and residual interface friction angle of the piles with or without TOSW was insignificant. Table 4.3 shows the results of conducted tests and the ratio between the interface friction angle and the sand angle of internal friction (δ/ϕ).

Table 4.4 Extracted cores compressive strength

Pile	Strength (MPa)
CFA C0	63
CFA C1	59
Bored C0	55
Bored C1	51

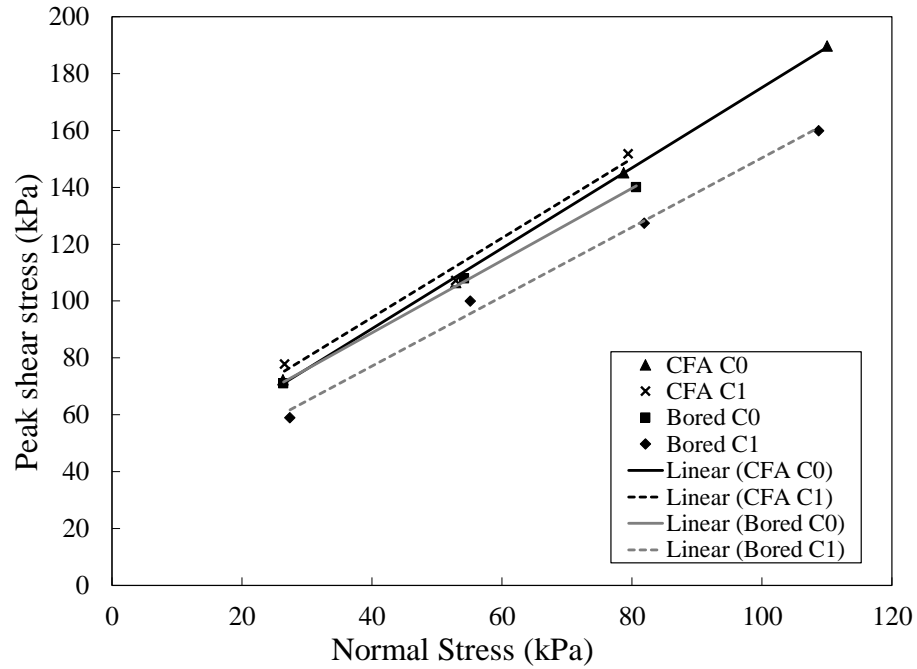


Figure 4.18 Soil-concrete peak interface friction angle using direct shear test

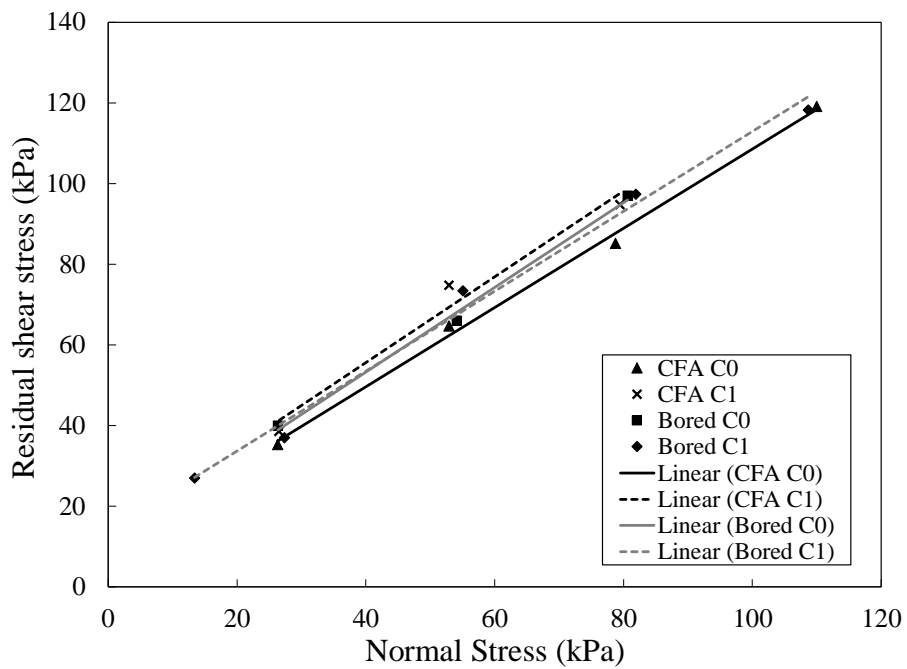


Figure 4.19 Soil-concrete residual interface friction angle using direct shear test

Interface friction angle of all piles was about the same, indicating a negligible effect of the method of installation or the type of concrete on that parameter. However, visual inspection showed a distinctive horizontal orientation for the particles on the CFA pile surface (Figure 4.20a) compared with the scattered particles on the bored pile surface (Figure 4.20b). The value δ was found to be higher than ϕ , indicating that the failure surface is going to be within the shear band of soil adjacent to the pile. The high interface angle can be attributed to the high surface roughness and the protruded particles from the pile surface. This would lead to particles rolling over each other inducing dilation and higher resistance. Similar behaviour was observed by (Giraldo and Rayhani 2013) between grout and clay and by (Chu and Yin 2006) between granite and cement grout.

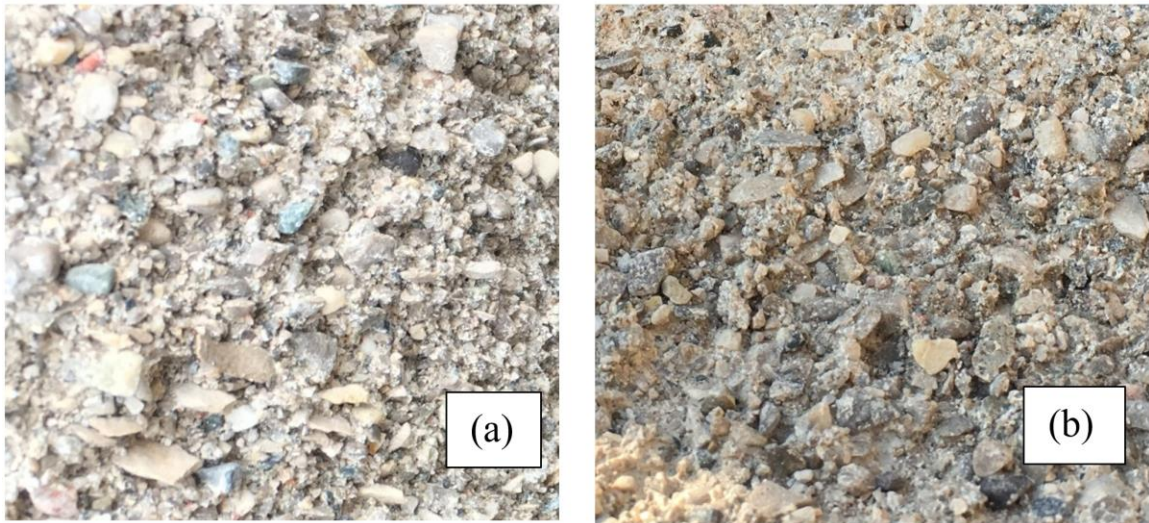


Figure 4.20 Particles orientation on the piles surface, (a) CFA pile, (b) bored pile

4.4.4 Roughness fractal dimension

The term “fractal” is associated with a scale-invariant object, which has similar features in all scales of view. The fractal geometry theory offers a powerful means for evaluating surface roughness. Several researchers have shown the possibility of quantifying roughness of natural rock joints and numerous empirical relationships have been proposed to estimate the joint roughness coefficient of a rock surface based on its fractal dimension (Kulatilake et al. 1997; Kulatilake and Um 1999; Li and Huang 2015). (Choi 2011) used fractal dimension as a measure of roughness to quantitatively analyze the effects of pile surface roughness on adfreeze bond strength. Recently, (Chen et al. 2015) examined the effect of surface roughness on interfacial shear behaviour of clay-concrete interface comparing the results of fractal dimension method with other roughness evaluation methods.

Several methods have been suggested in the literature to assess fractal dimension of rough profiles (Feder 2013). A compass-walking method was employed herein to determine fractal dimension of surface roughness for the different types test piles. The main concept of this method is to measure a curve by “walking a compass of radius r ” along the roughness profile as shown in Figure 4.21. For each compass of a certain radius, the number of divider steps, N , required to cover the entire profile is counted, and then multiplied by the span radius, r , to give an estimate of the profile length, L . The fractal dimension, D_R , is calculated by plotting N versus r in a log–log space and equating the slop according to:

$$D_R = -\frac{\Delta \log N}{\Delta \log r} \quad \text{Eq. 4.4}$$

The method was modified by (Bae et al. 2011) by measuring the remaining length shorter than the span radius, f , after excluding the length of Nr for the total profile length. Thus, the fractal dimension D_R , is calculated from:

$$D_R = - \frac{\Delta \log(N + f/r)}{\Delta \log r} \quad \text{Eq. 4.5}$$

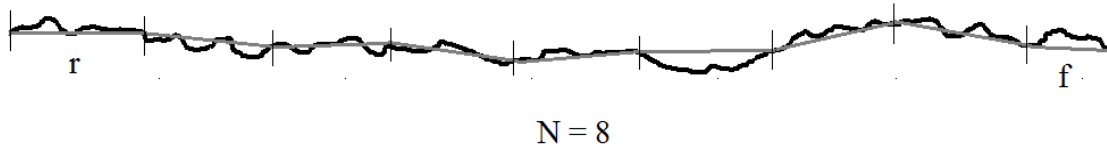


Figure 4.21 Schematic of compass-walking method for determination of fractal dimension of a profile

The roughness fractal dimension, D_R , of pile surface could be determined by fitting a regression line to the $\log(N + f/r) - \log(r)$ data obtained from compass-walking method. Figure 4.22 provides plots of roughness data used to attain the fractal dimensions for typical profiles of CFA and bored piles. To obtain a representative value of surface roughness for bored and CFA piles, 10 profiles at different locations along a typical pile shaft are used for each pile. The profiles of CFA and bored piles are denoted by C1-C10 and B1-B10, respectively.

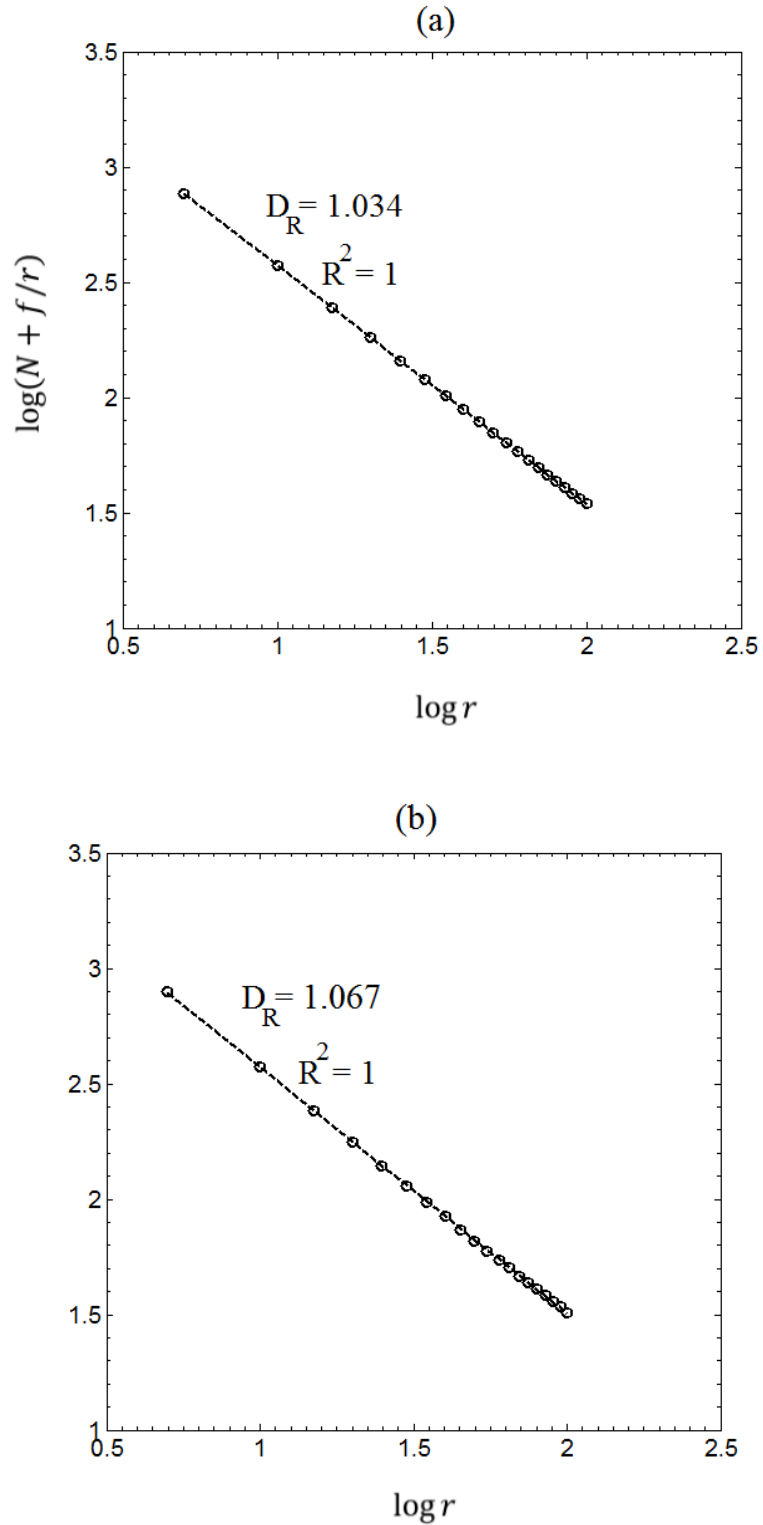


Figure 4.22 Schematic of compass-walking method for determination of fractal

dimension of a profile, (a) Bored pile, (b) CFA pile

Figure 4.23 presents all the surface profiles employed to evaluate the corresponding fractal dimension as a measure of surface roughness for each type of CFA and bored pile shafts. As illustrated, the fractal dimensions of shown profiles for the CFA piles varies from 1.049 to 1.110 with an average value of 1.069, while the roughness dimensions for the bored piles varies from 1.026 to 1.044 with an average value of 1.034. It is evident that the CFA piles surfaces provide rougher surface topology compared to the bored piles due to the difference in construction method that leads to formation of thicker shear band in the pile-soil interface.

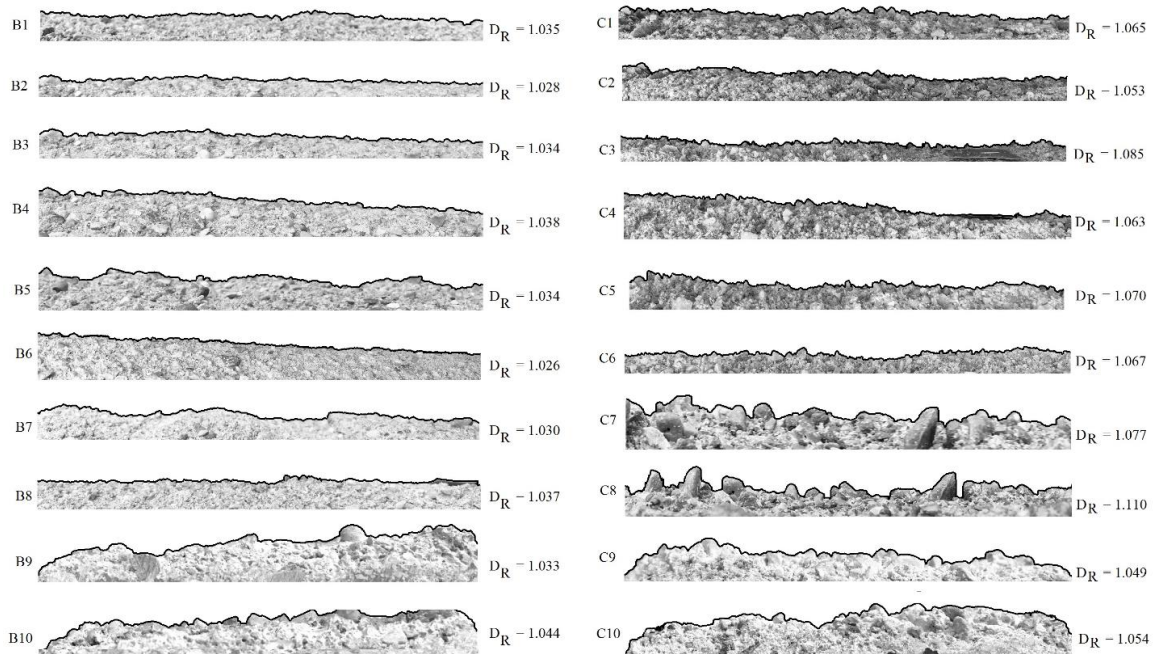


Figure 4.23 Profile of pile surface used to calculate D_R for different profiles of a) bored pile (labeled by B1-B10), b) CFA pile (labeled by C1-C10)

In fact, the pressurized concrete (or grout) used for the CFA piles' construction would result in higher penetration of concrete particles into the surrounding soils, and therefore, more complex particle-interlocking mechanisms. Additionally, the narrower range of

roughness values (i.e. smaller variance) in the bored piles indicates that there is a more uniform surface roughness along the bored piles compared to the CFA piles. The heterogeneity of surface roughness in the CFA pile could be due to variations in penetration and pumping rate during its construction procedure.

4.5 Conclusions

The behaviour of CFA and bored piles constructed with and without TOSW in sand was evaluated experimentally. This study and its results are limited to apply in sand soil. The length of the piles tested was limited to 3.5 m and by increasing the pile length in real life applications the results may differ. The piles were also constructed by graduate students which may be different from real life construction by technicians. The following conclusions can be drawn:

- The ultimate capacity of the CFA piles was approximately twice the capacity of bored piles.
- Incorporating TOSW in the piles concrete mixtures has insignificant effect on their geotechnical performance.
- For CFA piles, the shaft friction supported 77% of the total load, while for bored piles it contributed 66% of the total load capacity.
- The unit shaft resistance of the CFA piles was higher than the bored piles with maximum value of about 120 kPa.
- The unit end bearing resistance was similar for all piles. However, the CFA piles end bearing load was higher because of its larger cross-sectional area.

- The shaft friction measured in the pullout test was about 40 to 50% of that measured in the compression test due to the loading history, regardless of the pile type.
- The construction process of the CFA piles has increased its diameter by 25%.
- Concrete strength of CFA piles was higher than that of the bored piles due to the pressure applied on the concrete during piles construction.
- The shear failure around the pile happened in the soil in the shear band around the pile. The shear band thickness existed around the piles increased as the surface roughness increased.
- The concept of fractal dimension can be employed as a quantitative measure to evaluate roughness of pile surface. It is found that the CFA piles had a higher value of roughness fractal dimension compared to that of bored piles, which is mainly due to more complex particle-interlocking mechanism of CFA piles during the construction process.

4.6 References

2011. Standard Test Method for Direct Shear Test of Soils Under Consolidated Drained Conditions. ASTM International.
- 2013a. Standard Test Methods for Deep Foundations Under Static Axial Compressive Load. ASTM International.
- 2013b. Standard Test Methods for Deep Foundations Under Static Axial Tensile Load. ASTM International.
2015. Standard Test Method for Slump of Hydraulic-Cement Concrete. ASTM International.
2016. Standard Test Method for Compressive Strength of Cylindrical Concrete Specimens. ASTM International.
- Aboutabikh, M., Soliman, A.M., and El Naggar, M.H. 2016. Properties of cementitious material incorporating treated oil sands drill cuttings waste. *Construction and Building Materials* **111**: 751-757. doi: <http://dx.doi.org/10.1016/j.conbuildmat.2016.02.163>.
- Albuquerque, P., Carvalho, D., and Massad, F. 2005. Bored, continuous flight auger and omega instrumented piles: Behaviour under compression. *In Proceedings of The International Conference on Soil Mechanics and Geotechnical Engineering*. Osaka, Japan. p. 2075-2078.
- Albuquerque, P., da Fonseca, A.V., Santos, J., Esteves, E.C., Massad, F., and Carvalho, D. 2011. Effects of the construction method on pile performance: evaluation by instrumentation-part 2: experimental site at the Faculty of Engineering of the University of Porto.

- Bae, D.-s., Kim, K.-s., Koh, Y.-k., and Kim, J.-y. 2011. Characterization of joint roughness in granite by applying the scan circle technique to images from a borehole televiewer. *Rock mechanics and rock engineering* **44**(4): 497-504.
- Balamurugan, G., and Perumal, P. 2013. Use of quarry dust to replace sand in concrete—An experimental study. *International Journal of Scientific and Research Publications* **3**(12).
- Bowles, J.E. 1996. *Foundation analysis and design*. McGraw-Hill, New York.
- Brown, D.A., Dapp, S.D., Thompson, W.R., and Lazarte, C.A. 2007. *Design and Construction of Continuous Flight Auger (CFA) Piles*. Federal Highway Administration. Technical Report.
- Brown, D.A., Turner, J.P., and Castelli, R.J. 2010. *Drilled shafts: Construction procedures and LRFD design methods*. US Department of Transportation, Federal Highway Administration.
- Busch, P., Grabe, J., Gerressen, F., and Ulrich, G. 2010. Use of displacement piles for reinforcement of existing piles. *In Proceedings of DFI and EFFC 11th Int. Conf. in the DFI series, Geotechnical Challenges in Urban Regeneration in London/UK*. pp. 113-119.
- Carson, B. 2011. Sustainable solutions in the oil sands. *Policy Options Magazine*. pp. 12-22.
- Chen, X.B., Zhang, J.S., Xiao, Y.J., and Li, J. 2015. Effect of roughness on shear behaviour of red clay - concrete interface in large-scale direct shear tests. *Canadian Geotechnical Journal* **52**(8): 1122-1135. doi: 10.1139/cgj-2014-0399.
- Choi, C.-H. 2011. A study on the effect of pile surface roughness on adfreeze bond strength. *Journal of the Korean Geoenvironmental Society* **12**(12): 79-88.

- Chu, L.M., and Yin, J.H. 2006. Study on soil–cement grout interface shear strength of soil nailing by direct shear box testing method. *Geomechanics and Geoengineering* **1**(4): 259-273. doi: 10.1080/17486020601091742.
- Farrell, E.R., and Lawler, M.L. 2008. CFA pile behaviour in very stiff lodgement till. *Proceedings of the Institution of Civil Engineers-Geotechnical Engineering* **161**(1): 49-57.
- Feder, J. 2013. *Fractals*. Springer Science & Business Media.
- Fioravante, V. 2002. On The Shaft Friction Modelling of Non-Displacement Piles in Sand Soils and Foundations **42**(2): 23-33. doi: 10.3208/sandf.42.2_23.
- Fleming, W.G.K. 2009. *Piling engineering*. Taylor & Francis, New York;London;.
- Galbraith, A.P., Farrell, E.R., and Byrne, J.J. 2014. Uncertainty in pile resistance from static load tests database. *Proceedings of the Institution of Civil Engineers: Geotechnical Engineering* **167**(5): 431-446. doi: 10.1680/geng.12.00132.
- Gambhir, M.L. 2013. *Concrete Technology: Theory and Practice*.
- Gavin, K., Cadogan, D., Tolooiyan, A., and Casey, P. 2013. The base resistance of non-displacement piles in sand. Part I: field tests. *Proceedings of the Institution of Civil Engineers-Geotechnical Engineering* **166**(6): 540-548.
- Gavin, K.G. 2009. Shaft capacity of continuous flight auger piles in sand. *Journal of geotechnical and geoenvironmental engineering* **135**(6): 790-798.
- Giraldo, J., and Rayhani, M. 2013. Influence of fiber-reinforced polymers on pile–soil interface strength in clays. *Advances in civil engineering materials* **2**(1): 534-550.
- Gonen, T. 2016. The effect of inadequate compaction on compressive strength of concrete exposed to elevated temperature. *Scientia Iranica* **23**(1): 114-121.

- Ismael, N.F. 2001. Axial Load Tests on Bored Piles and Pile Groups in Cemented Sands. *Journal of Geotechnical and Geoenvironmental Engineering* **127**(9): 766-773. doi: doi:10.1061/(ASCE)1090-0241(2001)127:9(766).
- Jamwal, M.L.G.N. 2014. *Building and Construction Materials: Testing and Quality Control, 1e (Lab Manual)*. Tata McGraw-Hill Education.
- Joshi, R.C., Achari, G., and Kaniraj, S.R. 1992. Effect of loading history on the compression and uplift capacity of driven model piles in sand. *Canadian Geotechnical Journal* **29**(2): 334-341. doi: 10.1139/t92-038.
- Kulatilake, P., Um, J., and Pan, G. 1997. Requirements for accurate estimation of fractal parameters for self-affine roughness profiles using the line scaling method. *Rock Mechanics and Rock Engineering* **30**(4): 181-206. doi: 10.1007/bf01045716.
- Kulatilake, P.H.S.W., and Um, J. 1999. Requirements for accurate quantification of self-affine roughness using the roughness-length method. *International Journal of Rock Mechanics and Mining Sciences* **36**(1): 5-18. doi: 10.1016/S1365-1609(98)00170-1.
- Li, Y.R., and Huang, R.Q. 2015. Relationship between joint roughness coefficient and fractal dimension of rock fracture surfaces. *International Journal of Rock Mechanics and Mining Sciences* **75**: 15-22. doi: 10.1016/j.ijrmms.2015.01.007.
- Mandelbrot, B.B. 1985. Self-Affine Fractals and Fractal Dimension. *Physica Scripta* **32**(4): 257-260. doi: 10.1088/0031-8949/32/4/001.
- Ormeloh, J. 2014. Thermomechanical cuttings cleaner—qualification for offshore treatment of oil contaminated cuttings on the norwegian continental shelf and martin linge case study.

- Phillips, R., and Valsangkar, A. 1987. An experimental investigation of factors affecting penetration resistance in granular soils in centrifuge modelling. University of Cambridge Department of Engineering.
- Raman, S., Safiuddin, M., and Zain, M. 2007. Non-destructive evaluation of flowing concretes incorporating quarry waste. *Asian journal of civil engineering (Building and Housing)* **8**(6): 597-614.
- Söderbergh, B., Robelius, F., and Aleklett, K. 2007. A crash program scenario for the Canadian oil sands industry. *Energy Policy*. pp. 1931-1947.
- Uesugi, M., Kishida, H., and Tsubakihara, Y. 1988. Behaviour of Sand Particles in Steel-Friction. *Soils and Foundation* **28**(1): 107-118. doi: 10.3208/sandf1972.28.107.
- Zhu, H.H., Ho, A.N.L., Yin, J.H., Sun, H.W., Pei, H.F., and Hong, C.Y. 2012. An optical fibre monitoring system for evaluating the performance of a soil nailed slope. *Smart Structures and Systems* **9**(5): 393-410.

Chapter 5

5 LATERAL MONOTONIC AND CYCLIC BEHAVIOUR OF CONTINUOUS FLIGHT AUGER AND BORED PILES IN SAND

Continuous flight auger (CFA) and bored piles are two different types of piles used widely all over the world. The objective of this work is to identify the difference in behaviour between both types of pile highlighting the effect of construction method. In addition, the potential of constructing more sustainable piles through using green concrete mixture (i.e., incorporating treated oil sand waste (TOSW)) was investigated. Instrumented piles with the same nominal size were tested under one way cyclic and monotonic lateral loading in sand. Piles were exhumed after testing and pure bending moment test was performed on them to extract the moment-curvature relation. The results indicated that CFA piles have higher lateral capacity than that of bored piles. This behaviour can be attributed to the increase in CFA pile diameter and higher soil confinement resulting from this increase.

5.1 Introduction

Bored and continuous flight auger (CFA) piles are two popular types of cast-in-place reinforced concrete piles that have been used extensively in civil engineering applications. These piles are often subjected to static and cyclic lateral loads due to different hazards such as vessel impacts, traffic, waves, wind, and earthquakes leading to significant accumulated permanent pile displacements. In current design practice, similar procedure is being utilized to evaluate the lateral response of bored and CFA piles ignoring effect of

installation method (Brown et al. 2007). This is mainly due to limited number of published experimental results especially for CFA piles under lateral cyclic loading.

Bored and CFA piles construction technique can affect their behaviour and capacity. The concrete pressure used in the construction of CFA piles can increase its diameter. Consequently, the soil around the pile can experience densification due to the radial displacement during concrete pumping. Moreover, the surface roughness of the pile can increase due to the concrete intrusion into the surrounding soil. As a result, the skin friction and coefficient of lateral earth pressure can increase compared with that of the bored pile (Fleming 2009)

The “ p - y ” approach is the most commonly used method for analyzing the pile behaviour under lateral loading. This method considers the nonlinear nature of soil response by relating the pile deflection (y) at any point to the soil contact pressure (p) at that point, known as p - y curve. Although, empirical relationships provided in p - y curves have been obtained from back-analysis of instrumented full-scale load-tests, the results are very sensitive to the implemented p - y curves and the selection of suitable load-transfer curves is the most crucial issue in using this methodology for the analysis of laterally loaded piles. Previous research by Heidari et al. (2014) showed that the behaviour of pile under monotonic and cyclic lateral loading considerably influenced by pile properties as well as soil properties. These important parameters are the intrinsic characteristic of the developed p - y curves and difficult to be separated due to the limited number of full-scale tests (Ashford and Juirnarongrit 2005; Heidari et al. 2014). Despite various formulations for the load-transfer curves, there are still limited experimental data available to validate the reliability of the analytical methods for CFA piles in sand. These methods considered some

parameters while neglecting others. Moreover, compared to bored piles, relatively few published results are available for the cyclic and even static response of laterally loaded CFA piles in sand.

Therefore, the objective of this paper is to perform experimental full scale test to study the effect of pile installation on CFA and bored piles under static and cyclic lateral loading. In addition, the effect of incorporating TOSW on the behaviour of CFA and bored piles were investigated.

5.2 Experimental program

5.2.1 Soil preparation and investigation

Soil was placed in a testing soil pit 4.5x4.5m with a total depth of 6.0 m. The testing pit was backfilled with a natural washed concrete sand with fines less than 2%. The sand was placed in layers, 25 cm each, and was compacted by vibrating plate compactor on three passes. Sand cone test was performed on each layer to measure the soil density to assure uniform consistency. During backfilling, sand samples were collected and tested to determine the sand physical and mechanical properties.

The peak (ϕ_p) and residual (ϕ_r) angle of internal friction were measured with direct shear test and were 43 and 36°, respectively. Specific gravity and water content of the concrete sand were 3.3% and 2.71. The sand was well graded with sharp edged particles and mean particle size of (D_{50}) 0.95 mm.

5.2.2 Materials

Ordinary Portland cement Type 10 was used as a binder material. The same natural washed concrete sand used for backfilling was utilized as fine aggregates, while the coarse aggregates constituted 9 mm rounded gravel. The TOSW was added as a sand replacement at a rate of 30% by volume. The specific gravity and surface area of the TOSW were 2.81 and 4.85 m²/g, respectively. Concrete mixtures with and without TOSW were tested according to ASTM C143 (2015) and ASTM C39 (2016) to confirm their workability to be 200±20 mm and 28 days compressive strength to be 35 MPa (Brown et al. 2007).

5.2.3 Test piles and installation

CFA and bored piles were constructed using Big Beaver drilling machine. Five piles (i.e., P1 to P5) were excavated with 0.27 m diameter (D) auger. While one pile (i.e., P6) was constructed with 0.24 m diameter auger. Pile were spaced at a minimum distance of 5D to reduce the interaction effect between the piles (Phillips and Valsangkar 1987). During piles construction, the highest downward pressure was applied on the auger to reduce soil caving while rotating with the slowest speed possible. To assure the quality of the excavation, sand coming out of the hole was collected and weighted to calculate the occupied volume based on the measured soil density. After reaching the required depth the auger was filled with concrete and then retracted without applying pressure, while in CFA piles, concrete was pumped under pressure while retracting the auger with no rotation. Piles 1, 2, 3, and 4 were reinforced along their length with four 10M bars and 6M round stirrups every 15 cm and they were all tested laterally. Piles 5 and 6 was not reinforced as it was hard to insert the reinforcement cage in the concrete and hence, they were not tested laterally.

Piles 1 and 2 were bored piles, while piles 3, 4, 5 and 6 were CFA piles. Conventional concrete mixture without TOSW (C0) was used in piles 1, 3, 5 and 6, while concrete mixture with 30% TOSW (C1) was used in piles 2 and 4. Piles were tested under axial monotonic loading before performing the lateral testing demonstrated in the next sections. Table 5.1 summaries pile method of construction, material, acronyms, and testing sequence performed on each one.

Table 5.1 Piles configuration

Pile	Type	Concrete mixture	Acronym	Testing sequence
P1	Bored	C0	Bored C0	Compression then pullout
P2	Bored	C1	Bored C1	Compression then pullout
P3	CFA	C0	CFA C0	Compression then pullout
P4	CFA	C1	CFA C1	Compression then pullout
P5	CFA	C0	CFA C01	Compression only
P6	CFA	C0	CFA C02	Compression only

5.3 Instrumentation and test setup

5.3.1 Lateral loading

Figure 5.1 shows the lateral test setup. The load was applied using a hydraulic jack with capacity of 100 kN and maximum stroke of 10 in, reacting against steel struts affixed to the reinforced concrete wall of the test pit. The load applied at the pile head was measured using a load cell of 100 kN capacity, which was connected to the data acquisition system to record the load. The horizontal displacement was measured employing two linear

variable displacement transducers (LVDTs) positioned across each other. The average of the two LVDTs provides the lateral displacement of the pile head at each load increment.



Figure 5.1 Piles configuration

Each pile was instrumented with strain gauges on four levels attached to the reinforcement cage distributed along the pile shaft at distances from pile head of 0.8, 1.6, 2.5, and 3.5 m as shown in Figure 5.2a. Each strain gauge level comprised 4 strain gauges type CEA-06-250UW-120 provided by Micro-Measurements (Figure 5.2b). The strain gauges were connected to the data acquisition system through lead wires that were protected by 3 layers of M coat A, 2 layers of M coat B Nitrile Rubber and 2 layers of silicon inside the concrete body. The rotation along the pile shaft was calculated from the strain gauges' readings.

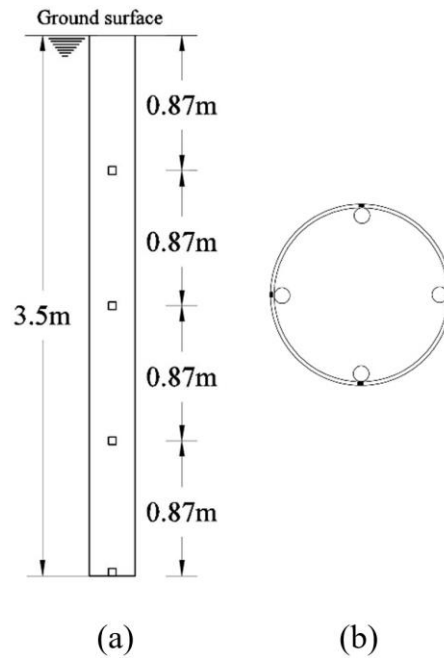
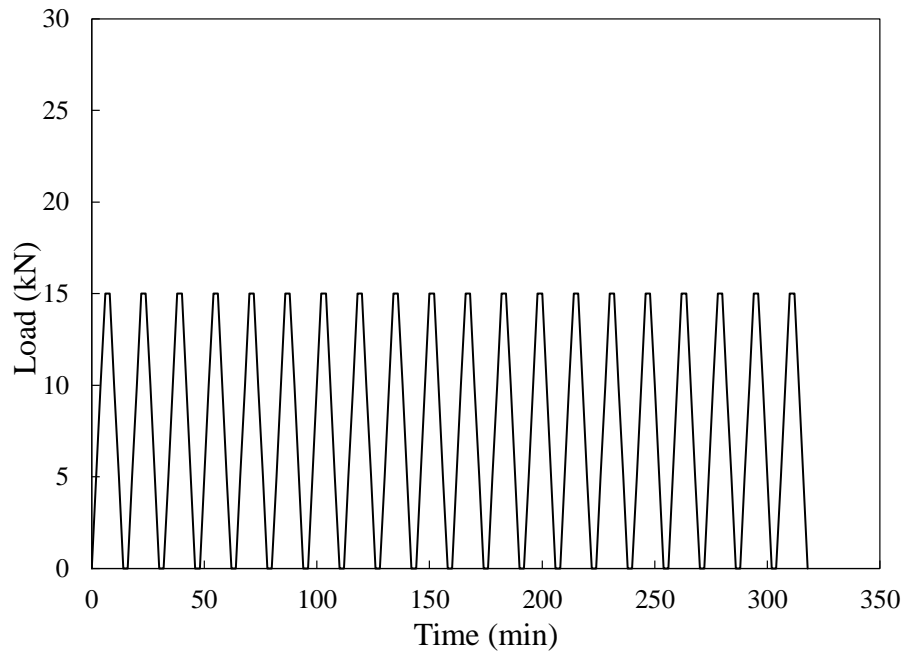


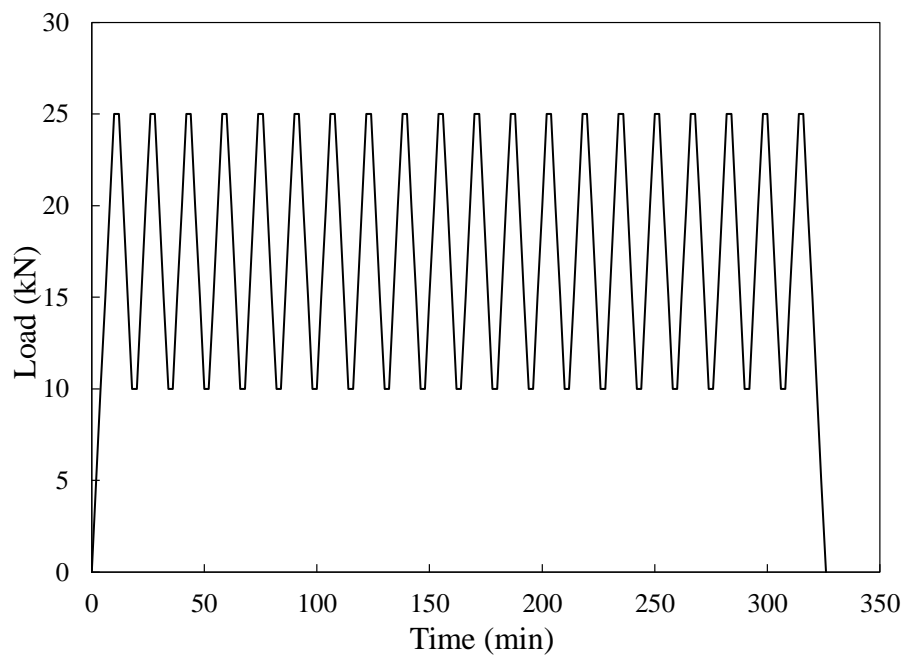
Figure 5.2 Piles instrumentation distribution (a) along pile length (b) cross section

5.3.2 Load test sequence and procedures

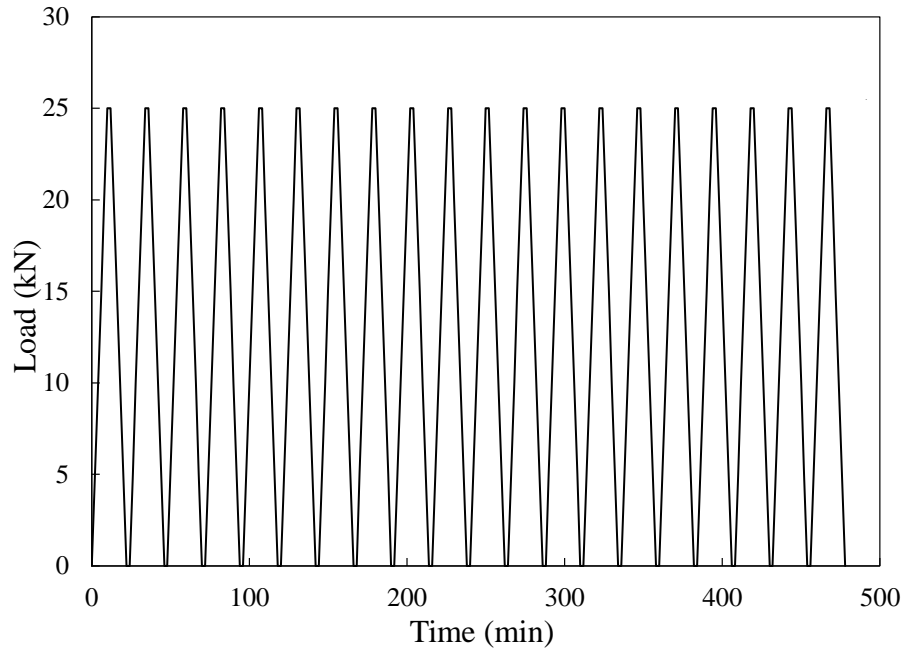
All piles, except pile Bored C1, were first tested under cyclic loading with three different amplitudes, 0 to 15 kN, 10 to 25 kN, and 0 to 25 kN as shown in Figure 5.3 (a, b, and c), respectively. One way cyclic load was applied in 5 kN increment for 2 minutes each with a total number of 20 cycles. Then the piles were tested monotonically until it reaches failure (25 mm). Monotonic load was applied in 5 kN increments every 5 minutes as illustrated in Figure 5.3d. Pile Bored C1 was first tested monotonically until it reached lateral displacement of 6.25 mm then the subsequent tests followed the same sequence as the other piles as mentioned beforehand. Piles were extracted after the lateral testing to examine the surface of the piles for cracks and to observe their actual geometry and surface roughness. Finally, the pure bending test was conducted on the piles to measure there moment-curvature.



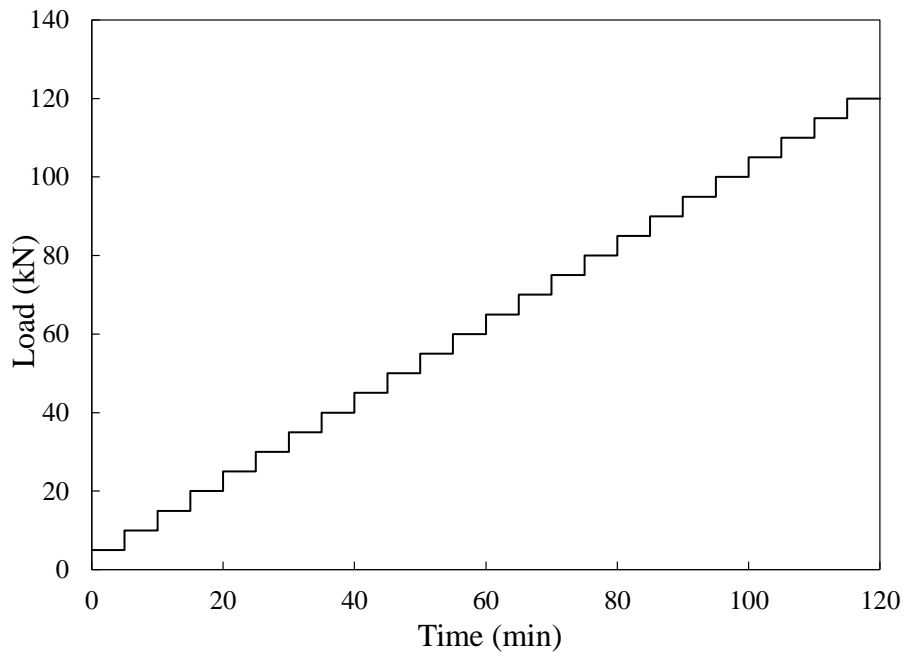
(a)



(b)



(c)



(d)

Figure 5.3 Lateral pile loading test patterns (a) Cyclic test (0-15 kN) (b) Cyclic test (10-25 kN) (c) Cyclic test (0-25 kN) (d) Monotonic test

5.3.3 Pure bending test

Piles were extracted from the soil after performing lateral tests and were tested structurally under pure bending to extract moment-curvature curves. Test 4-point setup was prepared as shown in Figure 5.4, where the load was applied at one and two thirds of the span length. The deflection was measured using nine linear displacement transducers (LVDTs) positioned along the span. The load was applied using a hydraulic jack with capacity of 250 kN and maximum stroke of 6 in on steel beam distributing the load equally on the pile. The pile was reacting against steel frame affixed to the ground. The load applied on the pile was measured using a load cell of 222 kN capacity, which was connected to the data acquisition system to record the load.



Figure 5.4 Bending test setup on extracted pile

5.4 Results and discussion

5.4.1 Monotonic loading

Figure 5.5 illustrates the load deflection curve of pile Bored C1 which was performed before the cyclic tests. The load deflection shape was hyperbolic in shape showing softer response as it reached the end of the test.

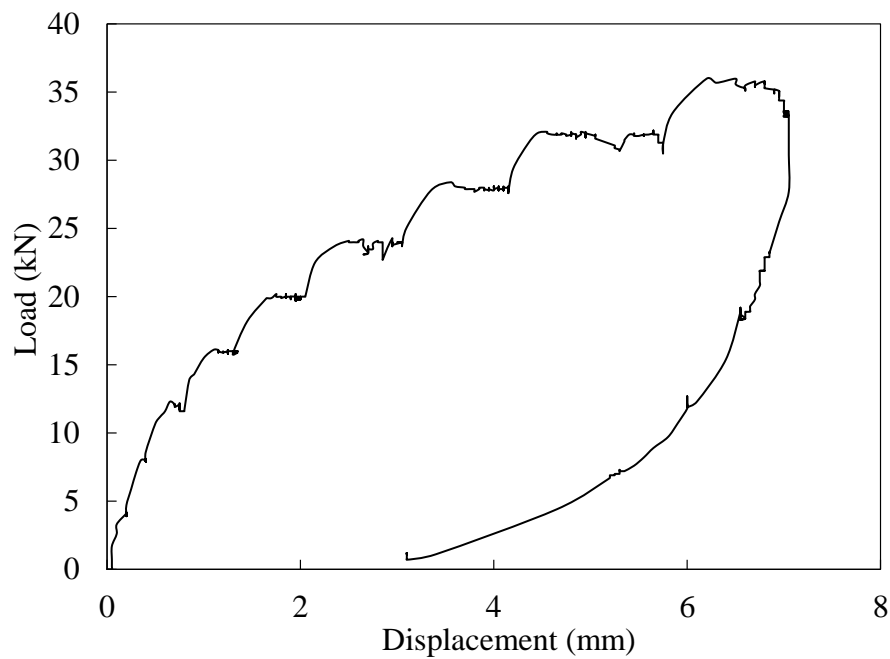


Figure 5.5 Lateral deflection curve of pile Bored C1 tested before cyclic loading

Figure 5.6 shows the load deflection curves of lateral monotonic tests on piles CFA C1, Bored C0, and Bored C1 performed after the cyclic tests. The initial stiffness was defined in this study as the slope of the initial linear part of the loading curve. Pile CFA C1, Bored C0 and Bored C1 initial stiffness were 11, 3, and 4 kN/mm, respectively. The ultimate load of pile CFA C0 was higher than that of the bored piles by about 93%. This can be attributed

to the increase of friction angle and soil densifying due to pressurized concrete pumping in CFA method of installation.

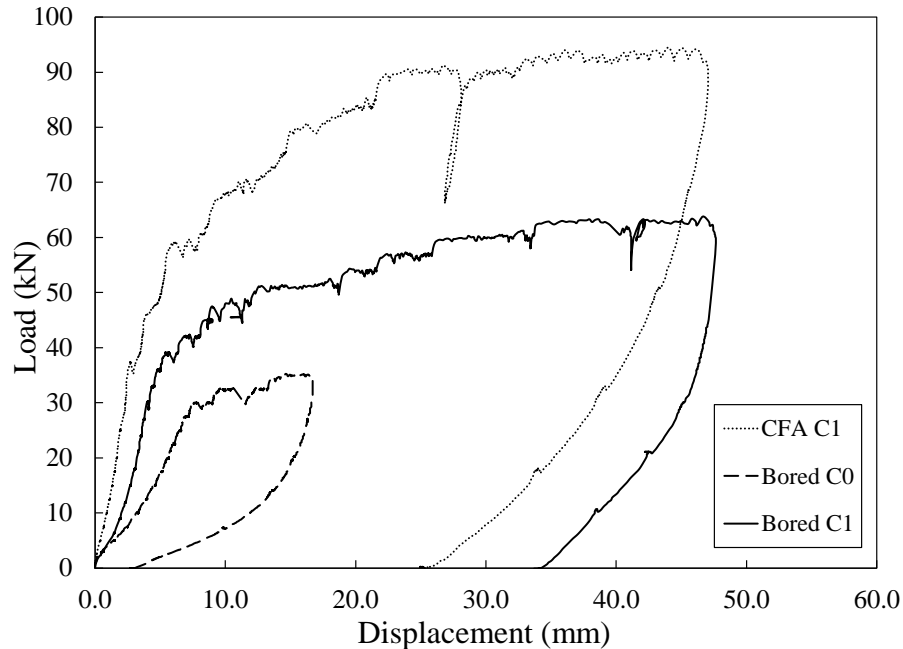
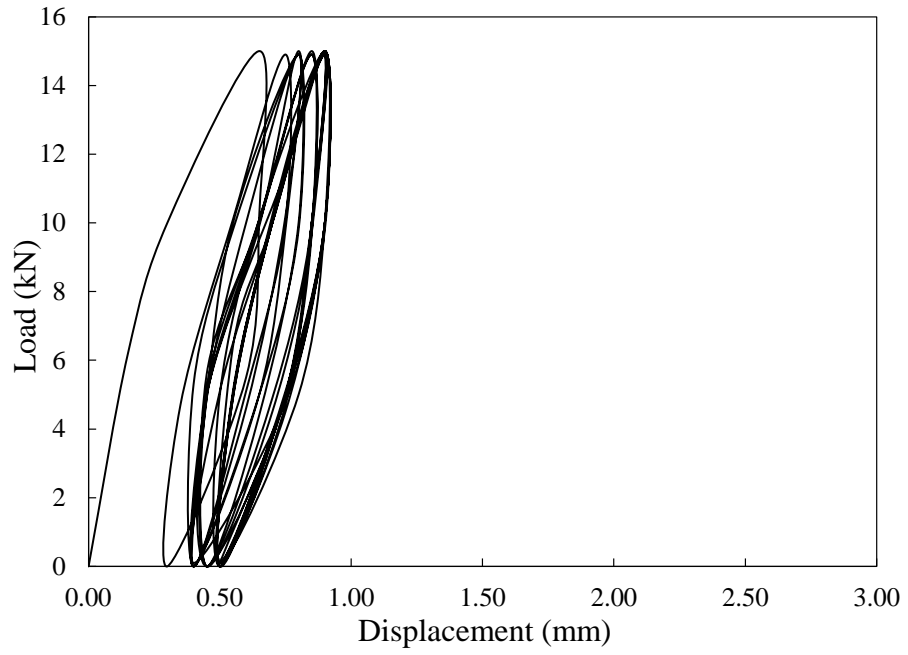


Figure 5.6 Lateral load deflection curves performed after the cyclic tests for piles CFA C1, Bored C0, and Bored C1

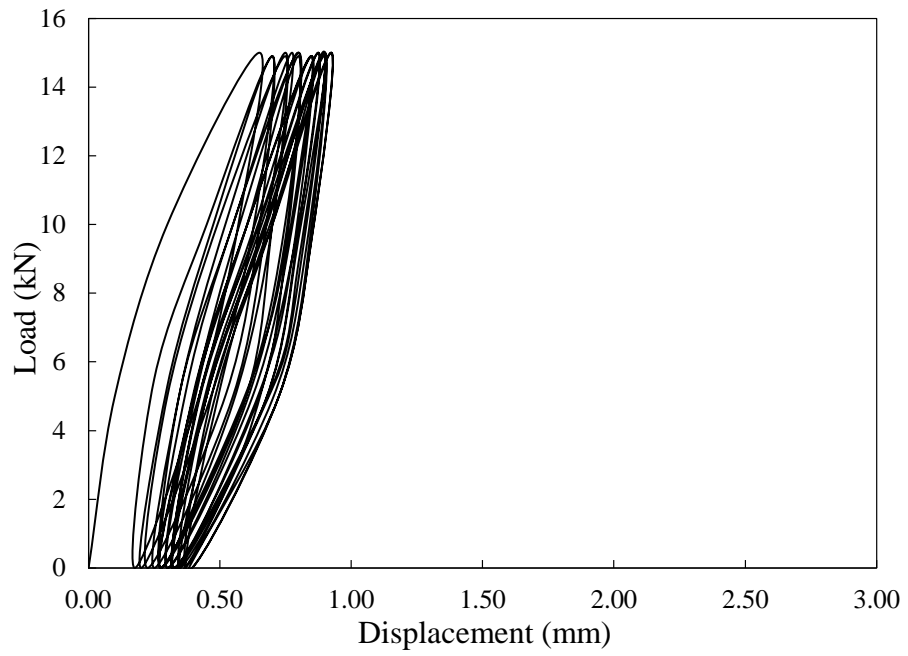
5.4.2 Cyclic loading

Figure 5.7 illustrates the load deflection curves of piles CFA C0, CFA C1, Bored C0, and Bored C1 tested under lateral cyclic loading amplitude 0 to 15 kN. The test results are presented in terms of hysteretic loops. It should be noted that this test was the first lateral test for all the piles except pile Bored C1. The initial stiffness of the first loading cycle for piles CFA C0 and CFA C1 were 41 and 50 kN/mm, respectively. On the other hand, pile Bored C0 and Bored C1 initial stiffness were 12.5 and 6.25 kN/mm, respectively.

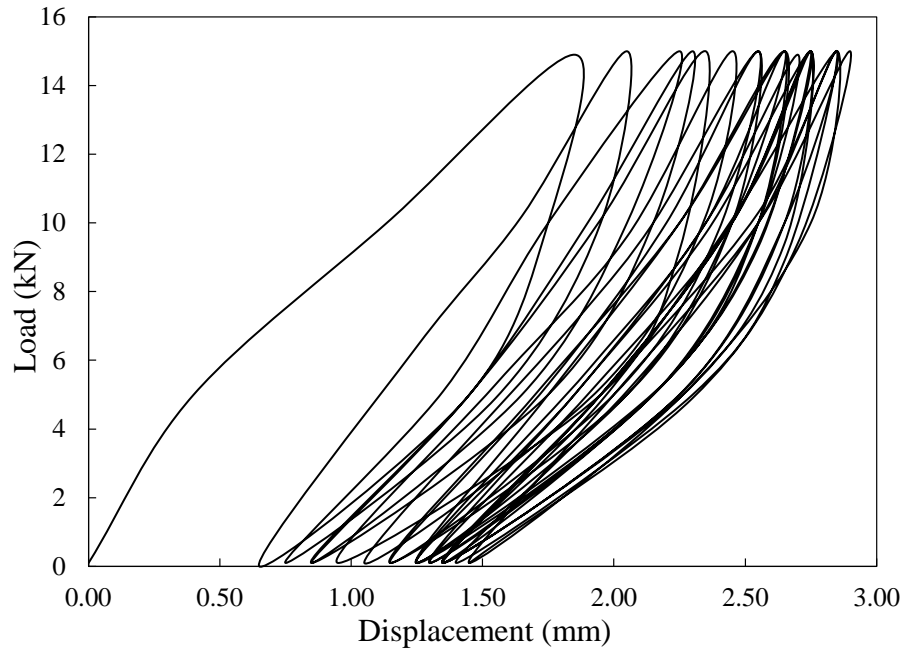
As depicted in Figure 5.7 the first loading cycle of the three piles CFA C0, CFA C1, and Bored C0, were convex shape because these were the virgin lateral loading experienced by these piles. On the contrary, pile Bored C1 first loading cycle was concave and its initial stiffness was 50% of pile Bored C0. The lower initial stiffness and different loading curve shape of pile Bored C1 can be attributed to its previous monotonic loading. The maximum lateral displacement experienced by the CFA piles at the end of this test (i.e., 0 to 15 kN) was about 0.9 mm, while the deflection of the bored piles was 3 times larger than that of the CFA piles under the same value of lateral load. This can be attributed to the additional confining pressure induced by the concrete pressure during installation, increase in pile diameter and improved piles' surface properties (at the macro scale). It is noticeable that even though the two bored piles experienced different loading history, and the displacement of the first cycle was different, but, their final displacement is about the same. This behaviour can be attributed to the shakedown condition presented by Matlock (1970) who stated that after large number of loading cycles, the soil-pile system starts to stabilize which was referred to as the shakedown condition. It can be noted that behaviour of piles with TOSW (i.e. CFA C1 & Bored C1) is very close to those without TOSW (i.e. CFA C0 & Bored C0).



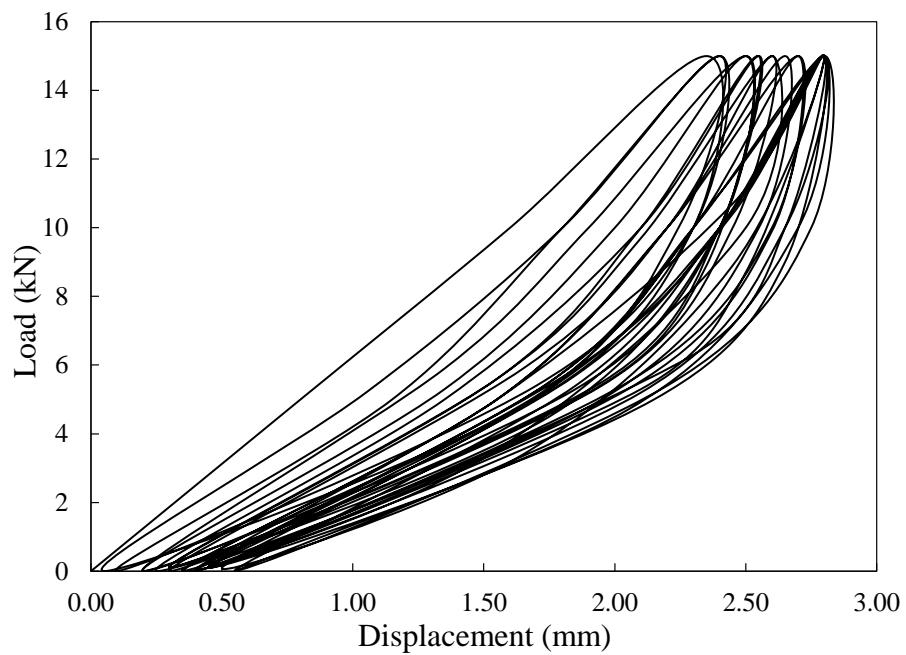
(a)



(b)



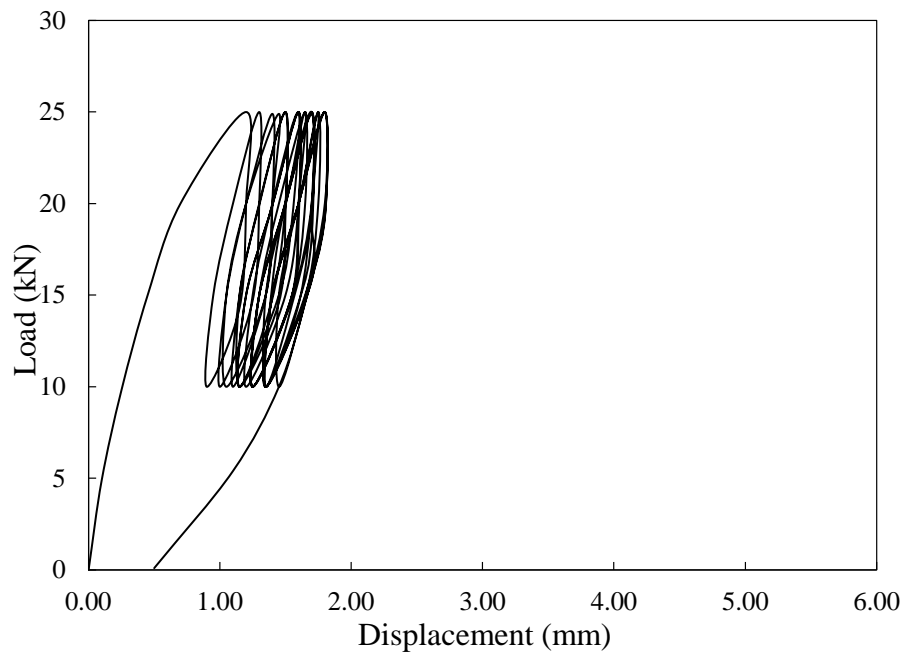
(c)



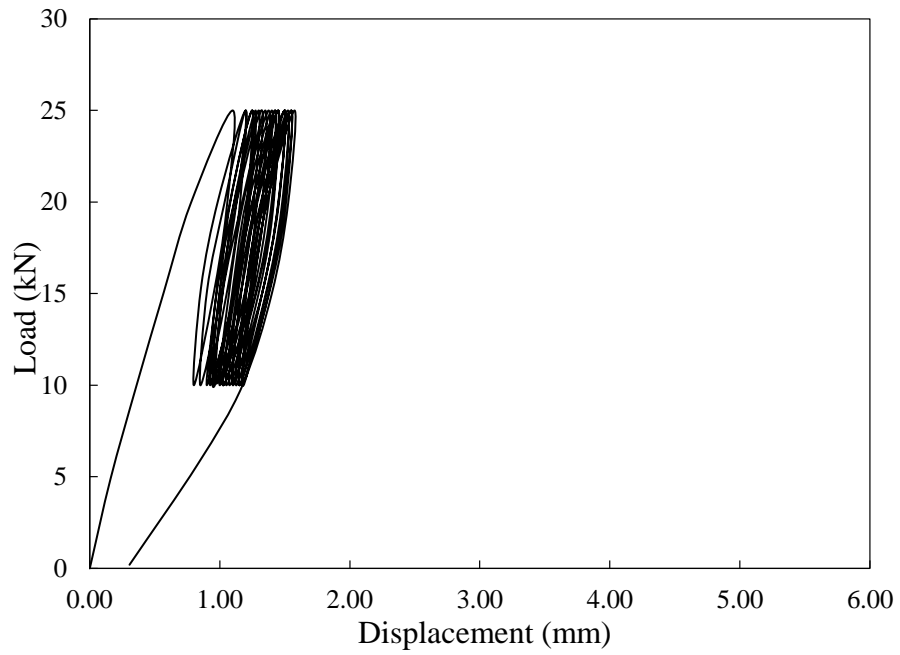
(d)

Figure 5.7 Lateral cyclic load displacement curve (0-15 kN range) (a) CFA C0 (b) CFA C1 (c) Bored C0 (d) Bored C1

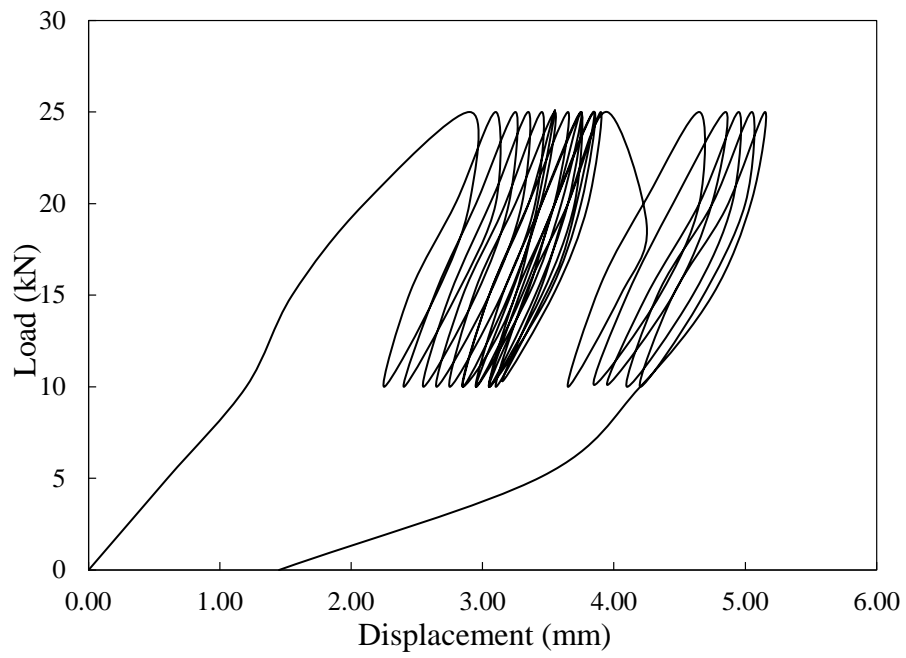
Figure 5.8 shows the load displacement relation for piles CFA C0, CFA C1, Bored C0, and Bored C1 under cyclic loading amplitude 10 to 25 kN, which was the second set of cyclic loading tests. The initial stiffness of piles CFA C0, CFA C1, Bored C0, and Bored C1 were 49, 30, 8, and 4 kN/mm. The difference in the stiffness between CFA and bored piles can be attributed to the effect of different installation method. The maximum deflection after 20 cycles for piles CFA C0 and CFA C1 were 1.8 and 1.6 mm. Pile Bored C0 cracked after 15 cycles which increased the settlement to 5.1 mm. However, using linear interpolation the settlement of this pile can be predicted at 4.15 mm. Bored pile C1 maximum settlement after 20 cycles was 4.0 mm. As mentioned before, the larger displacement experienced by the bored piles (i.e., 240% more) can be attributed to the installation method and its effect on soil density, surface roughness, and piles cross section.



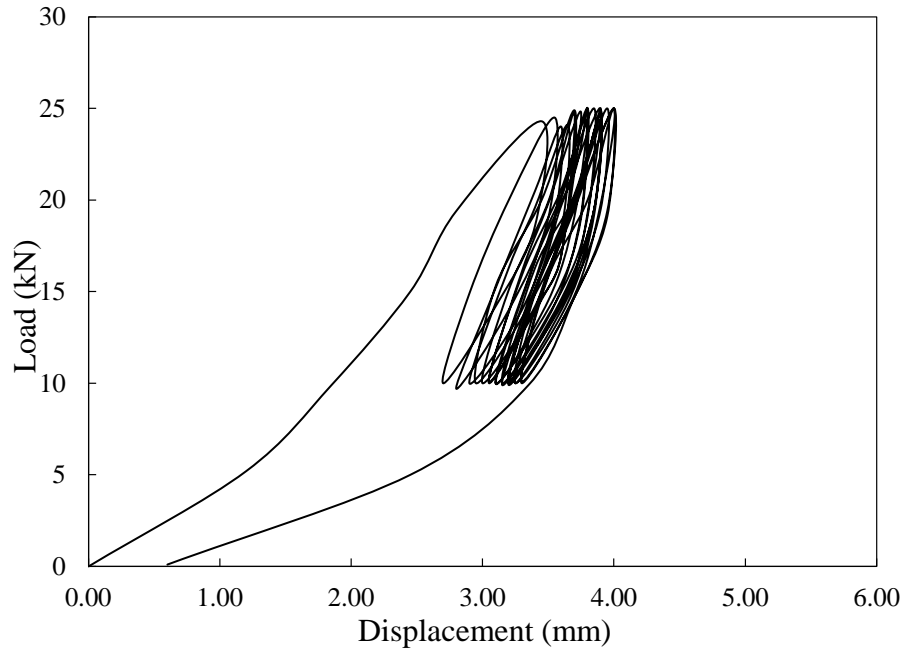
(a)



(b)



(c)



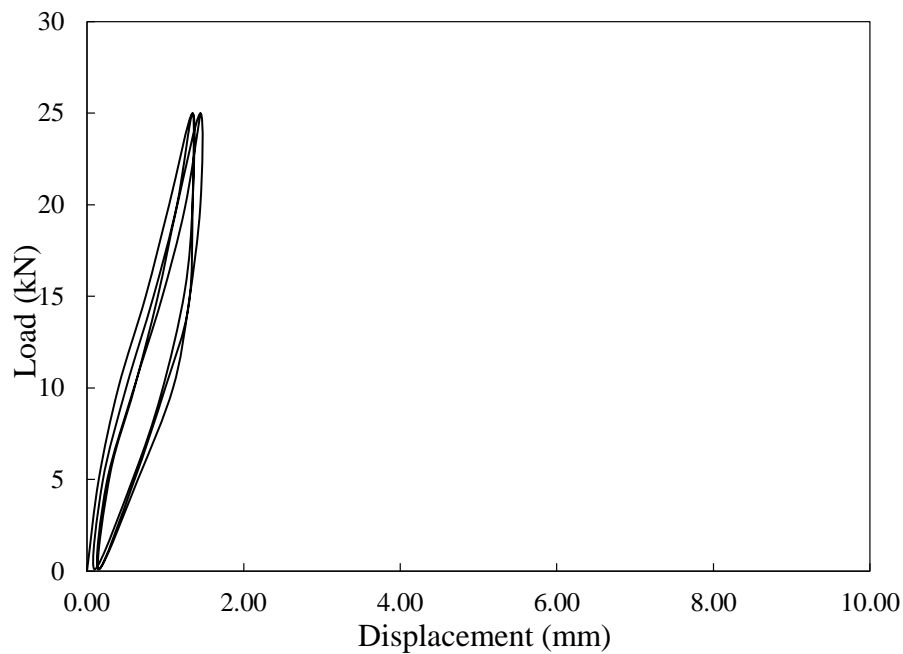
(d)

Figure 5.8 Lateral cyclic load displacement curve (10-25 kN range) (a) CFA C0 (b) CFA C1 (c) Bored C0 (d) Bored C1

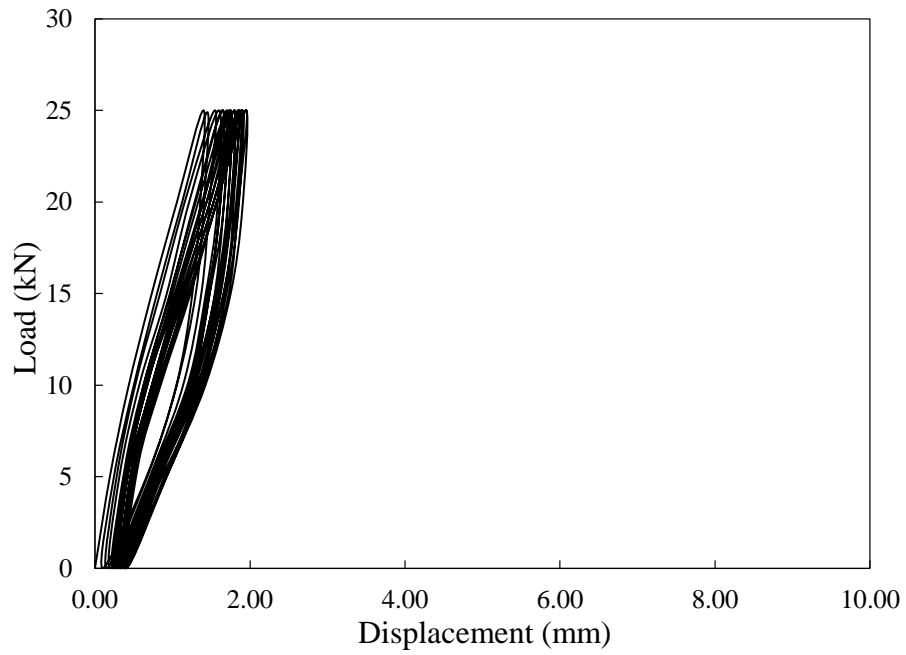
Figure 5.9 shows the load displacement relation for the four piles under cyclic loading amplitude 0 to 25 kN, which was the third set of cyclic loading tests. The loading test on pile CFA C0 was interrupted and did not continue due to breakage in the pile head at the application point. The initial stiffness of piles CFA C0, CFA C1, Bored C0, and Bored C1 were 33, 26, 5, and 4 kN/mm. The maximum displacement of pile CFA C0 after 20 cycles can be predicted by linear interpolation to be 2.1 mm. The maximum displacement of piles CFA C1, Bored C0, and Bored C1 after 20 cycles were 1.95, 8.25, and 4.1 mm, respectively. However, pile Bored C0 experienced cracking after 13 cycles resulted in displacement increase.

The cyclic loading affected the lateral monotonic test behaviour of the pile done on the pile. The initial stiffness of piles CFA C1 and Bored C1 decreased after the last cyclic test by 58% and 40%, respectively. However, it did not change for pile Bore C0 and stayed on the same value. The decrease in the stiffness values is due to the gapping effect. Pile Bored C0 constant stiffness can be attributed to the shakedown condition.

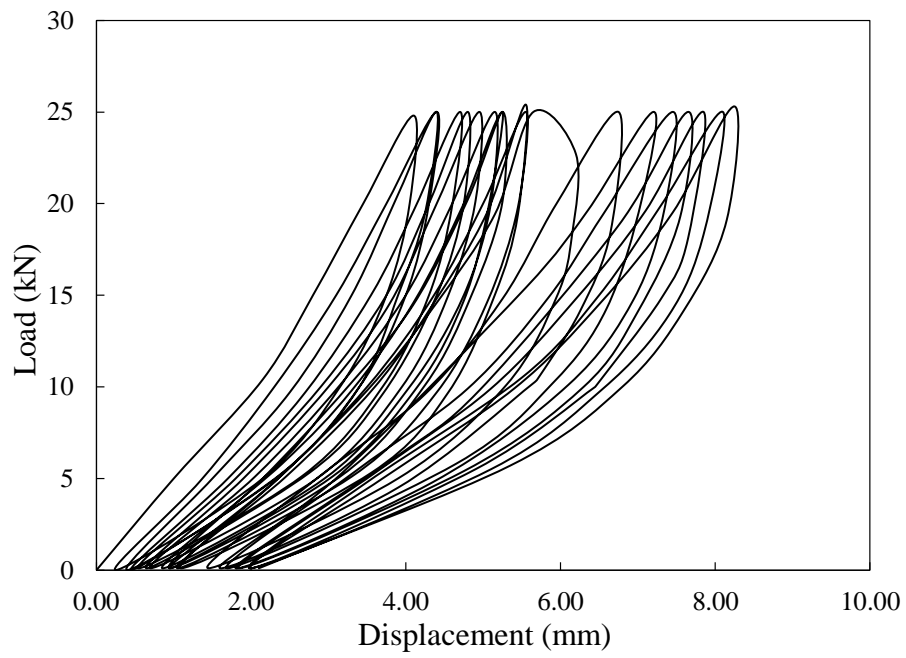
Through the series of lateral cyclic tests which performed on pile with and without TOSW, it was obvious that TOSW did not have significant effect on the geotechnical behaviour of the piles and both of the two mixtures behaved close to each other.



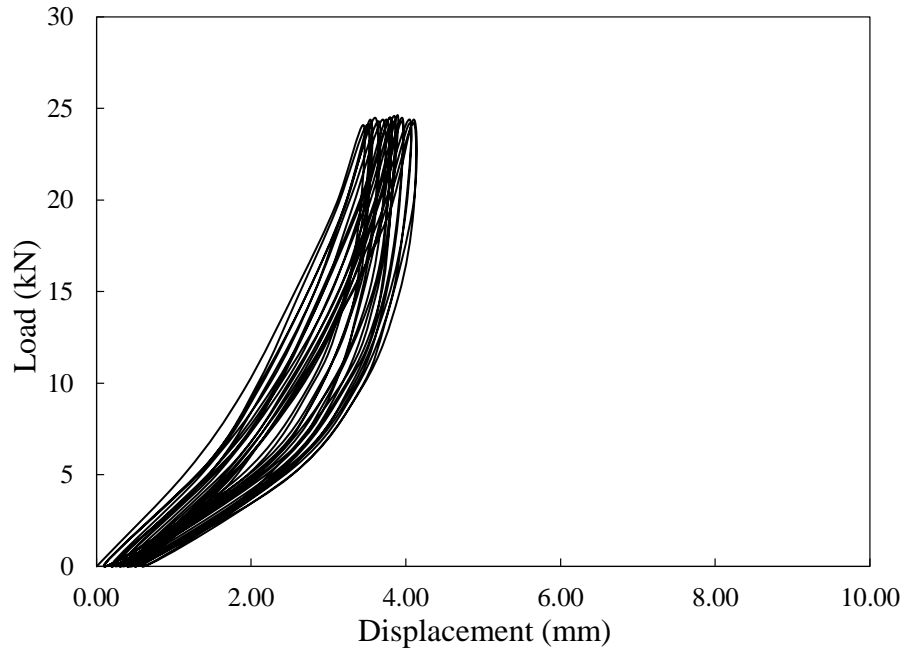
(a)



(b)



(c)



(d)

Figure 5.9 Lateral cyclic load displacement curve (0-25 kN range) (a) CFA C0 (b) CFA C1 (c) Bored C0 (d) Bored C1

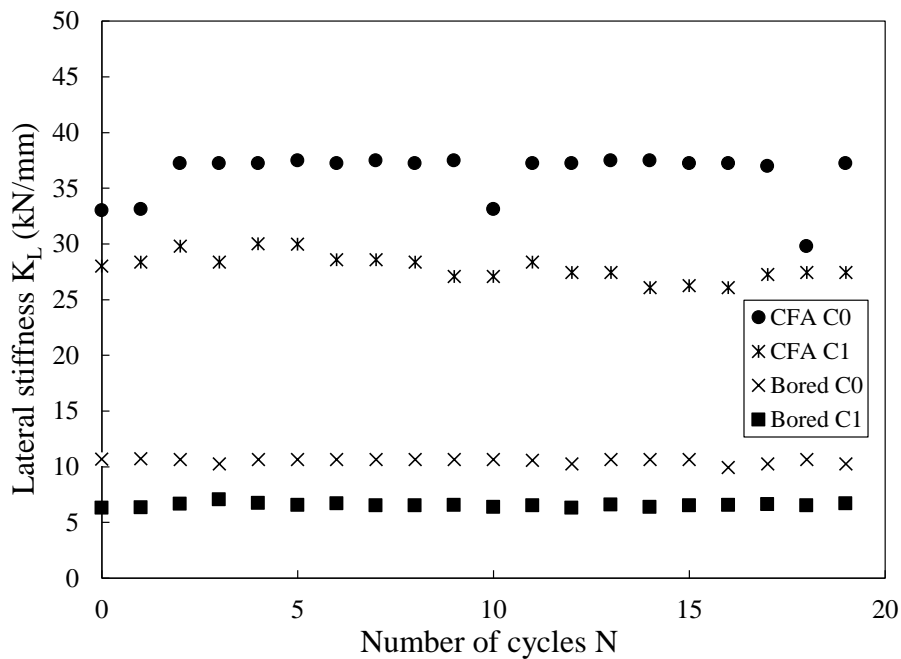
The change in pile lateral stiffness at each load cycle can be approximated by the slope of the loading curve, K_L , given by:

$$K_L = \frac{p_{max} - p_{min}}{y_{max} - y_{min}} \quad \text{Eq. 5.1}$$

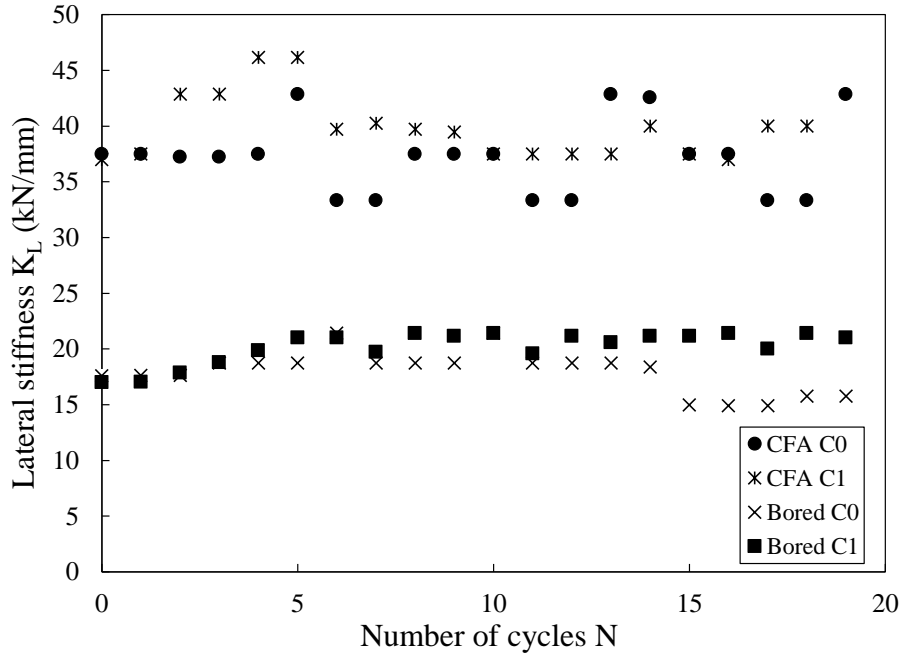
Where, K_L = pile lateral stiffness; p_{max} and p_{min} = maximum and minimum lateral load at each cycle; and y_{max} and y_{min} = the corresponding pile head deflection, respectively (Abd Elaziz and El Nagggar 2015).

Figure 5.10 illustrates the variation of the lateral stiffness with the number of loading cycles. The lateral stiffness of the first cyclic test in Figure 5.10a shows that K_L of CFA piles is higher than that of the bored piles by about 250%. On the other hand, the difference

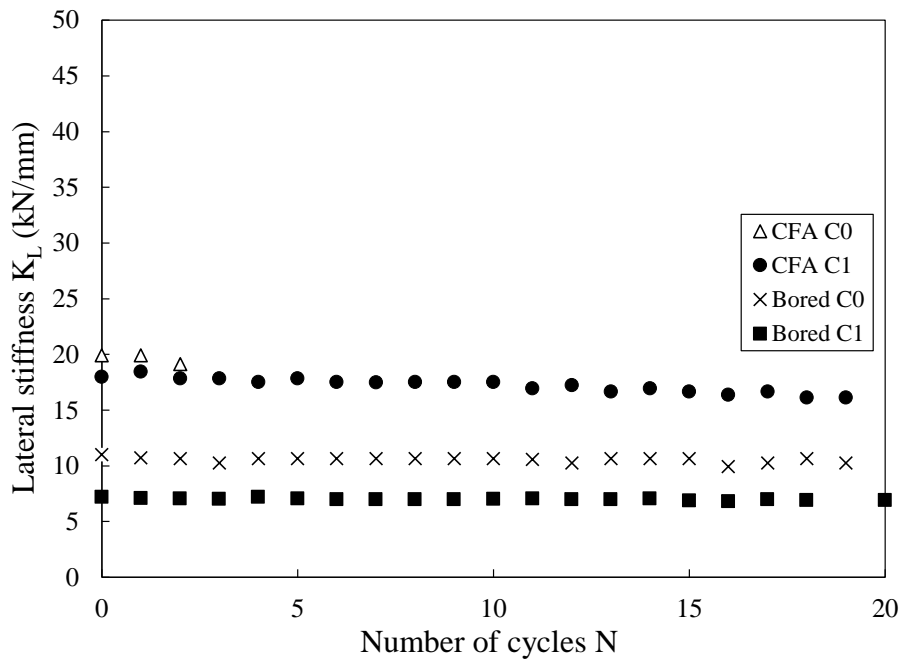
in lateral stiffness between CFA and bored piles, measured from the second cyclic test (i.e., 10 to 25 kN (Figure 5.10b)), decreased to 100% compared with the previous test. The CFA and the bored piles K_L increased by 18 and 100%, respectively, in the second cyclic test. the results of the second cyclic test was increased due to the preloading exerted in the piles during the test. However, it decreased again in the third test to (Figure 5.10c). The higher lateral stiffness experienced in the second test (i.e., 10 to 25 kN) can be attributed to the smaller gap occurred during the test. On the other hand, in the third test, the lateral stiffness decreased because the gapping increased as the pile bounded back to its original position as the load was totally released at the end of each cycle (Pender and Pranjoto 1996). It was found that incorporating TOSW in the concrete of both CFA and bored piles have in significant effect on their lateral stiffness.



(a)



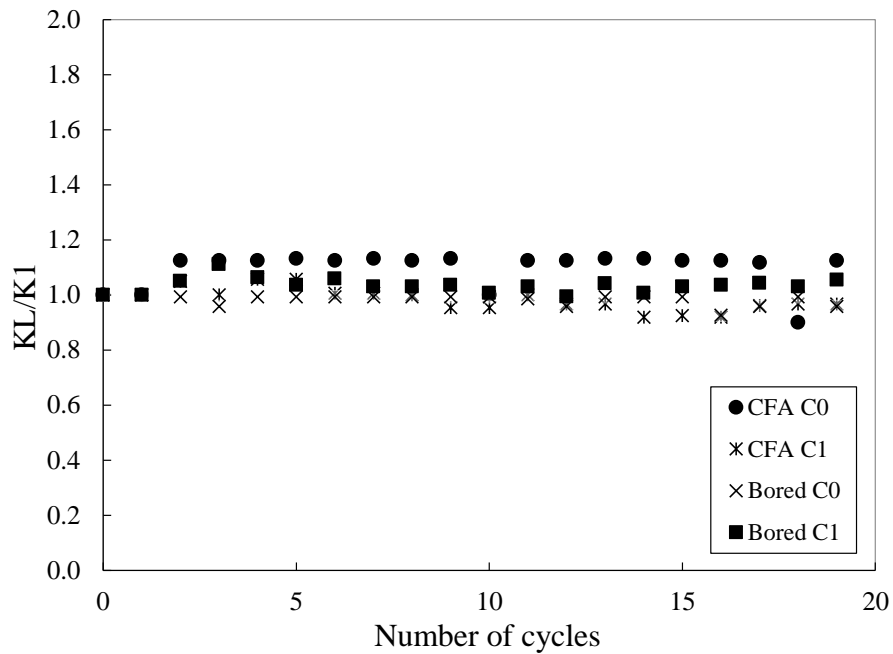
(b)



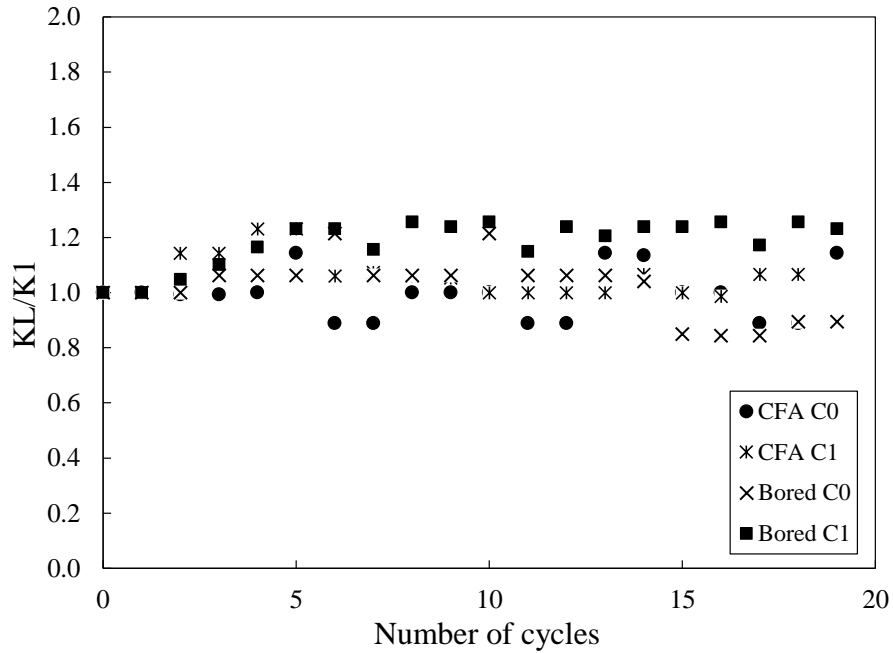
(c)

Figure 5.10 Variation of lateral stiffness with loading cycles (a) 0 to 15 kN (b) 10 to 25 kN (c) 0 to 25 kN

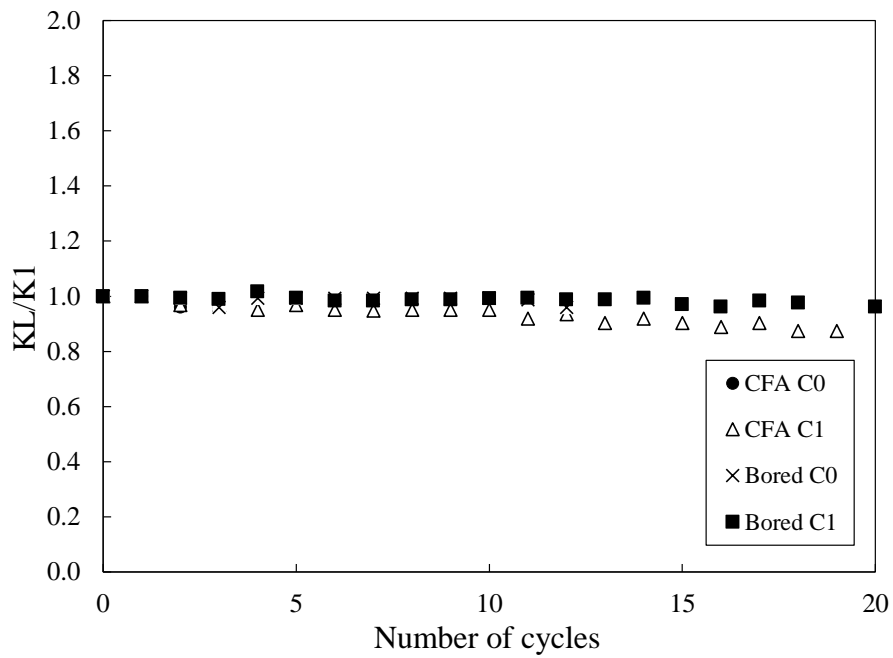
The degradation was represented by the ratio K_L/K_I (where, K_L is the lateral pile stiffness at the designated cycle, K_I is the lateral pile stiffness at the first cycle). Figure 5.11a shows the degradation of the first cyclic test. It can be noticed that the degradation is almost constant for all the piles during the first and third cyclic test (i.e., Figure 5.11a and c). Piles CFA C0, CFA C1, and Bored C0 experienced stiffness increase after the first and/or second cycle due to the soil densification in front of the pile. After that the degradation was minimal. There was almost no degradation for pile Bored C1. This behaviour can be attributed to the previous monotonic loading performed on it before the cyclic loading.



(a)



(b)



(c)

Figure 5.11 Variation of degradation with loading cycles for amplitude (a) 0 to 15

kN (b) 10 to 25 kN (c) 0 to 25 kN

The degradation results at each test for every pile can be related to the number of cycles with the degradation parameter, t (Idriss et al. 1978), such that:

$$K_N/K_1 = N^t \quad \text{Eq. 5.2}$$

where K_N and K_1 are the lateral stiffness at cycles N and 1, respectively. The values of the degradation parameters are shown in Table 5.2. Where the positive t value indicates increasing stiffness and the negative value indicates higher degradation. The third cyclic test of pile CFA C0 was terminated after four cycles as mentioned before. Therefore, there were no sufficient number of cycles to get reliable degradation value. Also, the degradation parameter of pile Bored C0 was calculated to the 14th and 12th cycles of the second and third cyclic tests, respectively, because after these cycles the pile was cracked and the degradation increased rapidly. It can be noted from Table 5.2 that the preloading of the second cyclic test increased the degradation parameter. Generally, there was no significant different between degradation parameters of CFA and bored piles constructed with or without TOSW.

Table 5.2 Variation of degradation parameter t for all cyclic tests

	0 to 15 kN	10 to 25 kN	0 to 25 kN
Amplitude (kN)	15	15	25
Preloading (kN)	0	10	0
CFA C0	-0.056	0.005	N.A.
CFA C1	0.003	-0.040	0.033
Bored C0	0.009	-0.039	0.022
Bored C1	-0.023	-0.087	0.006

5.4.3 Moment curvature

The moment curvature of piles CFA C1, Bored C0, and Bored C1 was obtained through pure bending moment experiment as shown in Figure 5.4. The measured moment-curvature is shown in Figure 5.12. These curves were used to transfer the measured curvature into moment as it is going to be illustrated in the next sections. The moment-curvature of bored pile incorporating TOSW was almost the same as that constructed without TOSW.

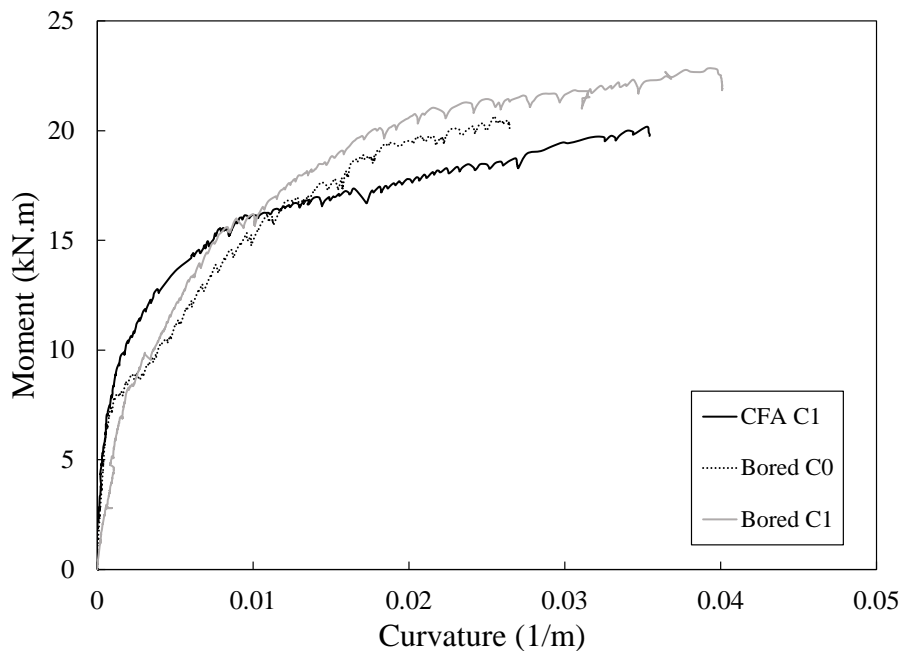


Figure 5.12 Piles moment-curvature

5.4.4 Curvature and moment profiles curve fitting

Curve fitting of the measured curvature is a key element in extracting deflection. The behaviour of the curve is important due to the sensitivity of the double-integration process required to extract the y curves. There are several curve fitting methods such as the

weighted residuals method (Janoyan et al. 2001; Wilson 1998), Fourier series fitting (Lin and Liao 2006), and a combination of B-spline fitting and weighted residuals (de Sousa Coutinho 2006). In this research, the latter method going to be applied.

Curvature data was calculated and analyzed along the pile using the data provided by the strain gauges. First, the readings of each strain gauge were observed along its response history, and any sensor with erroneous reading was given a weight of zero. The curvature value at any elevation of the pile is the result of two opposite strain readings and was calculated as follows (Welch and Reese 1972):

$$\psi = \frac{\varepsilon_1 - \varepsilon_2}{t} \quad \text{Eq. 5.3}$$

where, ε_1 and ε_2 are the measured tensile and compressive strain at to two opposite strain gauges, and t is the distance between the strain gauges parallel to the loading direction, and ψ is the calculated curvature.

To get a proper curvature data fitting, the curvature at the pile tip was set to zero as a boundary condition. This condition was set based on the observation of the strain gauges at the tip which indicated insignificant strain. An artificial point was added above the pile tip by 1mm with zero curvature value to ensure a smooth transition to zero curvature. The polynomial degree affects the sensitivity of the spline curve, and hence the displacement. Typically spline degree of 4 or 5, achieved satisfying results.

The moment profiles should be properly fitted to get acceptable soil reaction profile. Moment was interpreted from experimental moment-curvature relation illustrated previously. After transferring the curvature data points into moment, the moment data

points were fitted with the same procedures as described previously. The boundary condition at the pile tip was the same, but two more artificial points were added to impose the known values of moment and shear at the ground surface. The moment and shear was calculated at the ground surface knowing the applied lateral force and its distance from the ground. The two artificial points added were at the ground surface with the calculated ground surface moment and above it by 1 mm with moment value calculated the same way. The artificial points added in the curvature and moment was given a weight of 1000, to ensure the curves satisfy the conditions at these points.

5.4.5 Moment and deflection

Displacement was calculated by double integration of the measured curvature as illustrated previously. Moment was transferred from the curvature readings through the measured moment-curvature curve of each pile. Lateral deflection as well as the bending moment of each test group are illustrated together in the next section. Pile CFA C0 was not illustrated due to cutting in the strain gauges during previous tests.

5.4.5.1 Lateral Monotonic loading

Figure 5.13 shows the displacement and moment as a result of the monotonic tests performed after the cyclic tests on piles CFA C1 and Bored C0, and before and after the cyclic test for pile Bored C1. The bending moment of pile CFA C1 showed short pile behaviour, while the bored piles bending moment indicated semi long pile behaviour.

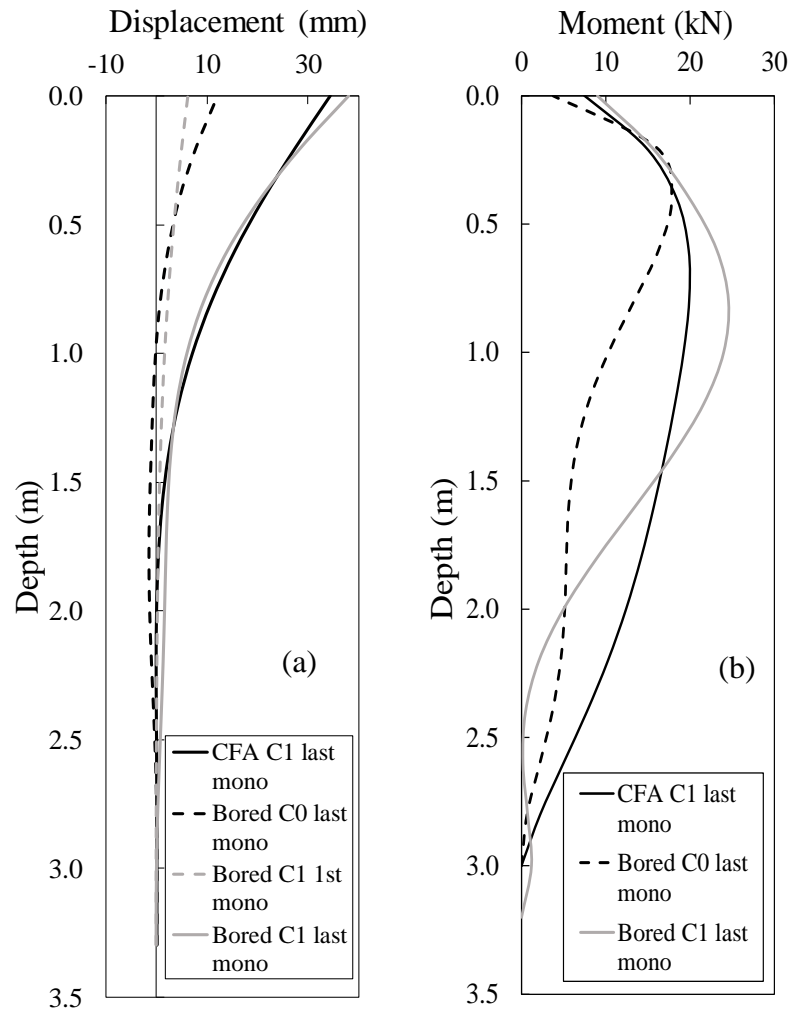


Figure 5.13 Monotonic test (a) deflection (b) moment

5.4.5.2 Lateral Cyclic loading

Figure 5.14a shows the deflection along the piles length of the first and last cycle of 0 to 15 kN cyclic test. It can be noted that the CFA pile experienced the smallest deflection along its length. On the other hand, even though the deflection of the last cycle in both bored piles is not identical, their profile and first cycle deflection is almost the same. The difference in the bored piles last cycle deflection can be attributed to integration minor errors.

Figure 5.14b shows the first and last cycle bending moment along the piles length subjected to 0 to 15 kN cyclic loading. The bending moment of the last cycle was noticed to have lower elevation of maximum bending moment as it should be. However, the maximum bending elevation of pile Bored C1 is lower than that of Bored C0. This behaviour is attributed to the previous monotonic loading of the pile Bored C1 which resulted in gapping and soil disturbance. The behaviour bending moment at the last cycle of pile CFA C1 is probably due to error in the strain gauges reading as it was expected that this pile behaves more as short pile which is confirmed by the bending moment of the following tests on the same pile.

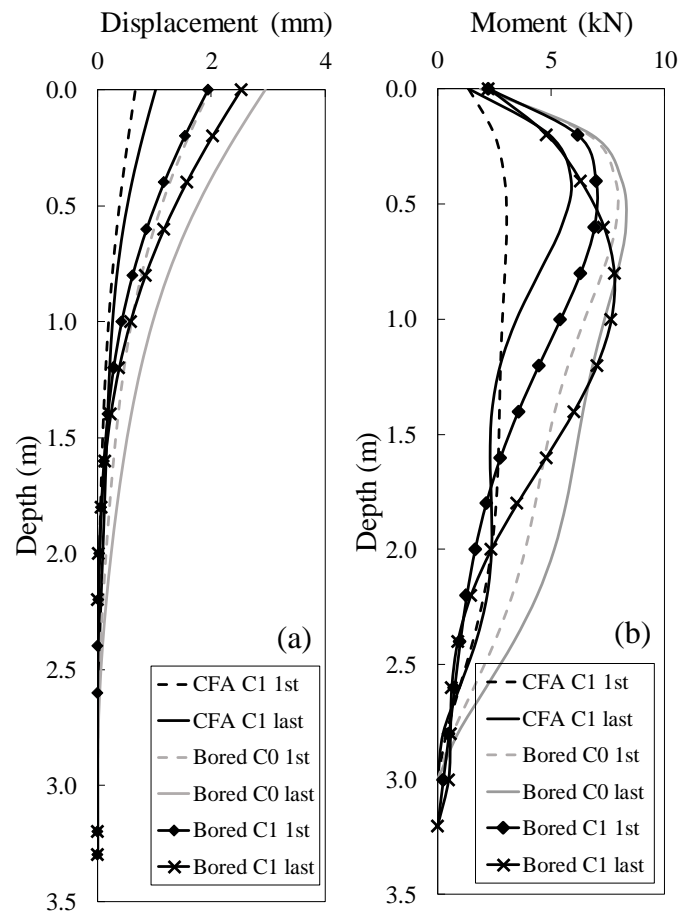


Figure 5.14 0-15 kN cyclic tests first and last cycle (a) deflection (b) moment

Figure 5.15a shows the lateral deflection of the piles along their length for the second cyclic test (i.e., 10-25 kN). The CFA pile deflection was the smallest while the bored piles experienced higher values. However, Bored C0 pile experienced increase in deflection that was not reflected in Figure 5.15a. It was noted that the strain gauges were not affected by the crack that happened at the 14th cycle which is shown in Figure 5.8c. This can be attributed to the high modulus of elasticity of concrete (i.e., 50GPa) which prevented the strain gauges from sensing the cracking in the pile.

The bending moment of the CFA C1 pile (Figure 5.15b) showed short pile behaviour while the bored piles showed semi long pile behaviour. It can be attributed to the increase in diameter due to the pile construction method which resulted in lower length to diameter ratio. The last cycle bending moment of pile Bored C1 showed lower maximum moment elevation following the same trend of the same pile in the previous cyclic test (i.e., 0-15 kN). Moreover, last cycle bending moment of pile Bored C0 was expected to be higher except it was not for the reasons mentioned previously.

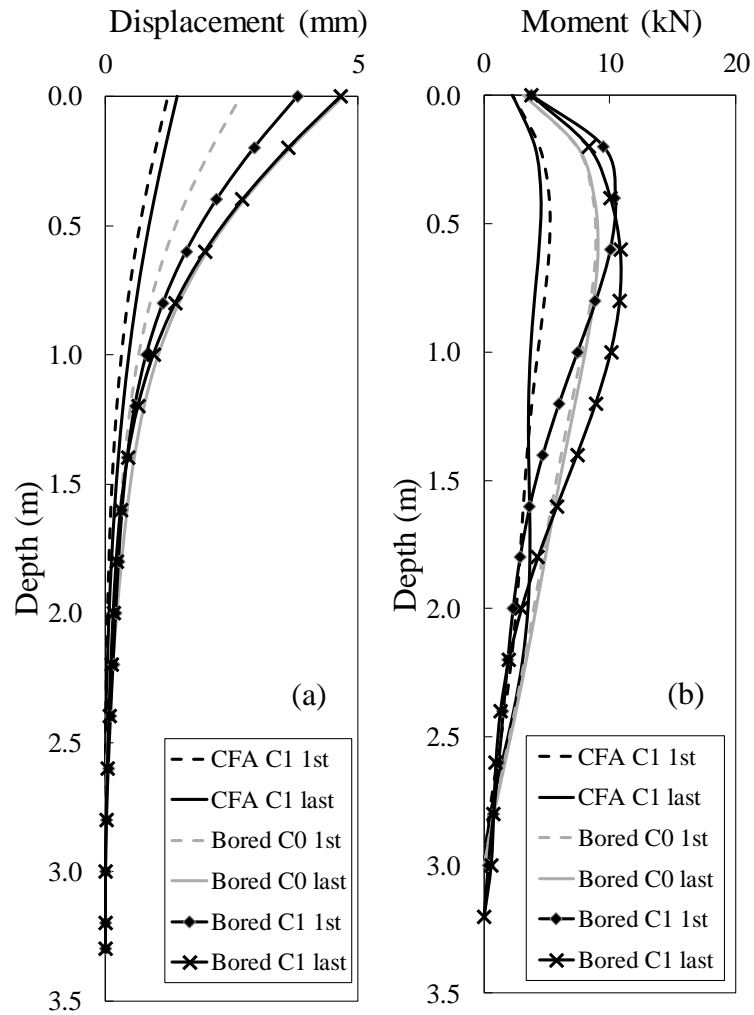


Figure 5.15 10-25 kN cyclic tests first and last cycle (a) deflection (b) moment

Deflection along the piles length of the last cyclic test (i.e., 0-25 kN) is shown in Figure 5.16a. Pile Bored C0 showed higher deflection due to the crack occurred after 12 cycles. It shows that the strain increase after the cracking was reflected on the strain gauges reading and as a result the deflection along the pile length.

CFA C1 bending moment showed in Figure 5.16b the same short pile behaviour. On the other hand, Bored C1 pile experienced higher bending moment due to the crack occurred during the test.

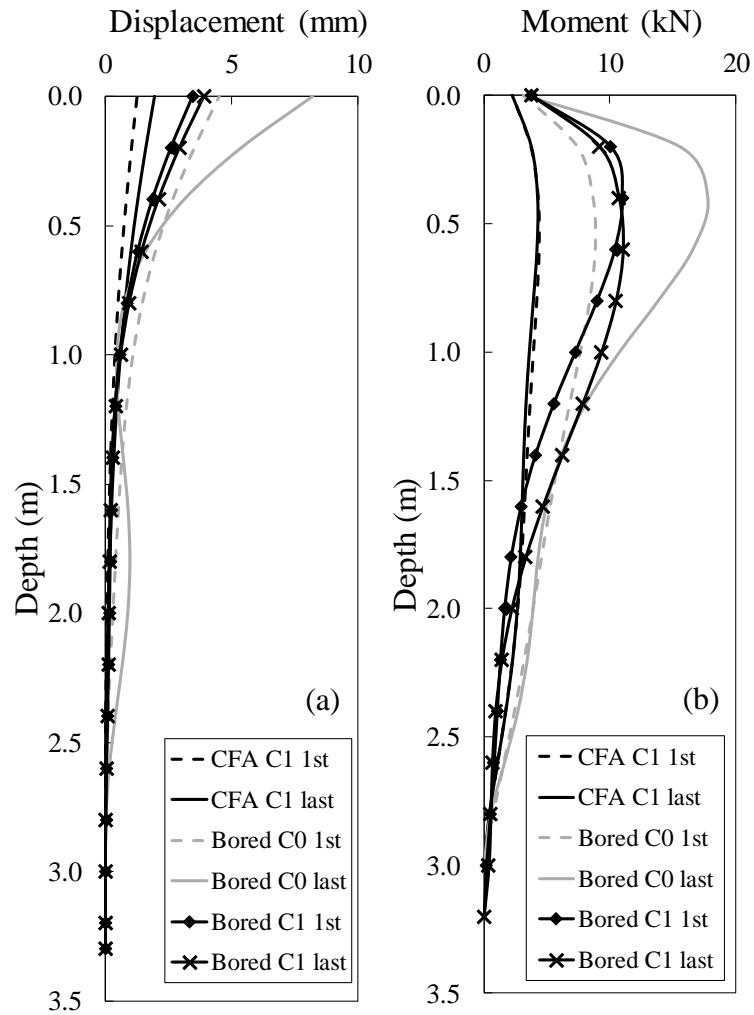


Figure 5.16 0-25 kN cyclic tests first and last cycle (a) deflection (b) moment

The sequence of testing has its effect on the behaviour of piles. Pile Bored C1 first monotonic test affected the behaviour of the next cyclic tests. It resulted in lower elevation of maximum bending moment. This behaviour can be attribute to the soil disturbance occurred during the first test.

5.4.6 Initial modulus of subgrade reaction

The initial modulus of subgrade reaction (k) was back calculated using LPile software. The load displacement for both bored and CFA piles was calculated using LPile for the initial linear part of the curve. Thereafter, it was compared to the measured experimental results. Figure 5.17 shows the experimental load displacement of the bored and the CFA pile compared to that calculated by LPile. To get a proper response using the numerical analysis, the initial modulus of subgrade reaction used by LPile (65000 kN/m) should be modified. It was found that k for the bored and CFA piles should be multiplied by 4 and 6, respectively, to get matching response.

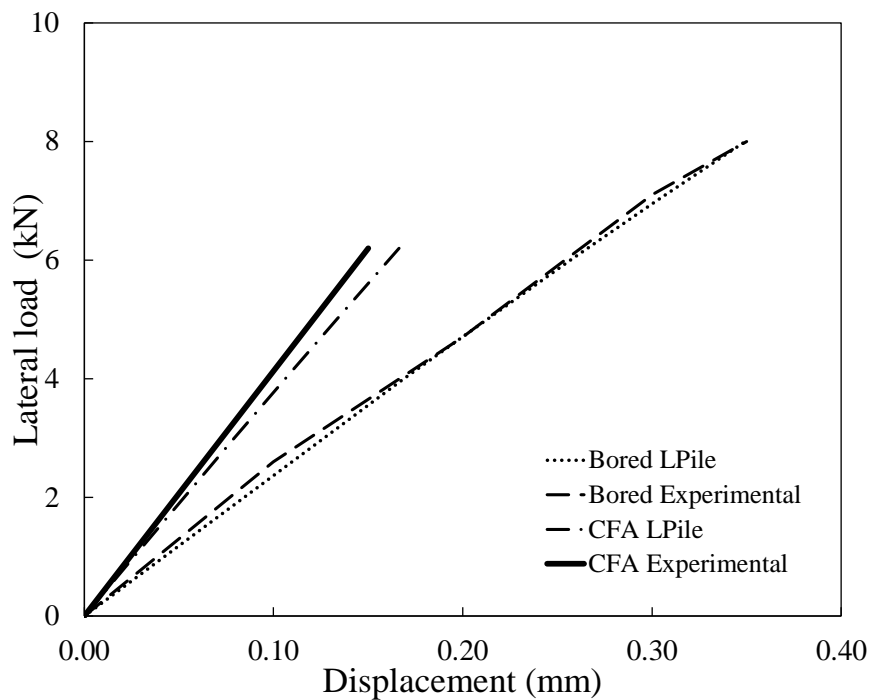


Figure 5.17 Experimental vs numerical load displacement

5.5 Conclusion

The effect of the construction method and incorporating TOSW in the piles on the lateral behaviour of the CFA and bored piles was investigated and the following conclusions were drawn:

- The ultimate capacity of the CFA pile incorporating TOSW was higher than that of the bored pile by about 47%. This difference can be attributed to the increase in CFA pile diameter and increased friction angle due to construction method which resulted in higher soil density and confinement.
- The virgin initial lateral stiffness of the CFA piles is about three times higher than that of the bored piles. After performing three cyclic tests on the piles the initial stiffness of the CFA piles was about six times higher than that of the bored piles.
- The maximum lateral deflection of the CFA piles was about 48% of that of the bored piles after the third cyclic testing indicating higher capacity of CFA piles.
- The lateral stiffness of the bored piles ranged from 32 to 50% of the lateral stiffness of CFA piles.
- The degradation parameter, t , is affected by preloading of the pile even though the load amplitude is the same.
- The construction method of the CFA piles increased the diameter by 13%, which thus increased the soil confining pressure and which in turn improved its overall performance.

5.6 References

2015. Standard Test Method for Slump of Hydraulic-Cement Concrete. ASTM International.
2016. Standard Test Method for Compressive Strength of Cylindrical Concrete Specimens. ASTM International.
- Abd Elaziz, A.Y., and El Nagggar, M.H. 2015. Performance of hollow bar micropiles under monotonic and cyclic lateral loads. *Journal of Geotechnical and Geoenvironmental Engineering* 141(5). doi: 10.1061/(ASCE)GT.1943-5606.0001279.
- Ashford, S.A., and Juirnarongrit, T. 2005. Effect of Pile Diameter on the Modulus of Subgrade Reaction. Department of Structural Engineering University of California, San Diego La Jolla, California: 92093-90085.
- Brown, D.A., Dapp, S.D., Thompson, W.R., and Lazarte, C.A. 2007. Design and Construction of Continuous Flight Auger (CFA) Piles. Federal Highway Administration. Technical Report.
- de Sousa Coutinho, A.G.F. 2006. Data reduction of horizontal load full-scale tests on bored concrete piles and pile groups. *Journal of Geotechnical and Geoenvironmental Engineering* 132(6): 752-769. doi: 10.1061/(ASCE)1090-0241(2006)132:6(752).
- Fleming, W.G.K. 2009. *Piling engineering*. Taylor & Francis, New York;London;.
- Frizzi, R.P., and Meyer, M.E. 2000. Augercast Piles: South Florida Experience. In *New Technological and Design Developments in Deep Foundations*. pp. 382-396.
- Hamid, T.B. 2014. Analysis of Lateral Load Tests on Auger Cast Piles. In *Tunneling and Underground Construction*.

- Heidari, M., El Naggar, H., Jahanandish, M., and Ghahramani, A. 2014. Generalized cyclic p-y curve modeling for analysis of laterally loaded piles. *Soil Dynamics and Earthquake Engineering* 63: 138-149.
- Idriss, I.M., Dobry, R., and Singh, R.D. 1978. Nonlinear behaviour of soft clays during cyclic loading. *Journal of the Geotechnical Engineering Division* 104(GT12): 1427-1447.
- Janoyan, K., Stewart, J.P., and Wallace, J.W. 2001. Analysis of py curves from lateral load test of large diameter drilled shaft in stiff clay. In *Proceedings of the 6th Caltrans workshop on seismic research*, Sacramento, CA.
- Lin, S.-S., and Liao, J.-C. 2006. Lateral response evaluation of single Piles using inclinometer data. *Journal of Geotechnical and Geoenvironmental Engineering* 132(12): 1566-1573. doi: 10.1061/(ASCE)1090-0241(2006)132:12(1566).
- Matlock, H. 1970. Correlations for design of laterally loaded piles in soft clay. *Offshore Technology in Civil Engineering's Hall of Fame Papers from the Early Years*: 77-94.
- O'Neill, M.W., Vipulanandan, C., and Hassan, K. 2000. Modeling of Laterally Loaded ACIP Piles in Overconsolidated Clay. In *New Technological and Design Developments in Deep Foundations*. pp. 471-485.
- Pender, M.J., and Pranjoto, S. 1996. Gapping effects during cyclic lateral loading of piles in clay. In *Proceedings of 11th World Conference on Earthquake Engineering*, Acapulco, Mexico. pp. 23-28.
- Phillips, R., and Valsangkar, A. 1987. An experimental investigation of factors affecting penetration resistance in granular soils in centrifuge modelling. *University of Cambridge Department of Engineering*.
- Tomlinson, M., and Woodward, J. 2014. *Pile design and construction practice*. CRC Press.

Welch, R.C., and Reese, L.C. 1972. Lateral load behaviour of drilled shafts. University of Texas at Austin.

Wilson, D.W. 1998. Soil-pile-superstructure interaction in liquefying sand and soft clay. Citeseer.

Chapter 6

6 NUMERICAL INVESTIGATION OF PERFORMANCE OF BORED AND CONTINUOUS FLIGHT AUGER PILES UNDER MONOTONIC LOADING

This chapter presents finite element (FE) analysis of the bored and continuous flight auger (CFA) piles constructed in the same soil conditions. Three-dimensional FE models were established using the non-linear soil hardening material model available in Plaxis. The models were calibrated and verified using controlled experimental data involving bored and CFA piles installed in sand and subjected to different loading conditions (i.e., compression, uplift and lateral loading). The developed numerical models accounted for the installation effects of the bored and CFA piles. The verified numerical models were then utilized to conduct a parametric study in order to examine the effects of the soil mechanical properties and pile geometry on the compressive, pullout, and lateral behaviour of the CFA piles in comparison with bored piles. The results demonstrated that a cylindrical soil zone with stiffer properties should be considered around the CFA pile to simulate the effect of soil densification resulting from its installation process.

6.1 Introduction

CFA and bored piles are two widely used types of reinforced concrete non-displacement piles. They are used worldwide for many applications for their reliable and safe performance. Bored piles are suitable for different geotechnical conditions owing to its low

cost, large capacity, and reliable performance. CFA piles offers no noise or vibration during installation, with high skin friction compared to the bored piles (Bowles 1996).

Due to the widespread usage of these piles, several researchers conducted experimental and numerical studies to evaluate their performance Ismael (2001), Albuquerque et al. (2005), Brown et al. (2007), Farrell and Lawler (2008), Gavin et al.(2009), Fleming (2009), Paulo Jose Rocha de et al. (2011), and Gavin et al. (2013). These investigations examined the performance of either bored or CFA piles, but a few studies examined numerically the behaviour of CFA piles in comparison with bored pile under the same field conditions.

Numerical analysis comparison on CFA piles was conducted by Holko and Stacho (2014) to assess the use of different FE software. The numerical analysis was carried out using two different types of software (i.e., Ansys (Ver) and Plaxis (Brinkgreve et al. 2015)). The results showed that Plaxis results was more accurate than the results of Ansys. Józefiak et al. (2015) modeled CFA piles using the finite element software ABAQUS (Manual 2010). They compared the bearing capacity obtained from the numerical analysis with the results obtained from experimental static load test. The lack of agreement between the measured and calculated results was attributed to the compaction of the soil below and around the pile resulted from the construction process.

Modeling the pile installation has an important effect on the pile behaviour. Pile installation can be simulated numerically by creating a cavity with a volume equal to the pile through applying prescribed displacement to the soil boundary, then placing the pile inside the cavity (Abu-Farsakh et al. 2003; Rosti and Abu-Farsakh 2015). Phuong et al. (2016) simulated the driven pile installation effect by using material point method to reduce the

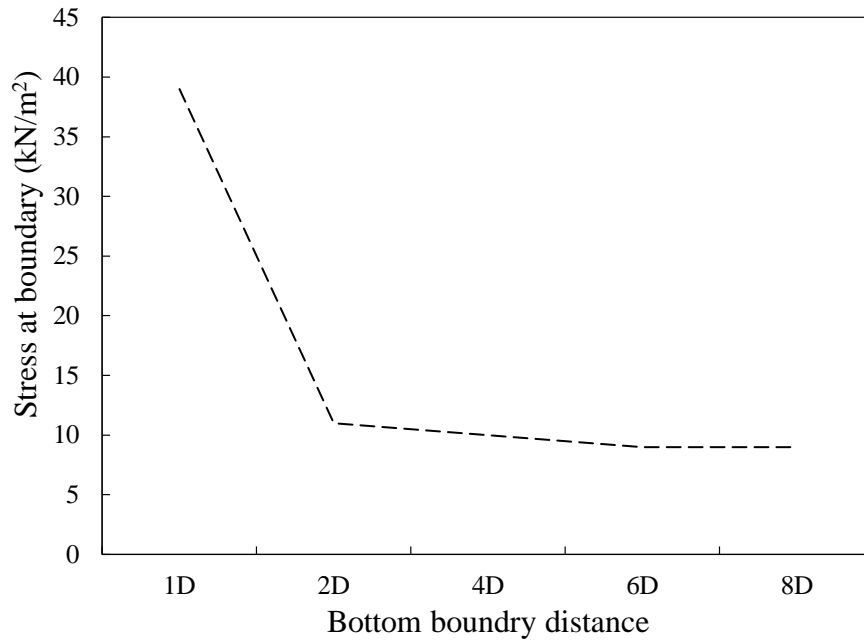
effect of large deformation that can lead to mesh distortion and non-converging solution. This method allowed a fine mesh to be maintained at the pile tip during the installation process and resulting in more accurate numerical results. Freitas et al. (2015) investigated the effect of pile installation using 3D FE models. Densification of the soil around a single driven pile was taken into account by predicting the densification after the pile installation using Alves (1998) equation. Their results demonstrated good agreement between the experimental and the calculated response.

CFA pile construction technique influences its performance and distinguishes it from the bored pile. In order to properly simulate the behaviour of CFA piles, the utilized numerical model should account for the installation effects. However, a limited number of research studies investigated the proper way to numerically model CFA piles. Therefore, this study investigates numerical modeling of bored and CFA piles installed in sand and verifying the modeling technique through comparing its predictions with observed experimental data of both types of piles constructed in the same sand. Moreover, a parametric study was carried out to compare the effect of soil properties and pile geometry on bored and CFA piles behaviour.

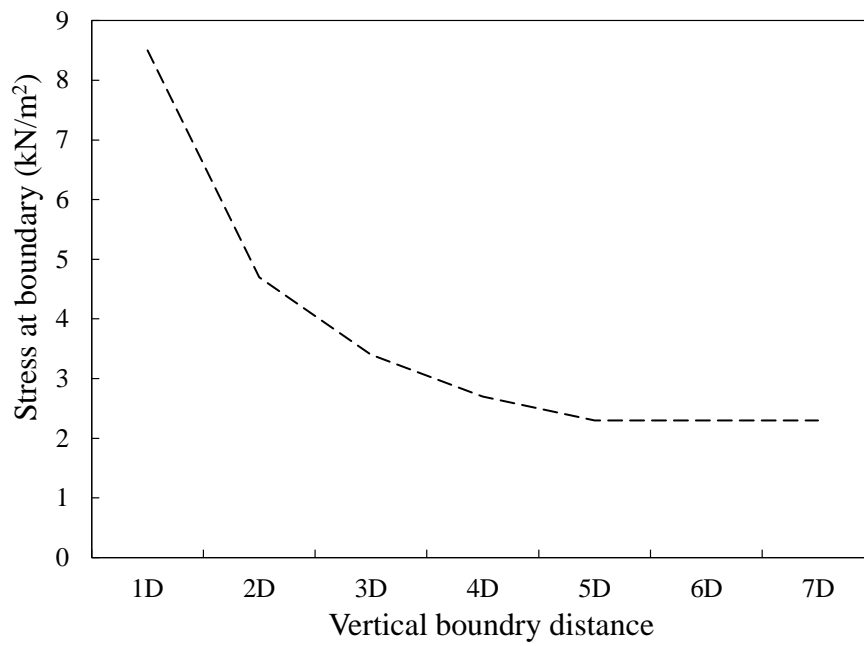
Three-dimensional finite element models were developed using Plaxis software (Brinkgreve et al. 2015) to examine the behaviour of bored and CFA piles under compression, pullout, and lateral loading conditions. The effects of soil strength as well as the pile diameter (D) on its performance were studied for both pile types.

6.2 Finite element model description

Different 3D Plaxis models were developed to simulate the soil-pile system. Each model simulated a single pile subjected to three loading cases: axial compression, uplift and lateral. The soil medium was modeled using ten-node tetrahedral elements that having three active transitional degrees of freedom at each node. The pile was placed at the center along the z -axis of the model, and it was modeled using embedded beam element available in the Plaxis element library (Brinkgreve et al. 2015). The locations of the boundaries were optimized through sensitivity analysis by measuring the stresses due to pile loading at the model boundaries. Stresses produced at the boundaries should be negligible. Stresses are measured while moving the boundaries away until there is no change in the stresses at the boundaries. Figure 6.1 shows the boundary condition sensitivity analysis for (a) the horizontal boundary at the bottom of the model, and (b) the vertical boundary around the pile. Based on the results from the sensitivity studies, the FE model was extended horizontally 1.6 m from the pile center (i.e., five times the largest pile diameter considered in the analysis), and extended vertically 2.5 m below the pile toe (i.e., approximately 8 times the largest pile diameter). Figure 6.2 shows the finite element pile model.



(a)



(b)

Figure 6.1 Boundaries sensitivity analysis for (a) bottom boundary (b) vertical boundary

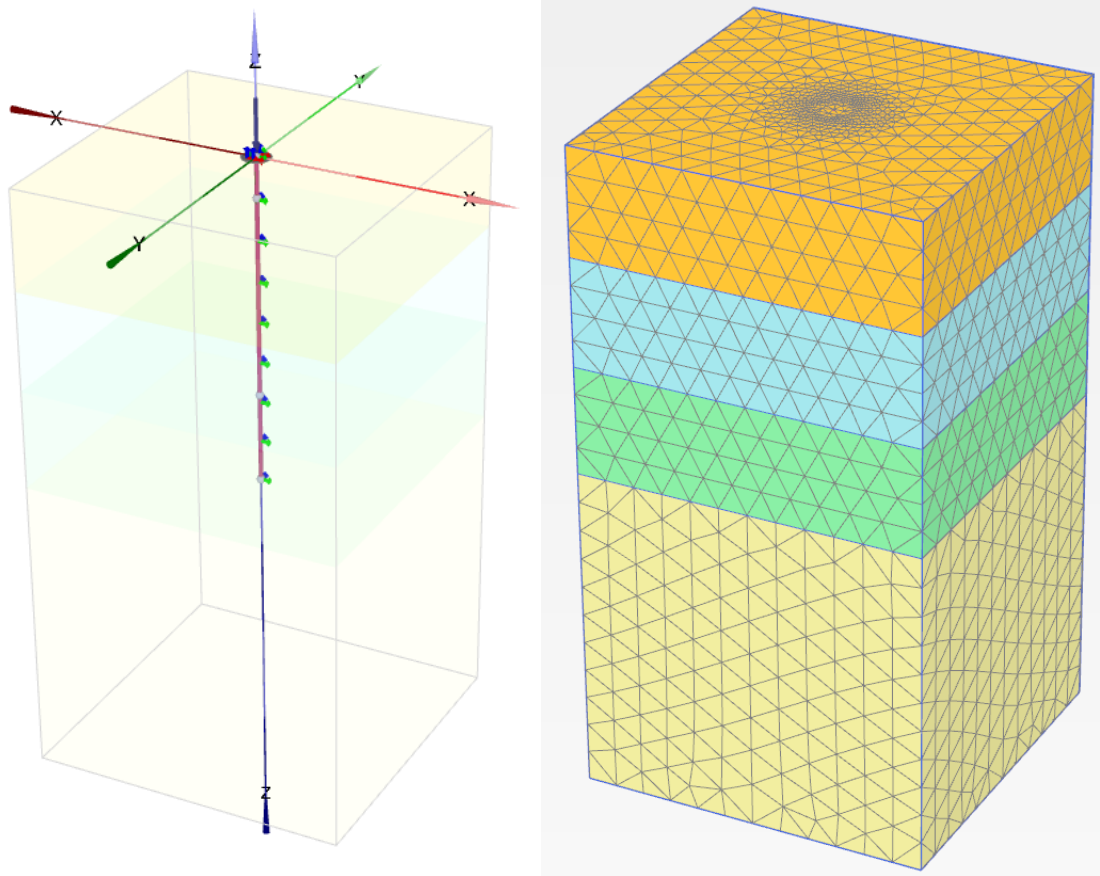


Figure 6.2 Pile model showing the different soil layers

The boundary condition at the top of the FE model was considered as stress-free. The vertical boundaries were free to move in Z-direction and constrained in the horizontal X and Y directions. The bottom boundary was restrained in X, Y, and Z directions. Appropriate meshing is important to ensure accurate and consistent results. Accordingly, a series of models was developed with different mesh refinement, and their results were compared. When the difference in deflection between two successive models was less than 2.5%, the coarser model was selected. Table 6.1 illustrates the mesh sensitivity analysis results for both types of loading, axial and lateral. The mesh was refined in the region along the pile-soil interface as shown in Figure 6.2. The meshing process resulted in a

configuration ranging from 15841 elements up to 24008 elements, the element size was smaller near the pile and increased far from the pile. The effect of pile construction technique on the properties of soil in its vicinity was accounted for as will be discussed later. The model was calibrated based on the field tests and measured soil parameters.

Table 6.1 Mesh sensitivity analysis

No. of elements	Compression		Lateral	
	Displacement (mm)	Error	Displacement (mm)	Error
2910	5.975		5.21	
5845	6.286	5.2%	5.59	7.5%
11095	6.416	2.1%	5.824	4.2%
19297	6.544	2.0%	5.935	1.9%
29625	6.655	1.7%	6.041	1.8%

6.2.1 Soil model – Soil Hardening material model

The soil was simulated by utilizing the Hardening Soil model available in Plaxis, which is characterized by a hardening plasticity yield surface that can expand in the principal stress space due to the plastic straining. This model offers several advantages over the conventional Mohr-Columb Model (elastic perfectly plastic) such as taking into account the effect of the stress on the stiffness modulus. This means that soil stiffness (modulus) increases as the pressure increases.

The soil domain was subdivided into four layers to simulate the change in soil properties with depth. The numerical thickness of each of the top three soil layers was 1 m, and the thickness of the last soil layer was 3 m. In order to account for the effect of CFA pile

construction technique, cylindrical soil bands were considered along the pile shaft, whose properties could be different than the in-situ soil.

The soil parameters adopted in the numerical model were based on the measured soil properties. Higher stiffness and strength was considered for the deeper soil layers as well as for the soil band around the CFA piles. The hardening soil model used to describe the soil constitutive behaviour is defined using the following parameters: secant stiffness from standard drained triaxial test (E_{50}^{ref}), tangent stiffness from primary odometer loading (E_{oed}^{ref}), unloading/reloading stiffness (E_{ur}^{ref}), cohesion (C'_{ref}), angle of internal friction (φ), dilation angle (ψ), and Poisson's ratio (ν).

6.2.2 Interface model

Pile interacts with the soil through joint interface elements. The interface are composed of 12-node interface elements. These elements are compatible with the existing 6-noded triangular soil elements having coinciding node coordinates resulting in zero thickness interface elements. The interaction can involve tip and shaft friction, which can be determined by the relative movement between the pile and the soil. The special interface elements are different from the conventional interface elements that are used along walls or volume piles. The special interface elements are created between the virtual nodes created by the beam element and the soil nodes. The strength properties of the embedded interfaces are linked to the strength properties of the soil layer. Each soil layer data set has an associated strength reduction factor for interfaces R_{inter} . The embedded interface properties are calculated from the soil properties and strength reduction factor by applying the following equations.

$$\tan\varphi_i = R_{inter}\tan\varphi_{soil} \quad \text{Eq. 6.1}$$

$$c_i = R_{inter}c_{soil} \quad \text{Eq. 6.2}$$

6.2.3 Test piles

Bored and CFA piles were installed inside a large-scale soil test pit at Western University. The test pit was filled with concrete sand compacted in layers. The piles length was 3.5 m; the diameter of the piles was measured after exhuming them from the ground. The modulus of elasticity for bored and CFA piles were calculated using Eq. 3.5 (ACI 318) based on the measured compressive strength shown in Table 4.3. The pile parameters are shown in Table 6.2. Figure 6.3 illustrates the modeled pile.

Table 6.2 pile properties of the different models

Properties	Bored pile	CFA pile
E (GPa)	41	44
γ (kN/m ³)	24	24
D (mm)	284	318

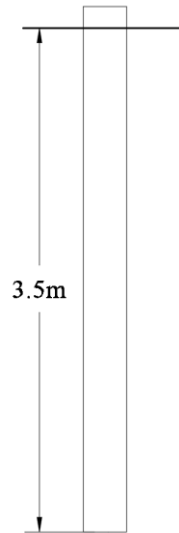


Figure 6.3 Pile diagram

6.2.4 Pile Model

The pile was simulated using embedded beam elements available in the Plaxis library. It consists of 3-node line elements with six degrees of freedom per node. The embedded beam can be placed in the soil medium and can interact with the surrounding soil through interface elements. The pile skin and tip forces can be determined by considering the relative movement between pile and soil. Embedded beam does not occupy volume, but a particular volume around the pile is assumed where the plastic behaviour of soil is excluded. The volume of the pile is specified through the diameter entered in material data set. Its behaviour can be defined by Young's modulus E , unit weight γ , and diameter D (Brinkgreve et al. 2015).

6.2.5 Loading sequence

An initial loading phase was carried out to apply geostatic stresses and equilibrium to consider in-situ stresses. A pile construction phase was then considered in which the pile replaced the soil and the effect of its own weight on the soil was evaluated. These two steps established the state of stress within the soil prior to applying the external loading on the pile. Consequently, the external loading was applied to the test pile following the same sequence that was applied in the experimental load tests in order to account for the effects of testing sequence on the piles behaviour.

6.3 Model calibration

The numerical models were calibrated by comparing the calculated results with the measured experimental load-displacement curves during the loading tests (Chapter 4 and 5). The measured soil parameters presented in Table 6.3 were used in the initial model. Secant stiffness in standard drained triaxial test (E_{50}^{ref}) was adopted after Poulos (1975) for medium dense soil between 20 to 50 kPa. Then E_{oed}^{ref} and E_{ur}^{ref} were calculated from Eq. 6.3 and Eq. 6.4 , respectively (Brinkgreve et al. 2015):

$$E_{oed}^{ref} = 0.75 * E_{50}^{ref} \quad \text{Eq. 6.3}$$

$$E_{ur}^{ref} = 3 * E_{50}^{ref} \quad \text{Eq. 6.4}$$

Table 6.3: Soil parameters before calibration

	Layer 1	Layer 2	Layer 3	Layer 4
Angle of internal friction φ (degrees)	34	34	34	34
Cohesion c' (kPa)	5	5	5	5
Dilation angle ψ (degrees)	5	5	5	5
Poisson's ratio ν	0.3	0.3	0.3	0.3
Secant stiffness in standard drained triaxial test E_{50}^{ref} (MN/m ²)	20	30	40	50
Effective unit weight γ' (kN/m ³)	18.5	18.5	18.5	18.5

These parameters were then fine-tuned through the calibration process to obtain best match between the calculated response and the measured load-displacement curves. The secant stiffness is responsible for the initial stiffness of the pile. While, the angle of internal friction and the cohesion has significant effect on the pile behaviour after the initial loading. Calibration first started by adjusting the secant stiffness to get a good agreement of the first part of the load displacement curve. Then, adjusting the interface strength to get better match of the non-linear part of the curve. Calibration results of each of the two models are illustrated in the next section.

Simplifications and assumptions were introduced to the modelling the mechanical behaviour of the soil. It was assumed the soil is homogeneous, isotropic material. The pile material was assumed to be elastic without reinforcement with equivalent section used. The effect of the soil disturbance due to previous loading was taken into account by using the interface reduction factor. All these assumptions are important facilitate the pile and soil modelling.

6.3.1 Compression loading

6.3.1.1 Bored pile

The calibrated soil parameters were the same as initial parameters except for E_{50}^{ref} for layers 2 and 3, which was increased to 35 and 50 MN/m², respectively. The comparison between the calculated and the measured load-displacement curves is shown in Figure 6.4. As can be noted from Figure 6.4, the calculated and measured response curves are in excellent agreement throughout the entire compressive loading range, indicating that both the stiffness and strength of the soil considered in the numerical model are representative of the in-situ conditions.

6.3.1.2 CFA pile

To account for the construction effect of the CFA pile in the numerical model, two soil bands were placed around the pile shaft. The diameters of these bands were 1.6 and 3 times the diameter of the CFA pile (Figure 6.5). The parameters of the soil bands, as well as the soil layers was initially estimated then it was calibrated to result in a proper pile response compared to the measured behaviour. Table 6.3 shows the initial parameters while the after calibration parameters are shown in Table 6.4. To capture the most appropriate behaviour for the end bearing resistance, a rigid plate 0.1 m thick with the same diameter as the pile, with linear elastic material was placed under the pile tip (Brinkgreve et al. 2015). Figure 6.6 compares the calculated and measured load deflection for the CFA pile under compression. It shows that the calibrated models can effectively simulate the experimental pile behaviour.

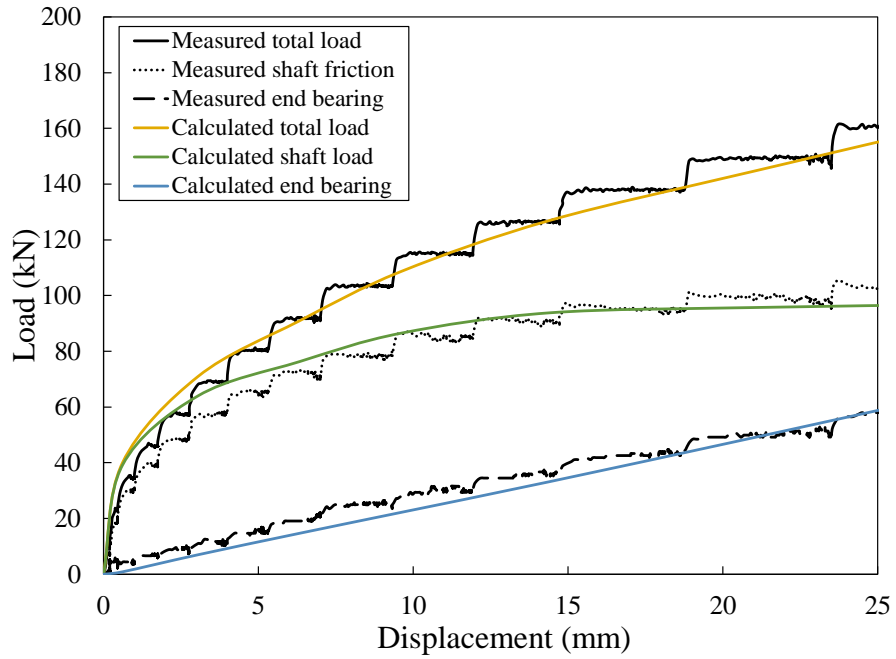


Figure 6.4: Comparison of measured and calculated compression load-settlement curves of bored pile

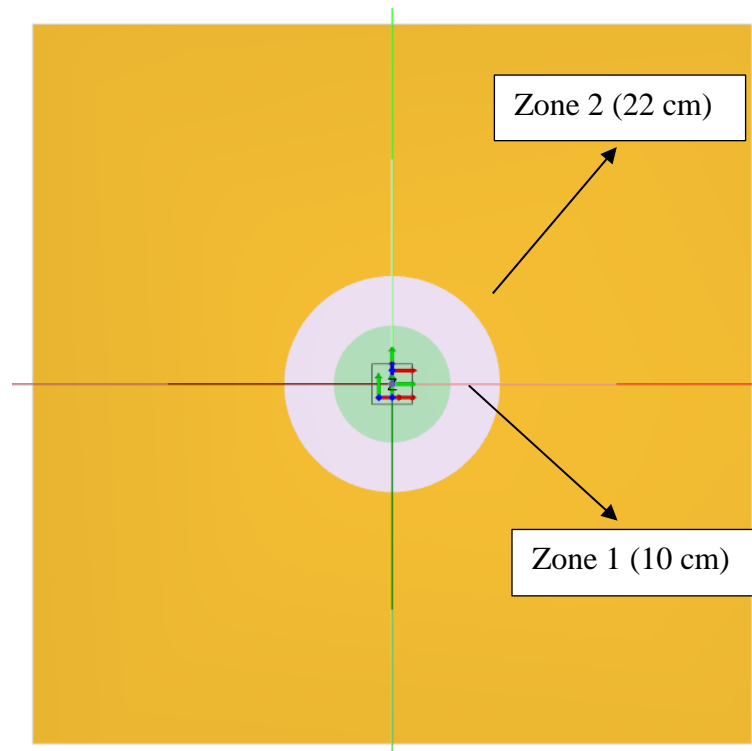


Figure 6.5: Plan view of the soil configuration around the CFA pile

Table 6.4: Soil properties of the CFA pile model

	Layer	Layer	Layer	Layer	Zone	Zone
	1	2	3	4	1	2
Angle of internal friction ϕ (degrees)	34	34	34	34	36	36
Cohesion c' (kPa)	0	0	5	5	5	5
Dilation angle ψ (degrees)	4	4	4	4	5	4
Secant stiffness in standard drained triaxial test E_{50}^{ref} (MN/m²)	45	45	50	60	100	80

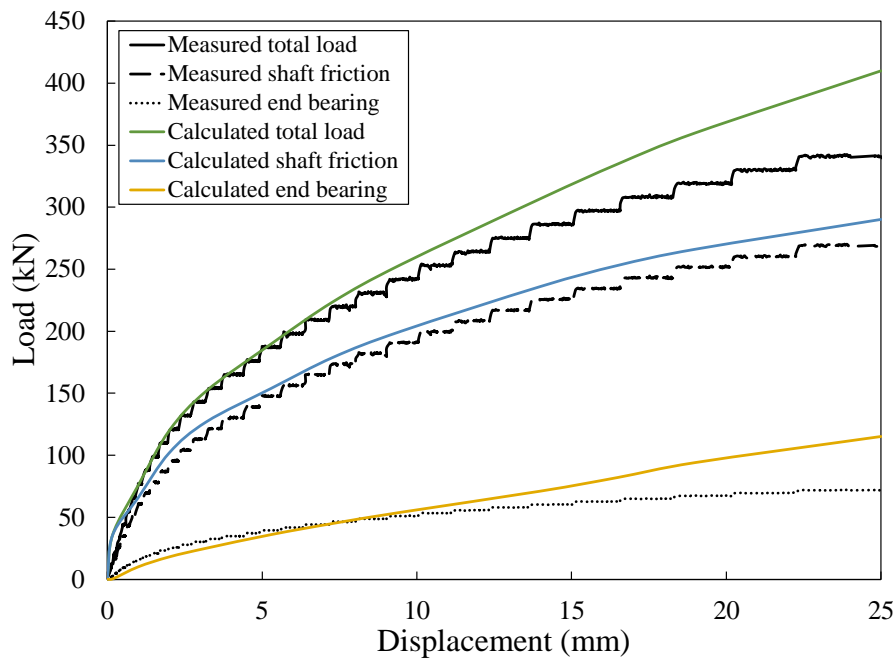


Figure 6.6: CFA pile measured and calculated compression load deflection comparison

6.3.2 Pullout loading

6.3.2.1 Bored pile

The soil parameters in the bored pile model simulating the pullout test was the same as that used in the compression test. However, the interface reduction factor was reduced to 0.3 to calibrate the pullout test properly. The lower interface reduction factor can be attributed to the high displacement that the pile was exposed to during the previous compression test which reduced the soil shear strength. Figure 6.7 shows the comparison between the measured and calculated load-deflection for the bored pile. Figure 6.7 shows good agreement between the experimental and the calculated results through the entire curve, indicating that the stiffness and the soil strength parameters represents the real pile behaviour.

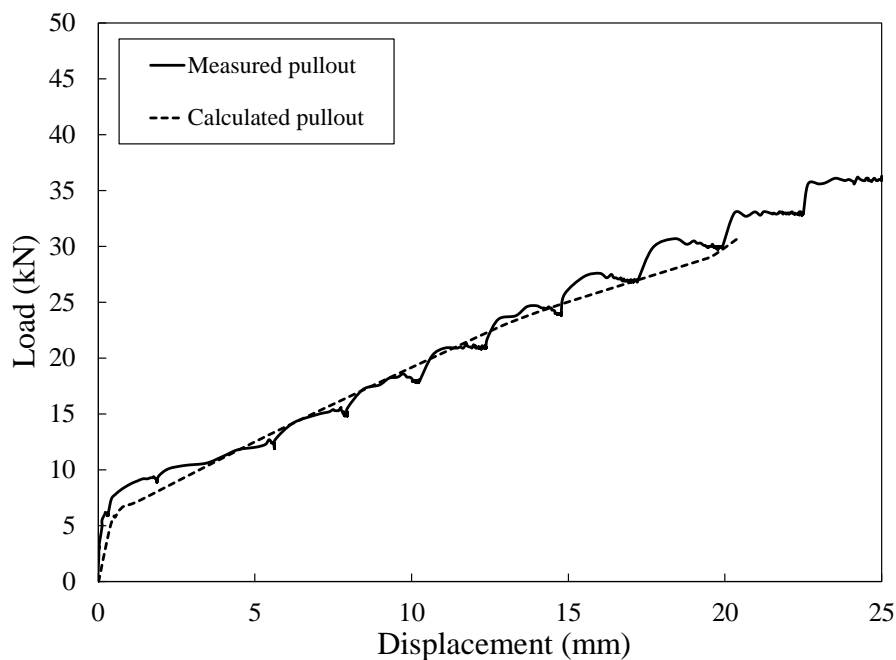


Figure 6.7: Comparison of measured and calculated pullout load-displacement curve for bored pile

6.3.2.2 CFA pile

In order to obtain good match between the calculated and measured responses, the interface reduction factor for the pullout model was reduced to 0.25. The reduction factor reflects the decrease that occurred in the shaft friction measured during the pullout test for the pile under consideration. This behaviour can be attributed to the reduction in the reduction of the friction angle from the peak to the residual. Similar behaviour was reported by (Joshi et al. (1992)). The rest of the soil parameters stayed the same. Figure 6.8 shows the comparison between the calculated and measured load-displacement for the CFA pile under pullout. It can be noted from Figure 6.8 that there is good agreement at the initial part of the curve which means the stiffness is representing the soil conditions.

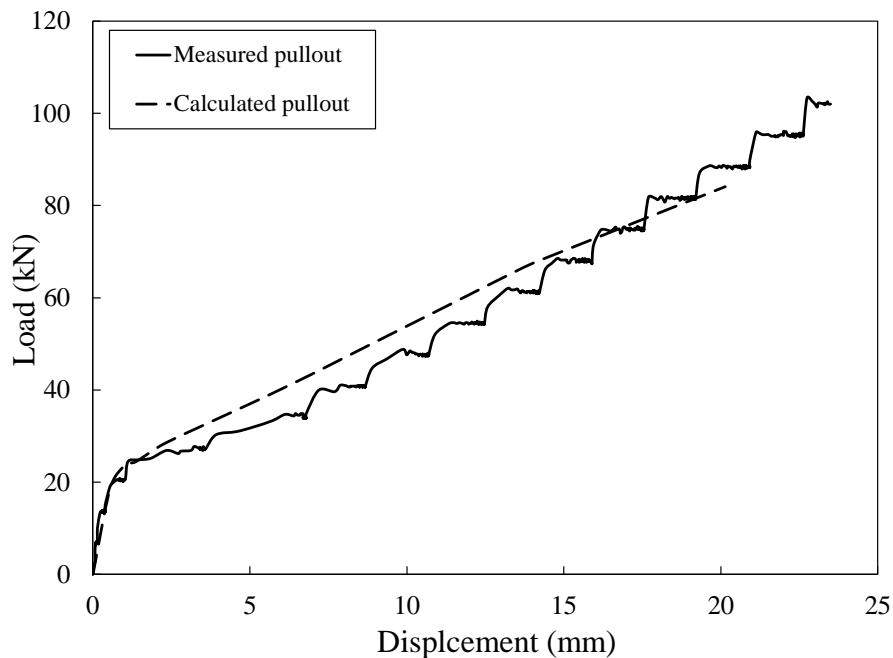


Figure 6.8: CFA pile measured and calculated pullout load deflection comparison

6.3.3 Lateral loading

6.3.3.1 Bored pile

The comparison between the measured and the calculated load-displacement curve is shown in Figure 6.9. As can be noted from Figure 6.9, there is good agreement between the measured and the calculated curves.

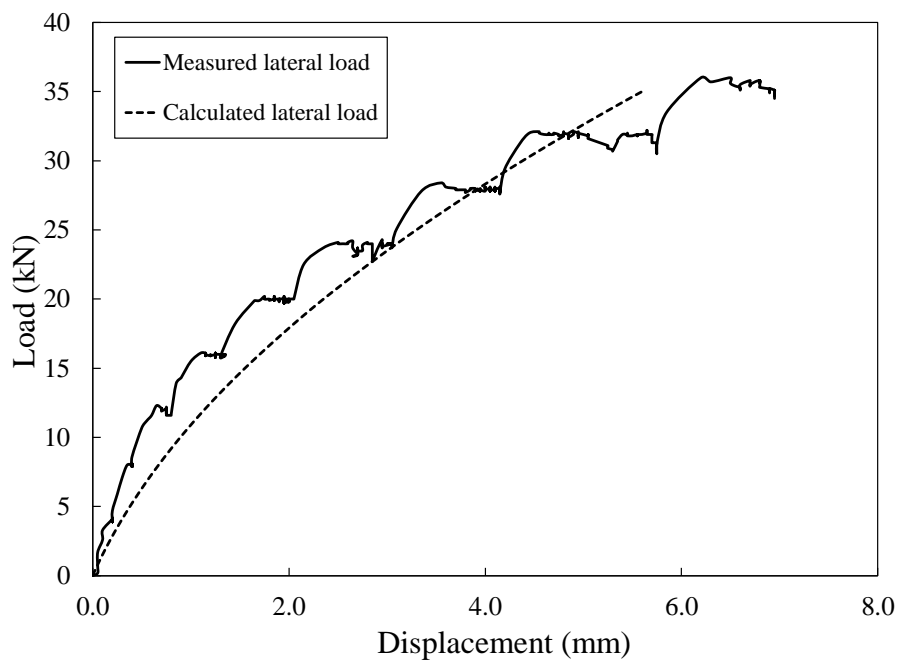


Figure 6.9: Comparison of measured and calculated lateral load-deflection curve for bored pile

6.3.3.2 CFA pile

The same model used for simulating compression and pullout loading behaviour was utilized for the lateral loading case. The interface reduction factor was equal to 0.7 in this case. This can be attributed to the new direction and soil that the pile is heading towards,

which is still with its full strength. Figure 6.10 compares the calculated and measured load-deflection curve for the CFA pile under lateral loading. the comparison in Figure 6.10 shows good agreement specifically at the first segment of the curve which indicates that the soil stiffness represents the field conditions.

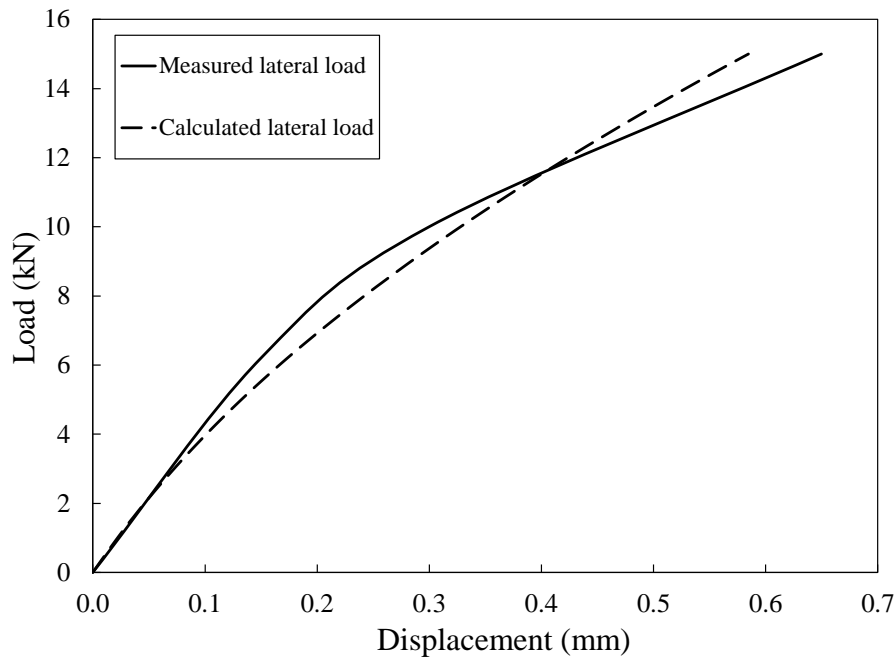


Figure 6.10: Comparison of CFA pile measured and calculated lateral load-deflection curves

6.4 Verification

The CFA compression model was verified using the measured data available from load testing of the CFA pile constructed with 240 mm diameter installed in the same conditions.

The pile was tested in compression only due to complications during inserting the steel reinforcement as this was the first pile to construct. And that is why the verification was done in compression only. The soil bands that were added around the pile stayed with the

same diameter. The only difference between the model used in calibration and the one used in verification was the diameter. Figure 6.11 shows the comparison between the measured and the calculated load deflection curves used for model verification. It can be noted from Figure 6.11 that there is excellent agreement between the measured and the calculated results. The model simulated the stiffness and the soil strength.

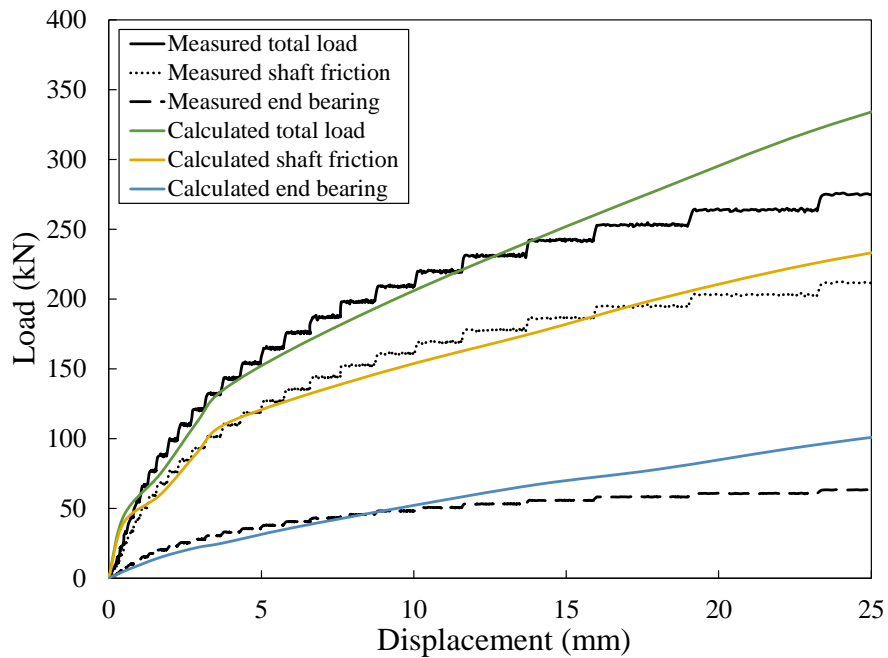


Figure 6.11 Verification comparison between measured and calculated compression load deflection curves

6.5 Parametric study

The calibrated numerical models were utilized to conduct a parametric study to investigate the comparative performance of bored and CFA piles considering different soil strength

(angle of internal friction) and pile diameter under different loading conditions. The results of the parametric study are presented and discussed in the following sections.

6.5.1 Effect of angle of internal friction

The values of friction angle of general soil medium considered in the parametric study were 30° , 35° , and 40° . The angle of friction of soil zones around the pile in the calibrated model had higher values than that of the general soil medium. The angle of friction of these zones were varied in the parametric study utilizing the same ratio of friction angle of the general soil model. For example, for the model with $\phi = 30^\circ$, the ratio is $30^\circ/34^\circ = 0.88$; the same ratio was applied to friction angle of soil zones around the pile.

6.5.1.1 Comparison of Compression Behaviour of Bored and CFA

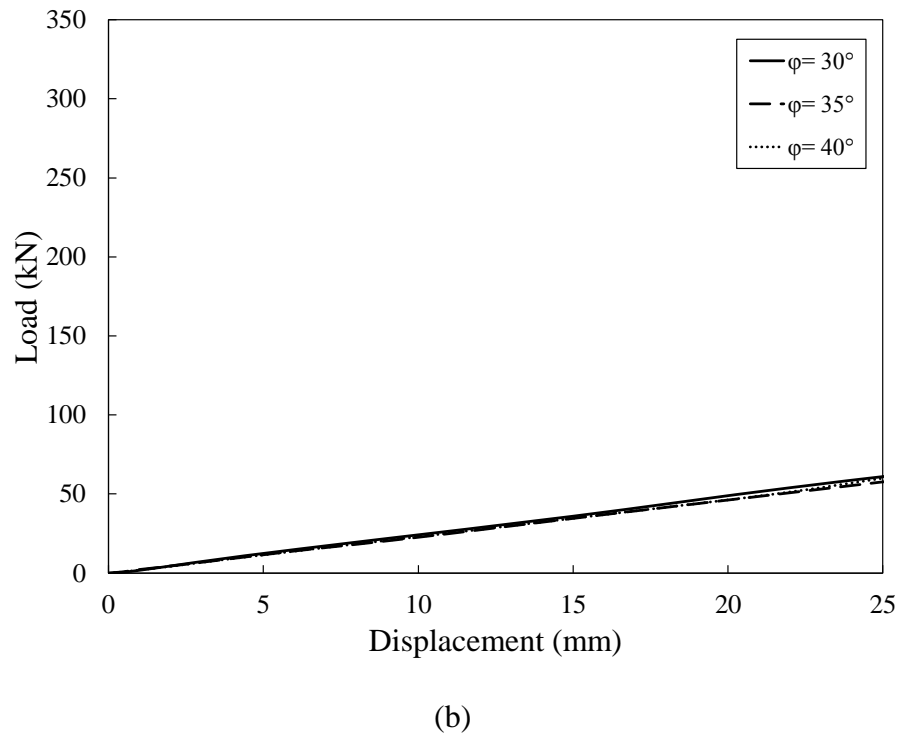
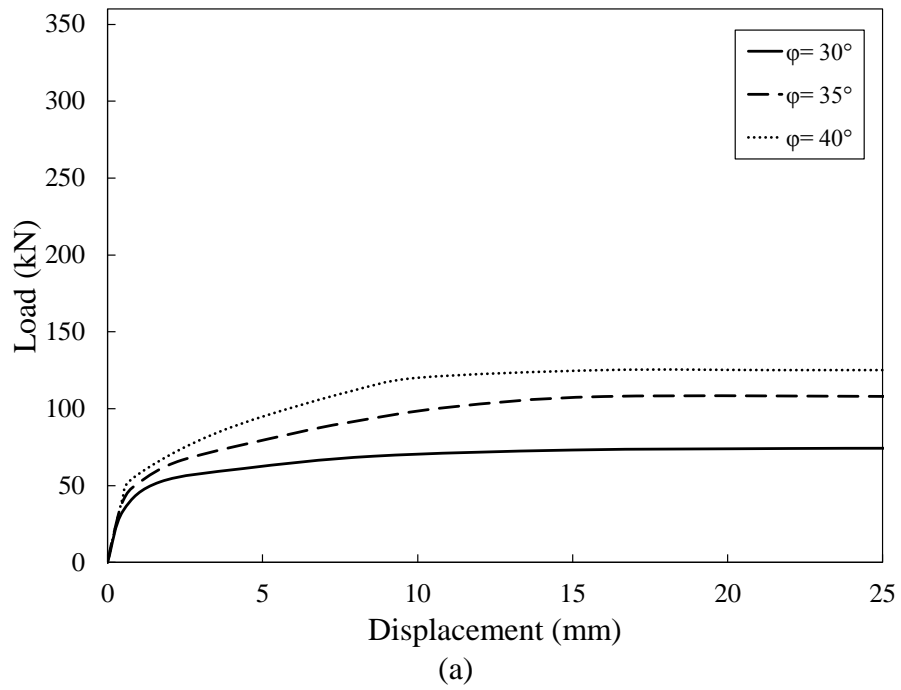
This section investigates the effect of the angle of internal friction on the response of both bored and CFA piles to compressive loading. Both the shaft and end bearing loads as well as the total load were calculated.

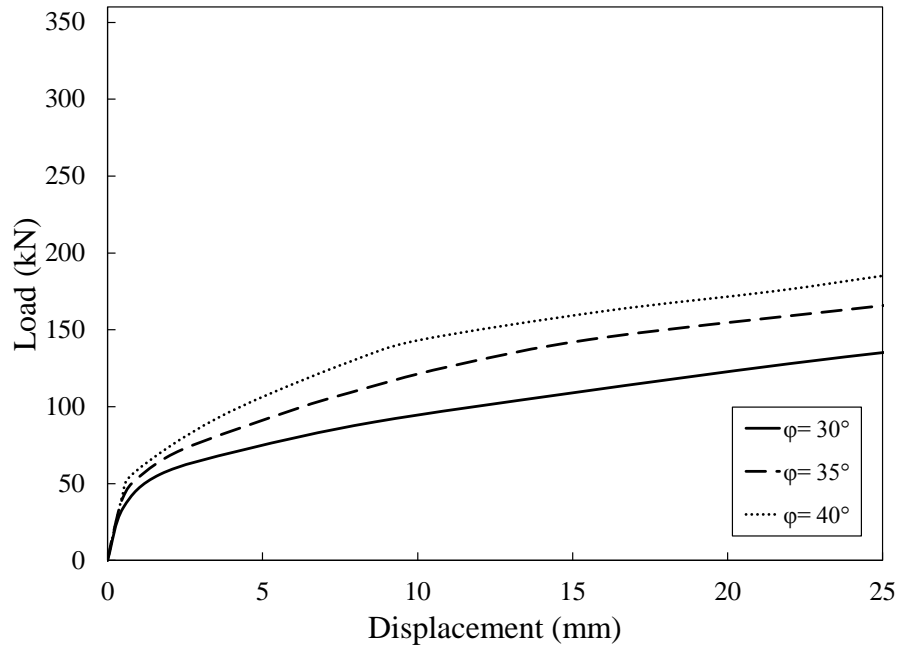
Figure 6.12a, b, and c presents the shaft load, end bearing load and, total load, respectively, of the bored pile for different values of angle of internal friction. As can be noted from Figure 6.12, the shaft friction and, consequently, the total load increases as the friction angle increased. It is also noted that the shaft resistance reached a maximum value at about 5 to 10 mm displacement (approximately 2-3% of the pile diameter). Full mobilization of shaft resistance occurred at higher displacement as the friction angle increased. On the other hand, the end bearing load was not affected by the change in friction angle. This can be attributed to the fact that the bearing resistance was not fully mobilized even for the case

with lower friction angle (30°) because end bearing resistance requires large displacement (as high as 10% of the pile diameter) to be fully mobilized.

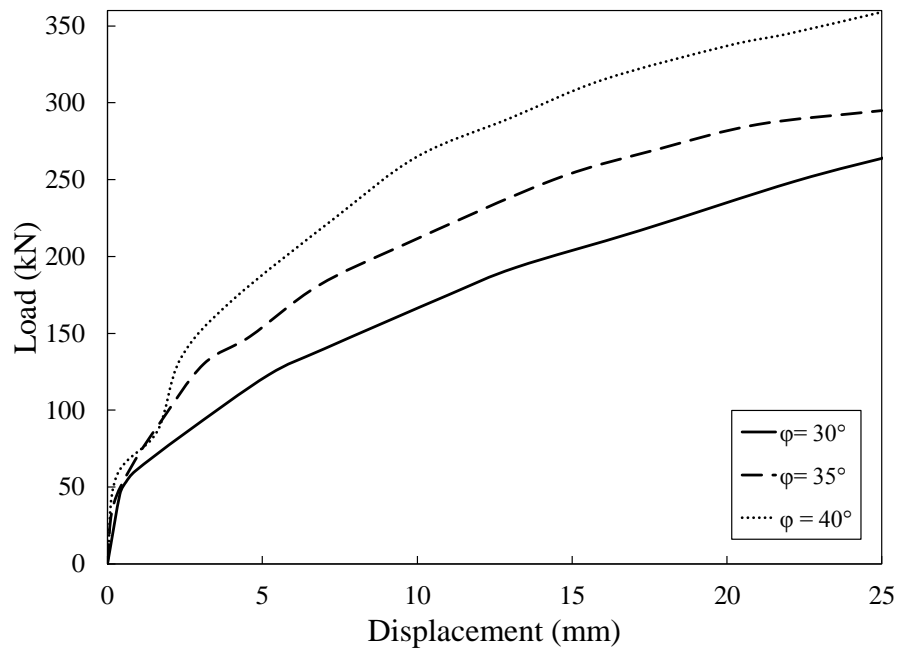
Figure 6.12 d, e, and f presents the shaft load, end bearing load and, total load, respectively, of the CFA pile for different values of angle of internal friction. It can be noted from Figure 6.12 that, similar to the bored pile case, the shaft load increased as the friction angle increased while the end bearing load remained unchanged. It is also noted that the shaft load of CFA pile continued to increase as the applied load increased, suggesting it was not mobilized fully for the range of load considered in the analysis. This could be attributed to the increased strength of the annular soil zone around the pile due to the construction technique.

Comparing the behaviour of both bored and CFA piles under compressive loading, it can be concluded that the CFA pile offers superior performance owing to the enhanced shaft friction and soil confinement due to the construction process.

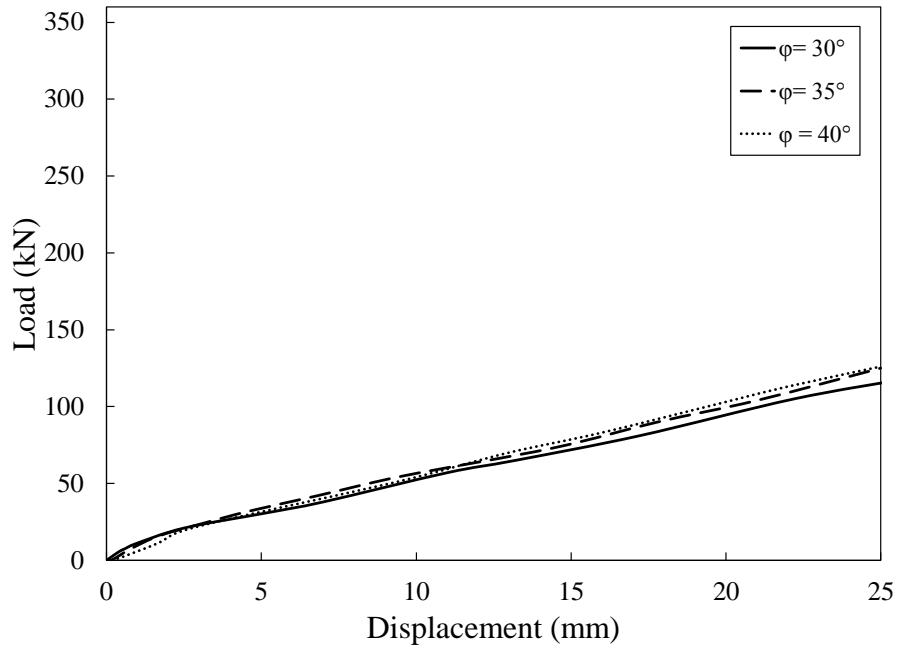




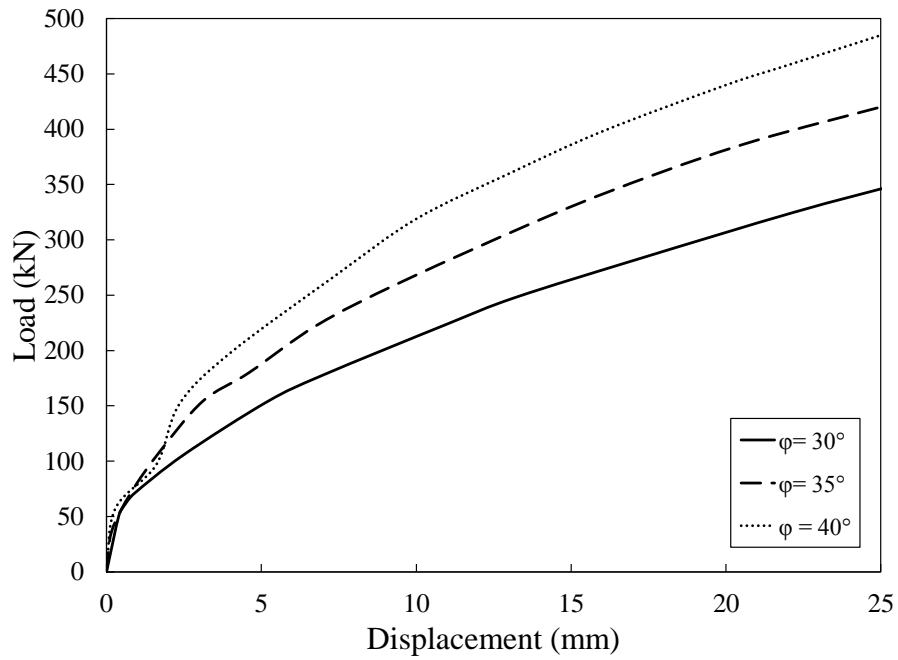
(c)



(d)



(e)

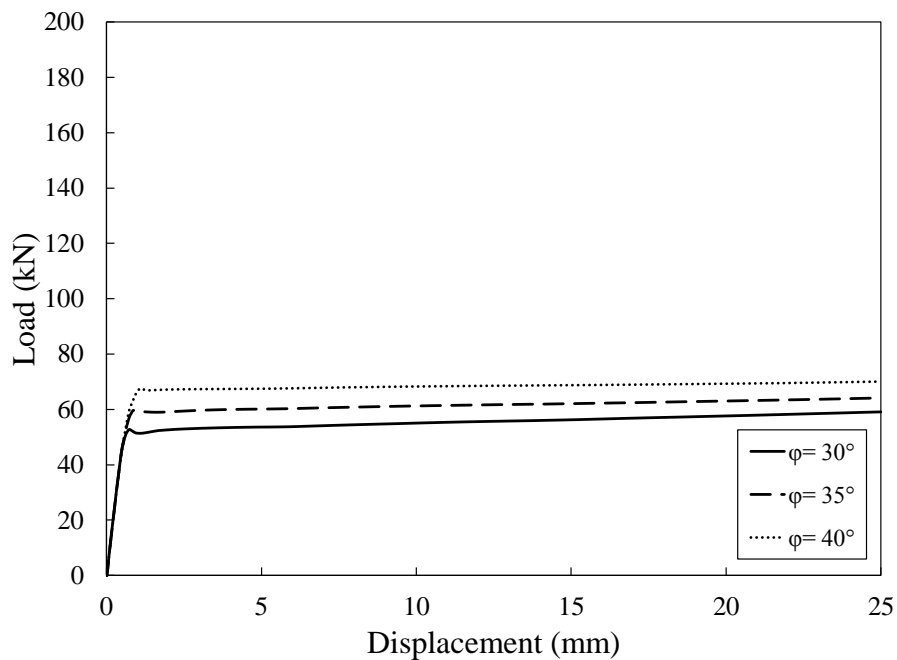


(f)

Figure 6.12 Effect of friction angle on (a) shaft friction, (b) end bearing, and (c) total load of the bored pile, and (d) shaft friction, (e) end bearing, and (f) total load of the CFA pile

6.5.1.2 Comparison of Pullout Behaviour of Bored and CFA

The effect of the change in angle of internal friction on the pullout response of bored and CFA piles was investigated. Figure 6.13a and b display the load-displacement curves of the bored and CFA piles, respectively. It is noted from Figure 6.13 that the change in friction angle has small effect on the pullout capacity of the CFA and bored pile. The shaft friction for the CFA pile (Figure 6.13b) shows the increasing in strength by increasing the displacement unlike the bored pile which reached the maximum capacity after small displacement and then stayed constant.



(a)

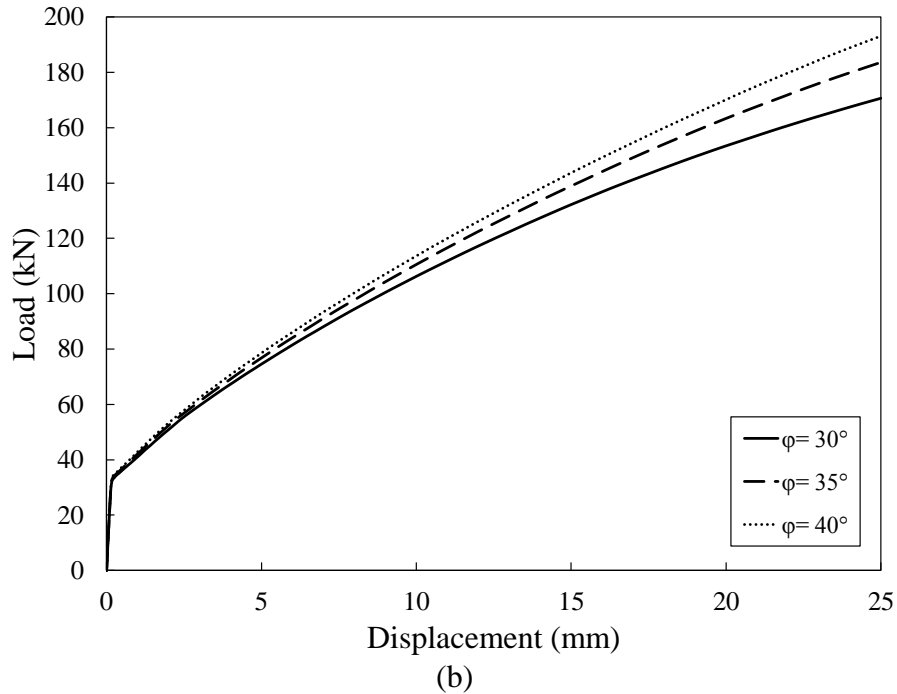
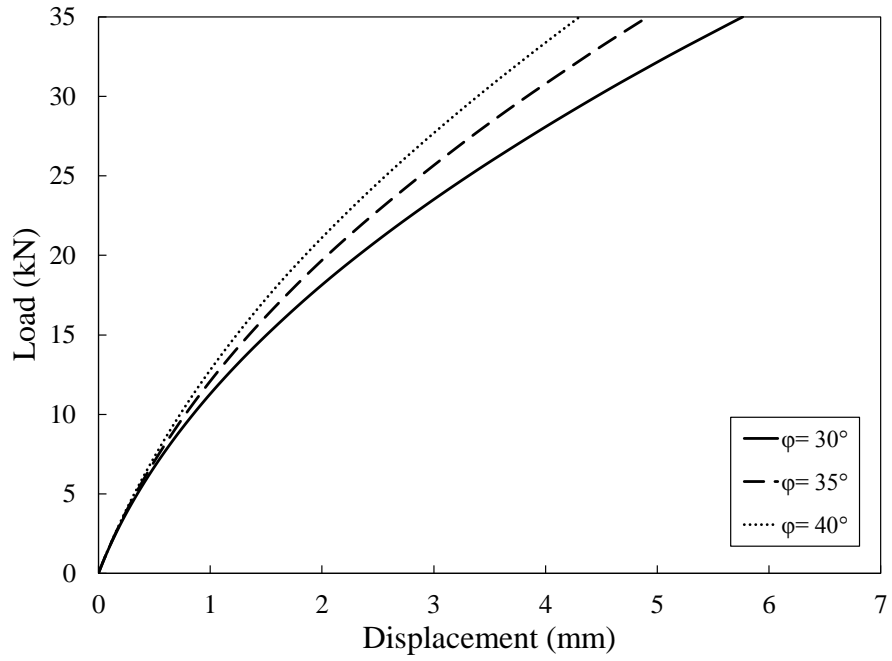


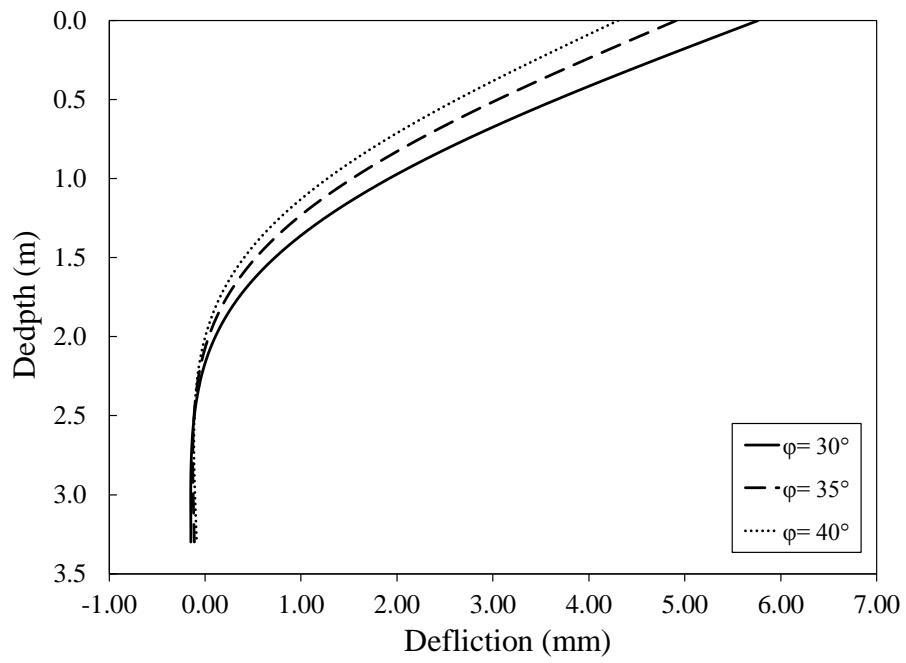
Figure 6.13 Effect of friction angle on pullout load displacement of (a) bored pile (b) CFA pile

6.5.1.3 Comparison of Lateral Behaviour of Bored and CFA

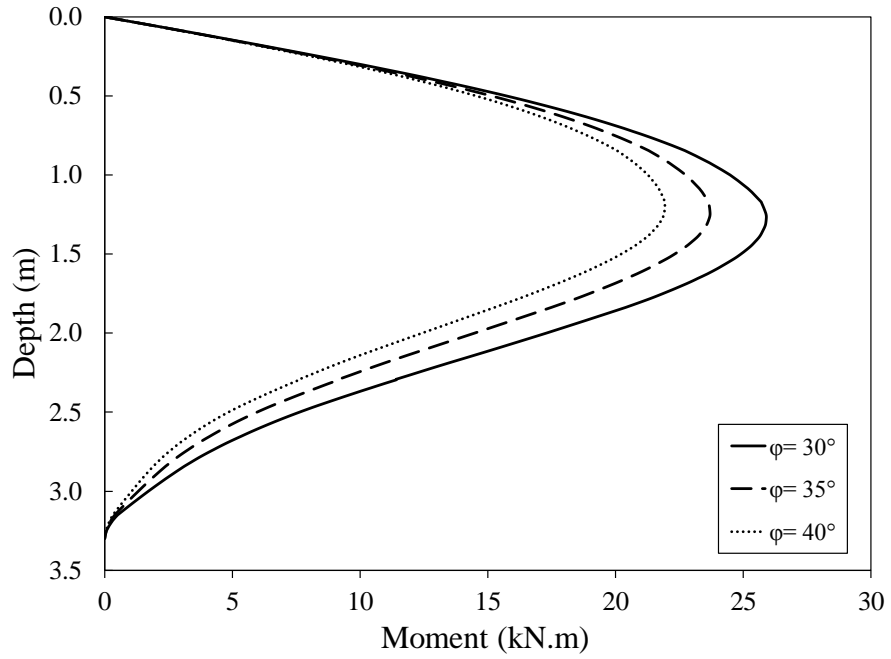
The effect of angle of internal friction on bored and CFA piles lateral behaviour was investigated. Figure 6.14a, b, and c shows the pile head displacement, deflection along the pile shaft, and moment distribution of the bored pile, respectively. The pile head movement and its deflection as well as its bending moment decreased by increasing the friction angle. Figure 6.14 d, e, and f show the head displacement, pile deflection, and moment distribution of the CFA pile. The CFA pile followed the same trend as the bored pile. The pile deflection decreased by increasing the angle of internal friction with about the same ratio. The position of the maximum bending moment of the CFA pile was higher than that of the bored pile. It can be attributed to the lower applied load on the pile.



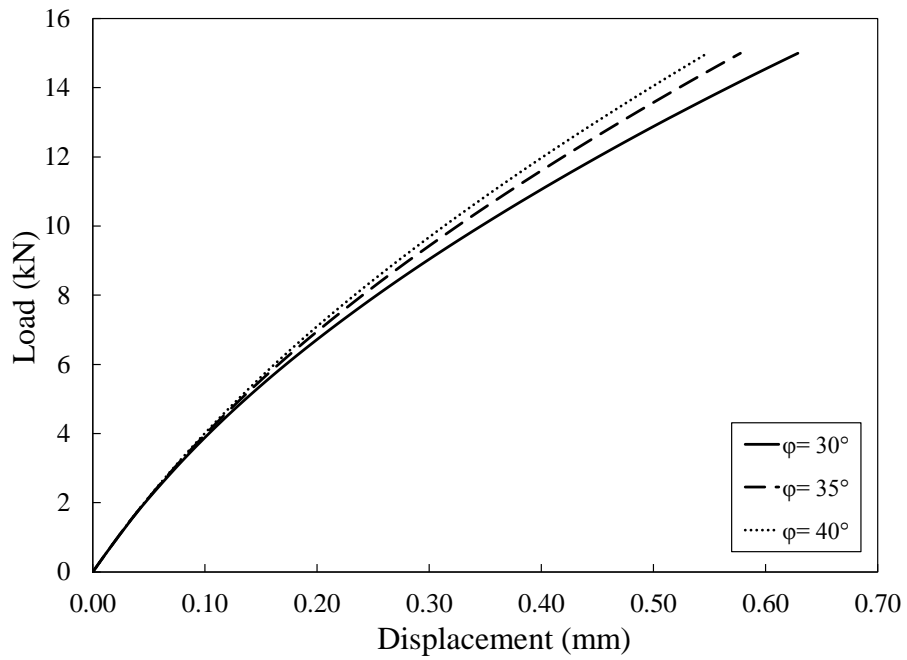
(a)



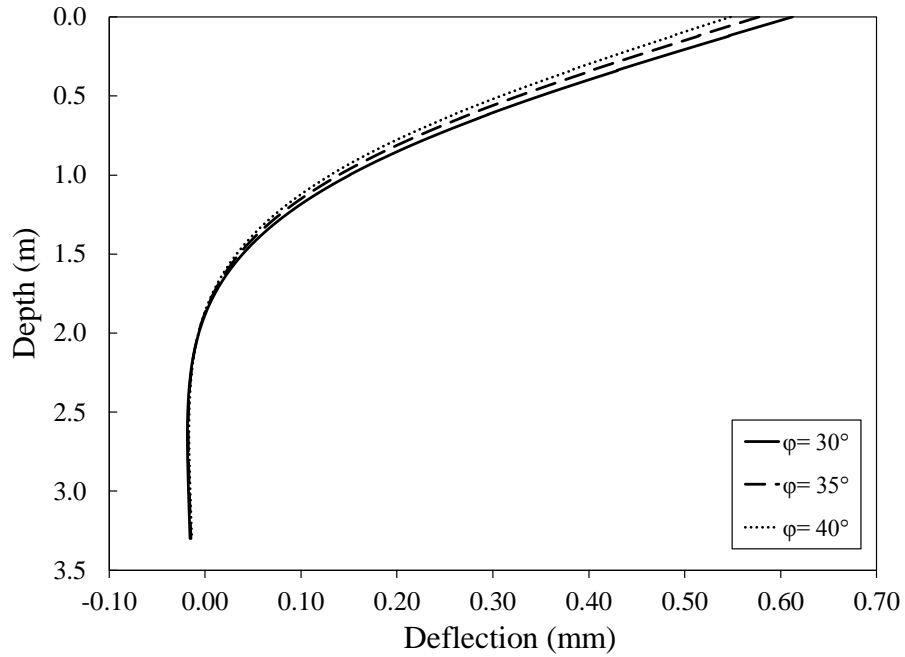
(b)



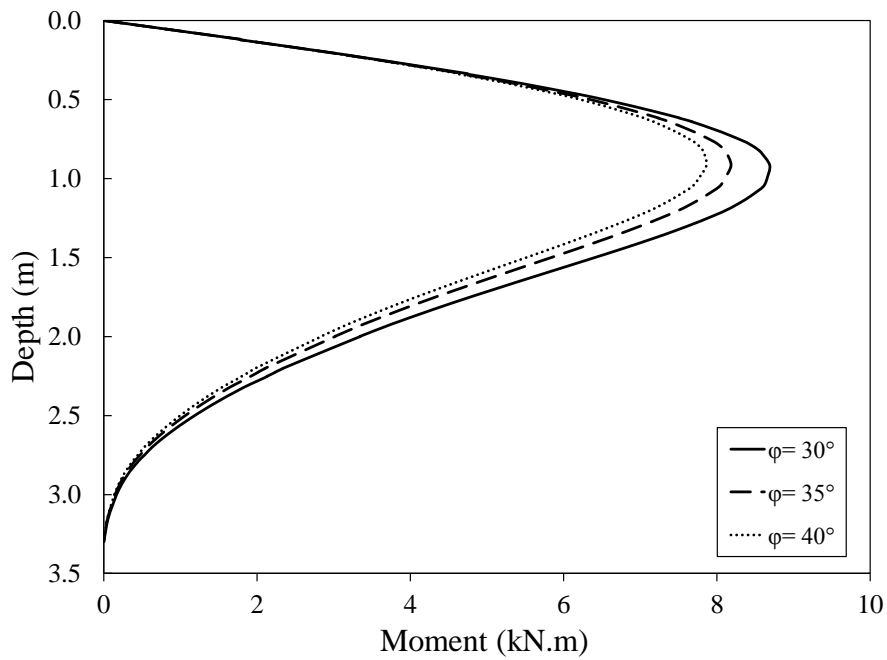
(c)



(d)



(e)



(f)

Figure 6.14 Effect of friction angle on (a) load displacement, (b) pile deflection, and (c) moment distribution of bored pile, and (d) load displacement, (e) pile deflection, and (f) moment distribution of CFA pile

6.5.2 Effect of Pile diameter

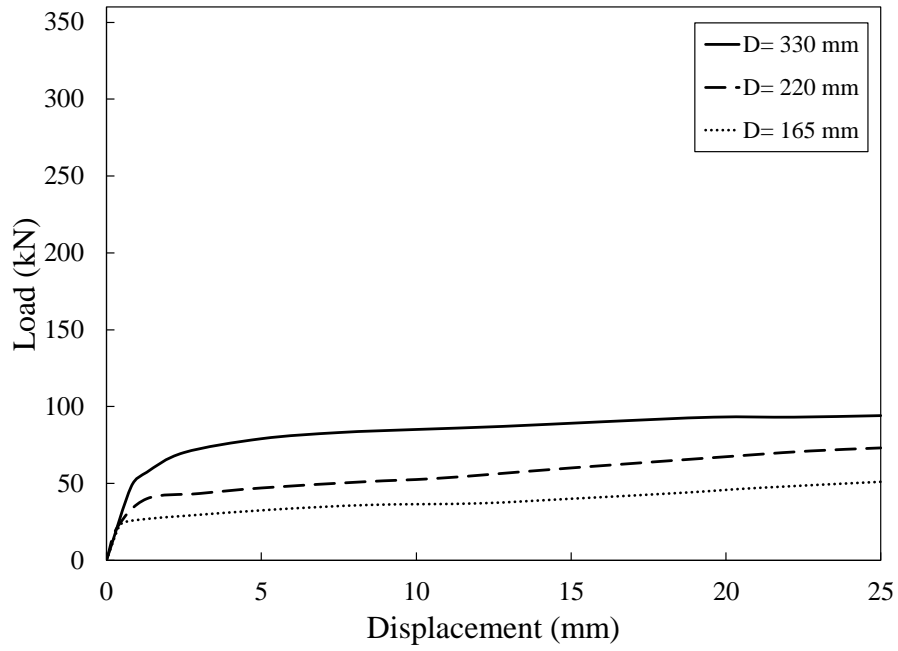
In this part of the study, the pile length was maintained constant and the pile diameter (D) values 330, 220, and 165 mm were used. The diameter of the stiffer annular soil zones around the CFA pile stayed the same.

6.5.2.1 Comparison of Compressive Behaviour of Bored and CFA piles

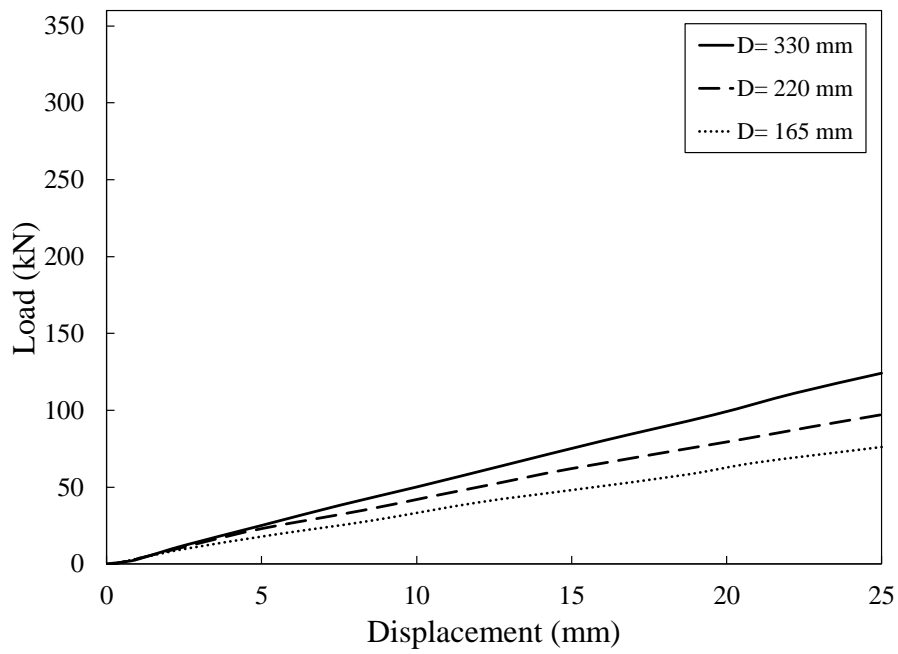
This section investigates the effect of D on the behaviour of both bored and CFA piles under compressive loading. Both the shaft and end bearing loads as well as the total pile load were calculated.

Figure 6.15 a, b, and c shows the shaft, end bearing and total loads for the bored pile with different D values. It can be noted that the pile capacity, as expected, decreased by reducing D . This can be attributed to the lower surface area of the pile due reducing the pile diameter, which in turn reduced the total load. The pile diameter decrease did not affect the end bearing which can be attributed to the soil disturbance below the pile toe during construction.

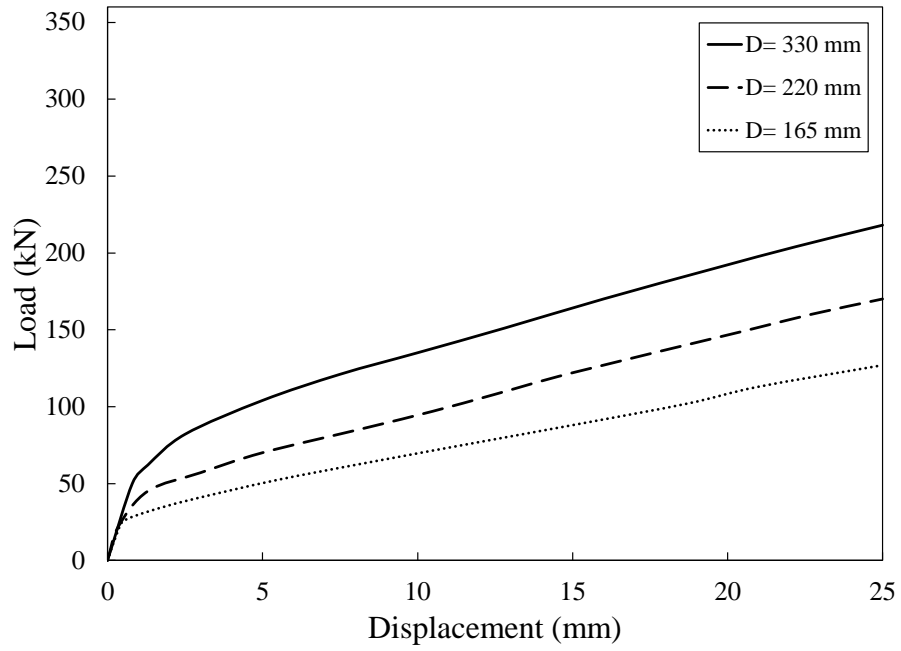
Figure 6.15 d, e, and f show the shaft, end bearing and total loads, respectively, of CFA pile with different D values. The behaviour of the pile with largest diameter was stiffer in both shaft and end bearing with the total load-displacement curve acting as expected.



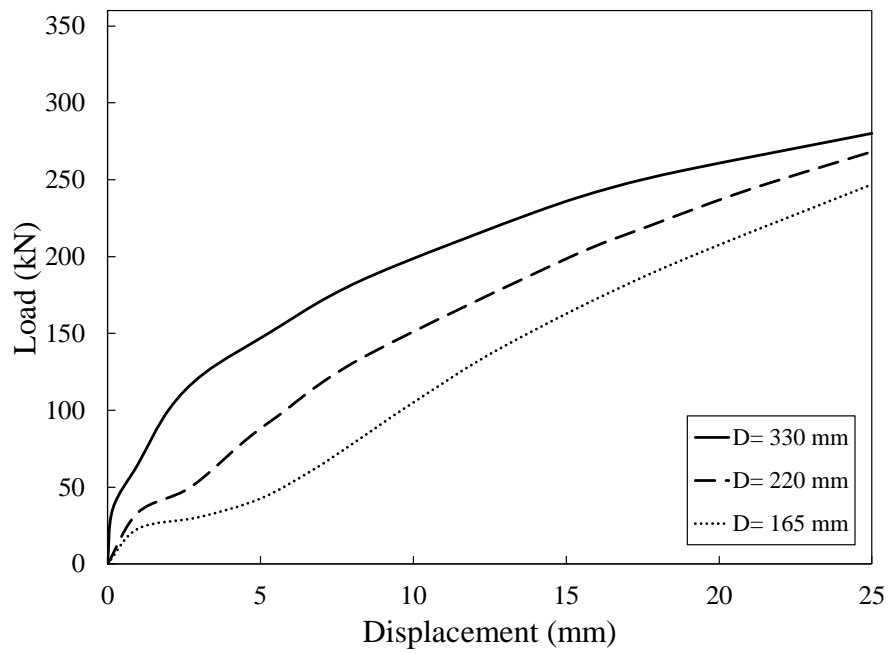
(a)



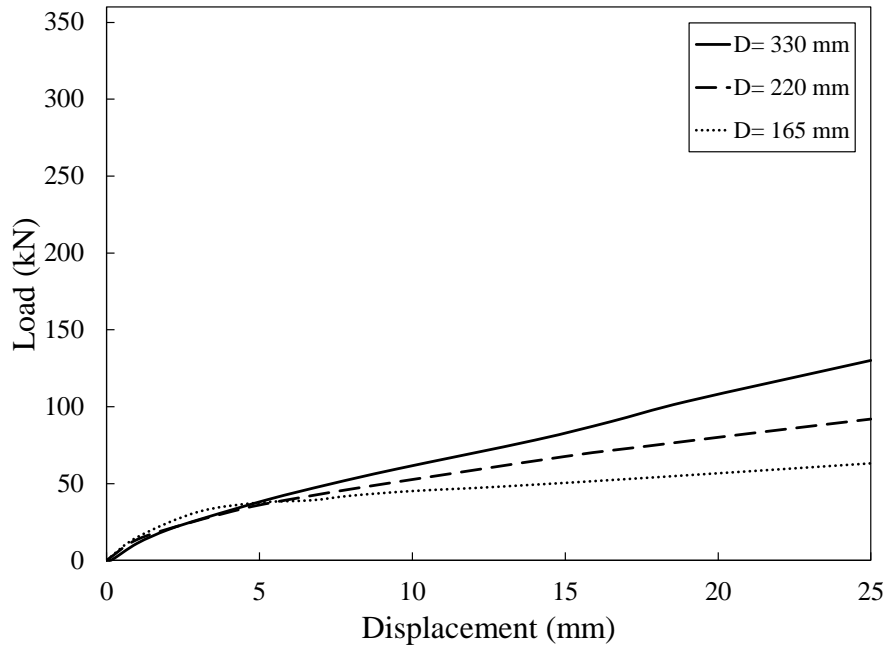
(b)



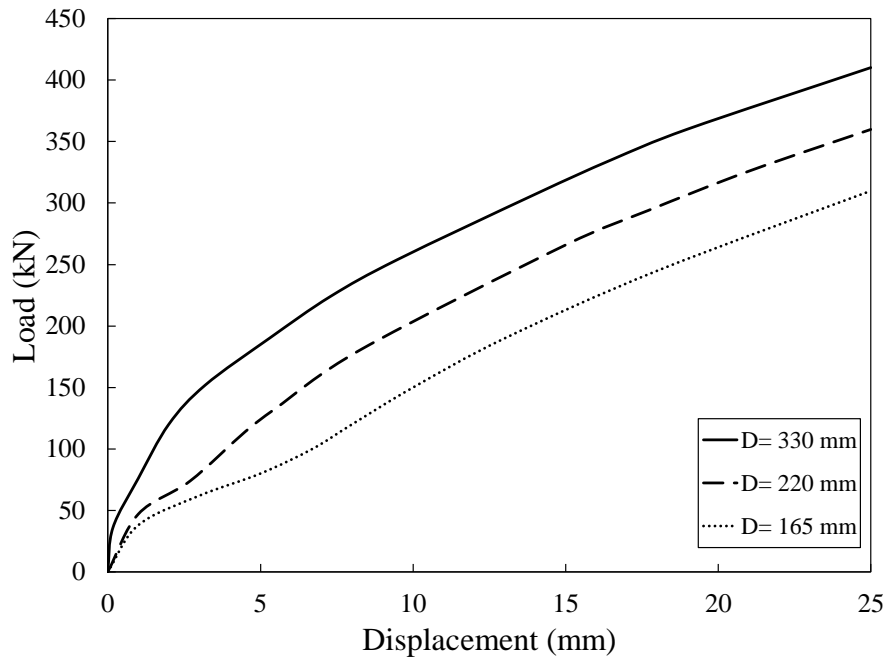
(c)



(d)



(e)



(f)

Figure 6.15 Effect of D on (a) shaft friction, (b) end bearing, and (c) total load of the bored pile, and (d) shaft friction, (e) end bearing, and (f) total load of the CFA

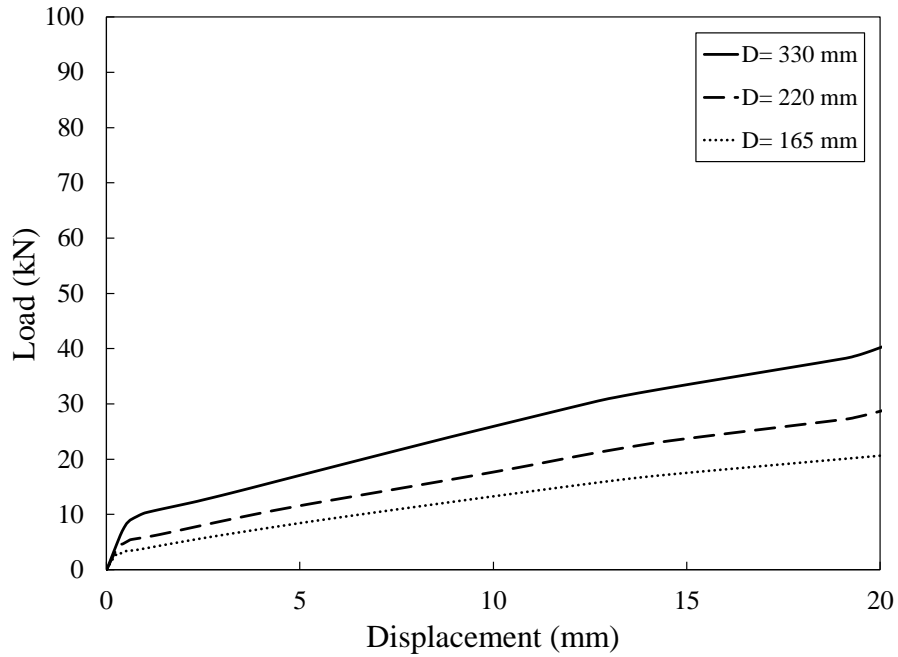
6.5.2.2 Pullout of bored and CFA

Pile diameter effect on the bored and CFA piles was investigated. Figure 6.16 shows the effect of D on pullout behaviour of bored and CFA piles. It was noted that the uplift capacity decreased by reducing D .

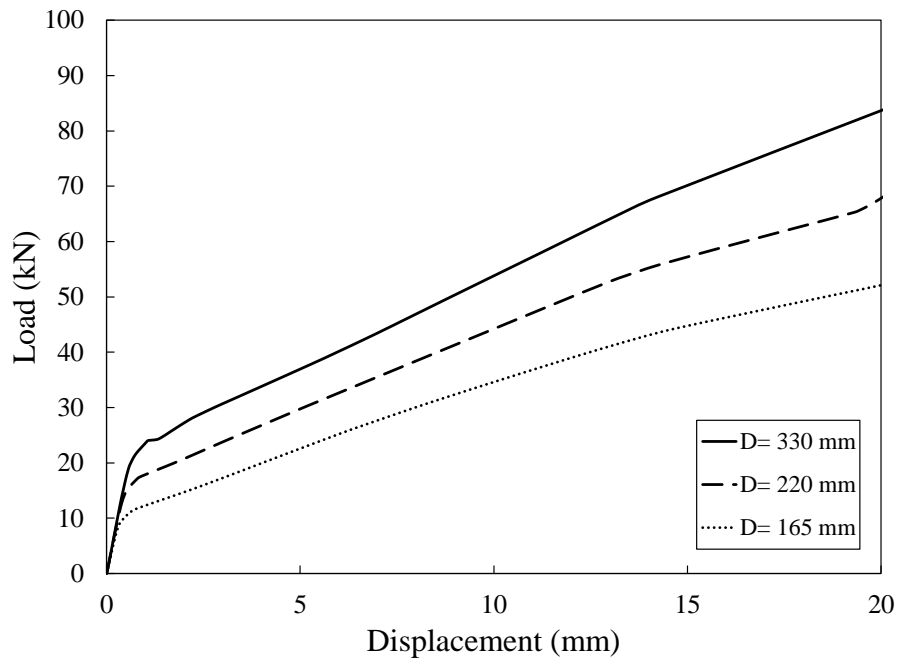
6.5.2.1 Lateral behaviour of bored and CFA

The effect of the change in pile diameter on the lateral behaviour of both bored and CFA pile was investigated. a, b, and c shows the load-displacement, deflection, and moment along the bored pile, respectively. It was noted that D affects the pile lateral response significantly. The pile head deflection and the deflection along the pile length were lower for higher D . This behaviour can be attributed to two factors. First, the smaller diameter which results in less soil volume supporting the pile. Second, the lower moment of inertia of pile cross-section for piles with lower D , which means less flexural resistance. As the diameter increased, the pile's behaviour shifted from long pile behaviour to short pile behaviour, which resulted in a downward shift of the location of the maximum bending moment.

The pile head deflection, pile deflection along the length, and the bending moment distribution of the CFA pile are shown in Figure 6.17 d, e, and f, respectively. The effect of the pile diameter is significant on the CFA pile behaviour following the same trend as the bored pile.

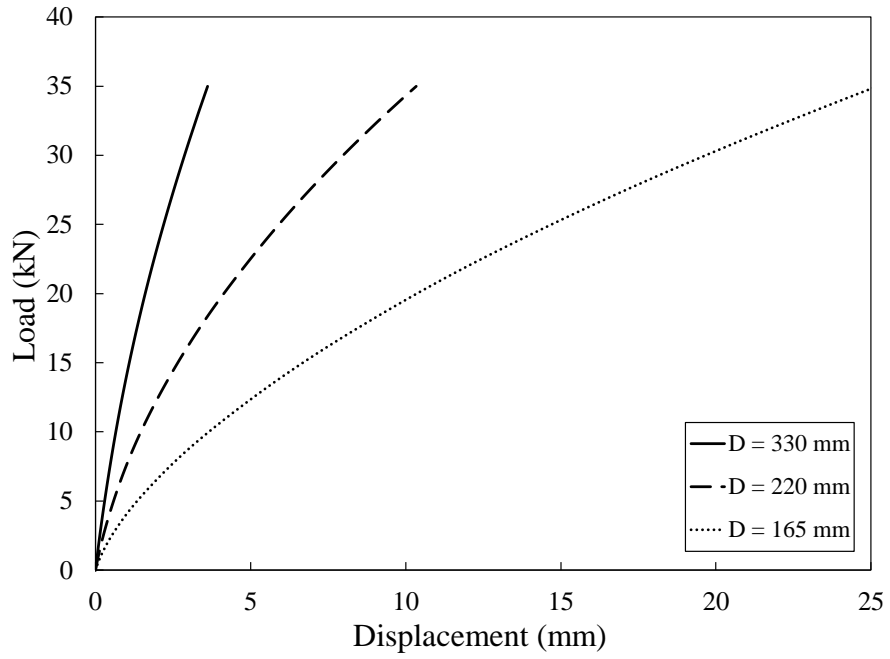


(a)

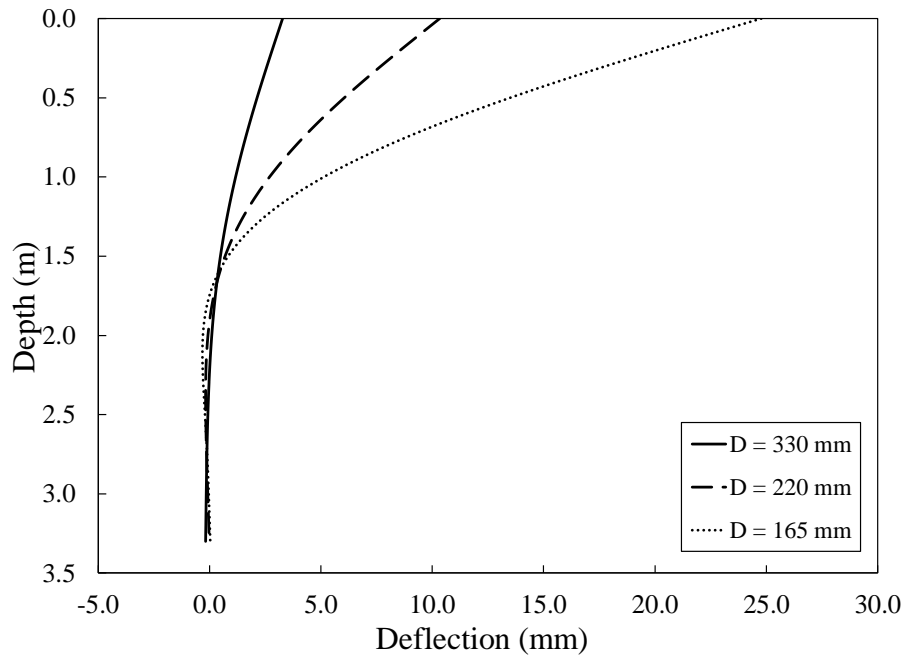


(b)

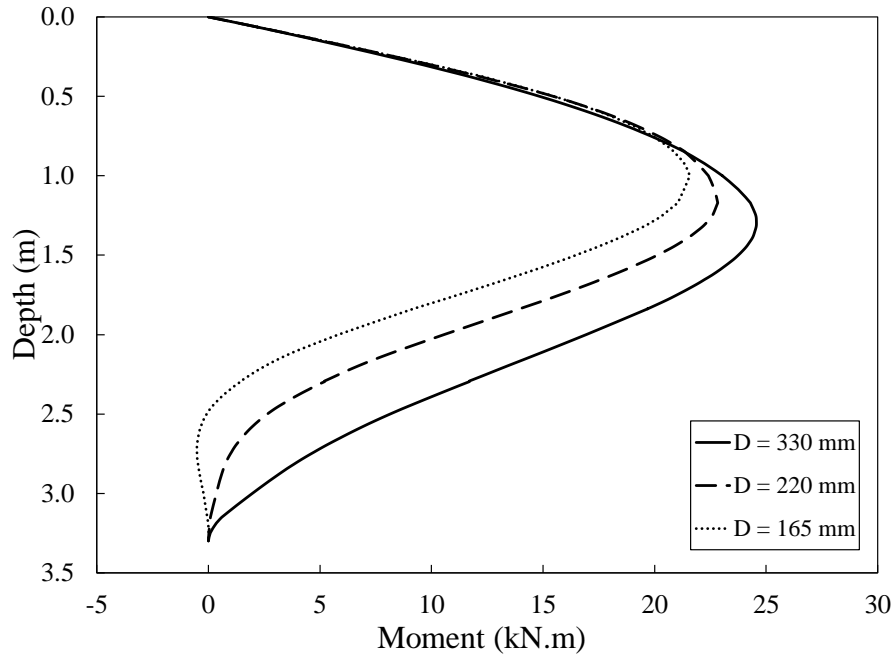
Figure 6.16 Effect of D on pullout load displacement of (a) bored pile (b) CFA pile



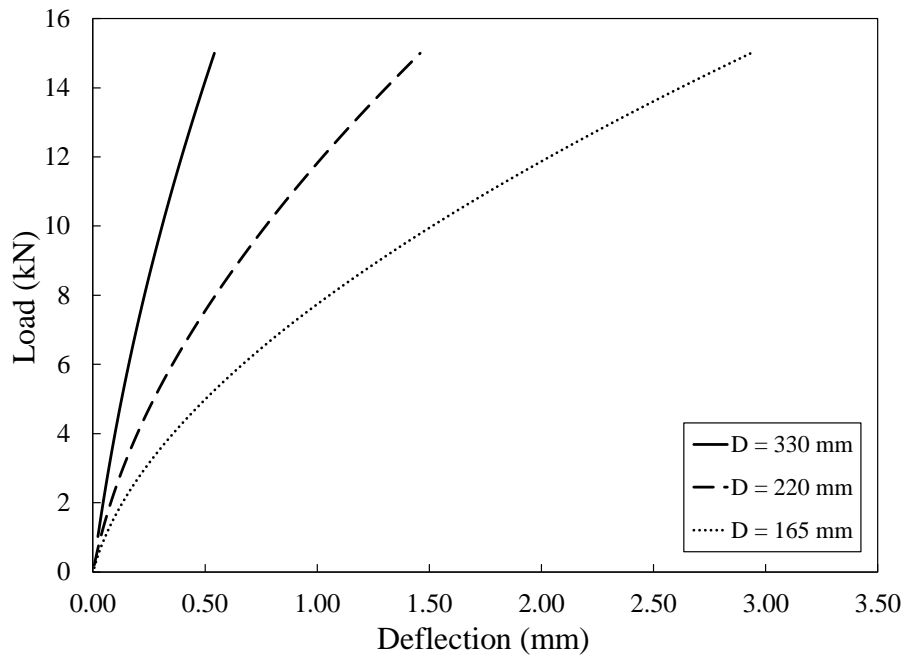
(a)



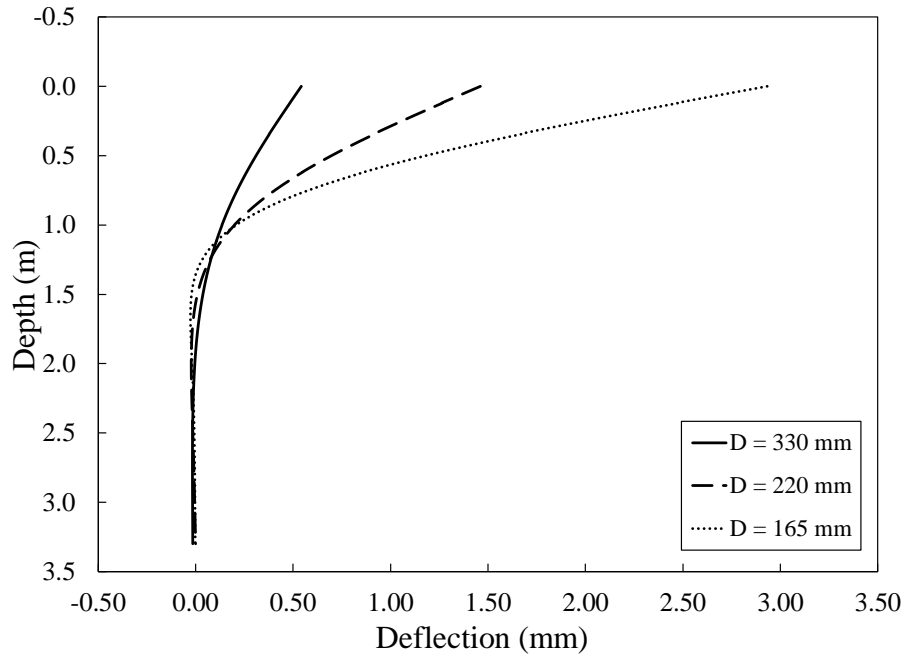
(b)



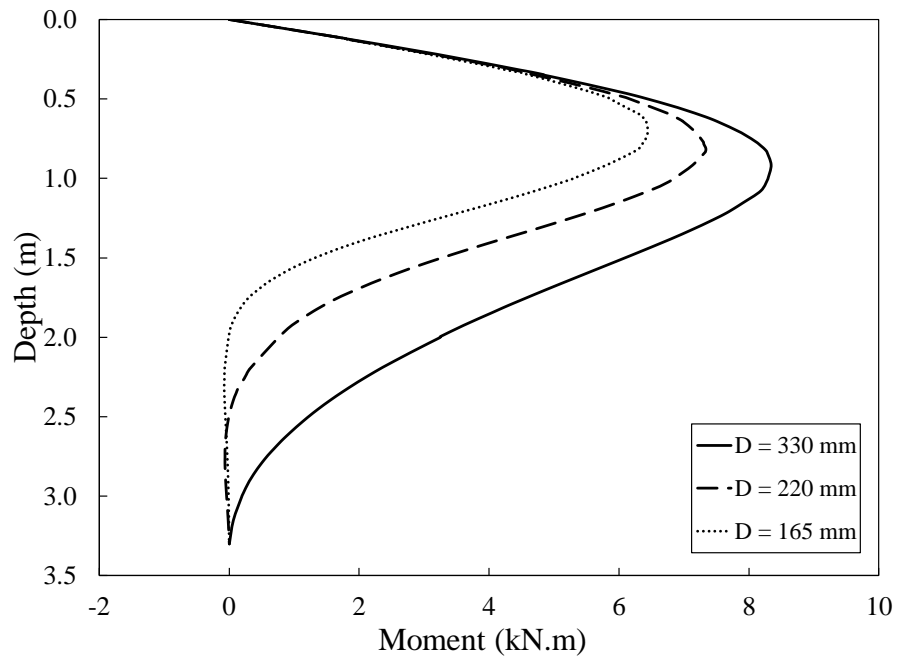
(c)



(d)



(e)



(f)

Figure 6.17 Effect of D on (a) load displacement, (b) pile deflection, and (c) moment distribution of bored pile, and (d) load displacement, (e) pile deflection, and (f) moment distribution of CFA pile

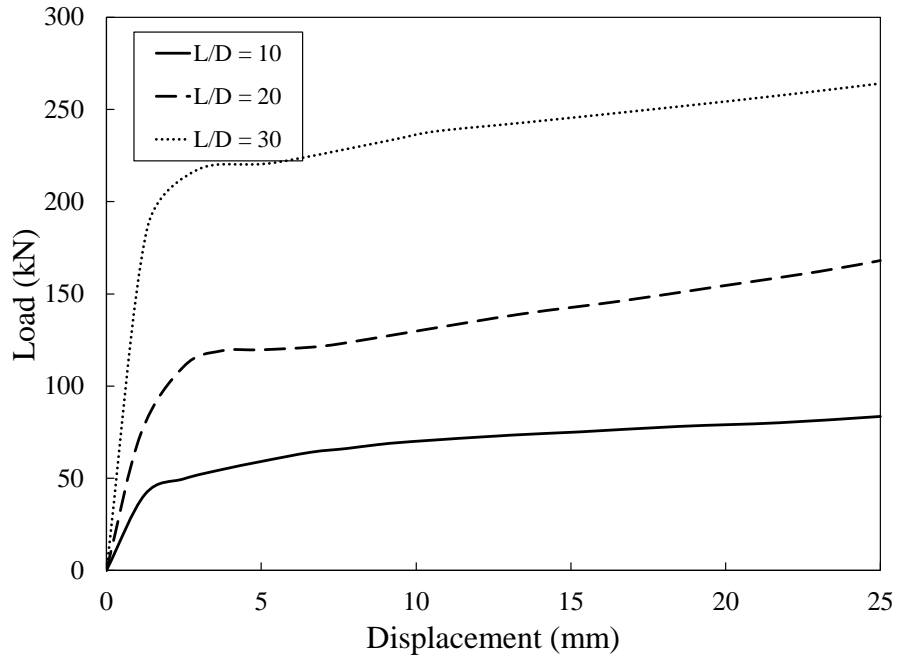
6.5.3 Effect of pile length to diameter ratio

In this part of the study the effect of length to diameter ratio (L/D) on the bored and CFA pile behaviour under compression and lateral loading was investigated. The ratios of L/D used in this investigation were 10, 20, and 30. The bored and CFA piles diameters did not change and were 280 mm and 320 mm, respectively. The lengths of the bored pile used in the investigation were 2.8 m, 5.6 m, and 8.4 m. While, the CFA pile lengths used in the investigation were 3.2 m, 6.4 m, and 9.6 m.

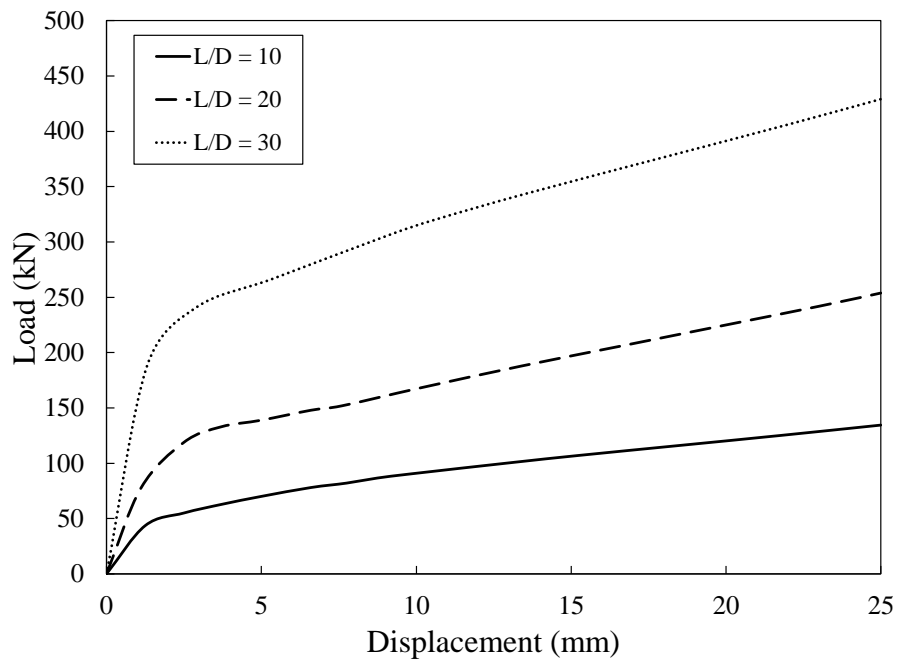
6.5.3.1 Compressive behaviour of bored and CFA piles

The bored and CFA piles compression response was investigated as a result of changing L/D ratio. Figure 6.18 shows the shaft friction, end bearing, and total load for the bored pile. Figure 6.18 a, b and c shows that both the stiffness and the capacity of the bored pile increased as the pile length increased, within the range considered in this analysis. This is because L/d for all cases were less than 30. It is also noted, as expected, the percentage contribution of the skin friction increased and the percentage contribution of the end bearing resistance decreased as the pile length increased.

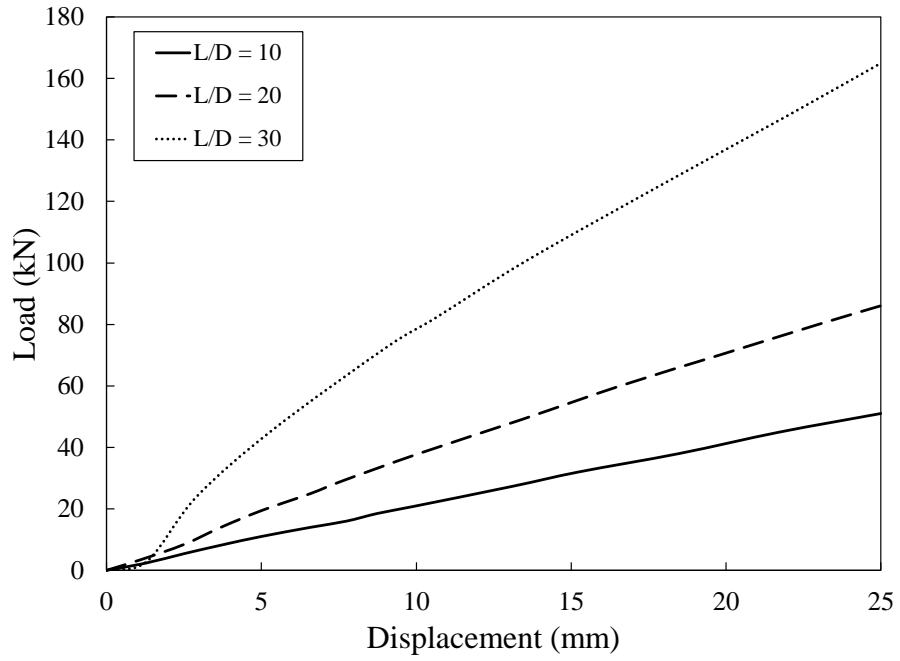
Figure 6.18 d, e, and f show similar trends for the shaft friction, end bearing, and total load of the CFA pile. Also, comparing the results of the CFA pile with those for the bored pile, it is clear that the advantage of the CFA pile over the bored pile increases as the pile length increases. This can be attributed to the higher shaft resistance due to increased soil confinement and soil friction around the pile because of the CFA pile construction process. It can be noted from Fig. 6.18 e that the end bearing is almost the same at 20 and 30 L/D .



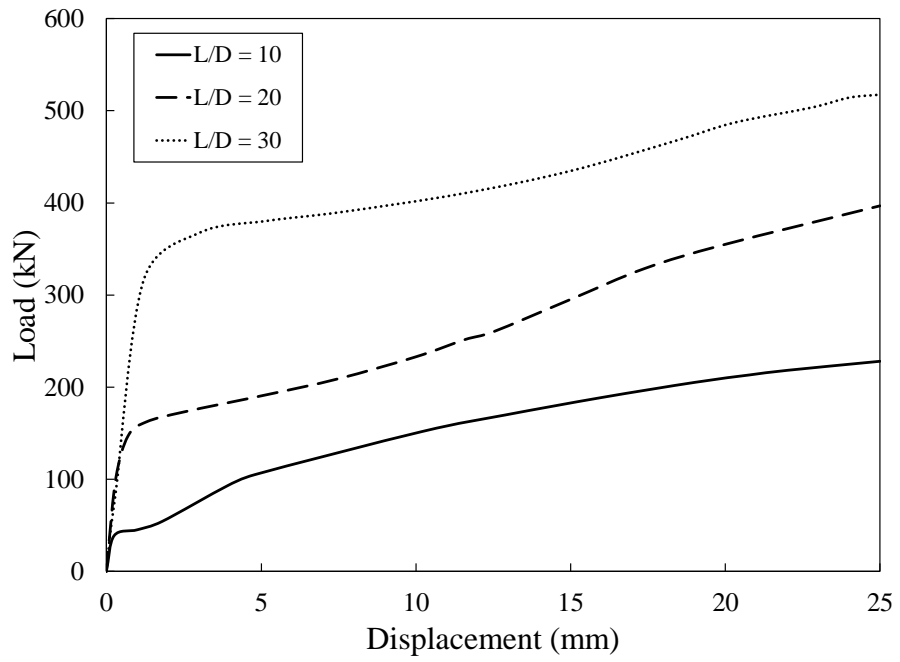
(a)



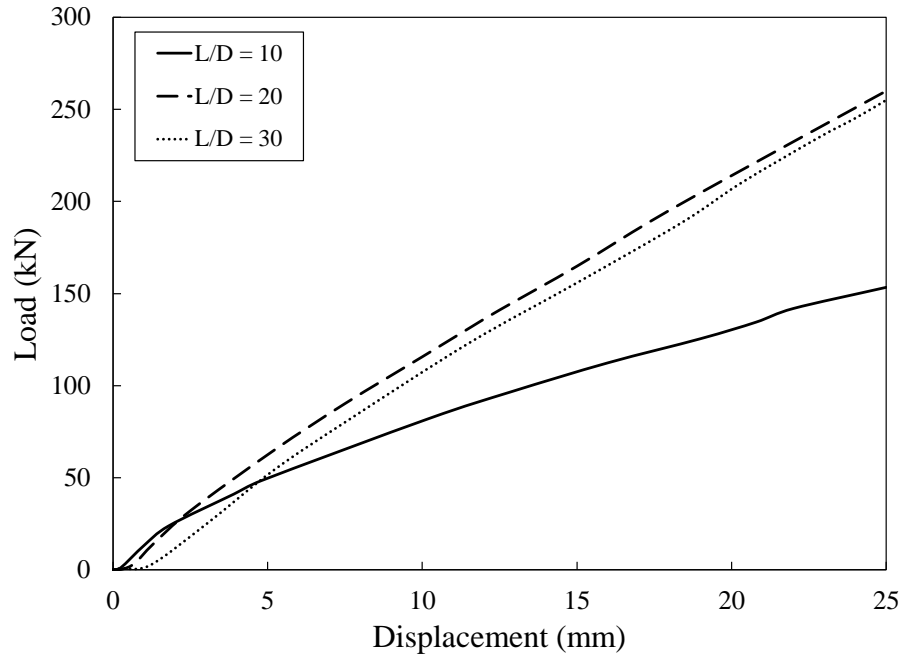
(b)



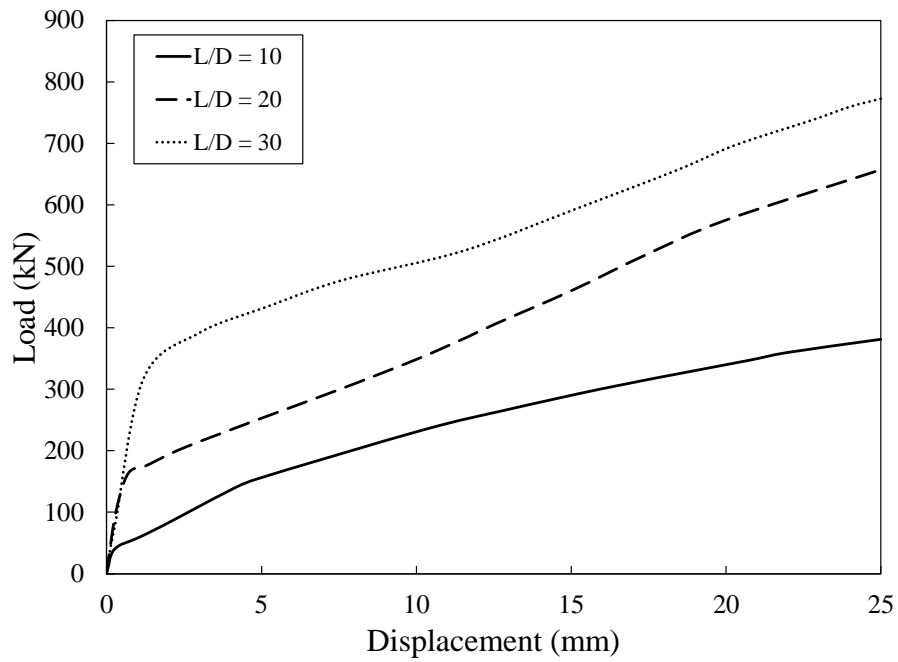
(c)



(d)



(e)



(f)

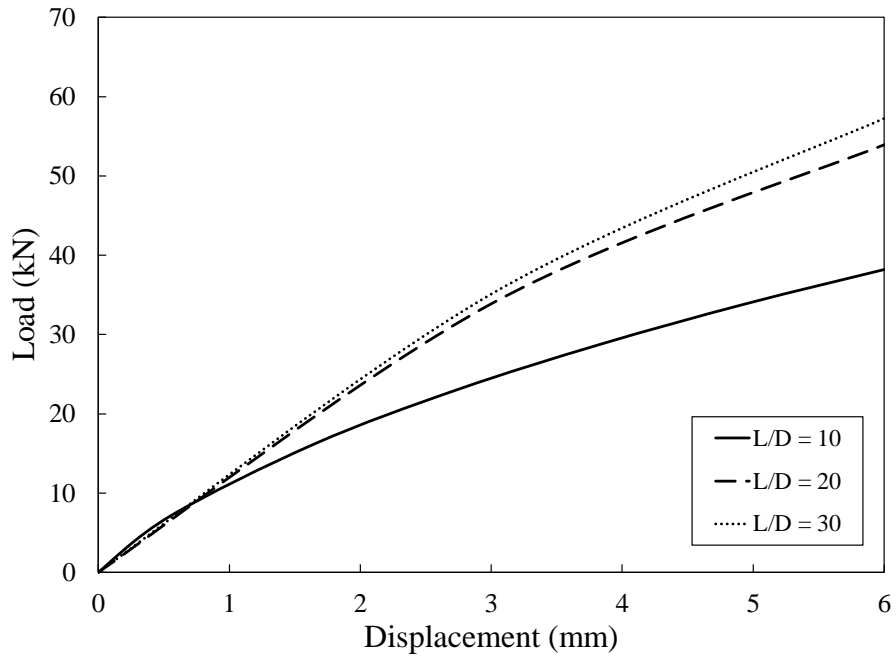
Figure 6.18 Effect of L/D on (a) shaft friction, (b) end bearing, and (c) total load of the bored pile, and (d) shaft friction, (e) end bearing, and (f) total load of the CFA pile

6.5.3.2 Lateral behaviour of bored and CFA piles

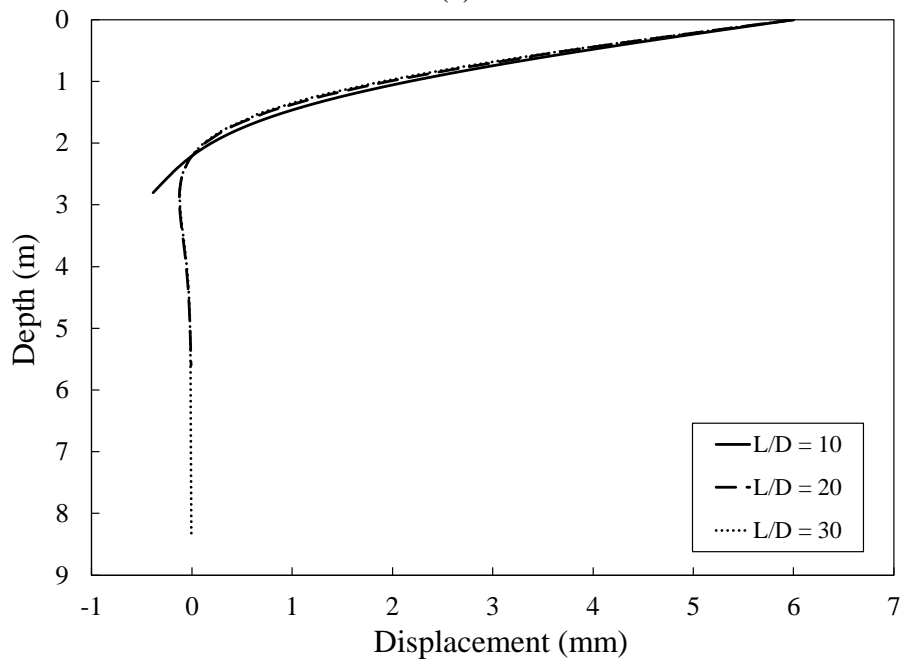
In this section the load-displacement, pile deflection, and bending moment distribution were calculated for bored and CFA piles. Lateral displacement of 6 mm was applied on the piles and the response was measured. Figure 6.19 a, b, and c show the load displacement at the pile head, pile deflection along its shaft, and moment distribution of the bored pile, respectively. It can be noted from Figure 6.19a that the load corresponding to pile deflection of 6 mm increased by about 30% as L/d increased from 10 to 20, but increased by only 5% as L/D increased from 20 to 30. This demonstrates that the pile lateral resistance is derived primarily from the soil along top $20d$ of the pile shaft, and any increase in the pile length over $20d$ has little contribution to the pile lateral performance. Figure 6.19b shows that at depth equal to $10D$, the pile deflection is almost zero. Thus, bored pile with $L/D = 10$ behaves as short pile, while piles with $L/D = 20$ and 30 behave as long piles. It can be noted from Figure 6.19 c that the bending moment increased as the pile length increase from $10D$ to $20D$, but marginal increase as the length increased from $20D$ to $30D$. This is attributed to the change from the short pile behavior to long pile behaviour at L/D about 20. Moreover, it can be noted that the location of the maximum bending moment did not change by increasing the L/D ratio.

Figure 6.19 d, e, and f present load-displacement at pile head, pile deflection along pile shaft, and moment distribution of the bored pile, respectively. Comparing the behaviour of the bored and CFA piles, it can be noted that the load corresponding to 6 mm deflection at the pile head for the CFA pile was almost twice that for the bored pile. The bending moment

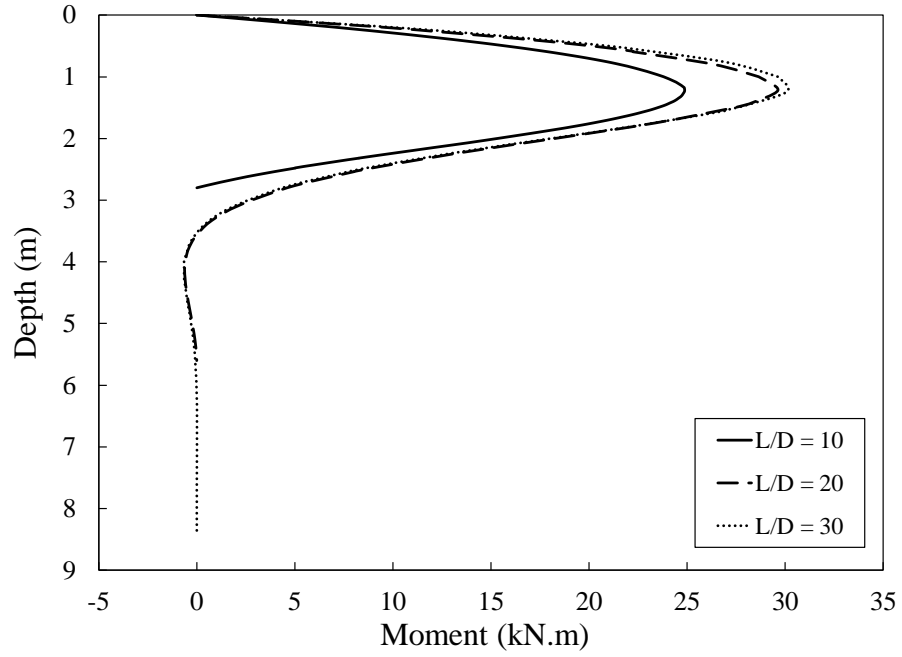
profiles shown in Figure 6.19 c and f demonstrate higher values for the CFA pile compared with that of the bored pile.



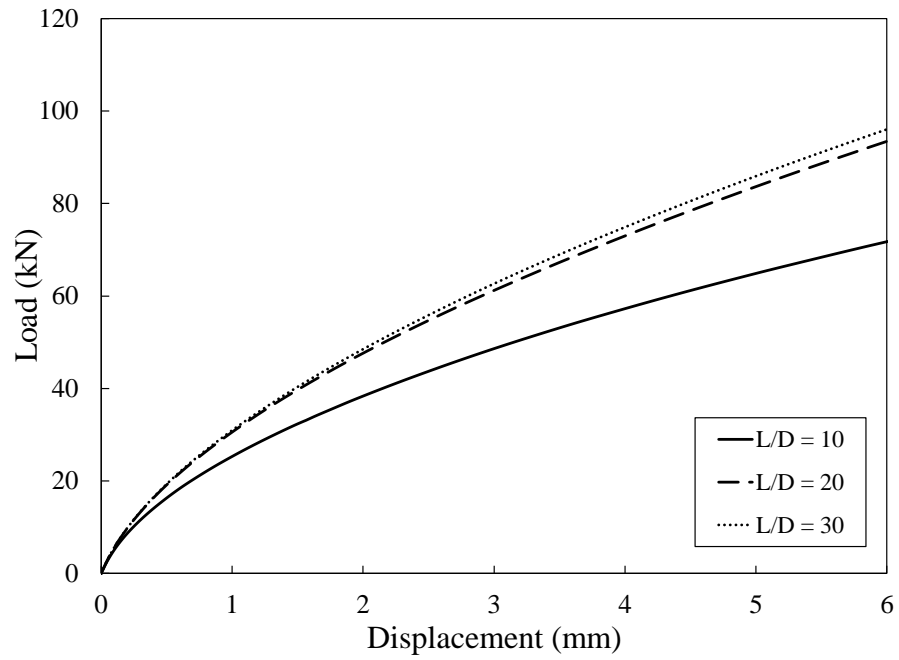
(a)



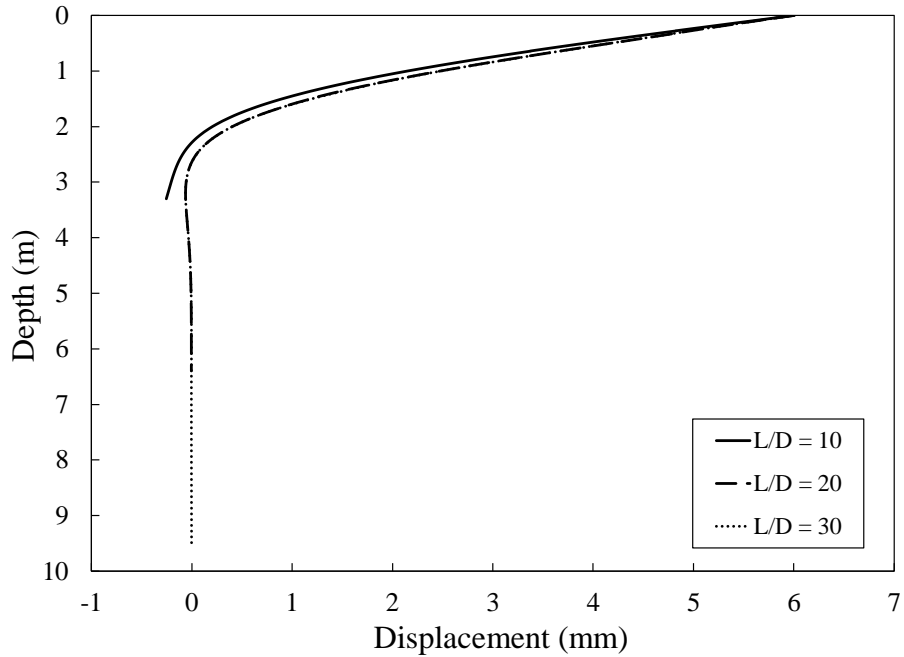
(b)



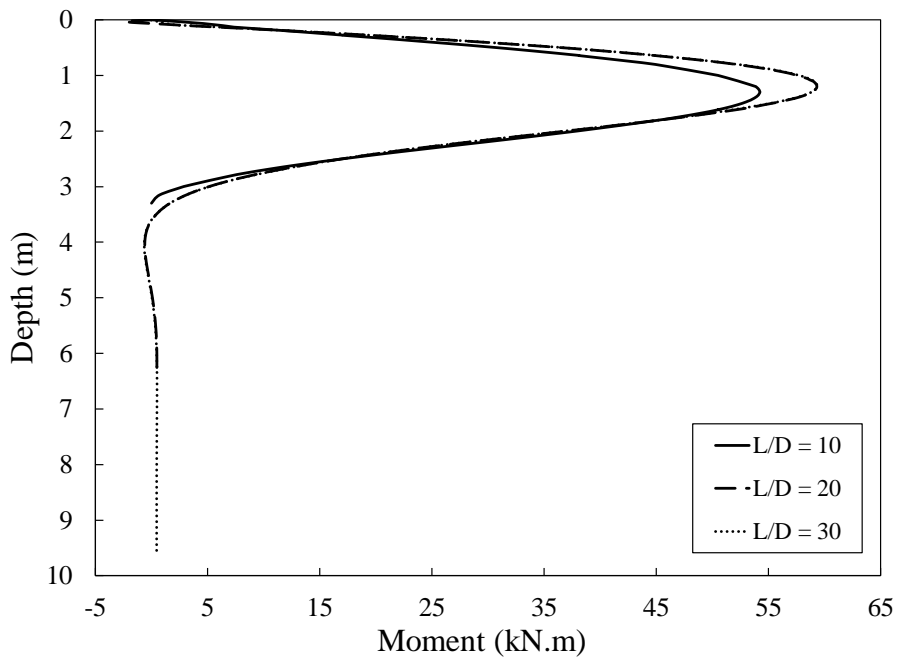
(c)



(d)



(e)



(f)

Figure 6.19 Effect of L/D on (a) load displacement, (b) pile deflection, and (c) moment distribution of bored pile, and (d) load displacement, (e) pile deflection, and (f) moment distribution of CFA pile

6.6 P-y curves

The p-y curves were back calculated using LPile software. The Load displacement curves for both CFA and bored piles were calculated for the initial part using LPile and it was then compared with the measured curves. The API initial modulus of subgrade reaction (65000kN/m) was multiplied by 4 and 6 for the bored and CFA piles, respectively. The corresponding p-y curves were then extracted for both bored and CFA piles and compared with the API p-y curves. Figure 6.20 shows the extracted p-y curves for the bored and CFA piles compared with API p-y curves at several depths of the piles. It is noted from Figure 6.20 that both bored and CFA piles had stiffer response than stipulated by the API curve. In addition, p-y curves for the CFA pile was stiffer than that for the bored pile, especially at larger depths. This should be considered when modeling CFA piles using the program LPile for proper prediction of its stiffness and response.

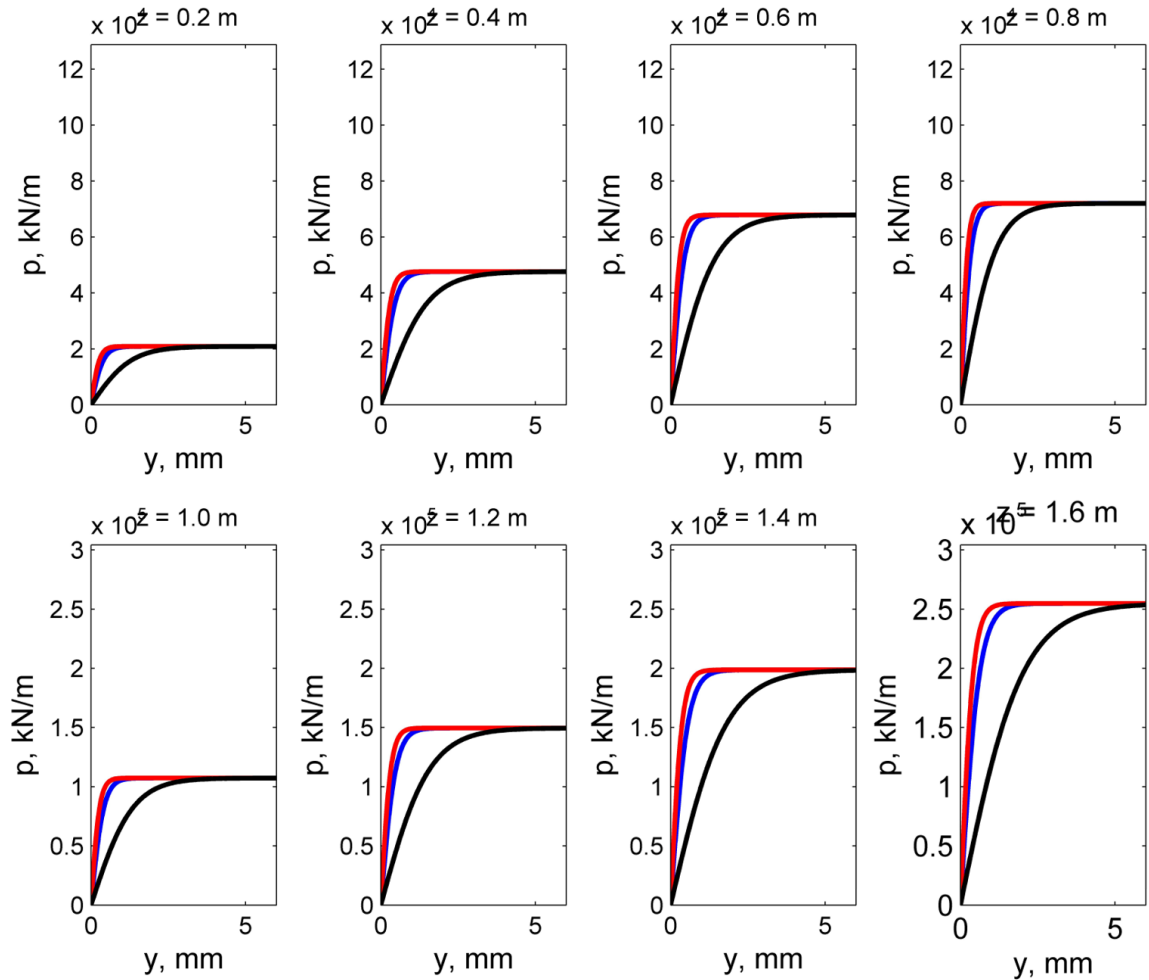


Figure 6.20 comparison between Bored, CFA and API p-y curves at several depths of the piles

6.7 Conclusions

Three-dimensional nonlinear finite element models of bored and CFA piles were developed to simulate their behaviour under compression, pullout, and lateral loading. CFA pile model calibration showed the need to simulate the construction effect, which resulted in densified zone of soil around the pile increasing its capacity. Two circular zones with stiffer

soil properties were added around the pile with diameters greater than the pile diameter by 60% and 200%.

A parametric study was performed on bored and CFA piles using the calibrated models to investigate the effect of the angle of internal friction and pile geometry on their behaviour under the different loading conditions. It was found that CFA piles are more affected by the increase in the friction angle than the bored pile. And the friction angle insignificantly affects the end bearing capacity in both types. The change of friction angle did not affect the pullout due to the loading sequence.

The larger D increased the shaft resistance of the piles during the compression test especially for the CFA pile. The CFA pile was insignificantly affected by the decrease in D , which was attributed to the high shear stress which initialized the residual shear strength. Both bored and CFA pile lateral capacity were affected significantly by D .

6.8 References

- Abu-Farsakh, M., Tumay, M., and Voyiadjis, G. 2003. Numerical parametric study of piezocone penetration test in clays. *International Journal of Geomechanics* 3(2): 170-181.
- Albuquerque, P., Carvalho, D., and Massad, F. 2005. Bored, continuous flight auger and omega instrumented piles: Behaviour under compression. In *Proceedings of The International Conference on Soil Mechanics and Geotechnical Engineering*. Osaka, Japan. p. 2075-2078.
- Bowles, J.E. 1996. *Foundation analysis and design*. McGraw-Hill, New York.
- Brinkgreve, R., Kumarswamy, S., and Swolfs, W. 2015. *Plaxis 3D Anniversary Edition Manual*. Plaxis bv. The Netherlands. Delft.
- Brown, D.A., Dapp, S.D., Thompson, W.R., and Lazarte, C.A. 2007. *Design and Construction of Continuous Flight Auger (CFA) Piles*. Federal Highway Administration. Technical Report.
- Farrell, E.R., and Lawler, M.L. 2008. CFA pile behaviour in very stiff lodgement till. *Proceedings of the Institution of Civil Engineers-Geotechnical Engineering* 161(1): 49-57.
- Fleming, W.G.K. 2009. *Piling engineering*. Taylor & Francis, New York;London;.
- Freitas, A.C.d., Danziger, B.R., Pacheco, M., and Gerscovich, D.M.S. 2015. 3-D predictions of installation and group effect on driven piles in sands. *International Journal of Geotechnical Engineering* 9(1): 101-112. doi: 10.1179/1939787914Y.0000000052.
- Gavin, K., Cadogan, D., Tolooiyan, A., and Casey, P. 2013. The base resistance of non-displacement piles in sand. Part I: field tests. *Proceedings of the Institution of Civil Engineers-Geotechnical Engineering* 166(6): 540-548.

- Gavin, K.G., Cadogan, D., and Casey, P. 2009. Shaft Capacity of Continuous Flight Auger Piles in Sand. *Journal of Geotechnical and Geoenvironmental Engineering* 135(6): 790-798. doi: doi:10.1061/(ASCE)GT.1943-5606.0000073.
- Holko, M., and Stacho, J. 2014. Comparison of Numerical Analyses with a Static Load Test of a Continuous Flight Auger Pile. *Slovak Journal of Civil Engineering* 22(4): 1-10.
- Ismael, N.F. 2001. Axial Load Tests on Bored Piles and Pile Groups in Cemented Sands. *Journal of Geotechnical and Geoenvironmental Engineering* 127(9): 766-773. doi: doi:10.1061/(ASCE)1090-0241(2001)127:9(766).
- Józefiak, K., Zbiciak, A., Maślakowski, M., and Piotrowski, T. 2015. Numerical modelling and bearing capacity analysis of pile foundation. *Procedia Engineering* 111: 356-363.
- Manual, A.U. 2010. Version 6.10. ABAQUS Inc.
- Paulo José Rocha de, A., Faiçal, M., Pereira Viana Da Fonseca, A., David de, C., Jaime, S., and Elisabete Costa, E. 2011. Effects of the construction method on pile performance: Evaluation by instrumentation. part 2: Experimental site at the faculty of engineering of the University of Porto. *Soils and Rocks* 34(1): 51-64.
- Phuong, N., van Tol, A., Elkadi, A., and Rohe, A. 2016. Numerical investigation of pile installation effects in sand using material point method. *Computers and Geotechnics* 73: 58-71.
- Poulos, H.G. 1975. *Settlement of Isolated Foundations*.
- Rosti, F., and Abu-Farsakh, M. 2015. Numerical Simulation of Pile Installation and Setup for Bayou Lacassine Site. In *IFCEE 2015*. pp. 1152-1161.
- Ver, A.F. Software Package. Ansys Fluent Inc., Canonsburg, PA, USA.

Chapter 7

7 SUMMARY, CONCLUSIONS, AND RECOMMENDATIONS

7.1 Summary and conclusions

The potential for increasing concrete sustainability through reusing treated oil sands waste (TOSW) as a replacement for natural sand was investigated. The experimental results demonstrated the high potential of recycling/reusing TOSW in concrete mixtures for different construction applications. Besides converting TOSW to a valuable product, this study provides an alternative solution for waste management of TOSW instead of sending to landfill. The following conclusions can be drawn from the first experimental phase:

- Mixtures incorporating up to 30% TOSW as a partial replacement of sand met the targeted compressive strength for CFA pile concrete mixtures at age 28 days (i.e. 35 MPa) along with adequate durability performance.
- Addition of TOSW did not alter the correlation between compressive strength and other mechanical properties.
- Solidification of TOSW in the cementitious matrix of concrete along with reduction in concrete porosity due to TOSW addition increase the potential of producing materials with a lower pollution potential than that characterizing the TOSW disposal.

Bored and continuous flight auger (CFA) piles are two widely used cast in place reinforced concrete pile types that are constructed employing different techniques, which affects their axial performance and capacity. Therefore, the second experimental phase of this thesis focused on comparing the axial performance of CFA and bored concrete piles in sand; and investigated the effect of utilizing a green concrete mixture (i.e. incorporating treated oil sand waste (TOSW)) in their construction. The following conclusions can be drawn from this experimental phase:

- The ultimate capacity of the CFA piles was approximately twice the capacity of bored piles.
- Incorporating TOSW in the piles concrete mixtures has insignificant effect on their geotechnical performance.
- For CFA piles, the shaft friction supported 77% of the total load, while for bored piles it contributed 66% of the total load capacity.
- The unit shaft resistance of the CFA piles was higher than the bored piles with maximum value of about 120 kPa.
- The unit end bearing resistance was similar for all piles. However, the CFA piles end bearing load was higher because of its larger cross-sectional area.
- The shaft friction measured in the pullout test was about 40 to 50% of that measured in the compression test due to the loading history, regardless of the pile type.
- The construction process of the CFA piles has increased its diameter by 13%.
- Concrete strength of CFA piles was higher than that of the bored piles due to the pressure applied on the concrete during pile construction.

- The shear failure around the pile happened in the soil in the shear band around the pile. The shear band thickness existed around the piles increased as the surface roughness increased.
- The concept of fractal dimension can be employed as a quantitative measure to evaluate roughness of pile surface. It is found that the CFA piles had a higher value of roughness fractal dimension compared to that of bored piles, which is mainly due to more complex particle-interlocking mechanism of CFA piles during the construction process.

In the third experimental phase, the lateral monotonic and cyclic behaviours of bored and continuous flight auger piles were compared, highlighting the effect of construction method. In addition, the effect of utilizing a green concrete mixture (i.e. incorporating treated oil sand waste (TOSW)) on their behaviour was highlighted. The following conclusions were drawn:

- Pile CFA C1 ultimate capacity was higher than that of pile Bored C1 by about 47%. This difference can be attributed to the increase in CFA pile diameter and increased friction angle due to construction method which resulted in higher soil density and confinement.
 - The virgin initial lateral stiffness of the CFA piles is about three time higher than that of the bored piles. After performing three cyclic tests on the piles the initial stiffness of the CFA piles was about six times higher than that of the bored piles.
-

- The maximum lateral deflection of the CFA piles was about 48% of that of the bored piles after the third cyclic testing indicating higher capacity of CFA piles.
 - The lateral stiffness of the bored piles ranged from 32 to 50% of the lateral stiffness of CFA piles.
 - The degradation parameter 't' is affected by preloading of the pile even though the load amplitude is the same.
-
- The construction method of the CFA piles increased the diameter by 13%, which thus increased the soil confining pressure and which in turn improved its overall performance.
 - Incorporating TOSW in the concrete mixtures of the piles did not affect their geotechnical behaviour.

Finally, a three-dimensional nonlinear finite element (FE) model was established using the software Plaxis 3D to analyze the bored and continuous flight auger (CFA) piles constructed in the same soil conditions. The models were calibrated and verified using controlled experimental data. In addition, the verified numerical models were utilized to conduct a parametric study in order to examine the effects of the soil mechanical properties and pile geometry on the compressive, pullout, and lateral behaviour of the CFA piles in comparison with bored piles. The following conclusions were drawn

- CFA pile model calibration showed the need to simulate the construction effect which resulted in densified zone of soil around the pile increasing its capacity. Two circular zones with stiffer soil properties were added around the pile with diameters greater than the pile diameter by 60% and 200%.

- CFA piles are more affected by the increase in the friction angle than the bored pile. And the friction angle insignificantly affects the end bearing capacity in both types. The change of friction angle did not affect the pullout due to the loading sequence.
- The larger D increased the shaft resistance of the piles during the compression test especially for the CFA pile. The CFA pile was insignificantly affected by the decrease in D , which was attributed to the high shear stress which initialized the residual shear strength. Both bored and CFA pile lateral capacity were affected significantly by D .

7.2 Contribution

- Highlighted advantages of using CFA pile compared to Bored pile under different realistic loading scenarios.
- Clarified the interrelationship between construction methods and geotechnical performance.
- Provided first time data about the moment-curvature for CFA and bored pile.
- Examined the potential of achieving sustainability in geotechnical application while maintain the desired performance.

7.3 Recommendations

- Further analytical studies should be done to provide design correlations to properly design the CFA piles and provide designers with proper tools.

- Studying the effect of CFA piles construction in different types of soils to further understand the soil effect on the pile behaviour.
- Further studies should be made to study the effect of concrete pumping pressure on the pile behaviour because the behaviour of the CFA pile is dependent on the pumping pressure.
- Investigate utilizing TOSW as full replacement of fly ash used in CFA concrete mixtures.
- More numerical simulation should be conducted to better develop the most effective way of modelling the CFA piles.

Curriculum Vitae

Name: Mahmoud Kassem

Post-secondary Education and Degrees: Arab Academy for Science and Technology
Cairo, Egypt
2001-2006 B.A.

Arab Academy for Science and Technology
Cairo, Egypt
2007-2011 M.Sc.

Honors and Awards: Arab Academy for Science and Technology Graduate Scholarship
2013-2017

Western University Graduate Scholarship
2013-2017

Related Work Experience Teaching Assistant
The University of Western Ontario
2013-2017